



FEUP Universidade do Porto
Faculdade de Engenharia

**OPERATIONAL MODAL ANALYSIS
FOR TESTING AND MONITORING
OF BRIDGES AND SPECIAL STRUCTURES**

Filipe Manuel Rodrigues Leite de Magalhães

A dissertation presented to the Faculty of Engineering of the University of Porto
for the degree of Doctor in Civil Engineering.

Supervisors: Álvaro Cunha (Full Professor); Elsa Caetano (Associate Professor).



ABSTRACT

Dynamic testing and continuous monitoring based on Operational Modal Analysis can play an important role in the management of important civil infrastructures, since these experimental tools permit the periodic or continuous assessment of bridges, dams, high-rise buildings, stadia or offshore structures through the analysis of their response to ambient excitation, while they are in normal operation.

Nowadays, the performance of dynamic tests has become very practical, even when carried out on large structures, as there are solutions that avoid the use of long electrical cables. Furthermore, the installation of continuous dynamic monitoring systems with remote control and data retrieving has become much more straightforward and economical due to the diversity of commercially available solutions. However, this highly sophisticated hardware has to be combined with powerful routines that should be able to efficiently extract useful information from data collected during dynamic tests or continuously recorded by permanent installations.

Therefore, this work was firstly focused on the development and implementation of processing procedures adequate to extract accurate modal parameter estimates from the time series recorded during ambient vibration tests of large civil engineering structures. The efficiency of the presented algorithms to simultaneously process several datasets was then validated with the analysis of databases collected in the dynamic tests of the Millau Viaduct and Humber Bridge. Additionally, the accuracy of modal damping ratio estimates provided by ambient vibration tests was evaluated using data from five relevant structures where both ambient and forced vibration tests were performed.

Afterwards, routines suitable for the on-line processing of data continuously collected by dynamic monitoring systems were developed and integrated in a monitoring software package. One of the most important features of the software is the automatic identification of modal parameters from the collected acceleration time series through the adoption of a new procedure suitable to be used together with the state-of-the-art algorithms: SSI-COV and p-LSCF. This is complemented by algorithms that minimize the effects of environmental and operational factors on the identified natural frequencies, and by statistical tools that provide indexes adequate to automatically identify changes in the natural frequencies due to abnormal causes, as for instance, the occurrence of damages. The implemented monitoring tools were tested with two applications: one in a large arch bridge (Infante D. Henrique Bridge) and another in the roof of a stadium (Braga Stadium). In particular, the system installed in the bridge, in continuous operation for more than two years, permitted to demonstrate the usefulness and robustness of all the components included in the monitoring software.

RESUMO

A monitorização contínua e os ensaios dinâmicos baseados na Análise Modal Operacional podem desempenhar um papel muito relevante na gestão de infra-estruturas importantes, dado que estas ferramentas experimentais permitem a avaliação periódica ou contínua de pontes, barragens, edifícios, estádios ou estruturas offshore através da análise da sua resposta a acções ambientais, sem perturbar o seu normal funcionamento.

Actualmente, a realização de ensaios dinâmicos tem-se tornado muito prática, mesmo quando estes são efectuados em estruturas de grandes dimensões, pois existem soluções que evitam o uso de longos cabos eléctricos. Além disso, a instalação de sistemas de monitorização contínua dinâmica com controlo e transmissão de dados à distância tornou-se muito mais simples e económica, devido à diversidade de soluções disponíveis no mercado. No entanto, estes equipamentos têm que ser combinados com rotinas que devem ser capazes de extrair informação útil dos dados colhidos durante ensaios dinâmicos ou continuamente registados por instalações permanentes.

Assim, numa primeira fase, este trabalho focou-se no desenvolvimento e aplicação de técnicas para obter estimativas precisas de parâmetros modais a partir dos dados adquiridos durante ensaios de vibração ambiental de estruturas de grandes dimensões. A eficiência dos algoritmos apresentados para processar simultaneamente series temporais medidas em diferentes setups foi validada com a análise dos dados recolhidos nos ensaios dinâmicos do Viaduto de Millau e da Ponte Humber. Além disso, a precisão das estimativas de coeficientes de amortecimento modal obtidas através de ensaios de vibração ambiental foi avaliada utilizando dados de cinco estruturas relevantes onde foram realizados ensaios de vibração ambiental e forçada.

Posteriormente, foram desenvolvidas e integradas num software de monitorização rotinas para realizar o processamento on-line de dados continuamente registados por sistemas de monitorização dinâmica. Uma das características mais importantes do software consiste na utilização de um novo procedimento para realizar a identificação automática dos parâmetros modais, adequado para ser utilizado em conjunto com os algoritmos: SSI-COV e p-LSCF. Este software contém ainda algoritmos que minimizam os efeitos dos factores ambientais e operacionais nas frequências naturais identificadas e ferramentas estatísticas que fornecem índices adequados para identificar automaticamente alterações nas frequências naturais, que poderão estar associadas à ocorrência de danos. Estas ferramentas foram testadas em duas aplicações: na Ponte Infante D. Henrique e na cobertura do Estádio de Braga. Em particular, o sistema instalado na ponte, em funcionamento contínuo há mais de dois anos, permitiu demonstrar a utilidade e robustez de todas as componentes incluídas no software de monitorização.

RÉSUMÉ

Les essais dynamiques et la surveillance continue basée sur l'analyse modale opérationnelle ont un rôle significatif dans la gestion des infrastructures civiles importantes, puisque ces outils expérimentaux permettent l'évaluation périodique ou continue des ponts, barrages, bâtiments de grande hauteur, stades ou structures offshore en analysant leur réponse sous excitation ambiante, sans perturber leur fonctionnement normal.

Actuellement, les essais dynamiques ont devenu très pratiques, même quand les objets d'étude sont de grands ouvrages, car il est possible d'utiliser des solutions qui ne nécessitent pas de longs câbles électriques. En outre, l'installation de systèmes de surveillance continue dynamique avec contrôle et transmission des données à la distance est devenue plus simple et économique en raison de la diversité des solutions disponibles. Toutefois, ces dispositifs doivent être combinés avec des routines qui peuvent extraire des informations utiles à partir des données recueillis lors des essais dynamiques ou à partir de celles qui sont amenés continuellement avec des systèmes de mesure permanents.

Ainsi, ce travail s'est concerné d'abord sur le développement et la mise en œuvre de techniques pour obtenir des estimations précises des paramètres modaux à partir des données enregistrées pendant les essais de vibration ambiante de grands ouvrages. L'efficacité des algorithmes présentés pour traiter simultanément des séries temporelles mesurées dans les configurations différentes a été validée avec l'analyse des données recueillies dans les essais dynamiques du viaduc de Millau et du pont Humber en Angleterre. En outre, la précision des estimations des coefficients d'amortissement modal obtenus lors des essais de vibration ambiante a été évaluée en utilisant les données provenant de cinq structures essayées en conditions de vibration ambiante et sous charge.

Dans une seconde phase, une intégration dans un logiciel a été faite des routines pour effectuer le traitement en ligne des données continuellement enregistrées par des systèmes de surveillance dynamique. Une des caractéristiques les plus importantes de ce logiciel est l'utilisation d'une nouvelle procédure pour effectuer une identification automatique des paramètres modaux adaptés pour être utilisées avec des algorithmes: SSI-COV et de p-LSCF. Ce logiciel est complété par des algorithmes qui permettent minimiser les effets des facteurs environnementaux et opérationnels sur les fréquences naturelles identifiées, ainsi que par les outils statistiques qui fournissent des indices suffisants pour identifier automatiquement le changement de fréquence naturelle qui peuvent être associées à l'apparition du dommage. Ces outils ont été testés avec deux applications: un pont de grande arche, le Pont Infante D. Henrique, et la couverture du stade de Braga. En particulier, le système installé dans le pont, en fonctionnement continu depuis plus de deux ans, a permis de démontrer l'utilité et la robustesse de l'ensemble des éléments inclus dans le logiciel de surveillance.

ACKNOWLEDGEMENTS

To all who have accompanied me during my PhD journey, family, friends and colleagues that, through their friendship and understanding, contributed to the achievement of this work, here I present my sincere gratitude. However, I have to express special thanks:

- to Professor Álvaro Cunha for providing all the necessary resources for the development of the experimental work, for encouraging me to participate in important international conferences, for the final review of the text and, most important, for the total willingness to support, motivate and guide me throughout my academic career;
- to Professor Elsa Caetano for challenging me with interesting and rewarding projects, for sharing her experience and knowledge, for her important contributions on some of the experimental work and also for her example of commitment to achieve the best results in every project;
- to Professor Guido De Roeck and Doctor Edwin Reynders, from Katholieke Universiteit Leuven (Belgium), for receiving me at their group during one month, for their hospitality and for the generous insights they gave me in the area of system identification;
- to Professor James Brownjohn, from University of Sheffield (UK), for his invitation to participate in the dynamic tests of the Humber Bridge, and for the interesting discussions we had during all our meetings along the last years.
- to Doctors Gérard Grillaud and Olivier Flamand, from CSTB (France), for the opportunity to be involved in the processing of data collected during the dynamic tests of the Millau Viaduct and Grande Ravine Bridge.
- to Doctor Bart Peeters, from LMS, for his support on the use of the Test.Lab software and for all the stimulating conversations we had during the last years.
- to Professor Rune Brincker for sharing with me several interesting ideas during the preparation of a joint publication about the estimation of modal damping ratios.
- to Professor Adão da Fonseca and Engineer Renato Bastos for their support concerning the application at the Infante D. Henrique Bridge and also to Engineer Paulo Ferreira from Metro do Porto (owner of the bridge) for his interest in the monitoring project and for the provided assistance.
- to Engineers Carlos Quinaz (design team) and Luis Afonso (construction company) for their interest in the monitoring project started in the suspended roof of the Braga Stadium, as well as, to Engineers

Afonso Bastos, Amaral and Canedo from Câmara Municipal de Braga (owner of the Stadium) for all the supported provided during the installation of the monitoring equipment.

- to my work colleagues and friends Azenha, Carlos, Ferraz, Mário, Noites, Pedro, Raposo and Topa, partners during our fun and relaxed daily snacks, lunches and extra-work activities, for their fellowship essential to balance the moments of intense work.

- aos meus pais, à minha irmã e à Helena pelo apoio e afecto que alimentam o meu entusiasmo.

CONTENTS

1. INTRODUCTION.....19

1.1 RESEARCH CONTEXT19

1.2 OBJECTIVES AND MAIN CONTRIBUTIONS.....22

1.3 ORGANIZATION OF THE TEXT24

2. OPERATIONAL MODAL ANALYSIS.....29

2.1 INTRODUCTION TO OPERATIONAL MODAL ANALYSIS.....29

2.2 MODELS OF DYNAMIC SYSTEMS32

2.2.1 *Introduction*.....32

2.2.2 *Time Domain Models*33

 Finite Element Model.....33

 Continuous-Time State-Space Model33

 Discrete-Time State-Space Model.....36

 Introduction to Stochastic Processes38

 Stochastic State-Space Model39

2.2.3 *Frequency Domain Models*41

 Laplace, Fourier and z-Transforms41

 Transfer Function and Frequency Response Function43

 Laplace Transform of the State-Space Model.....45

 Modal Model.....46

 Common-Denominator Model47

 Left Matrix-Fraction Description48

 Right Matrix-Fraction Description49

 Output Spectrum and Half-Spectrum50

2.3 MODAL PARAMETERS IDENTIFICATION53

2.3.1 *Overview of OMA Methods*.....53

2.3.2 *Pre-Processing*.....56

 Reference outputs.....56

 Correlations56

 Spectra and Half Spectra57

2.3.3	<i>FDD and EFDD Methods</i>	59
	Alternative Implementation of the EFDD Method.....	62
	Numerical Simulations	62
2.3.4	<i>SSI-COV Method</i>	68
	Numerical Simulations	72
2.3.5	<i>p-LSCF Method</i>	76
	Numerical Simulations	83
2.4	AUTOMATED OPERATIONAL MODAL ANALYSIS	87
2.4.1	<i>Introduction</i>	87
2.4.2	<i>Automated FDD</i>	89
2.4.3	<i>Cluster Analysis for Automated OMA</i>	91
2.4.4	<i>Proposed Methodology for Automated OMA</i>	93
	Illustration with simulated data	96
2.5	MERGING STRATEGIES FOR MULTIPLE SETUP TESTS	98
2.5.1	<i>Introduction</i>	98
2.5.2	<i>Post Separate Estimation Re-scaling</i>	99
2.5.3	<i>Post Global Estimation Re-scaling</i>	101
2.5.4	<i>Pre Global Estimation Re-scaling</i>	102
2.5.5	<i>A Combined Methodology</i>	103
2.6	FINAL CONSIDERATIONS	105
3.	AMBIENT VIBRATION TESTS	109
3.1	INTRODUCTION	109
3.2	EXPERIMENTAL PROCEDURE AND EQUIPMENT	111
3.3	MILLAU VIADUCT	114
3.3.1	<i>Introduction</i>	114
3.3.2	<i>Bridge Description</i>	115
3.3.3	<i>Dynamic Tests</i>	116
3.3.4	<i>Preliminary Analysis</i>	117
3.3.5	<i>Modal Parameters Identification</i>	118
	p-LSCF, PoSER.....	119
	p-LSCF, PoGER.....	122
	p-LSCF, PreGER.....	126
3.3.6	<i>Conclusions</i>	128

3.4	HUMBER BRIDGE.....	130
3.4.1	<i>Introduction</i>	130
3.4.2	<i>Bridge Description</i>	131
3.4.3	<i>Ambient Vibration Test</i>	132
3.4.4	<i>Preliminary Analysis</i>	134
3.4.5	<i>Modal Parameters Identification</i>	137
	SSI-COV, PoGER.....	138
	p-LSCF, PoGER.....	142
	SSI-COV, Combined Procedure.....	145
3.4.6	<i>Conclusions</i>	147
3.5	DAMPING ESTIMATION WITH AMBIENT VIBRATION AND FREE VIBRATION TESTS.....	149
3.5.1	<i>Introduction</i>	149
3.5.2	<i>Free vibration tests: testing and processing procedures</i>	149
3.5.3	<i>Millau Viaduct</i>	151
3.5.4	<i>Vasco da Gama Cable-stayed Bridge</i>	154
3.5.5	<i>Pedro e Inês Footbridge</i>	155
3.5.6	<i>La Grande Ravine Bridge</i>	157
3.5.7	<i>Braga Stadium Suspended Roof</i>	160
3.5.8	<i>Conclusions</i>	163
4.	CONTINUOUS DYNAMIC MONITORING.....	167
4.1	INTRODUCTION.....	167
4.2	STRUCTURAL HEALTH MONITORING BASED ON MODAL PARAMETERS.....	170
4.3	REMOVING ENVIRONMENTAL AND OPERATION EFFECTS ON NATURAL FREQUENCIES.....	173
4.3.1	<i>Introduction</i>	173
4.3.2	<i>Input-Output methods</i>	174
	Multiple Linear Regression.....	174
	Multivariate Linear Regression.....	178
	Dynamic regression models.....	179
	The ARX model.....	179
4.3.3	<i>Output only methods</i>	180
	Principal Components Analysis.....	180
	Factor Analysis.....	183
4.3.4	<i>Control Charts</i>	186

4.3.5	<i>Conclusions</i>	189
4.4	A DYNAMIC MONITORING SOFTWARE – DYNAMO.....	191
5.	DYNAMIC MONITORING OF THE INFANTE D. HENRIQUE BRIDGE	199
5.1	INTRODUCTION	199
5.2	BRIDGE DESCRIPTION	200
5.3	PRELIMINARY EXPERIMENTAL AND NUMERICAL STUDIES	202
5.3.1	<i>Ambient Vibration Test</i>	202
5.3.2	<i>Numerical modelling</i>	205
5.4	MONITORING SYSTEM DESCRIPTION.....	208
5.5	MONITORING RESULTS	213
5.5.1	<i>Characterization of the measured signals</i>	213
5.5.2	<i>Automatic modal parameters identification</i>	216
Automated Frequency Domain Decomposition	216	
Automated Covariance driven Stochastic Subspace Identification	222	
Automated poly Least Squares Complex Frequency Domain	227	
5.5.3	<i>Analysis of the modal parameters variation</i>	230
5.6	REMOVING ENVIRONMENTAL AND OPERATIONAL EFFECTS ON NATURAL FREQUENCIES. 235	
5.7	DAMAGE DETECTION.....	244
5.8	CONCLUSIONS.....	250
6.	DYNAMIC MONITORING OF THE BRAGA STADIUM SUSPENDED ROOF	255
6.1	INTRODUCTION	255
6.2	DESCRIPTION OF THE STRUCTURE	256
6.3	PRELIMINARY EXPERIMENTAL AND NUMERICAL STUDIES	258
6.3.1	<i>Ambient Vibration Test</i>	258
6.3.2	<i>Numerical modelling</i>	259
6.4	MONITORING SYSTEM DESCRIPTION.....	261
6.5	MONITORING RESULTS	263
6.5.1	<i>Characterization of the measured signals</i>	263
6.5.2	<i>Automatic modal parameters identification</i>	265
Automated SSI-COV	266	
Automated p-LSCF	268	

6.5.3 *Analysis of the modal parameters variation*.....270

6.6 CONCLUSIONS273

7. CONCLUSIONS AND FUTURE RESEARCH277

7.1 CONCLUSIONS..... 277

7.2 FUTURE RESEARCH..... 281

8. REFERENCES285

Chapter 1

INTRODUCTION



1. INTRODUCTION

1.1 Research Context

Nowadays, the concern with the ageing and structural degradation of a large number of civil infrastructures, as reported for instance in (Federal Highway Administration 2008), together with the need to validate the behaviour of new structures with a high level of complexity (IABSE 2009) and the construction of very flexible structures more prone to the occurrence of excessive levels of vibration induced by different types of dynamic loads (wind, high speed railway traffic or pedestrians) have contributed to significantly increase the interest of designers, constructors and owners of important structures on dynamic tests and vibration-based health monitoring programs.

Dynamic tests permit the identification of natural frequencies, mode shapes and modal damping ratios of relevant modes of vibration and the characterization of the vibration amplitude associated with normal operation conditions or motivated by recreated load scenarios, as for instance controlled train passages or tests done in footbridges with crowds trained to walk with a predefined pacing rate. Figure 1.1 shows some examples: (i) a view from the top of one of the Humber Bridge towers during the performance of a dynamic test while the bridge was under normal operation (test described in section 3.4); (ii) the S. João Bridge, a railway bridge over the Douro river at Porto, tested during the passage of a train; (iii) one of the load scenarios (three pedestrians running) recreated during the dynamic tests of a cable-stayed footbridge (Magalhães et al. 2008b).



Figure 1.1 – Dynamic test of the Humber Bridge during normal operation, of the S. João Bridge (Porto, Portugal) during the passage of a train and of a cable-stayed footbridge (Viana do Castelo, Portugal) crossed by a group of three pedestrians.

In particular, the identification of modal properties is useful to check, and if necessary update, numerical models of new structures, to tune vibration control devices that might have been adopted, to evaluate the safety of structures in the context of inspection programs, to characterize existing structures before the development of rehabilitation projects or to obtain a baseline characterization of a new structure to be used in the future as reference to check the evolution of the corresponding dynamic

characteristics. As examples, Figure 1.2 shows the Luiz I Bridge (Porto, Portugal), where dynamic tests were performed before and after its recent rehabilitation (Cunha et al. 2006), and the Pedro e Inês Footbridge (Coimbra, Portugal), where extensive dynamic tests had to be done to tune the installed control devices (several Tune Mass Dampers control both vertical and lateral vibrations) (Caetano et al. 2010b).

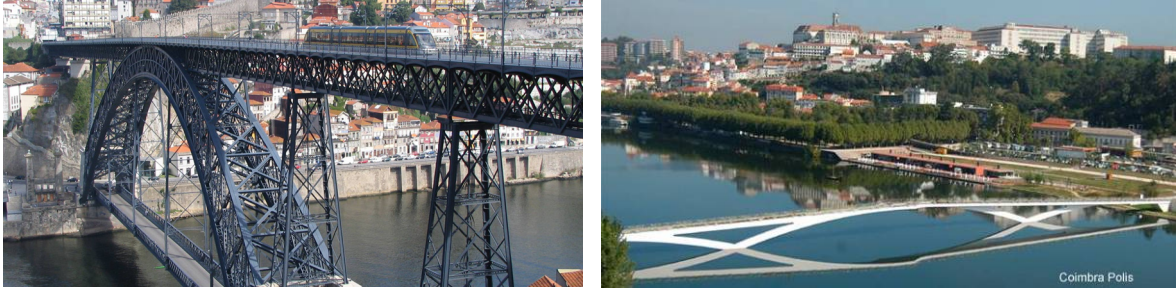


Figure 1.2 – Luiz I Bridge after rehabilitation and Pedro e Inês Footbridge.

The experimental identification of modal parameters (natural frequencies, mode shapes and modal damping ratios) can be based on the measurement of the response of the structure under analysis to different types of controlled excitations (e.g. impact produced by a hammer or vibrations induced by a shaker). These tests are called Forced Vibration Tests (FVT). However, as civil engineering structures are usually tested outside the laboratory, they are continuously excited by ambient forces, like wind or traffic circulating over or nearby the structure. Taking that into account, new techniques have been devised to perform the identification of modal parameters profiting from the structural dynamic response to ambient excitation. This type of dynamic test, designated Ambient Vibration Test (AVT), is quite simple, practical and economical, because it only consists of measuring the structural dynamic response, normally using accelerometers, while the structure is under normal operation.

Furthermore, as ambient excitation is always present, the techniques used to analyse data collected during ambient vibration tests can be applied to continuously process time series acquired by a permanent installation of a set of accelerometers. This permits to track the evolution of modal parameters over time. As the structural deterioration or the occurrence of damages due to some extreme event, like an earthquake, implies a stiffness reduction and consequently a decrease of the natural frequencies, an accurate characterization of the variation of natural frequencies over time can be adopted to detect structural problems. This is the core idea behind vibration-based health monitoring systems.

In both applications, dynamic tests and health monitoring systems, the most important operation is the accurate identification of modal parameters from measured structural responses. This is designated Operational Modal Analysis (OMA). OMA can be performed through the use of several alternative

algorithms, which have evolved significantly during the last decade. Despite the observed progress, some improvements have still to be done, especially to make data processing more straightforward by the reduction of the needed manual operations. The standard algorithms, already implemented in commercial software, still present several steps where some experienced judgment is needed to then manually select some parameters. On the one hand, this makes the processing of data collected during ambient vibration tests of large structures very cumbersome and time consuming. On the other hand, it precludes the use of OMA in the context of continuous monitoring programs, where all the data processing has to be automatic.

Particularly in the context of development of vibration-based health monitoring systems, there is a huge need of efficient and robust routines able to perform an online and automatic processing of large amounts of continuously collected data. The recent technological advances already permit the construction of very reliable, accurate and efficient monitoring equipment, which can be remotely configured and also permit an easy remote access to the acquired data. This encouraged the installation of dynamic monitoring systems on a considerable number of important civil infrastructures, as the examples presented in Figure 1.3 (Boller et al. 2009). However, this highly developed equipment has to be combined with processing routines able to timely convert large amounts of data into relevant information or ideally into an index suitable to provide an alert in case of detection of an abnormal structural behaviour.

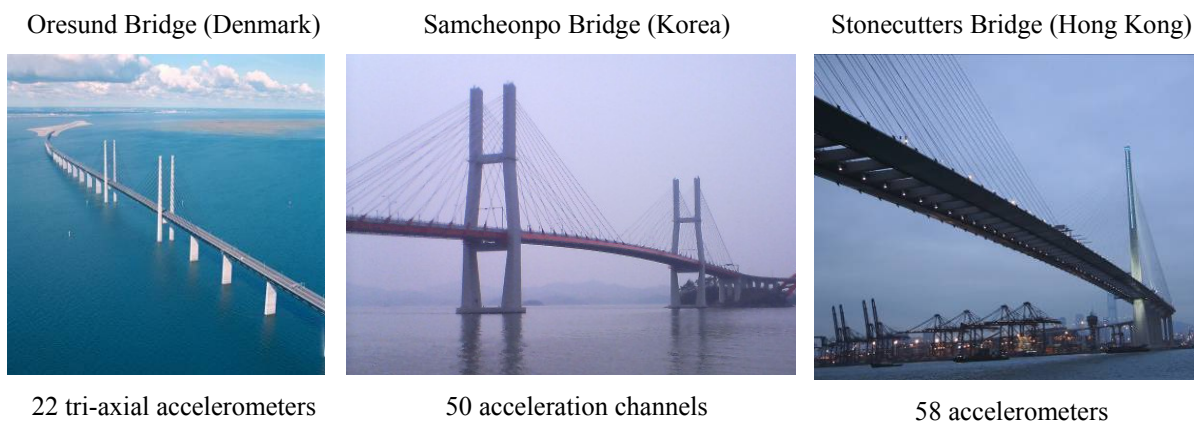


Figure 1.3 – Examples of bridges with dynamic monitoring systems.

The processing of data collected by dynamic monitoring systems with the aim of identifying structural deficiencies comprehends not only the automatic identification of modal parameters, but also the elimination of environmental and operational effects on natural frequencies. As the identification of very small structural changes is aimed to permit the detection of damages in an early phase of development, the minute effects of for instance the temperature or the traffic intensity over a bridge on the estimated natural frequencies have to be minimized. Therefore, monitoring software based on

OMA has to include three components: (i) automatic identification of modal parameters, (ii) elimination of environmental and operational effects on modal parameters, (iii) calculation of an index able to flag relevant frequency shifts. These steps are illustrated in Figure 1.4 using results from one of the monitoring applications that will be present in this thesis.

As important as the development of new processing tools is the performance of full-scale applications with the goal of testing and improving the algorithms and also to obtain practical evidences of their usefulness to definitely convince designers, constructors and owners of civil engineering structures about the relevance of dynamic testing and monitoring based on Operational Modal Analysis.

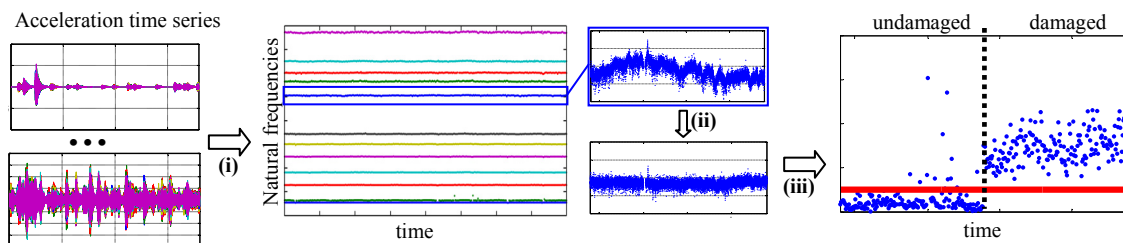


Figure 1.4 – Main processing steps of a vibration-based health monitoring system.

1.2 Objectives and main contributions

Taking into account the needs identified in the previous introduction, this thesis aimed the achievement of the following main objectives:

- development, implementation and validation of processing procedures to efficiently obtain accurate modal parameter estimates from data collected during ambient vibration tests of large civil engineering structures;
- development of routines and their integration in a software package to automatically extract useful information from data continuously collected by dynamic monitoring systems;
- conception and implementation of long-term dynamic monitoring programs in relevant civil engineering structures to test the implemented routines and demonstrate the usefulness of vibration-based health monitoring systems.

The development and improvement of algorithms to extract useful information from data collected during dynamic tests or by dynamic monitoring systems will certainly contribute to make the use of

these experimental tools more common and, as a consequence, to a better control, increase of safety and extension of lifetime of vital civil infrastructures.

More specifically, the main contributions of the present work are the following:

- evaluation of the effect of user-defined variables on the accuracy of modal parameter estimates provided by three state-of-the-art identification algorithms (Enhanced Frequency Domain Decomposition, Covariance driven Stochastic Subspace Identification and poly-Least Squares Complex Frequency Domain method) using numerical simulations (section 2.3);
- alternative implementation of the Enhanced Frequency Domain Decomposition method that permits the identification of more accurate modal damping ratios with shorter time series (section 2.3.3);
- development of a new algorithm to perform the automatic identification of modal parameters using parametric identification methods, which was tested together with the SSI-COV and p-LSCF methods (section 2.4.4);
- development of a new strategy to efficiently process data from multiple setups, which combines a first global processing of all the setups with an automatic individual processing of each setup (section 2.5.5);
- test of the developed and implemented routines in the analysis of databases collected during the ambient vibration tests of two outstanding structures: Millau Viaduct, in France, and Humber Bridge, in the United Kingdom (sections 3.3 and 3.4);
- comparison of modal damping ratio estimates provided by ambient vibration tests with the ones obtained from free vibration tests in five different structures (Millau Viaduct, Vasco da Gama Cable-stayed Bridge, Pedro e Inês Footbridge, La Grande Ravine Bridge and Braga Stadium suspended roof) with the goal of characterizing the accuracy that is possible to achieve in the estimation of damping with Operational Modal Analysis (section 3.5);
- synthesis of the theory behind the available methods to extract the influence of environmental and operational factors on modal parameters with the goal of obtaining indexes that permit an automatic identification of structural deficiencies (section 4.3);

- creation of a dynamic monitoring software package, called DynaMo, that combines tools to manage the acquired files and the processing outputs with algorithms to perform the online automatic identification of modal parameters, to eliminate the influence of environmental and operational factors and to construct control charts that permit the automatic detection of small structural anomalies (section 4.4);
- conception, assembly and operation for more than two years of a dynamic monitoring system on a long span arch bridge (Infante D. Henrique Bridge, Portugal), where all the features of the dynamic monitoring software (online identification of the modal parameters of 12 modes with three alternative identification algorithms, elimination of the effects of environmental and operational factors on the identified natural frequencies by multiple linear regression models and principal components analysis, and construction of control charts) were tested, and that permitted to prove the ability of the adopted methodology to detect small damages (numerically simulated) and the creation of a very complete database that can be used in the future to test alternative monitoring methodologies (chapter 5);
- conception, assembly and operation for more than 9 months of a dynamic monitoring system on the suspended roof of a stadium (Braga Stadium, Portugal), which was important to demonstrate that the routines for online automatic identification of modal parameters are adequate to be applied in a large variety of structures, as in this application they also provided a very detailed characterization of the variation of the modal parameters of 12 vibration modes (chapter 6).

1.3 Organization of the text

The relation between the seven chapters of this thesis is characterized in Figure 1.5. A description of the contents of each chapter is given in the following paragraphs.

Chapter 1 introduces the thesis with a contextualization of the developed research, followed by the presentation of the main objectives and major contributions of the work and by the present description of the organization of the text.

Chapter 2 starts with a review of the models of dynamic systems used by identification algorithms. Then, it is given an overview of the existent algorithms for operational modal analysis, followed by a

detailed description of three state-of-the-art identification techniques (Frequency Domain Decomposition – FDD, Covariance driven Stochastic Subspace Identification – SSI-COV and poly-Least Squares Complex Frequency Domain – p-LSCF) illustrated with some numerical simulations. Afterwards, it is explained a new methodology to perform an automated operational modal analysis, after a review of other available procedures. Finally, alternative strategies to process data belonging to different setups of the same ambient vibration test are presented.

Chapter 3 is essentially dedicated to the application of the algorithms presented in Chapter 2 in the analysis of data collected during the ambient vibration tests of two large structures: Millau Viaduct and Humber Bridge. These two applications are complemented by a synthesis of the results obtained in five structures where both ambient and free vibration tests were performed, which was important to characterize the level of accuracy that is possible to achieve in the estimation of modal damping ratios with ambient vibration tests.

Chapter 4 begins with an introduction to the main concepts associated with the continuous dynamic monitoring of civil infrastructures. Then, the theoretical background of the methods available to eliminate the effects of environmental and operational factors on natural frequencies are presented together with statistical tools that permit the automatic detection of abnormal changes on the evolution of the identified natural frequencies. The chapter ends with the description of the software package that was developed for dynamic monitoring.

Chapter 5 presents a complete description of the monitoring program implemented on the Infante D. Henrique Bridge. The application uses the algorithms for operational modal analysis detailed in Chapter 2 and the specific tools for dynamic monitoring presented in Chapter 4, providing therefore a very complete test of the created monitoring software.

Chapter 6 describes the dynamic monitoring program started on the suspended roof of the Braga Stadium. This is another application where it was possible to test the procedure for automatic identification of modal parameters using the SSI-COV and the p-LSCF methods.

Chapter 7 summarizes the conclusions of this thesis and points out some future research topics.

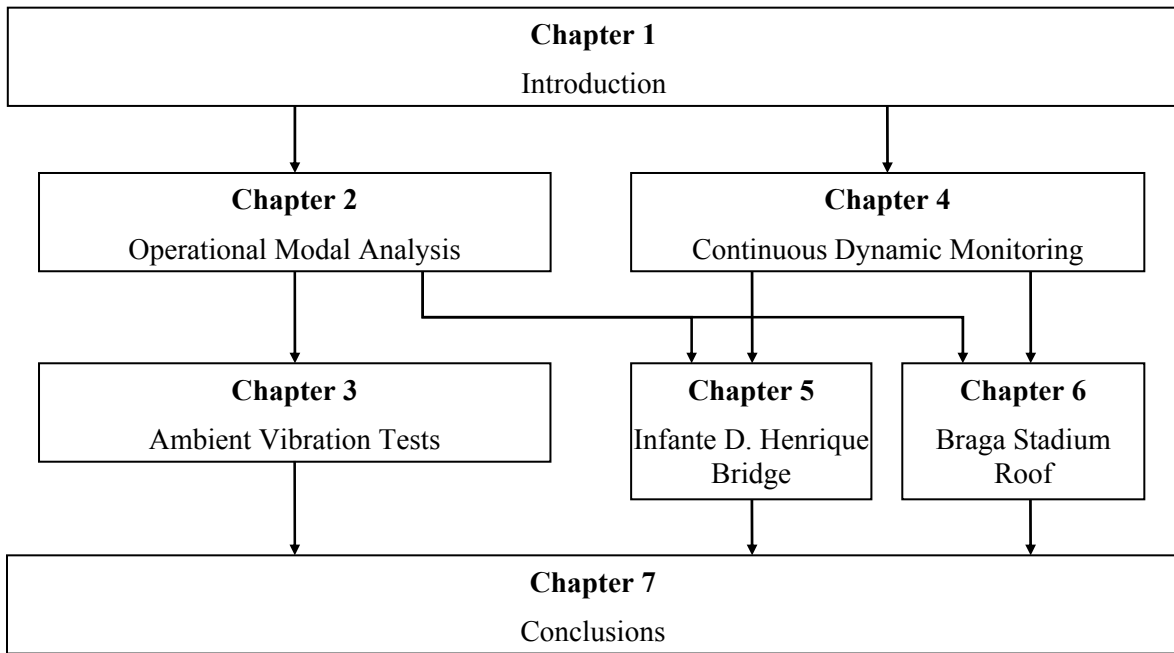
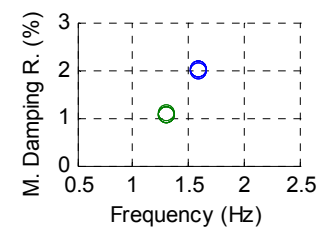
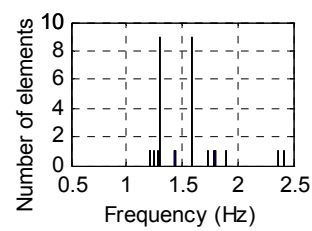
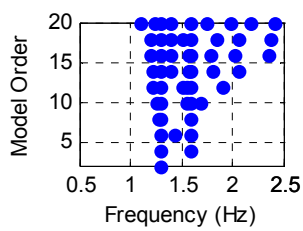
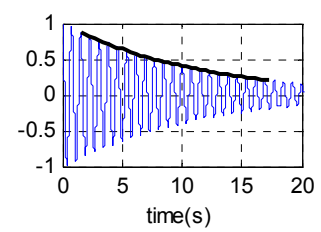
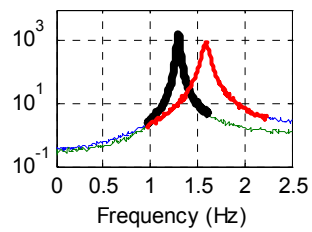
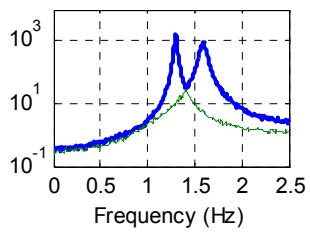


Figure 1.5 – Organization of the text.

Chapter 2

OPERATIONAL MODAL ANALYSIS



2. OPERATIONAL MODAL ANALYSIS

2.1 Introduction to Operational Modal Analysis

Experimental Identification of modal parameters is a research topic that has been developed during the last six decades. It started to be applied in mechanical engineering to characterize the dynamic behaviour of relatively small structures tested in a controlled environment, inside a laboratory. This first approach, nowadays called Experimental Modal Analysis (EMA), is based on the measurement of the structure response to one or several also measured dynamic forces. From the relation between the applied input and the observed output it is possible to identify the modal parameters. Since the first practical applications until now, the testing equipment and the algorithms for data processing have evolved significantly. Therefore, EMA is currently a well-established field founded on solid theoretical bases documented in reference books (Ewins 2000; Heylen et al. 2007; Maia and Silva 1997) and largely used in practice, for instance in the aerospace and automotive industries (several applications are documented in the proceedings of the International Modal Analysis Conference – IMAC, an annual conference organized since 1982).

EMA techniques can also be adopted for identification of modal parameters of civil engineering structures, like bridges, dams or buildings. Though, their large size imposes additional challenges. In particular, the application of a controlled and measurable dynamic excitation requires the use of very heavy and expensive devices. Despite the complicated logistics, these Forced Vibration Tests (FVT) have already been successfully performed either on massive dams (Figure 1.5) or on bridges (Figure 2.2) (Cunha and Caetano 2006).

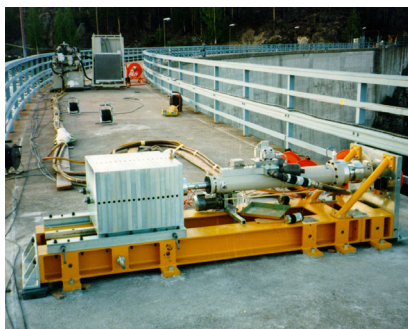


Figure 2.1 – Servo-hydraulic shaker used by EMPA (www.empa.ch) to excite a dam in horizontal direction.



Figure 2.2 – Shakers used in the Forced Vibration Tests of Tataro cable-stayed Bridge in Japan

However, in the case of civil engineering structures, Ambient Vibration Tests (AVT) are much more practical and economical, since the heavy shakers are replaced by freely available ambient forces, like the wind or the traffic circulating over or nearby the structure. As a consequence, AVT have the very

relevant advantage of permitting the dynamic assessment of important civil infrastructures, like bridges, without disturbing their normal operation. Furthermore, as structures are characterized using real operation conditions, in case of existence of non-linear behaviour, the obtained results are associated with realistic levels of vibration and not with artificially generated vibrations, as it is the case when forced vibration tests are used.

Nevertheless, as the level of excitation is low, very sensitive sensors with very low noise levels have to be used and even so, one should expect much lower signal to noise ratios than the ones observed in traditional tests. Besides this, AVT have two additional disadvantages when compared to FVT: the modal mass is not estimated (or the mode shapes are not scaled in an absolute way) and the frequency content of the excitation may not cover all the frequency band of interest, especially when very stiff structures with high natural frequencies are under analysis.

Since the first applications of this alternative testing procedure, many new powerful algorithms for modal parameter identification have been developed. Still, most of them are based on techniques previously established for EMA. As modal information is derived from structural responses (outputs) while the structure is in operation, this process is usually called Operational Modal Analysis (OMA) or Output-only Modal Analysis (in opposition to input-output modal analysis). Given that the knowledge of the input is replaced by the assumption that the input is a realization of a stochastic process (white noise), the determination of a model that fits the measured data is also named Stochastic System Identification.

Recently, combined modal testing techniques, called Operational Modal Analysis with eXogenous inputs (OMAX), have been explored. In this type of dynamic test an artificial force is used in operational conditions. The main difference between OMAX and EMA is that the operational forces are included in the identified system model instead of being assumed as noise. In this way, the amplitude of the applied artificial force can be of the same level or even lower than the always present ambient excitation. As a consequence, relatively small excitation devices can be adopted. The theoretical background of this approach as well as the details of its application to civil engineering structures are described in (Reynders 2009). The presented applications show that OMAX algorithms can be useful to process data collected in FVT using shakers (as the ambient vibration that cannot be avoided during the test is explicitly considered in the model) or to process data collected in footbridges where the ambient excitation was complemented by an artificial excitation produced by a small excitation device (e.g. impact hammer).

The present work is only focused on the use of Operational Modal Analysis. Therefore, in this chapter, after a brief characterization of the models of dynamic systems adopted by the identification methods, it is given an overview of the available OMA algorithms, followed by a detailed description of three of the most powerful and representative identification methods that are extensively used in civil engineering applications.

Then, it is highlighted the use of operational modal analysis in the framework of dynamic monitoring projects. In this context, the continuously measured data has to be processed automatically and so algorithms to perform an automatic operational modal analysis are needed. A new methodology for that purpose is presented after an overview of other available tools. The efficiency of the proposed methodology is then demonstrated on the basis of the continuous monitoring applications presented in chapters 5 and 6.

As ambient vibration tests are usually performed with a number of sensors that is inferior to the total number of points to be measured, several setups have to be considered. Thus, this chapter ends with the presentation of alternative techniques to process data collected in different setups. It is given special attention to procedures that are suitable to efficiently process a large number of setups, in particular taking profit from the previously presented tools for automatic modal analysis. These are then used in the applications presented in chapter 3.

2.2 Models of Dynamic Systems

2.2.1 Introduction

The identification of modal parameters is usually performed with the purpose of obtaining accurate experimental estimates of natural frequencies, mode shapes and modal damping ratios, which can then be correlated with the corresponding values numerically estimated from a finite element model of the structure under analysis.

On the other hand, the majority of modal identification methods are based on models, designated experimental models, of the tested dynamic system that are fitted to the recorded data and from which it is then possible to extract estimates of modal parameters. This section is devoted to the characterization of alternative experimental models and to the description of their relation with finite element models.

This subject has already been extensively explored in some reference books (Ewins 2000; Juang 1994). So, only the essential concepts needed for the understanding of the identification methods described in section 2.3 are presented here.

First of all, it is important to point out that models are always idealizations of real dynamic systems that necessarily contain simplifications. The ones adopted throughout this work assume linear and time-invariant behaviour of the described system.

Models of dynamic systems can be established either in time or frequency domain with continuous-time equations (analytical models) or discrete-time equations, being the latter the ones that are usually used to fit experimental data, which is always discrete. In the next section, the relationships between different model types are presented together with the procedures to calculate the modal parameters from their matrices. Emphasis will be given to models that consider an unknown or stochastic input, since these are the ones used for Operational Modal Analysis.

2.2.2 Time Domain Models

Finite Element Model

The analysis of a complex dynamic system imposes its previous discretization through the construction of a finite element model with a finite number of degrees of freedom (n_2). After this first step, the equilibrium of such system is expressed by the following differential equation expressed in matrix form:

$$M \cdot \ddot{q}(t) + C_1 \cdot \dot{q}(t) + K \cdot q(t) = p(t) = B_2 \cdot u(t) \quad (2.1)$$

where $M, C_1, K \in \mathbb{R}^{n_2 \times n_2}$ are the mass, damping and stiffness matrices; $\ddot{q}(t), \dot{q}(t), q(t)$ are time functions organized in column vectors that characterize the evolution of the acceleration, velocity and displacement of each degree of freedom (each dot over a time function denotes one derivation with respect to time) and $p(t)$ is a column vector with the forces applied to the system. As normally not all the degrees of freedom (*dof*) are excited, the load vector with n_2 lines can be replaced by a vector of inferior dimension ($n_i < n_2$) containing the time evolution of the n_i applied inputs. This vector, designated by $u(t)$, is multiplied by a matrix that maps the n_i inputs with the n_2 *dof* of the system: B_2 , a n_2 -by- n_i matrix composed by ones and zeros.

Continuous-Time State-Space Model

The previous second-order system of differential equations can be transformed into a first-order one using several alternative mathematical manipulations. One possibility is based on the use of the following definitions:

$$x(t) = \begin{bmatrix} q(t) \\ \dot{q}(t) \end{bmatrix} \quad (2.2)$$

$$A_C = \begin{bmatrix} 0 & I \\ -M^{-1} \cdot K & -M^{-1} \cdot C_1 \end{bmatrix}; \quad B_C = \begin{bmatrix} 0 \\ M^{-1} \cdot B_2 \end{bmatrix}$$

where 0 represents a matrix full of zeros and I is a n_2 -by- n_2 diagonal matrix with ones in the main diagonal (identity matrix).

The equilibrium equation (2.1) may then be transformed into the so-called state equation:

$$\dot{x}(t) = A_C \cdot x(t) + B_C \cdot u(t) \quad (2.3)$$

where A_C , designated state matrix, is a n -by- n matrix, with n equal to $2 \cdot n_2$ and $x(t)$ is the state vector, which contains the displacement and the velocity vectors of the dynamic system.

A state-space model is obtained by combining the state equation with the observation equation. The observation equation establishes the relation between a subset of n_o measured outputs organized in vector $y(t)$ and the displacement, velocity and acceleration associated with all *dof*:

$$y(t) = C_a \cdot \ddot{q}(t) + C_v \cdot \dot{q}(t) + C_d \cdot q(t) \quad (2.4)$$

C_a , C_v and C_d are n_o -by- n_2 matrices that select the *dof* of the finite element discretization that are measured by the adopted transducers: accelerometers, velocity or displacement sensors. Moreover, these matrices can be used to combine pairs of displacements in order to obtain strains, which can be measured on the prototype by strain gauges.

Solving equation (2.1) for $\ddot{q}(t)$, substituting into equation (2.4) and using the definitions:

$$\begin{aligned} C_C &= \begin{bmatrix} C_d - C_a \cdot M^{-1} \cdot K & C_v - C_a \cdot M^{-1} \cdot C_1 \end{bmatrix} \\ D_C &= \begin{bmatrix} C_a \cdot M^{-1} \cdot B_2 \end{bmatrix} \end{aligned} \quad (2.5)$$

a compact equation with the relation between the outputs $y(t)$ with the state vector $x(t)$ and the inputs $u(t)$ can be achieved:

$$y(t) = C_C \cdot x(t) + D_C \cdot u(t) \quad (2.6)$$

C_C is the output matrix and D_C is designated direct transmission matrix, as it directly relates the applied forces with the measured accelerations. If only displacements and velocities are measured, C_a is equal to zero and, as a consequence, there is no direct transmission (see equation (2.5)).

Finally, a continuous-time state-space model of order n (dimension of the A_C matrix) results from placing together equations (2.3) and (2.6):

$$\begin{aligned} \dot{x}(t) &= A_C \cdot x(t) + B_C \cdot u(t) \\ y(t) &= C_C \cdot x(t) + D_C \cdot u(t) \end{aligned} \quad (2.7)$$

Once the model has been constructed, the modal parameters of the dynamic system can be extracted from the state matrix A_C . In (Peeters 2000) it is demonstrated that the matrices with the eigenvalues and eigenvectors of A_C (A_C and Ψ , respectively) have the following structure:

$$\begin{aligned}
A_C &= \Psi \cdot A_C \cdot \Psi^{-1} \\
A_C &= \begin{bmatrix} \Lambda & 0 \\ 0 & \Lambda^* \end{bmatrix}, \quad \Psi = \begin{bmatrix} \Theta & \Theta^* \\ \Theta \cdot \Lambda & \Theta^* \cdot \Lambda^* \end{bmatrix} \\
\Lambda &= \begin{bmatrix} \ddots & & \\ & \lambda_k & \\ & & \ddots \end{bmatrix}, \quad \Theta = [\dots \ \varphi_k \ \dots] \quad k = 1, \dots, n_2
\end{aligned} \tag{2.8}$$

where \bullet^* means complex conjugate. The λ_k are related with the structure frequencies (ω_k - natural frequencies in rad/s) and modal damping ratios (ξ_k) by the expression:

$$\lambda_k = -\xi_k \cdot \omega_k + i \cdot \sqrt{1 - \xi_k^2} \cdot \omega_k \tag{2.9}$$

where $i = \sqrt{-1}$.

The mode shapes are represented in equation (2.8) by φ_k . However, as only a subset of the *dof* is measured, the observable modal components are given by:

$$\Phi = C_C \cdot \Psi \tag{2.10}$$

As one would expect, the number of modes (n_m) is equal to the dimension of the finite element model (n_2) from which the state-space model was derived and equal to one half of the dimension of the state-space model: $n_m = n/2$ (n , dimension of the state vector).

At this point, it is important to clarify that the relation between inputs and outputs of the dynamic system characterized by the state-space model presented in equation (2.7) is not unique. There exist an infinite number of state-space representations that produce the same input-output description (Juang 1994). An alternative model can be established by the application of a transformation to the state vector:

$$x(t) = T \cdot z(t) \tag{2.11}$$

where T is any non-singular square matrix. Introducing the previous relation in the state-space model equations, a new model is obtained:

$$\begin{aligned}
\dot{z}(t) &= T^{-1} \cdot A_C \cdot T \cdot z(t) + T^{-1} \cdot B_C \cdot u(t) \\
y(t) &= C_C \cdot T \cdot z(t) + D_C \cdot u(t)
\end{aligned} \tag{2.12}$$

This alternative model is characterized by the matrices: $T^{-1} \cdot A_C \cdot T$, $T^{-1} \cdot B_C$, $C_C \cdot T$ and D_C . Due to the transformation applied to the state vector, its physical meaning (structure displacements and velocities, as presented in equation (2.2)) is lost. Therefore, when a state-space model is identified from experimental data, it is one over an infinite number of models that can describe the same observed data, and thus, the components of the state vector of the identified model can not be associated with displacements or velocities of the tested structure.

If the inverse of the matrix that contains the eigenvectors of A_C is used as transformation matrix $T = \Psi$, one obtains the modal state-space form (subscript m):

$$\begin{aligned} \dot{x}_m(t) &= A_C \cdot x_m(t) + \Psi^{-1} \cdot B_C \cdot u(t) \\ y(t) &= C_C \cdot \Psi \cdot x_m(t) + D_C \cdot u(t) \end{aligned} \tag{2.13}$$

where A_C is a diagonal matrix whose elements are related with the natural frequencies and modal damping ratios of the structure (equations (2.8) and (2.9)), $C_C \cdot \Psi$ contains, as already mentioned, the observable modal components (equation (2.10)) and $\Psi^{-1} \cdot B_C$ contains the modal participation factors. This model is adequate to perform a model order reduction by considering only the contribution of selected modes (Peeters 2000).

Discrete-Time State-Space Model

In a dynamic test, the analog signals recorded by the transducers are converted to digital data by an analog to digital converter (A/D) so that, they can be stored and processed by a computer. Therefore, in practice, the available information of the dynamic system under study is discrete in time. Consequently, a discrete time version of the previously presented model is more adequate to fit experimental data.

A discrete-time state-space model is characterized by the following equations:

$$\begin{aligned} x_{k+1} &= A \cdot x_k + B \cdot u_k \\ y_k &= C \cdot x_k + D \cdot u_k \end{aligned} \tag{2.14}$$

The time functions $x(t)$, $y(t)$ and $u(t)$ are replaced by their values at discrete time instants $k \cdot \Delta t$, where k is an integer and Δt is the adopted sampling interval: $x_k = x(k \cdot \Delta t)$.

In (Juang 1994) it is demonstrated that, if it is assumed that the time functions are constant between consecutive discrete samples (zero-order-hold assumption, ZOH), the discrete-time model matrices are related with their continuous-time counterparts by the following expressions:

$$A = e^{A_C \cdot \Delta t} = I + A_C \cdot \Delta t + \frac{1}{2!} \cdot (A_C \cdot \Delta t)^2 + \frac{1}{3!} \cdot (A_C \cdot \Delta t)^3 + \dots$$

$$B = \int_0^{\Delta t} e^{A_C \cdot \tau} \cdot d\tau \cdot B_C = \left[I \cdot \Delta t + \frac{1}{2!} \cdot A_C \cdot (\Delta t)^2 + \frac{1}{3!} \cdot A_C^2 \cdot (\Delta t)^3 + \dots \right] \cdot B_C \quad (2.15)$$

$$C = C_C$$

$$D = D_C$$

The relation between the modal parameters of discrete and continuous-time state-space models is obtained by inserting the eigenvalue decomposition of the continuous-time state matrix into the first expression of equation (2.15):

$$A_C = \Psi \cdot \Lambda_C \cdot \Psi^{-1} \quad (2.16)$$

$$A = e^{A_C \cdot \Delta t} = e^{\Psi \cdot \Lambda_C \cdot \Psi^{-1} \cdot \Delta t} = \Psi \cdot e^{\Lambda_C \cdot \Delta t} \cdot \Psi^{-1} = \Psi \cdot \Lambda_D \cdot \Psi^{-1}$$

The third equality of the second expression is easily proven using the series expansion of the exponential function.

Thus, it is demonstrated that the eigenvectors of matrix A coincide with the ones of matrix A_C . The eigenvalues of the discrete model, designated by μ_k , are related with the ones of the continuous model λ_k by the following equation:

$$\mu_k = e^{\lambda_k \cdot \Delta t} \Leftrightarrow \lambda_k = \frac{\ln(\mu_k)}{\Delta t} \quad (2.17)$$

Consequently, it is proven that once a discrete-time state-space model has been identified from experimental data, it is possible to estimate the modal parameters of the tested structure. The natural frequencies and model damping ratios are obtained from the eigenvalues of A using equations (2.17) and (2.9). Taking into account that C is equal to C_C and that the eigenvectors of A coincide with the eigenvectors of A_C , the observable modal components are given by equation (2.10).

Discrete-time state-space models are also very convenient to simulate experimental data, which can then be used to test identification algorithms. This is done in section 2.3, in the numerical simulations used throughout the presentation of the identification algorithms.

Introduction to Stochastic Processes

The previously presented models assume that the input time functions are known or in other words, that the input is deterministic. However, in the context of operational modal analysis, the input is unknown and therefore it has to be represented by a stochastic process, which is also adequate to take into account the effects of the noise in the model.

A stochastic process is a set of n (with $n \rightarrow \infty$) time dependent random functions, designated by realizations, associated with the characterization of one or several variables (as for instance a set of excitation forces). Its characterization is based on statistical properties.

In practical applications, it is common to assume that stochastic processes are stationary, ergodic and zero mean. Stationarity means that the statistical properties of the process are constant over time. Ergodicity means that statistical properties can be calculated either considering average values over many realizations at a certain time instant, or using the average values of just one realization over time. The zero mean assumption is valid because measured time signals are commonly detrended before being processed.

In the framework of time domain models, the most relevant statistical property of the adopted stochastic processes is the correlation function. For a continuous time stochastic process $g(t)$ with n_g components, the correlation matrix is defined by the following expression:

$$R_{gg}(\tau) = \lim_{T \rightarrow \infty} \frac{1}{T} \int_{-T/2}^{+T/2} g(t) \cdot g(t + \tau)^T dt \quad (2.18)$$

where \bullet^T means transpose and $R_{gg}(\tau)$ is a n_g -by- n_g square matrix that is a function of the considered time lag (τ). The elements in the diagonal are designated auto-correlations and the others cross-correlations. If the signal is discrete and is only defined for $t \geq 0$, the integral is replaced by a summation:

$$R_{gg}(\tau) = E[g_k \cdot g_{k+\tau}^T] = \lim_{n_t \rightarrow \infty} \frac{1}{n_t} \cdot \sum_{k=0}^{n_t-1} g_k \cdot g_{k+\tau}^T \quad (2.19)$$

where $E[\bullet]$ is the expected value operator, which gives the average value of \bullet when the number of realizations of the stochastic process approaches infinite, and g_k is the value of $g(t)$ at the time instant $k \cdot \Delta t$. In real applications, an infinite number of samples is not available and thus, an estimate of the correlation is obtained by limiting the summation to a finite number of samples.

Similarly, the correlation matrix between two stochastic processes g and h can also be calculated with the expression:

$$R_{gh}(\tau) = E[g_k \cdot h_{k+\tau}^T] = \lim_{n_t \rightarrow \infty} \frac{1}{n_t} \cdot \sum_{k=0}^{n_t-1} g_k \cdot h_{k+\tau}^T \quad (2.20)$$

Correlation functions describe how a particular instantaneous observation depends upon previously occurring observations. They are even, real valued functions that go to zero as the time lag between observations (τ) becomes larger (both positively and negatively).

Due to the zero mean assumption, the covariance functions coincide with the correlation functions. Therefore, in signal processing, it is common to use indistinctively both terms: correlation and covariance.

Stochastic State-Space Model

Experimental data includes noise, which is not measurable, but that must be considered in the models. The stochastic state-space model is a better approximation of the real world that is obtained by adding a stochastic component to the previously presented discrete-time state-space model:

$$\begin{aligned} x_{k+1} &= A \cdot x_k + B \cdot u_k + w_k \\ y_k &= C \cdot x_k + D \cdot u_k + v_k \end{aligned} \quad (2.21)$$

where the vectors w_k and v_k model the noise due to disturbances and modelling inaccuracies, and the measurement noise due to sensor inaccuracy, respectively. Both vector signals with dimension n are assumed to be zero mean realizations of stochastic processes with the following correlation matrices:

$$\begin{aligned} E\left(\begin{bmatrix} w_p \\ v_p \end{bmatrix} \cdot \begin{bmatrix} w_p^T & v_p^T \end{bmatrix}\right) &= \begin{bmatrix} Q & S \\ S^T & R \end{bmatrix} \\ E\left(\begin{bmatrix} w_p \\ v_p \end{bmatrix} \cdot \begin{bmatrix} w_q^T & v_q^T \end{bmatrix}\right) &= 0, \quad p \neq q \end{aligned} \quad (2.22)$$

where the indexes p and q represent generic time instants. As the correlations matrices of the processes w_k and v_k , $E(w_p \cdot w_q^T)$ and $E(v_p \cdot v_q^T)$, are assumed to be equal to zero for any time delay $\tau = q - p$ different from zero, each new observation of these processes is independent from the previous ones. Such purely random stochastic processes are designated white noise processes.

In the context of Operational Modal Analysis, the system input is unknown. Therefore, the terms of the state-space model in u_k are included in the noise terms:

$$\begin{aligned} x_{k+1} &= A \cdot x_k + w_k \\ y_k &= C \cdot x_k + v_k \end{aligned} \tag{2.23}$$

This model assumes that the system inputs are also realizations of a white noise process. This is of course an approximation of the reality that has consequences on the results of the identification methods. These are discussed in section 2.3.

Stochastic state-space models present several properties that are essential for the justification of the identification algorithms presented later. These are described and proven in (Van Overschee and De Moor 1996), here only the more relevant aspects are referred.

These properties are based on the assumptions already mentioned for the noise terms, equation (2.22), and on the assumption that the state vector can be characterized by a stationary stochastic process with zero mean. Due to stationarity, the correlation matrix of the state vector, designated state covariance matrix and represented by Σ , is independent of the time instant k :

$$\Sigma = E[x_k \cdot x_k^T] \tag{2.24}$$

Since w_k and v_k are zero mean white noise vector sequences independent of x_k ,

$$E[x_k \cdot w_k^T] = 0 \quad , \quad E[x_k \cdot v_k^T] = 0 \tag{2.25}$$

Taking into account equations (2.23), (2.24) and (2.25), the following deduction can be made:

$$\begin{aligned} \Sigma &= E[x_{k+1} \cdot x_{k+1}^T] = E[(A \cdot x_k + w_k) \cdot (A \cdot x_k + w_k)^T] = \\ &= A \cdot E[x_k \cdot x_k^T] \cdot A^T + E[w_k \cdot w_k^T] \Leftrightarrow \\ \Sigma &= A \cdot \Sigma \cdot A^T + Q \end{aligned} \tag{2.26}$$

Given that the correlation matrix of the outputs for any arbitrary time lag $\tau = j \cdot \Delta t$ is calculated by the expression (in order to simplify the notation $R_{yy}(\tau = j \cdot \Delta t)$ is represented by R_j):

$$R_j = E[y_k \cdot y_{k+j}^T] \tag{2.27}$$

and that the “next state-output” correlation matrix is defined as:

$$G = E \left[x_{k+1} \cdot y_k^T \right] \quad (2.28)$$

it is possible to demonstrate, with mathematical manipulations similar to the ones presented in (2.26), the following properties:

$$\begin{aligned} R_0 &= C \cdot \Sigma \cdot C^T + R \\ G &= A \cdot \Sigma \cdot C^T + S \\ R_j &= C \cdot A^{j-1} \cdot G \\ R_{-j} &= G^T \cdot (A^{j-1})^T \cdot C^T = R_j^T \end{aligned} \quad (2.29)$$

As it is going to be shown in section 2.3, the third expression of the previous equation is crucial for the system identification methods based on state-space models, since it relates the correlation matrix of the measurable structural responses with the state-space matrix, from which it is possible to extract the modal parameters of the dynamic system.

2.2.3 Frequency Domain Models

This section starts with the description of the mathematical tools needed to make the transition from the time domain to the frequency domain. Then, the most relevant formulations to model dynamic systems in the frequency domain are detailed. Firstly, it is presented the modal model, which is the one that provides the best physical understanding from an engineering point of view, but that is not adequate to be directly fitted to experimental data, as it is highly non-linear. Afterwards, matrix fraction models are presented. These more abstract models that can be more easily fitted to the measured data are then used to obtain estimates of modal parameters. At the end, it is justified the extension of the presented models to dynamic systems with stochastic inputs.

Laplace, Fourier and z-Transforms

The Laplace or s-Transform of a function $f(t)$ is expressed as:

$$F(s) = \mathcal{L}[f(t)] = \int_0^{\infty} f(t) \cdot e^{-st} \cdot dt \quad (2.30)$$

The scalar s is a complex variable: $s = \sigma + i \cdot \omega$, where σ and ω are the real and complex parts of s . The adopted integral limits imply that $f(t)$ is not defined for negative values; this is always the case for data collected in experimental tests. The Laplace Transform has the ability of converting a derivative into a multiplication:

$$\mathfrak{L}[\dot{f}(t)] = -f(0) + s \cdot \mathfrak{L}[f(t)] \quad (2.31)$$

where $f(0)$ is the value of $f(t)$ at $t = 0$. This property is very convenient, as it enables the transformation of linear differential equations into algebraic equations.

The Fourier Transform equals the Laplace Transform restricted to the imaginary axis, also designated frequency axis: $F(\omega) = F(s)|_{s=i\omega}$. Thus, it is calculated by the expression:

$$F(\omega) = \mathfrak{F}[f(t)] = \int_0^{\infty} f(t) \cdot e^{-i\omega t} \cdot dt \quad (2.32)$$

The Fourier Transform can be interpreted as a generalization of the Fourier series, which expresses a periodic signal as the sum of an infinite number of harmonic signals, and in simple words it can be said that it characterizes the frequency content of the time signal.

Since experimental data is sampled at discrete times, it is convenient to develop a transform similar to the s-transform for discrete-time systems. Such discrete-time analogy is the z-transform, which is defined by the expression:

$$F(z) = \mathfrak{Z}[f(k \cdot \Delta t)] = \sum_{k=0}^{n_t-1} f_k \cdot z^{-k} \quad (2.33)$$

f_k is the value of function $f(t)$ evaluated at the time instant $k \cdot \Delta t$, where Δt is the sampling interval and k is an integer varying from 0 to $n_t - 1$. In (Juang 1994), it is shown that the z-transform coincides with the s-transform of a sampled time signal after setting $z = e^{s \cdot \Delta t}$.

Expressions in the z-domain for discrete-time system descriptions are similar to expressions in the Laplace domain for continuous-time system descriptions.

Finally, the Discrete Fourier Transform (DFT) coincides with the s-Transform of a sampled time signal restricted to the imaginary axis. This is expressed by the formula:

$$F(\omega_j) = \mathcal{F}_d[f(k \cdot \Delta t)] = \sum_{k=0}^{n_t-1} f_k \cdot e^{-i \cdot \omega_j \cdot k \cdot \Delta t} \quad (2.34)$$

As only a limited number (n_t) of values of the time function are available at time intervals of amplitude Δt , the DFT is only uniquely determined for discrete values of ω , $\omega_j = j \cdot 2 \cdot \pi / (n_t \cdot \Delta t)$, with j varying from 0 to $n_t/2$ (Maia and Silva 1997). The maximum frequency captured in this process, designated Nyquist frequency, is $\omega_j = \pi / \Delta t$, in rad/s, or $f_j = 1 / (2 \cdot \Delta t)$, in Hz. This means that when a signal is recorded with a sampling frequency $f_s = 1 / \Delta t$, only its frequency content between 0 and $f_s/2$ can be correctly characterized.

The DFT is usually calculated with a very efficient algorithm called Fast Fourier Transform (FFT) (Cooley and Tukey 1965).

Transfer Function and Frequency Response Function

The application of the Laplace transform to the second order differential equation of equilibrium (2.1), assuming zero initial conditions, leads to the following algebraic equation:

$$\begin{aligned} M \cdot s^2 \cdot Q(s) + C_1 \cdot s \cdot Q(s) + K \cdot Q(s) &= P(s) \\ [M \cdot s^2 + C_1 \cdot s + K] \cdot Q(s) &= P(s) \\ Z(s) \cdot Q(s) &= P(s) \end{aligned} \quad (2.35)$$

where $Z(s)$ is designated dynamic stiffness matrix.

Therefore, it is possible to relate the Laplace transform of the outputs $Q(s)$ with the Laplace transform of the inputs $P(s)$ through a matrix function called Transfer Function:

$$\begin{aligned} Q(s) &= H(s) \cdot P(s) \\ H(s) &= Z(s)^{-1} = [M \cdot s^2 + C_1 \cdot s + K]^{-1} \end{aligned} \quad (2.36)$$

Each element of the transfer function matrix is a complex valued function and therefore, it can be graphically represented by two surfaces defined in the Laplace or s-plane (x axis – σ ; y axis – $i\omega$): the real and the imaginary parts or the absolute value and the phase angle. Figure 2.3 shows the absolute value of the element (1,1) of the transfer function matrix of a dynamic system with two degrees of freedom, with the characteristics presented in section 2.3, Figure 2.10 (Model SM). At the observed

peaks, the amplitude of the transfer function is equal to infinite (the figure was constructed with a finite resolution and consequently the peaks present finite values). The values of s in which the elements of the transfer function matrix present infinite values are designated poles.

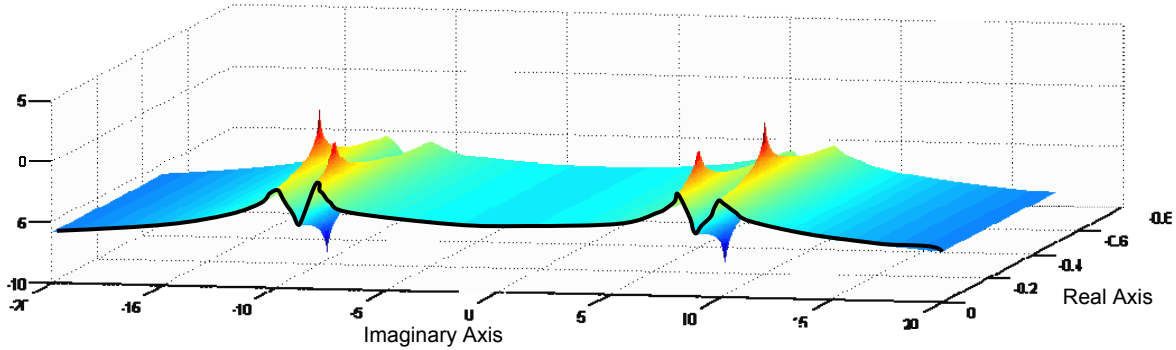


Figure 2.3 – Absolute value of the element (1,1) of the transfer function of a dynamic system with two degrees of freedom (vertical axis in logarithmic scale).

The poles, represented by λ_k , are complex numbers whose real and imaginary components are related with the natural frequencies and modal damping ratios of the dynamic system by equation:

$$\lambda_k = -\xi_k \cdot \omega_k + i \cdot \sqrt{1 - \xi_k^2} \cdot \omega_k$$

The real part depends on the natural frequency and on the modal damping ratio, whereas the imaginary part coincides with the damped natural frequency ($\sqrt{1 - \xi_k^2} \cdot \omega_k$), which is close to the natural frequency when damping is small. As it can be observed in Figure 2.3, the poles appear in complex conjugate pairs. Figure 2.4 represents the poles identified in the presented transfer function plot in a top view of the s -plane and defines the so-called unstable region, associated with poles with negative modal damping ratios. The expression for the poles coincides with the one presented for the eigenvalues of the continuous-time state space model (equation (2.9)).

Taking into account that in section 2.3.5 it is presented an identification algorithm in the z -domain, it is relevant to illustrate the relation between the geometric representation of the poles in the s and z -domains. Therefore, considering the relation $z = e^{s \cdot \Delta t}$, Figure 2.5 represents the same poles of Figure 2.4 in the z -domain (note: $e^{a+i \cdot b} = e^a \cdot e^{i \cdot b}$, where e^a is the absolute value of the complex number and b is its phase). In this domain the stable region is limited by the unit circle, whose equation is $z = e^{i \cdot \omega \cdot \Delta t}$.

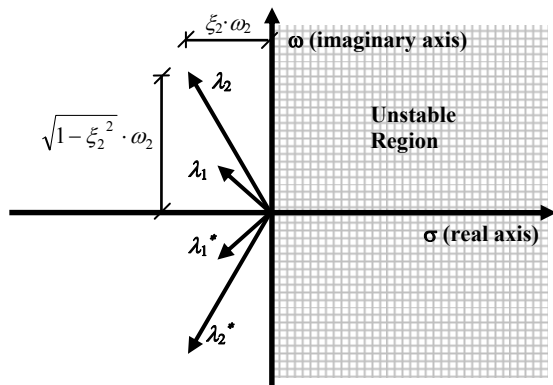


Figure 2.4 – Poles of a dynamic system with two modes represented in the s-plane.

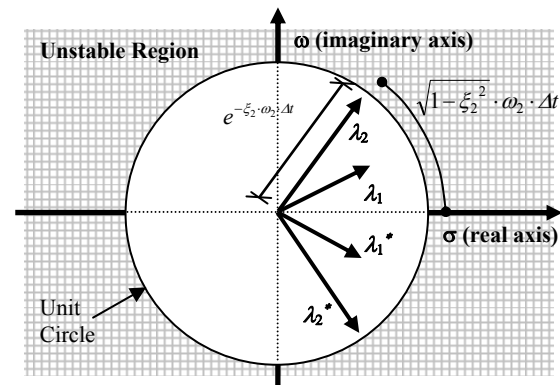


Figure 2.5 – Poles of a dynamic system with two modes represented in the z-plane.

The matrix of Frequency Response Functions (FRF) is composed by the cross sections of the elements of the transfer function matrix along the imaginary axis: $s = i \cdot \omega$. In the presented plot of the transfer function (Figure 2.3) the absolute value of the corresponding FRF element is marked with a black line. Consequently, the FRF is simply a particular case of the transfer function. However, in practice, it may replace the transfer function with no loss of useful information (Heylen et al. 2007). The FRF elements present peaks with finite amplitude (for damped structures) for ω equal to the system damped natural frequencies, with a bell shape that becomes sharper when the damping decreases.

Laplace Transform of the State-Space Model

The application of the s-transform to the continuous-time state-space model, equation (2.7), gives:

$$\begin{aligned} s \cdot X(s) &= A_C \cdot X(s) + B_C \cdot U(s) \\ Y(s) &= C_C \cdot X(s) + D_C \cdot U(s) \end{aligned} \quad (2.37)$$

where $X(s)$, $Y(s)$ and $U(s)$ are the s-transforms of the state vector, of the system outputs and of the system inputs, respectively. By eliminating the state vector, it is obtained a relation between the structure outputs and inputs that defines an alternative expression for the transfer function:

$$\begin{aligned} Y(s) &= [C_C \cdot (s \cdot I - A_C)^{-1} \cdot B_C + D_C] \cdot U(s) \\ H(s) &= [C_C \cdot (s \cdot I - A_C)^{-1} \cdot B_C + D_C] \end{aligned} \quad (2.38)$$

The transfer function presented in the previous equation is more general and at the same time more close to the experimental world than the transfer function derived from the finite element model (equation (2.36)). This one enables to relate a subset of outputs, containing displacements, velocities and accelerations, selected by the matrices C_a , C_v and C_d , with an excitation vector that may only

contain the elements that are not identically zero (selected by matrix B_2 , equation (2.1)), whereas the transfer function derived from the finite element model relates the displacements of all n_2 *dof* with the n_2 components of the applied forces. Thus, it corresponds to the particular case:

$$\begin{aligned} C_a &= 0 & ; & & C_d &= 0 & ; & & C_d &= I_{n_2 \times n_2} \\ B_2 &= I_{n_2 \times n_2} \end{aligned} \quad (2.39)$$

$I_{n_2 \times n_2}$ is a identity matrix n_2 -by- n_2 . In this case $C_C = [I_{n_2 \times n_2} \ 0]$ and $D_C = 0$ (equation (2.5)).

Modal Model

The transfer function, or equivalently the frequency response function (substituting s by $i\omega$), can be expressed by the sum of the contributions of the dynamic system modes (Heylen et al. 2007):

$$H(s) = V \cdot (s \cdot I - A)^{-1} \cdot L^T = \sum_{k=1}^{n_2} \frac{\varphi_k \cdot \gamma_k^T}{s - \lambda_k} + \frac{\varphi_k^* \cdot \gamma_k^H}{s - \lambda_k^*}$$

with

$$V = \begin{bmatrix} \varphi_1 & \dots & \varphi_{n_2} & \varphi_1^* & \dots & \varphi_{n_2}^* \end{bmatrix} \quad L = \begin{bmatrix} \gamma_1 & \dots & \gamma_{n_2} & \gamma_1^* & \dots & \gamma_{n_2}^* \end{bmatrix} \quad A = \begin{bmatrix} \lambda_1 & & & & & \\ & \ddots & & & & \\ & & \lambda_{n_2} & & & \\ & & & \lambda_1^* & & \\ & 0 & & & \ddots & \\ & & & & & \lambda_{n_2}^* \end{bmatrix} \quad (2.40)$$

where n_2 is the number of modes, \bullet^* is the complex conjugate of a matrix or vector, \bullet^H is the complex conjugate transpose of a matrix or vector, φ_k is a column vector containing the n_2 components of mode shape k , γ_k^T is a line vector with the n_2 components of the modal participation factor of mode k and λ_k , for $k = 1, \dots, n_2$, are the poles.

In the experimental field, the Frequency Response Function is more commonly used and its matrix is limited to a subset of inputs and outputs (or a subset of lines and columns of the complete matrix). Furthermore, the analysis is performed on a limited frequency band that only contains a subset of the structure modes. In this context, the FRF is defined by the expression (Heylen et al. 2007):

$$H(\omega) = \sum_{k=1}^{n_m} \frac{\phi_k \cdot l_k^T}{i \cdot \omega - \lambda_k} + \frac{\phi_k^* \cdot l_k^H}{i \cdot \omega - \lambda_k^*} + UR - \frac{LR}{\omega^2} \quad (2.41)$$

where n_m is the number of modes in the frequency band under analysis, ϕ_k is a column vector containing the n_o (number of measured outputs) observable components of mode shape k and l_k^T is a

line vector with n_i (number of inputs) components of the modal participation factor of mode k . UR and LR are n_o -by- n_i matrices that represent the influence of the modes below (Lower Residue) and above (Upper Residue) the frequency band under analysis. This effect is illustrated in Figure 2.6, which schematically presents the plot of the absolute value of one element of the FRF matrix of a structure with four modes and its modal decomposition. It can be observed that the mode below the frequency band under analysis has an influence that depends on the frequency (thicker blue line), whereas the mode above the selected frequency band has a residual influence that is approximately constant (thicker orange line). It is also evident that the expressions for the residuals are only valid if the modes are not close to the limits of the selected frequency band, therefore some care should be taken on the selection of those limits.

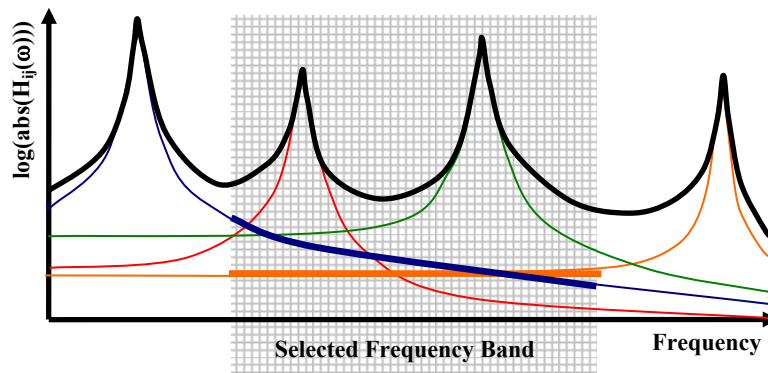


Figure 2.6 – Influence of the modes outside the frequency band under analysis.

Common-Denominator Model

The common-denominator model is inspired on the relation between the transfer function and the dynamic stiffness matrix and on the use of the Cramer's rule to calculate de inverse of $Z(s)$:

$$H(s) = Z(s)^{-1} = \frac{\text{adj}(Z(s))}{|Z(s)|} \quad (2.42)$$

where $|\bullet|$ means the determinant of \bullet , and $\text{adj}(\bullet)$ is the adjoint matrix of \bullet . Each element of the ajoint matrix $a(i,j)$ is equal to $(-1)^{i+j} \cdot |A_{ji}|$, where A_{ji} is the original matrix (\bullet) without line j and column i .

The equation of the denominator is designated characteristic equation, because its roots are the system poles, λ_k and λ_k^* in equation (2.40).

In order to obtain a transfer function that relates measured outputs with applied inputs, instead of displacements and forces of all the *dof* of a finite element model, the Cramer's rule can also be applied to the transfer function derived from the state-space model (equation (2.38)):

$$H(s) = \frac{C_C \cdot \text{adj}(s \cdot I - A_C) \cdot B_C + \det(s \cdot I - A_C) \cdot D_C}{\det(s \cdot I - A_C)} \quad (2.43)$$

Hence, the common-denominator model is generally expressed as:

$$H(s) = \frac{\begin{bmatrix} B_{1,1}^C(s) & \cdots & B_{1,N_i}^C(s) \\ \vdots & \ddots & \vdots \\ B_{N_o,1}^C(s) & \cdots & B_{N_o,N_i}^C(s) \end{bmatrix}}{a^C(s)} \quad (2.44)$$

$$a^C(s) = \sum_{r=0}^{p_a^C} a_r^C \cdot s^r$$

$$B^C(s) = \sum_{r=0}^{p_b^C} B_r^C \cdot s^r$$

where $B^C(s)$ is a n_o -by- n_i matrix with polynomials of order p_b^C and $a^C(s)$ is a scalar polynomial of order p_a^C (the subscript C is used to identify the model type: Common-denominator). Making the analogy between the model and the theoretical expressions of equations (2.42) and (2.43), it follows that the order of the denominator polynomial is equal to the number of roots of the characteristic equation and so equal to two times the number of modes ($2 \cdot n_m$), and that the order of the numerator polynomial matrix is also equal to $2 \cdot n_m$ when the outputs are accelerations (the direct transmission term D_C is different from zero) and equal to $2 \cdot n_m - 1$ when displacements and/or velocities are measured.

The identification algorithms based on common-denominators models face some problems in the estimation of mode shapes, especially when closely space modes are present (Cauberghe 2004). This justifies the use of the slightly more complex models that are presented next.

Left Matrix-Fraction Description

A very general polynomial model can be used to relate the system inputs and outputs:

$$\left[\sum_{r=0}^{p_a^L} A_r^L \cdot s^r \right] \cdot Y(s) = \left[\sum_{r=0}^{p_b^L} B_r^L \cdot s^r \right] \cdot U(s) \quad (2.45)$$

$$A^L \cdot Y(s) = B^L \cdot U(s)$$

The transfer function associated with the previous equation is:

$$H(s) = (A^L)^{-1} \cdot B^L$$

$$H(s) = \left[\sum_{r=0}^{p_a^L} A_r^L \cdot s^r \right]^{-1} \cdot \left[\sum_{r=0}^{p_b^L} B_r^L \cdot s^r \right] \quad (2.46)$$

This last equation defines the left matrix-fraction description (LMFD), which parameterizes the transfer function by the left division (A\B) of the polynomial matrix $B^L(s)$ by the polynomial matrix $A^L(s)$. The coefficients of the denominator polynomial A_r^L are n_o -by- n_o matrices, whereas the ones of the numerator polynomial B_r^L are n_o -by- n_i matrices. Bearing in mind the existence of a direct transmission term between inputs and outputs when accelerations are measured, it is natural to adopt, in this situation, the same order for the A and B polynomials ($p_a^L = p_b^L$). The poles of the system are the zeros of the characteristic equation, which is for this model equal to the determinant of the A^L matrix. This determinant is a polynomial with a degree equal to $p_a^L \cdot n_o$. Therefore, a left matrix-fraction model of order p_a^L represents a dynamic system with $p_a^L \cdot n_o / 2$ modes, since the poles appear in complex conjugate pairs.

Right Matrix-Fraction Description

As an alternative to the LMFD, the right matrix-fraction description (RMFD) can also be used to describe the relation between inputs and outputs of a dynamic system. This is based on the right division (B/A) of two polynomial matrices, which leads to this transfer function:

$$H(s) = B^R \cdot (A^R)^{-1}$$

$$H(s) = \left[\sum_{r=0}^{p_b^R} B_r^R \cdot s^r \right] \cdot \left[\sum_{r=0}^{p_a^R} A_r^R \cdot s^r \right]^{-1} \quad (2.47)$$

where the matrices B_r^R remain n_o -by- n_i and the matrices A_r^R are now n_i -by- n_i . Adopting the same justification that was presented for the LMFD, it is usually assumed that $p_a^R = p_b^R$.

Once the model matrices have been estimated, the natural frequencies and the modal damping ratios can be extracted from the coefficients of the denominator polynomial and the mode shapes determined from the coefficients of B . Instead, it is also possible to convert the estimated right matrix-fraction model (or with equivalent expressions the LMFD model) into a state-space model (equation (2.7)). The equations needed to make this transposition have been derived in (Reynders 2009), assuming $p_a^R = p_b^R = p^R$ and that the degree of the polynomial with the determinant of $A(s)$ is equal to $p^R \cdot n_i$. In order to simplify the notation, the subscript R is dropped:

$$\begin{aligned}
 A_C &= \begin{bmatrix} -A_p^{-1} \cdot A_{p-1} & -A_p^{-1} \cdot A_{p-2} & \dots & -A_p^{-1} \cdot A_1 & -A_p^{-1} \cdot A_0 \\ I & 0 & \dots & 0 & 0 \\ \vdots & \ddots & \dots & \vdots & \vdots \\ 0 & 0 & \dots & I & 0 \end{bmatrix} \\
 B_C &= \begin{bmatrix} A_p^{-1} \\ 0 \end{bmatrix} \\
 C_C &= \begin{bmatrix} B_{p-1} - B_p \cdot A_p^{-1} \cdot A_{p-1} & \dots & B_0 - B_p \cdot A_p^{-1} \cdot A_0 \end{bmatrix} \\
 D_C &= B_p \cdot A_p^{-1}
 \end{aligned} \tag{2.48}$$

After this step, the modal parameters can be estimated from the state-space model matrices, following the procedure presented in the previous sub-section. As the A_C matrix is a square matrix with dimension $p^R \cdot n_i$, the model represents a dynamic system with $p^R \cdot n_i / 2$ modes. Despite the similarity between the LMFD and RMFD models, it was the second one that was adopted in the frequency domain identification algorithm that has shown better performance for operational modal analysis. This is described in section 2.3.5.

Output Spectrum and Half-Spectrum

The previously presented models in the frequency domain assume a deterministic input. As already referred while describing the time domain models, during an ambient vibration test the input is not measured and therefore it must be idealized by a stochastic process.

In frequency domain, stochastic processes are characterized by their spectra. The spectrum of a stationary stochastic process $g(t)$ with n_g components is defined as the double-sided s-transform (between $+\infty$ and $-\infty$) of its correlation function $R_{gg}(t)$ (see definition in equation (2.18)):

$$S_{gg}(s) = \int_{-\infty}^{+\infty} R_{gg}(t) \cdot e^{-s \cdot t} \cdot dt \tag{2.49}$$

S_{gg} is a n_g -by- n_g matrix composed by auto or power spectra (elements in the diagonal) and cross spectra (the remaining elements). In case of discrete signals, the discrete-time spectrum is given by the Discrete Fourier Transform of the also discrete-time correlation function:

$$S_{gg}(\omega_j) = \sum_{k=-j_m}^{j_m} R_{gg}(k \cdot \Delta t) \cdot e^{-i \cdot \omega_j \cdot k \cdot \Delta t} \tag{2.50}$$

where $R_{gg}(k \cdot \Delta t)$ is evaluated for time lags varying between $-j_m \cdot \Delta t$ and $j_m \cdot \Delta t$ (maximum time lag of the correlation function).

In order to estimate the modal parameters of a dynamic system using only its output, it is of special relevance the output spectrum, which obviously depends on the input spectrum and on the characteristics of the dynamic system. If the inputs are assumed as white noise processes, their continuous-time correlation matrix function is given by:

$$R_{uu}(\tau) = R_{uu} \cdot \delta(\tau) \quad (2.51)$$

where R_{uu} is a n_i -by- n_i constant matrix and $\delta(\tau)$ is the Dirac delta function, which has the following properties:

$$\begin{aligned} \delta(\tau) &= \infty \text{ at } t = 0; \\ \delta(\tau) &= 0 \text{ elsewhere;} \\ \int_{-\infty}^{+\infty} f(t) \cdot \delta(t - a) \cdot dt &= f(a) \text{ for any function continuous at } a. \end{aligned} \quad (2.52)$$

This definition of white noise is equivalent to the definition given in the description of the discrete-time stochastic state-space model (equation (2.22)).

Consequently, due to properties of the $\delta(\tau)$ function, the input spectrum, or the Laplace transform of the input correlation, is a constant matrix:

$$S_{uu}(s) = \int_{-\infty}^{+\infty} R_{uu}(t) \cdot e^{-st} \cdot dt = R_{uu} \quad (2.53)$$

This implies that the spectrum is “flat”, which means that the energy of the input signals is uniformly distributed along the frequency axis.

The output spectrum S_{yy} , restricted to $s = i \cdot \omega$, is related with the input spectrum S_{uu} by the following equation (Ljung 1999):

$$S_{yy}(\omega) = H(\omega) \cdot S_{uu}(\omega) \cdot H^H(\omega) \quad (2.54)$$

In the particular case where the input is assumed to be a white noise, the output spectrum only depends on the system transfer function $H(\omega)$ and on a constant matrix:

$$S_{yy}(\omega) = H(\omega) \cdot R_{uu} \cdot H^H(\omega) \quad (2.55)$$

Taking into account the modal decomposition of the transfer function (equation (2.41)), it is also possible to express the output spectrum as a superposition of the contribution of the structure modes. Considering the contribution of all the system modes (n_2), the following equation is obtained (Peeters 2000):

$$S_{yy}(\omega) = \sum_{k=1}^{n_2} \frac{\phi_k \cdot g_k^T}{i \cdot \omega - \lambda_k} + \frac{\phi_k^* \cdot g_k^H}{i \cdot \omega - \lambda_k^*} + \frac{g_k \cdot \phi_k^T}{-i \cdot \omega - \lambda_k} + \frac{g_k^* \cdot \phi_k^H}{-i \cdot \omega - \lambda_k^*} \quad (2.56)$$

where the vectors g_k , called operational reference vectors, take the place of the modal participation factors. However, these vectors do not depend only on the characteristics of mode k . As it proven in (Peeters 2000), each g_k theoretically depends on all the structure modal parameters, on the input locations and on the input correlation matrix.

The modal decomposition of the output spectrum shows that this has four poles ($\lambda_k, -\lambda_k, \lambda_k^*$ and $-\lambda_k^*$) for each mode. This imposes the use of models with orders that are twice the modal order needed to model the transfer function of the same dynamic system. This disadvantage can be avoided by the use of the so-called Positive or Half-Spectrum. In practical applications, where only discrete time signals are available, this is calculated from the correlation matrix limiting the DFT to positive time lags:

$$S_{yy}^+(\omega_j) = \frac{R_{yy}(0)}{2} + \sum_{k=1}^{j_m} R_{yy}(k \cdot \Delta t) \cdot e^{-i \cdot \omega_j \cdot k \cdot \Delta t} \quad (2.57)$$

It is demonstrated, for instance in (Cauberghe 2004), that the modal decomposition of the half-spectrum is given by:

$$S_{yy}^+(\omega) = \sum_{k=1}^{n_2} \frac{\phi_k \cdot g_k^T}{i \cdot \omega - \lambda_k} + \frac{\phi_k^* \cdot g_k^H}{i \cdot \omega - \lambda_k^*} \quad (2.58)$$

As this equation has exactly the same structure as the modal decomposition of the transfer function, or of the frequency response function, all the previously described models can also be adopted to model half-spectrum matrices. Still, it cannot be forgotten that operational reference vectors unlike modal participation vectors do not have any specific physical meaning.

2.3 Modal Parameters Identification

2.3.1 Overview of OMA Methods

The methods available to perform the identification of modal parameters of dynamic systems based on their response to ambient excitation are usually classified as frequency domain or time domain methods.

Frequency domain methods start from output spectrum or half-spectrum matrices previously estimated from the measured outputs. These methods can be either non-parametric or parametric. The non-parametric frequency domain methods are simpler and therefore were the first ones to be used (MacLamore et al. 1971). Among these, the Peak-Picking method is the most well-known, being still widely applied nowadays in dynamic testing of civil engineering structures. It is the most adequate method to make a first check of the quality of collected data and get a first insight into the system dynamic properties.

The Peak-Picking method is a very simple and fast method that estimates the resonant frequencies by selecting the peaks of the auto-spectra of the measured outputs. The mode shapes are derived from the analysis of one row or column of the spectrum matrix, as it can be shown that, under the conditions of low damping and well separated modes, a single row or column of the spectrum matrix, evaluated near a natural frequency, can be considered as an estimate of the mode shape associated with that frequency (Bendat and Piersol 1980). The violation of these assumptions leads to the identification of operational deflection shapes that stem from the superposition of two or more closely spaced modes. However, particularly in the case of bridges, it is possible to pre-combine the collected signals, so that different types of modes (e.g. vertical bending and torsion) are analysed separately, avoiding or limiting the existence of closely spaced modes in each analysis (see chapter 3). The modal damping ratios can be estimated directly from the spectra using the half-power bandwidth method (Bendat and Piersol 1980), but this procedure is not very accurate. Felber (1993) refers several practical aspects related with the implementation of this method in the context of dynamic bridge testing.

The Frequency Domain Decomposition (FDD) is a slightly more sophisticated non-parametric frequency domain method that overcomes some of the limitations of the Peak-Picking method. This method is going to be described with some detail in section 2.3.3.

Alternatively, the identification in the frequency domain can be based on the fitting of a model to the output spectrum, from which modal parameters are extracted in a second phase. The models that can

be used for such purpose have already been succinctly described in the previous section (the modal model, the common-denominator model, the right and left matrix-fraction descriptions). The fitting of experimental data to a model is an optimization problem based on a cost function, which can be solved either through the linear least squares method or with the Maximum Likelihood (ML) estimator (Guillaume et al. 1999). All the possible combinations of these models and fitting procedures are explored in (Cauberghe 2004), together with a different class of methods (realization algorithms) that use frequency domain state-space models, designated stochastic frequency-domain subspace identification methods. Furthermore, in (Devriendt and Guillaume 2007), it is introduced an alternative frequency domain identification algorithm based on the concept of Transmissibility Functions. Still, it has to be said that most of the parametric frequency domain methods for operational modal analysis resulted from the transposition of algorithms previously developed for input-output modal analysis.

In the present work, only one frequency domain parametric method is described with detail: the poly-Least Squares Complex Frequency domain method (p-LSCF). This was selected because it is the most commonly used in civil engineering applications among this class of methods. This is due to its good performance, but also to its implementation on a commercial software package (Test.Lab from LMS) under the name PolyMax.

The similarity between the mathematical expressions of the transfer function and of the output spectrum of a system excited by white noise, presented in section 2.2.3, is in correspondence with the similarity, in the time domain, between the output correlations of a system excited by white noise and the impulse responses (Bendat and Piersol 1980). This was explored in the early ages of operational modal analysis based on time domain methods, in order to adapt the existing techniques for the analysis of impulse responses recorded in the context of forced vibration tests. For instance, the well known ERA (Eigensystem Realization Algorithm) method (Juang and Pappa 1985) was converted to an OMA method, the NExT, by James et al. (1992).

Nowadays, the available time domain methods for operational modal analysis, extensively explored in (Peeters 2000), are essentially based on two types of models: discrete-time stochastic state-space models and ARMA (Auto-Regressive Moving Average) or just AR (Auto-Regressive) models.

The formulations that use state-space models, designated stochastic subspace identification (SSI) methods, constitute the parametric approach that is more commonly adopted for civil engineering applications. The model can be identified either from correlations (or covariances) of the outputs: Covariance driven Stochastic Subspace Identification – SSI-COV; or directly from time series

collected at the tested structure by the use of projections (Van Overschee and De Moor 1996): Data driven Stochastic Subspace Identification – SSI-DATA. As reported in (Peeters 2000), these two methods are very closely related. Still, the SSI-COV has the advantage of being faster and based on simpler principles, whereas the SSI-DATA permits to obtain some further information with a convenient post-processing, as for instance, the decomposition of the measured response in modal contributions. In the present work, only the algorithm of the SSI-COV method is described.

On the other hand, methods based on ARMA or AR models, investigated for instance in (Andersen 1997), are not so frequently used by the civil engineers community. ARMA models can be for instance identified from the output correlations using the Instrumental Variable (IV) method (Peeters 2000). If the output correlations are substituted by impulse responses, the equations of this method coincide with the ones of a standard method for EMA: the Polyreference Time Domain (PTD) method. It is also possible to estimate ARMA or AR models directly from the output time signals using the least squares method. However, these approaches have not yet reached a level of robustness adequate for practical applications.

All the output-only modal identification methods assume that the ambient excitation, known to provide multiple inputs with wide band frequency content, is a zero mean white noise. As this assumption is not fully realistic, the true excitation can be considered as the output of a linear filter subjected to a white noise, which means that the identified modal parameters are not only associated with the tested structure but also with the imaginary system that produced the real excitation. Generally, in practice, it is possible to separate the modal parameters associated with the structural system from the others, since it is known that the vibration modes of civil engineering structures have usually low damping and smooth mode shapes with real components.

Considering the existence of a large number of alternative algorithms for OMA developed during the last decades, which are however based on just few basic principles, this work is only concentrated on the description of three methods with completely distinct theoretical backgrounds. Therefore, in the following sub-sections (2.3.3 to 2.3.5), it is presented the description of three methods that have also proven to provide good results in civil engineering applications: Frequency Domain Decomposition (FDD), Covariance driven Stochastic Subspace Identification (SSI-COV) and poly-Least Squares Complex Frequency Domain (p-LSCF).

The description of the methods is complemented by some parametric analyses based on simulated data, with the main goal of evaluating the quality of the estimates provided by each identification

technique and also to illustrate the influence of the parameters of the identification algorithms on their results, in order to define rules to help on the choice of the user-defined variables.

The next sub-section (2.3.2) is devoted to alternative procedures that can be used to obtain, from the measured raw time series, accurate estimates of both correlations and spectra, which are the starting point of the OMA algorithms.

In chapters 3, 5 and 6, the identification techniques presented herein are applied to data collected on full-scale dynamic tests of large structures and in the context of dynamic monitoring projects.

2.3.2 Pre-Processing

Reference outputs

The majority of output-only modal identification techniques start with the calculation of a matrix either with correlations or spectra. This can be a square matrix containing all the cross-correlations or spectra between all the measured outputs or a rectangular matrix which only contains some columns of the complete matrix. The measured signals associated with the selected columns are designated reference outputs. The reduction of the size of these matrices leads to algorithms that are faster and require less computer memory without losing accuracy, provided that the reference sensors are well chosen. A good selection of the reference sensors corresponds to the choice of the ones that present in average higher modal components for all the modes to be characterized by the experimental test.

In the context of ambient vibration testing of large structures with a limited number of sensors, it is current practice to cover the whole structure by performing several setups moving some sensors and keeping others in the same positions, so that the results from different setups can be linked. The *dof* measured during all setups are also designated reference outputs. These should also measure the response of *dof* that present in average higher modal components for all the modes to be characterized by the experimental test. In the data processing of each setup, both types of references may coincide or not. However, as the criterion for their selection is the same, the reference sensors adopted during the test are usually also adequate for the processing.

Correlations

The definition of the correlation function of a discrete signal has already been presented in equation (2.19). As during dynamic tests only a finite number of samples are collected, the summation cannot be extended until infinite. Therefore, we can only get an estimate of the correlation (\hat{R}).

The following formula already takes into account a previous selection of n_r reference outputs (y^{ref}):

$$\hat{R}_j^{ref} = \frac{1}{n_t - j} \cdot \sum_{k=0}^{n_t-j-1} y_k \cdot y_{k+j}^{ref T} \quad \text{with } j = 1, 2, \dots, j_m \quad (2.59)$$

where \hat{R}_j^{ref} is a n_o -by- n_r matrix, n_t represents the total number of collected samples and $j_m \cdot \Delta t$ is the maximum time lag of the correlation functions. Note also that, in order to simplify the notation, $R_{yy}(\tau = j \cdot \Delta t)$ is represented by R_j .

The calculation of the correlation matrix with direct application of the previous formula is very time consuming. However, it is possible to obtain the same results using of a high-speed FFT-based approach, described in (Oppenheim and Schaffer 1975) and implemented in the Signal Processing Toolbox of Matlab (MatLab 2000a).

Spectra and Half Spectra

The output spectrum matrix can be obtained following two classical alternative approaches for the estimation of the spectra between all outputs and the reference outputs: the periodogram and the correlogram.

The Periodogram approach, also known as Welch estimator (Welch 1967), calculates the spectra directly from the measured time series and involves the following steps. First, the response records are divided in n_b segments y_b with the same length (n_{tb}), which may present some percentage of overlap. Then, it is calculated the Discrete Fourier Transform (DFT) of each block after the application of a window w_k :

$$Y_b(\omega_j) = \sum_{k=0}^{n_{tb}-1} w_k \cdot y_{b,k} \cdot e^{-i \cdot \omega_j \cdot k \cdot \Delta t} \quad (2.60)$$

The window aims the minimization of leakage, an error expressed by the spreading of the true spectrum components along other neighbouring frequencies and motivated by the finite nature of the time segments (Maia and Silva 1997). Since the window reduces the contribution of the data at the beginning and end of each block, the adoption of some overlap between adjacent blocks is advisable. A Hanning window (Maia and Silva 1997) is very commonly used together with an overlap of 50%.

Afterwards, the estimate of the output spectrum matrix, a n_o -by- n_r matrix represented by $\hat{S}_{yy}^{ref}(\omega_j)$, is the average of the spectra associated with the several data blocks, given by $Y_b(\omega_j) \cdot Y_b^{ref}(\omega_j)^H$:

$$\hat{S}_{yy}^{ref}(\omega_j) = \frac{1}{n_b} \sum_{b=1}^{n_b} Y_b(\omega_j) \cdot Y_b^{ref}(\omega_j)^H \quad (2.61)$$

The selection of the length of each block and consequently the number of blocks is a trade-off between frequency resolution and irregularity of the spectra or, in other words, between bias and variance of the estimates. Selecting longer blocks increases the resolution and reduces the effect of leakage, but the number of averages is smaller and thus the uncertainty is higher.

The Correlogram approach uses the definition expressed by equation (2.50) and so calculates the output spectrum from the DFT of the output correlation matrix, which can be estimated with the previously referred very efficient algorithm. If the DFT is extended to the negative and positive time lags of the correlation function, as expressed in equation (2.50), a spectrum is obtained; if the DFT is restricted to the positive time lags, as expressed in equation (2.57), a half-spectrum is estimated. The evaluation of the DFT should be preceded by the application of a window to reduce the leakage. However, the application of this window influences the decay of the correlations and therefore has implications on the damping that is then estimated. Nevertheless, if an exponential window is used, the effect introduced by the window can be corrected later from the estimated modal damping ratios. Furthermore, this window also reduces the influence of noise in the tails of the correlations, where the correlation values are already very small. The exponential window is a symmetric function defined by the following equation:

$$w_k = e^{-\beta|k|\Delta t} \quad \text{with} \quad -j_m \leq k \leq j_m \quad (2.62)$$

where factor β defines the decay rate of the window (a higher β leads to the introduction of more artificial damping) and thus influences the value of the window associated with the maximum time lag of the correlation functions, j_m . The modal damping ratios estimated from the windowed correlations ($\xi_{estimated}$) are corrected by removing the artificial damping added by β :

$$\xi_{estimated} = \xi_{real} + \frac{\beta}{\omega} \quad (2.63)$$

Note that the added damping is inversely proportional to the frequency (ω). Therefore, the influence of the exponential window is more pronounced on the modes with lower natural frequencies.

2.3.3 FDD and EFDD Methods

The so called Frequency Domain Decomposition method (FDD) was presented by Brincker et al. (2000). However, the concepts behind the method had already been used in the analysis of structures subjected to ambient excitation by Prevosto (1982) and Corrêa et al. (1992), and on the identification of modal parameters from FRF (Shih et al. 1988). The method aims to be a simple and user-friendly technique, as the Peak-Picking, allowing at the same time the separation of closely spaced modes and the identification of modal damping ratios. It is a frequency domain non-parametric method that interprets output spectrum matrices previously calculated with the Welch method.

According to the modal decomposition of the transfer function, presented in equation (2.40), and taking into account the relationship between the output spectrum and the transfer function (equation (2.55)), the following matrix expression for the output spectrum is obtained:

$$S_{yy}(\omega) = V \cdot (i \cdot \omega \cdot I - \Lambda)^{-1} \cdot L^T \cdot R_{uu} \cdot L^* \cdot (i \cdot \omega \cdot I - \Lambda)^{-1*} \cdot V^H \quad (2.64)$$

If it is assumed that the inputs are not correlated (R_{uu} is a diagonal matrix) and that the mode shapes are orthogonal, and so the modal participation factors are also orthogonal, then the previous equation can be written as:

$$S_{yy}(\omega) = V \cdot C(\omega) \cdot V^H \quad (2.65)$$

where $C(\omega)$ is a diagonal matrix composed by functions of ω , each of them dependent on the natural frequency and modal damping ratio of only one mode of the structure, and V is a matrix whose columns represent the mode shapes. The same simplification can be done even if the inputs are correlated, but the modal inputs ($L^T \cdot u(t)$) are uncorrelated.

On the other hand, the singular value decomposition (SVD) of the complete output spectrum matrix (a square Hermitian matrix, $S = S^H$) estimated from the measured signals gives:

$$\hat{S}_{yy}(\omega_j) = U_j \cdot S_j \cdot U_j^H \quad (2.66)$$

where U_j is a orthonormal matrix ($U_j \cdot U_j^H = I$) that contains the singular vectors of $\hat{S}_{yy}(\omega_j)$ and S_j is a diagonal matrix holding the corresponding singular values.

The comparison between equations (2.65) and (2.66) shows that the singular vectors provided by the SVD can be associated with the mode shapes of the tested structure and that the singular values are

related with the ordinates of scalar spectra of single degree of freedom systems with the same modal parameters as the modes that contribute to the response of the multi degree of freedom system under analysis. The singular value decomposition provides the singular values in ascending order, which means that for each discrete value of ω , the first singular value contains an ordinate of the spectrum associated with the dominant mode at that frequency. The number of non-zero singular values represents the rank of the spectrum matrix at a specific frequency, or in other words, the number of modes with significant contribution to the system response at that particular frequency.

If the modes are well separated, the graphic of the first singular values as a function of ω (first singular value spectrum) presents peaks at all the natural frequencies and the values of the other singular values are negligible. The first singular vectors associated with the frequencies of the peaks are good estimates of the mode shapes. In the presence of two or more closely spaced modes, in the vicinity of their natural frequencies, there are two or more singular values with significant amplitudes. The mode shape of each mode is determined looking at the singular vectors associated with the peaks of the singular values with significant amplitudes.

If the structure is lightly damped, as it is the case of the majority of civil engineering structures, in the neighbourhood of the resonant frequencies, the modal decomposition of the output spectrum through its singular value decomposition is still approximately true even if there is some correlation between the inputs or the modal inputs, as it may occur if for instance the wind is the dominant excitation. However, the condition of orthogonality of the mode shapes has to be respected at least between closely spaced modes (Brincker et al. 2000).

The points belonging to the spectra associated with each mode can be selected by comparing the singular vectors associated with the points in the vicinity of an identified resonant frequency with the singular vector associated with the peak that represents that frequency. Once a set of points with similar singular vectors is selected for a given mode, this segment of an auto-spectrum may be converted to the time domain. An auto-correlation function with the contribution of a single mode is obtained. As the output correlation of a dynamic system excited by white noise is proportional to its impulse response, it is possible to estimate the modal damping ratio of the mode under analysis from the obtained correlation. This can be simply performed by fitting an exponential function to the relative maxima of the correlation function and extracting the modal damping ratio from the parameters of the fitted expression, taking into account the classical expression for the impulse response of a single degree of freedom (Clough and Penzien 1993):

$$y(t) = a \cdot e^{-\xi_k \cdot \omega_k \cdot t} \cdot \sin(\omega_k \cdot t) \quad (2.67)$$

where a is constant and ξ_k and ω_k are the damping ratio and the natural frequency in rad/s. Before the determination of the modal damping ratio, an enhanced estimate of the natural frequency may be obtained from the time intervals between zero crossings of the correlation function.

The selection of the points of the singular value spectra with similar singular vectors is usually performed establishing a limit for an index designated Modal Assurance Criterion (MAC), which measures the correlation between two mode shapes (ϕ_1 , ϕ_2) by the expression (Allemang and Brown 1982):

$$MAC_{\phi_1, \phi_2} = \frac{(\phi_1^T \cdot \phi_2)^2}{(\phi_1^T \cdot \phi_1) \cdot (\phi_2^T \cdot \phi_2)} \quad (2.68)$$

This index varies from 1, when the modes only differ on a scale factor, to zero, when the modes are orthogonal.

The above described procedure to estimate modal damping ratios was firstly detailed in (Brincker et al. 2001) under the name of Enhanced Frequency Domain Decomposition (EFDD) method.

However, the previously presented algorithm, used together with the Welch method to calculate the output spectrum matrix, produces circular correlations, which means that the calculated correlation is a superposition of the desired function and its mirror image, as represented in Figure 2.7 (Bendat and Piersol 1980). In order to avoid the circular error that introduces bias on the modal damping ratio estimates when short time segments are used, an alternative algorithm based on a procedure for the calculation of unbiased correlation functions described in references (Bendat and Piersol 1980; Brincker et al. 1992) was developed.

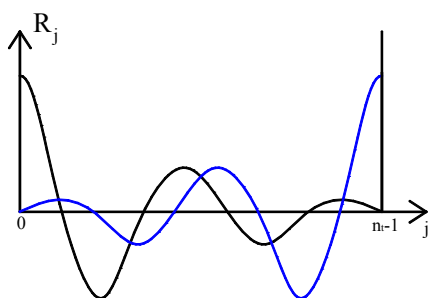


Figure 2.7 – Circular correlation.

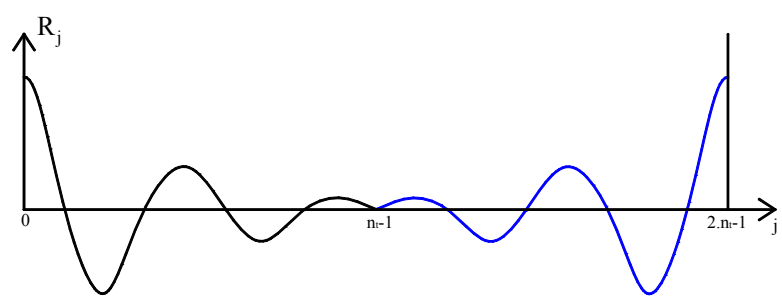


Figure 2.8 – Correlation calculated with the alternative procedure.

Other alternative implementation of the EFDD method are presented in (Rodrigues et al. 2004) and in (Jacobsen et al. 2008).

Alternative Implementation of the EFDD Method

This alternative implementation of the EFDD method comprehends the following steps: (i) selection of time segments from the measured signals without application of windows, (ii) doubling of the length of the time segments by adding zeros at the end (this operation produces a translation of the mirrored correlation from the position presented in Figure 2.7 to the position represented in Figure 2.8), (iii) calculation of auto-spectra and cross-spectra functions to construct the spectrum matrix, (iv) averaging of the spectra estimates to reduce random errors, (v) singular value decomposition of the spectrum matrix, (vi) selection of the singular values associated to a particular mode using the MAC (Modal Assurance Criterion) values, (vii) inverse FFT of the spectrum formed by the selected points and zeros at the remaining abscises, and finally, (viii) division of the resulting auto-correlation function by a triangular window ($w(t)=(T-t)/T$, where T is the length of the selected time series). The modal damping ratio of the mode under analysis is then estimated from the fitting of an exponential function to the relative maxima of the auto-correlation function. The steps after step (v) are repeated as many times as the number of modes to be identified. The algorithm of this improved version is illustrated in Figure 2.9 and it is tested with the following numerical simulations.

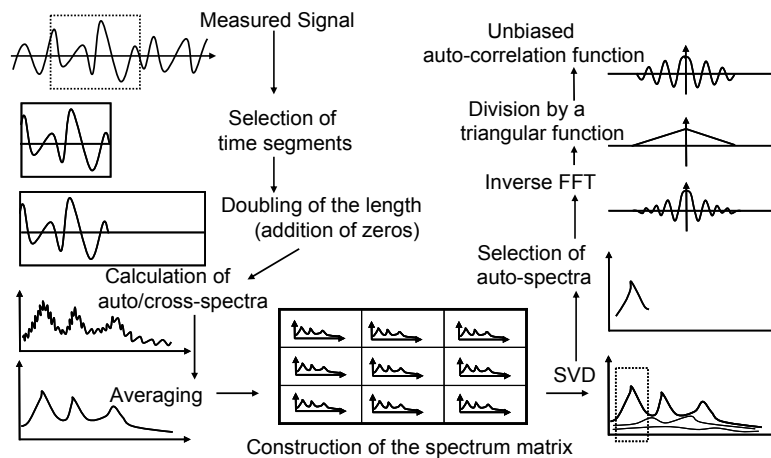


Figure 2.9 – Alternative implementation of the EFDD method

Numerical Simulations

The previously presented methodology for modal identification, as well as the others that will be described afterwards, are applied to data collected in full scale tests of civil engineering structures in chapter 3. In this chapter, the algorithms are explored using simulated data from two simple models (SM and CM) with two degrees of freedom, which are characterized in Figure 2.10 by the stiffness (K), mass (M) and damping (C_1) matrices and by the corresponding modal parameters: natural frequencies (f_i), modal damping ratios (ξ_i) and mode shapes (ϕ_i). The damping is viscous (damping

forces proportional to velocity) and proportional (the damping matrix is a linear combination of the stiffness and mass matrices). The system matrices were defined aiming to achieve modal parameters with values of the same order of magnitude of the ones usually found in current civil engineering structures. Model SM presents well-separated modes, whereas model CM presents closely spaced modes.

The broadband ambient excitation is replicated by time series with normally distributed random numbers assuming independent inputs for the two *dof* of the models. The relation between the artificially generated inputs and the system outputs is established following the methodology described by Juang (1994). This is based on a discrete-time state-space model constructed from the models matrices characterized in Figure 2.10 using the relations presented in equations (2.2), (2.5) and (2.15). Considering the values of the frequencies of the model (lower than 2.5Hz), it was adopted a sampling frequency of 5Hz. In order to study the bias and variance of the estimates provided by the identification algorithms, for each studied situation, 100 simulations were performed, which means that 100 different inputs and subsequent outputs were generated. The simulated outputs, which are time series with the accelerations of the two degrees of freedom of the models, were corrupted with noise that mimics the influence of the sensors and measuring chain noise. This was simulated by normally distributed random numbers with a standard deviation equal to 10% the standard deviation of the simulated outputs (this percentage of noise is quite conservative in case of well conducted ambient vibration tests).

Model SM (well separated modes)	Model CM (closely spaced modes)
$K = \begin{bmatrix} 100 & 0 \\ 0 & 100 \end{bmatrix} (kN/m)$	$K = \begin{bmatrix} 100 & 0 \\ 0 & 100 \end{bmatrix} (kN/m);$
$M = \begin{bmatrix} 1.25 & 0.25 \\ 0.25 & 1.25 \end{bmatrix} (ton)$	$M = \begin{bmatrix} 1.0125 & 0.0125 \\ 0.0125 & 1.0125 \end{bmatrix} (ton);$
$C_1 = \begin{bmatrix} 0.3275 & -0.0725 \\ -0.0725 & 0.3275 \end{bmatrix} (kN.s/m)$	$C_1 = \begin{bmatrix} 0.303 & -0.098 \\ -0.098 & 0.303 \end{bmatrix} (kN.s/m)$
$f_1 = 1.2995 \text{ Hz}; \quad \xi_1 = 1.041 \%$	$f_1 = 1.5720 \text{ Hz}; \quad \xi_1 = 1.012 \%$
$f_2 = 1.5915 \text{ Hz}; \quad \xi_2 = 2.000 \%$	$f_2 = 1.5915 \text{ Hz}; \quad \xi_2 = 2.005 \%$
$\phi_1 = \begin{bmatrix} 1 \\ 1 \end{bmatrix}; \quad \phi_2 = \begin{bmatrix} -1 \\ 1 \end{bmatrix}$	$\phi_1 = \begin{bmatrix} 1 \\ 1 \end{bmatrix}; \quad \phi_2 = \begin{bmatrix} -1 \\ 1 \end{bmatrix}$

Figure 2.10 – Characteristics of the simulated models

Firstly, the influence of the parameters of the identification algorithm in the quality of the estimated modal parameters is studied using model SM. In the case of the EFFD method, the parameters that have a stronger influence on the results are the number of points considered in the time segments used for the spectra calculation (Welch method) and the total duration of the collected signals. Therefore, this method was tested varying the total duration of the acceleration time series from 5 to 80 minutes and using five alternative time segments lengths that lead to spectra with frequency resolution between 0.039 and 0.0024Hz. Table 2.1 characterizes the 44 considered scenarios (named from 1a to 5i). Scenario 5a is not possible because the length of each time segment would be higher than the total time length (the sampling frequency is 5Hz, so 2048 points correspond to 409.6 s or 6.83 min > 5min).

Table 2.1 – Scenarios for the application of the EFDD method

Number of points of the time segments	Total time length (minutes)								
	5	10	20	30	40	50	60	70	80
128 (-●-)*	1a	1b	1c	1d	1e	1f	1g	1h	1i
256 (-x-)	2a	2b	2c	2d	2e	2f	2g	2h	2i
512 (-○-)	3a	3b	3c	3d	3e	3f	3g	3h	3i
1024 (-□-)	4a	4b	4c	4d	4e	4f	4g	4h	4i
2048 (-◇-)	-	5b	5c	5d	5e	5f	5g	5h	5i

* symbols used in the graphics of Figure 2.13

The large number of datasets to be analysed (44x100) forced the use of a procedure without any user interaction. In section 2.4 an automated version of the FDD method will be presented, here it is used a less robust procedure that is however adequate for this particular application. The two peaks of the singular value spectra are automatically selected and then the selection of the auto-spectra is based on the MAC relating the singular vectors (equivalent to the mode shapes) of the peaks with the ones of the points in their neighbourhood, the points with a MAC higher than 0.6 are selected. The fit of the exponential decay to the relative maxima of the auto-correlations is performed after the application of an interpolation algorithm (Matlab command – *spline*) to increase the resolution and consequently increase the accuracy on the identification of the relative maxima. In this example, only the relative maxima with amplitude lower than 90% and higher than 20% of the absolute maximum are used in the fitting. The application of this procedure to one of the simulated dataset is illustrated in Figure 2.11. Complementary identifications with small variations on the adopted parameters (MAC limit and bounds for the amplitude of the auto-correlation functions) proved that, in the processing of simulated data, they do not affect significantly the results.

Figure 2.12 presents the results obtained with the standard version of the EFDD method using the parameters defined in scenario 4i for 100 simulations. It shows that the variance of the modal damping

ratio estimates is much higher than the variance of the natural frequency estimates. Moreover, the analysis of the results obtained for all considered scenarios demonstrated that the estimates of the natural frequencies and mode shapes are always very close to their theoretical values. Therefore, the performance of the method is essentially conditioned by the quality of the modal damping estimates.

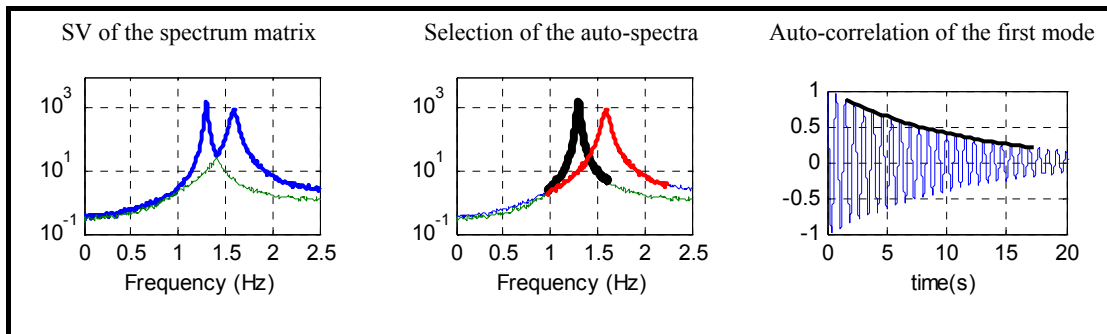


Figure 2.11 – Application of the EFDD method to one dataset of Model SM.

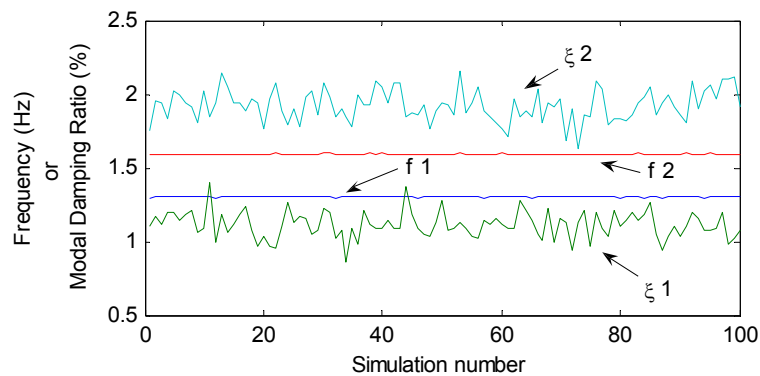


Figure 2.12 – Modal parameters of model SM estimated from the 100 simulations performed for scenario 4i.

Figure 2.13 characterizes the modal damping ratio estimates obtained with the standard algorithm of the EFDD method, representing the mean and the standard deviation values of the results obtained with the 100 simulations performed for all the scenarios characterized in Table 2.1.

It is clear that, if the number of points of the time segments is not well chosen, the estimates can present high bias (more than 100 %). In practice, it is possible to check if the damping estimate is likely to be biased looking at the estimated auto-correlation. If the estimated correlation does not contain some points after the vanishing of the decay, this indicates that the length of the estimated correlation is not long enough to characterize the full decay and thus, that damping is biased by errors introduced in the estimation of the spectra (Brincker et al. 2001). This is evidenced with the scheme presented in Figure 2.14 that shows the theoretical modal decay of the first mode and the limits of the auto-correlation functions calculated using the time segment lengths defined in Table 2.1. The first two vertical lines are clearly before the end of the decay, consequently the corresponding estimates are biased (-o- and -x- lines of the top left plot of Figure 2.13). The effect of the introduced errors can also be observed comparing, for instance, the auto-correlation estimated using time segments with 256

points (Figure 2.15) with its theoretical counterpart (Figure 2.14): the estimated decay vanishes just at the end of the estimated segment, approximately at 20 seconds, 30 seconds before the theoretical result.

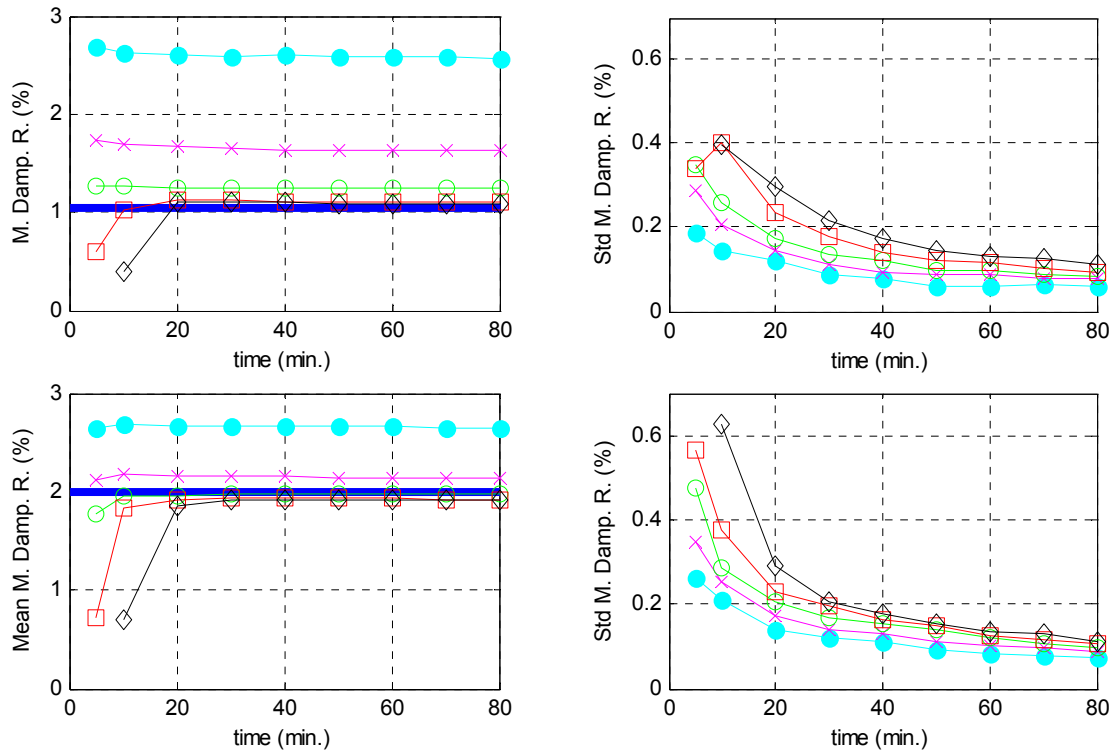


Figure 2.13 – Mean values and standard deviations of the estimates obtained with the standard algorithm of the EFDD method for the 2 modes of model SM using the parameters characterized in Table 2.1 (mode 1 at top, mode 2 at bottom theoretical values represented by a horizontal solid line, symbols of the lines defined in Table 2.1).

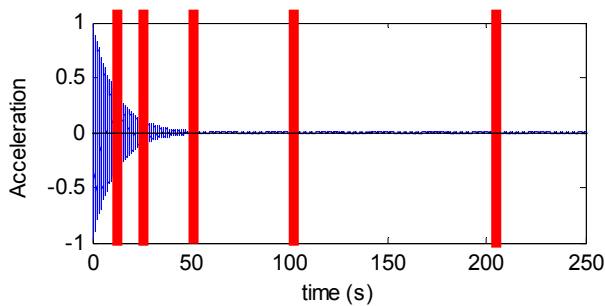


Figure 2.14 – Theoretical modal decay of the first mode and limits of the auto-correlation functions calculated using the time segment lengths defined in Table 2.1

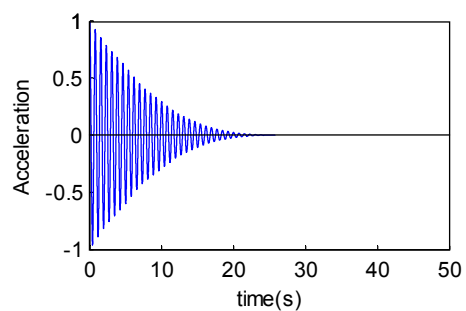


Figure 2.15 – Modal decay estimated using time segments with 256 points.

Therefore, the correct choice of the time segments length depends on the natural frequencies and modal damping ratios of the modes under analysis. Lower natural frequencies and higher modal damping ratios demand longer time segments (as also stems from the comparison of the bias of modes 1 and 2 estimates using 256 points).

The plots of Figure 2.13 also show that, for the model under analysis, the total time length should be longer than 20 minutes. Increasing it further, the number of performed averages increases and therefore, the standard deviation is reduced. However, it is relevant to observe that even using time series longer than one hour, the standard deviation is still quite high (around 0.1%), as is also evidenced by the scatter of the estimates presented at Figure 2.12. An additional set of simulations using the parameters of scenario 4i applied to 100 simulations of structural responses without the inclusion of noise showed that, even in this ideal case, the standard deviations kept values around 0.1% (relative standard deviation of about 10% for the 1st mode). Therefore, this uncertainty cannot be reduced increasing the number of averages or improving the quality of the signals.

Figure 2.16 presents the results obtained with the application of the alternative implementation of the EFDD method detailed in Figure 2.9. Only the mean values are presented because no significant differences were observed in the values of the standard deviations. It is clear that bias errors motivated by the use of short time segments are reduced or in some cases almost eliminated (results for mode 1 with 512 points and results for mode 2 with 128 and 256 points). Hence, the proposed alternative algorithm permits to improve the results when only short time series are available without increasing the computational effort.

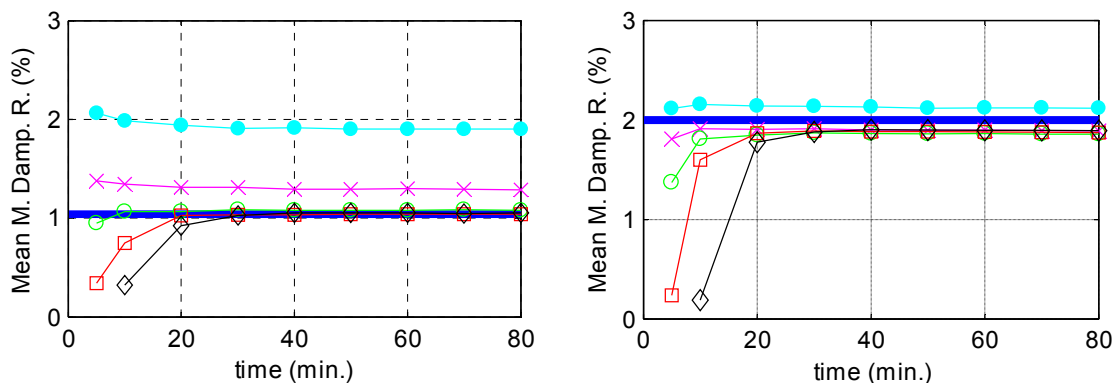


Figure 2.16 – Mean values of the estimates obtained with the alternative algorithm of the EFDD method for the 2 modes of model SM using the parameters characterized in Table 2.1 (mode 1 at the left, theoretical values represented by a horizontal solid line, symbols of the lines defined in Table 2.1).

In order to test the capability of this method to deal with closely spaced modes, model CM characterized in Figure 2.10 was used to generate 100 simulations that were then processed with the standard version of the EFDD method using the parameters of scenario 4c (see Table 2.1). Figure 2.17 illustrates the processing of one data set, showing the selection of the auto-spectra associated with the two closely spaced modes (black and red lines). Figure 2.18 compares the results obtained for the modal damping ratios of model CM with the ones previously obtained for model SM with the same parameters, representing the mean (x marks) and the standard deviation (amplitude of the error bars)

values associated with the 100 performed identifications. It can be concluded that the proximity of the natural frequencies does not affect significantly the results. However, it has to be noted that the simulations were performed considering independent inputs and assuming a proportional damping matrix. The existence of closely spaced modes with correlated modal inputs or non-diagonal modal damping matrices has a negative impact on the performance of this identification algorithm. The effect of non-proportional damping is studied in (Magalhães et al. 2009f), using numerical simulations based on the same model that was adopted herein.

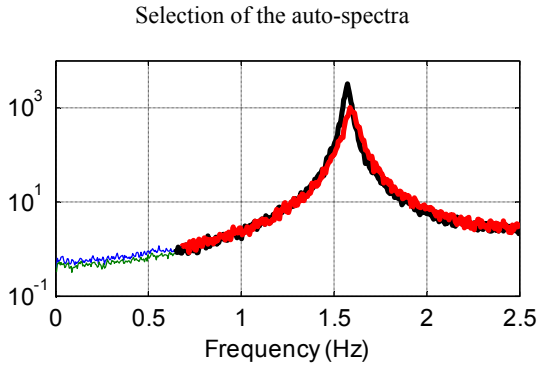


Figure 2.17 – Application of the EFDD method to one of the datasets simulated for model CM.

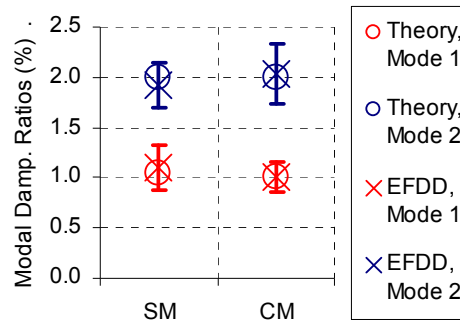


Figure 2.18 – Modal damping estimates for models SM and CM (scenario 4c).

2.3.4 SSI-COV Method

The Covariance driven Stochastic Subspace Identification method identifies a stochastic state-space model, equation (2.23), from the output covariance matrix (or correlation, as the mean of the signals is assumed to be zero). The algorithm described here is the version presented in (Peeters and De Roeck 2000), which only uses the columns of the correlation matrix associated with previously selected reference outputs (see section 2.3.2).

The starting point of this method is the output correlation matrix evaluated for positive time lags varying from $1 \cdot \Delta t$ to $(2 \cdot j_b - 1) \cdot \Delta t$ represented by R_1^{ref} to $R_{2 \cdot j_b - 1}^{ref}$ and organized in a $n_o \cdot j_b$ -by- $n_r \cdot j_b$ block Toeplitz matrix (n_o – number of outputs; n_r – number of reference outputs):

$$T_{1|j_b}^{ref} = \begin{bmatrix} R_{j_b}^{ref} & R_{j_b-1}^{ref} & \cdots & R_1^{ref} \\ R_{j_b+1}^{ref} & R_{j_b}^{ref} & \cdots & R_2^{ref} \\ \cdots & \cdots & \cdots & \cdots \\ R_{2 \cdot j_b - 1}^{ref} & R_{2 \cdot j_b - 2}^{ref} & \cdots & R_{j_b}^{ref} \end{bmatrix} \quad (2.69)$$

If the factorization property of the correlation matrix presented in equation (2.29)

$$R_j = C \cdot A^{j-1} \cdot G \quad (2.70)$$

is applied to all the R_j^{ref} matrices stored in the Toeplitz matrix, $T_{1|j_b}^{ref}$ can be decomposed in the product of the following matrices:

$$T_{1|j_b}^{ref} = \begin{bmatrix} C \\ C \cdot A \\ \dots \\ C \cdot A^{j_b-1} \end{bmatrix} \cdot \begin{bmatrix} A^{j_b-1} \cdot G^{ref} & \dots & A \cdot G^{ref} & G^{ref} \end{bmatrix} = O_{j_b} \cdot \Gamma_{j_b}^{ref} \quad (2.71)$$

The second equality defines the matrices: O_{j_b} - extended observability matrix; and $\Gamma_{j_b}^{ref}$ - reversed extended stochastic controllability matrix. The first one is a column of j_b blocks with dimensions n_o -by- n (n is the dimension of the state-space model). The second one is formed by j_b n -by- n_r matrices organized in a row. According to the previous equation, the Toeplitz matrix results from the product of a matrix with n columns by a matrix with n rows. Therefore, if $n < n_r \cdot j_b$, the rank of $T_{1|j_b}^{ref}$ is equal to n .

On the other hand, the singular value decomposition of the Toeplitz matrix yields:

$$T_{1|j_b}^{ref} = U \cdot S \cdot V^T = \begin{bmatrix} U_1 & U_2 \end{bmatrix} \cdot \begin{bmatrix} S_1 & 0 \\ 0 & 0 \end{bmatrix} \cdot \begin{bmatrix} V_1^T \\ V_2^T \end{bmatrix} = U_1 \cdot S_1 \cdot V_1^T \quad (2.72)$$

The number of non-zero singular values gives the rank of the decomposed matrix, which, in this case, coincides with n (assuming $n < n_r \cdot j_b$), the dimension of the state-space matrix A .

The comparison of equations (2.71) and (2.72) shows that the observability and the controllability matrices can be calculated from the outputs of the SVD using, for instance, the following partition of the singular values matrix:

$$\begin{aligned} O_{j_b} &= U_1 \cdot S_1^{1/2} \\ \Gamma_{j_b}^{ref} &= S_1^{1/2} \cdot V_1^T \end{aligned} \quad (2.73)$$

There are alternative implementations of the SSI-COV method that pre and/or post multiply the Toeplitz matrix by weighting matrices before the SVD. These weighting matrices determine the state-space basis in which the model is identified. More details can be found in (Van Overschee and De Moor 1996). In the present work, it was used an implementation without weighting matrices.

Taking into account the structure of the observability and controllability matrices presented in equation (2.71), once these have been obtained, the identification of the state-space model matrices A and C is quite straightforward. Matrix C can be extracted from the first n_o lines of the observability matrix. The most efficient and robust procedure to obtain matrix A is based on the shift structure of the observability matrix (Kung 1978). Thus, A is the solution of a least squares problem expressed by the following equation:

$$\begin{bmatrix} C \\ C \cdot A \\ \dots \\ C \cdot A^{j_b-2} \end{bmatrix} \cdot A = \begin{bmatrix} C \cdot A \\ C \cdot A^2 \\ \dots \\ C \cdot A^{j_b-1} \end{bmatrix} \Leftrightarrow A = \begin{bmatrix} C \\ C \cdot A \\ \dots \\ C \cdot A^{j_b-2} \end{bmatrix}^\dagger \cdot \begin{bmatrix} C \cdot A \\ C \cdot A^2 \\ \dots \\ C \cdot A^{j_b-1} \end{bmatrix} = O_{j_b}^{to \dagger} \cdot O_{j_b}^{bo} \quad (2.74)$$

where $O_{j_b}^{to}$ contains the first $n_o \cdot (j_b - 1)$ lines of O_{j_b} and $O_{j_b}^{bo}$ contains the last $n_o \cdot (j_b - 1)$ lines of O_{j_b} . The symbol \bullet^\dagger represents the Moore-Penrose pseudo-inverse of a matrix, which is used to solve least squares problems (minimizes the sum of the squared errors of the individual equations of an overdetermined system of equations) and that can be calculated, for instance, with the expression: $A^\dagger = (A^T \cdot A)^{-1} \cdot A^T$. Still, there are mathematical algorithms to calculate it in a more efficient way (MatLab 2000b).

At this point, a state-space model that can represent the dynamics of the system under analysis has already been obtained. Please note that, as stressed in section 2.2.2, this solution is not unique.

As already referred in the presentation of the state-space models (section 2.2.2), the modal parameters can be easily extracted from matrices A and C . First, the eigenvalues of A (μ_k), which are the poles of the discrete-time state-space model, have to be related by equation (2.17) with the poles of the continuous-time model (λ_k , equations (2.8) and (2.9)). Then, the poles with a positive imaginary component are used to obtain natural frequencies (f_k , in Hz) and modal damping ratios (ξ_k):

$$\begin{aligned} \lambda_k &= \frac{\ln(\mu_k)}{\Delta t} \\ f_k &= \frac{\text{Abs}(\lambda_k)}{2 \cdot \pi} \\ \xi_k &= -\frac{\text{Re}(\lambda_k)}{\text{Abs}(\lambda_k)} \end{aligned} \quad (2.75)$$

Abs(\bullet) and Re(\bullet) are the absolute value and the real part of the complex number \bullet .

The multiplication of matrix C by the matrix with the eigenvectors of A gives a n_o -by- n matrix, which contains in its columns the observable components of the mode shapes. Due to the existence of complex conjugate pairs, only the columns associated with eigenvalues with positive imaginary components are selected. In this way, a state-space model of order n provides modal parameters for $n/2$ modes.

In the context of practical applications, the method is based on estimates of the output correlation matrices, which are calculated from a limited number of samples. In addition to this, the tested structure may not have a perfect linear behaviour (modelling inaccuracies) and the collected signals are always contaminated by noise. Therefore, the derived state-space model matrices and the obtained modal parameters have to be considered also as estimates. Furthermore, the SVD of the Toeplitz matrix does not permit the identification of the model order, because the higher singular values that theoretically should be zero in practice present residual values. Current practice showed that using data collected in large structures, it is even not possible to identify any gap between consecutive singular values that would at least permit to obtain a reasonable estimate of the most adequate model order.

As a result, the most appropriate way to overcome this difficulty is to estimate models with orders within an interval previously fixed in a conservative way (the upper limit should be much higher than two times the number of physical modes of the system within the frequency range under analysis) and then, select the best model by the analysis of the corresponding modal parameters.

This can be accomplished in an efficient way, because the SVD of the Toeplitz matrix, which is the most demanding calculation, has only to be performed once. As long as, the maximum model order, n_x , is defined, a Toeplitz matrix with at least n_x/n_r blocks has to be constructed. Then, the SVD of the complete Toeplitz matrix is calculated. Models with successively decreasing orders are estimated by selecting a successively decreasing number of singular values and vectors for the calculation of the observability and controllability matrices.

However, the use of high model orders leads to the introduction of numerical modes (also called spurious or noise modes), which have little to none physical relevance but are needed to model the noise and to overcome the modelling inaccuracies.

Separation of physical and spurious modes is then a crucial step of the identification algorithm. The most popular approach to achieve that is based on the creation of stabilization diagrams. In these diagrams the modal parameter estimates provided by all the models are represented together (x axis – natural frequency of the mode estimates; y axis – order of the model), allowing the identification of the modal parameters that are stable for models of increasing orders. Modes that appear in most of these models with consistent frequency, mode shape and damping are classified as stable and are

likely to be physical. Modes that only appear in some models are considered spurious. Examples of such diagrams are presented in Figure 2.19.

The quality of the stabilization diagrams (better quality means clearer alignments of stable poles), depends on the values of the parameters of the algorithm, on the signal to noise ratio of the time series under analysis and also on the adequacy of the state-space model to represent the tested structure.

Recently, a methodology that permits the estimation of the variance of modal parameters identified with the SSI-COV method has been developed (Reynders et al. 2008a). This is based on the study of the propagation of the uncertain observed on the estimated correlation matrices to the modal parameters. Therefore, the estimated variances only reflect the influence of the factors observed during the data collection period and, as a consequence, the obtained confidence intervals of the modal parameters are associated with the very particular conditions (temperature, vibration intensity,...) observed during that relatively small period. Practical applications show that these can present significant variations during a dynamic test composed by several setups (Reynders et al. 2008a). Still, the obtained variances can be used as an additional criterion in the selection of stable poles (numerical poles are expected to present higher variances) and as measure of the quality of the modal parameters identified for each mode.

Numerical Simulations

The numerical simulations of model SM used to test the FDD method were also adopted to explore the SSI-COV identification algorithm. Therefore, the same outputs generated with a sampling frequency of 5Hz and afterward corrupted with 10% of noise were processed by this method.

In the case of the SSI-COV method, the parameter with a more relevant influence on the results is the number of blocks that compose the Toeplitz matrix used in the identification, j_b in equation (2.69). Therefore, 45 scenarios were considered by the combination of five different values for this parameter and the same nine total time length values adopted in the study of the EFDD method. These are characterized in Table 2.2.

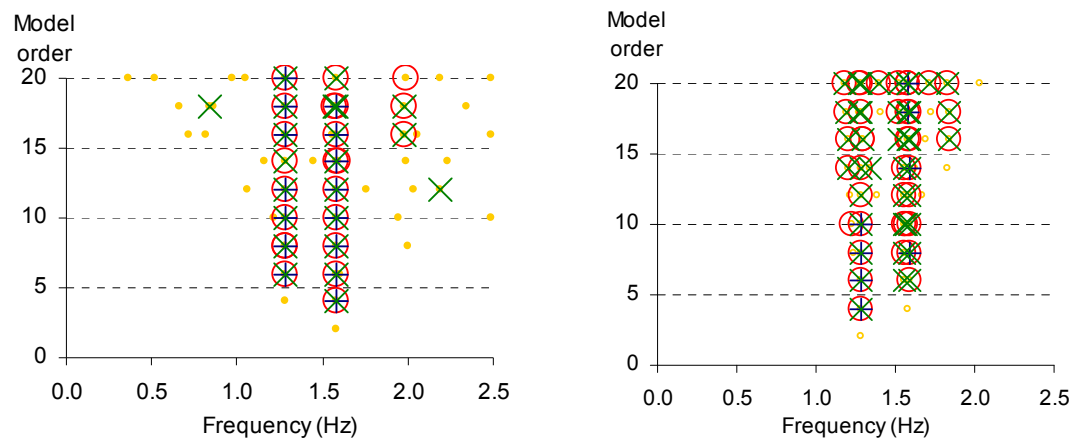
The parameter j_b limits the maximum model order (n_x) of the stochastic state-space models: $n_x = j_b \cdot n_r$. In this example, all outputs are considered reference outputs, so $n_r = 2$. Consequently, for the scenarios of the first line of Table 2.2, models with orders between 2 and 10 were used. For the other scenarios, the maximum model order was limited to 20 (already a very conservative limit taking into account that in the absence of noise and numerical inaccuracies, a model with two degrees of freedom is represented by a state-space model of order four).

Table 2.2 – Scenarios for the application of the SSI-COV method

Number of blocks of the Toeplitz matrix	Total time length (minutes)								
	5	10	20	30	40	50	60	70	80
5 (-●-)*	1a	1b	1c	1d	1e	1f	1g	1h	1i
10 (-x-)	2a	2b	2c	2d	2e	2f	2g	2h	2i
20 (-○-)	3a	3b	3c	3d	3e	3f	3g	3h	3i
30 (-□-)	4a	4b	4c	4d	4e	4f	4g	4h	4i
40 (-◇-)	5a	5b	5c	5d	5e	5f	5g	5h	5i

* symbols used in the graphics of Figure 2.20

Figure 2.19 presents the stabilization diagrams provided by the application of the SSI-COV method to one of the simulated dataset using two different values for j_b : 10 and 40. The stabilization criteria applied to estimates provided by models with consecutive orders were the following: stable frequencies - relative differences lower than 1%; stable modal damping ratios - relative differences lower than 2%; stable mode shapes - MAC higher than 0.95. Both diagrams present two vertical alignments of stable poles approximately at frequencies 1.3 and 1.6 Hz. However, the influence of j_b on the quality of the stabilization diagrams is evident. The justification for the worse quality of the stabilization diagram associated with a higher j_b will be presented later.



Symbols used in the stabilization diagrams:

All Poles - ● ; Stable frequencies - ○ ; stable modal damping ratios - + ; stable mode shapes - X

Figure 2.19 – Stabilization diagrams for scenarios 2d (left) and 5d (right).

The processing of 100 simulations for each scenario (4500 datasets) cannot be based on a manual analysis of stabilization diagrams. Therefore, it was used a procedure that permits the automation of parametric identification techniques based on the use of several model orders. The description of the adopted algorithm and practical details of its application are presented in section 2.4.4. Here, it is assumed that it is able to group all the estimates derived by models of different orders that represent

the same physical mode and to provide an average value of the modal parameters associated with each mode.

For all scenarios, the estimates of the natural frequencies and mode shapes are almost coincident with their theoretical values. So, the analysis is concentrated on the modal damping ratios. The results are shown in Figure 2.20 using the same type of plots that were adopted to evaluate the performance of the EFDD method (Figure 2.13). It is evident that, in this example, the SSI-COV method could provide good estimates using just 5 minutes of data (one quarter the time needed by the EFDD method). Another advantage is that the results are less dependent on the main parameters of the method (the vertical scales of the plots with the mean values shown in Figure 2.20 are much more detailed than their counterparts presented in Figure 2.13). Still, a good selection of j_b can improve the results, especially if short time series are used.

With respect to the standard deviations of the estimates, the plots of Figure 2.20 demonstrate that they decrease with the increasing of the used time length, reaching minimum values of about 0.10 %. Therefore, the scatter of the estimates provided by this method is similar to the observed with the EFDD. Additional simulations have also demonstrated that it is not significantly reduced if the artificial noise is not considered.

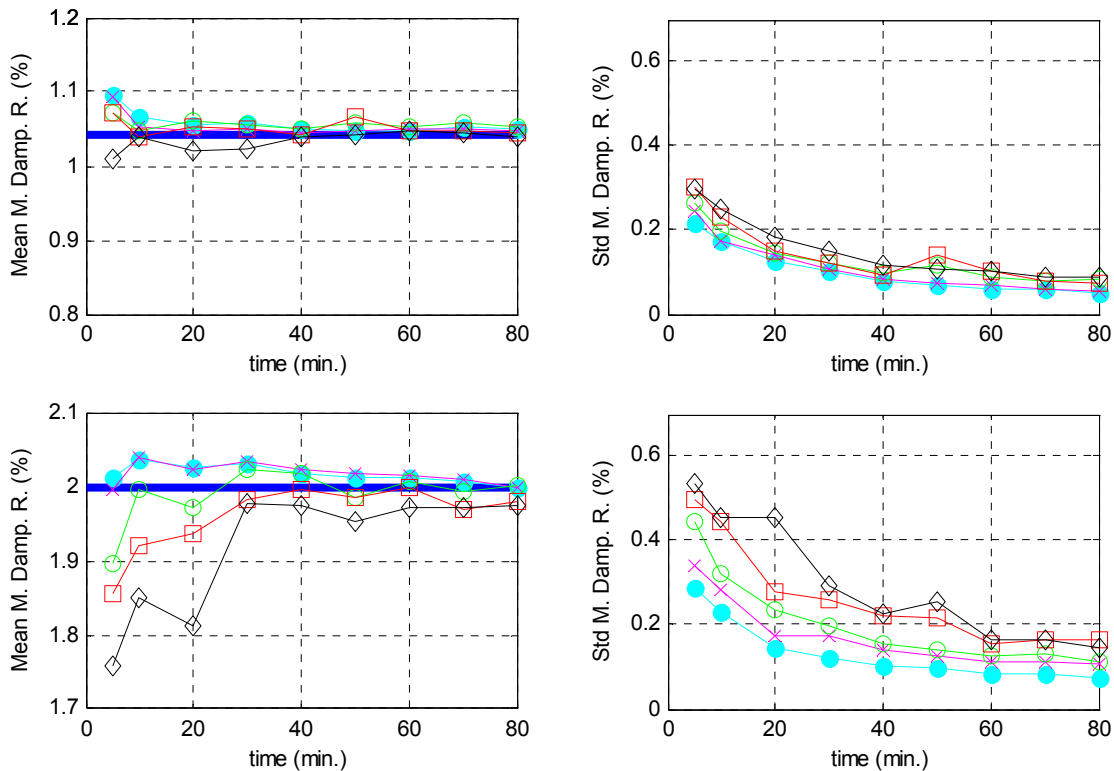


Figure 2.20 – Mean values and standard deviations of the estimates obtained with the SSI-COV method for the 2 modes of model SM using the parameters characterized in Table 2.2 (mode 1 at top, mode 2 at bottom, theoretical values represented by a horizontal solid line, symbols of the lines defined in Table 2.2).

The presented results also show that an increase of j_b , besides increasing the calculation effort (the SVD is applied to a larger matrix), may lead to worse estimates. The number of blocks of the adopted Toeplitz matrix (j_b) is directly related with the maximum time lag of the correlation functions (j_m) used in the identification: $j_m = 2j_b - 1$ (see equation (2.69)). So, the observed behaviour is explained by the fact that the first points of the correlations present richer information, since the amplitudes are higher and therefore the noise effect is smaller. The latter points tend to contain very few information of the modes with higher damping and are more influenced by the signals noise. This also justifies the worse quality of the second stabilization diagram presented in Figure 2.19.

With the goal of trying to establish a rule for the choice of j_b , or in other words, for the length of the adopted correlation functions, an additional set of simulations with a sampling frequency of 40Hz was performed. The higher value of the sampling frequency permits to adopt shorter correlation functions, without reducing the values of j_b , which also influences the maximum model order. In the previously presented simulations, the minimum value adopted for j_b was 5, which leads to the selection of correlation function time lags from 1 to 9, or equivalently to the use of correlation functions with a length of $9/5 = 1.8$ seconds (sampling frequency of 5Hz), which is still quite higher than the lower period of the structure ($1/1.3 = 0.77$ seconds).

The values adopted for j_b in this new set of simulations are presented in Table 2.3, together with the indication of the correlation functions length and the number of complete periods of the structure modes included in the correlation functions. For each value of j_b , 100 simulations and identifications were performed using time series with a total length of 30 minutes.

Table 2.3 – Values of j_b adopted in the simulations with a sampling frequency of 40Hz

j_b	5	10	20	30	40	80	160	240	320
Correlation length (points)	9	19	39	59	79	159	319	479	639
Correlation length (s)	0.225	0.475	0.975	1.475	1.975	3.975	7.975	11.975	15.975
n° of cycles of the 1 st mode	0	0	1	1	2	5	10	15	20
n° of cycles of the 2 nd mode	0	0	1	2	3	6	12	19	25

The values of the natural frequency estimates are close to the reference values for all the simulations except for the one with the lowest value of j_b . The results achieved in terms of modal damping ratios are condensed in Figure 2.21, where the mean values and the limits established by the mean values plus/minus the observed standard deviations are represented together with a horizontal line with the theoretical values. It is observed that the best results are obtained using correlation functions that contain a number of cycles of the model modes varying from 1 to 10. As we would expect, good

estimates can not be obtained if it is not considered at least one complete cycle of the structure larger period.

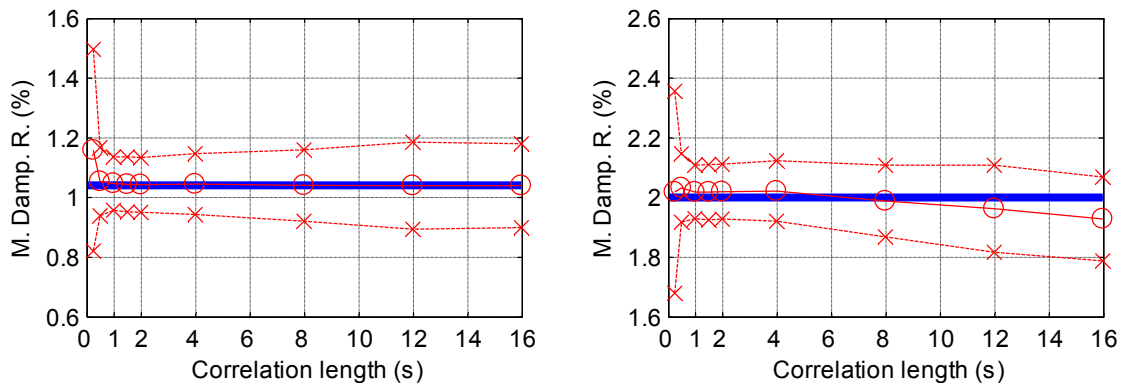


Figure 2.21 – Mean values and standard deviations of the estimates obtained with the SSI-COV method with a sampling frequency of 40Hz and a total length of 30 minutes (mode 1 at left, mode 2 at right; -o- mean value; -x- mean values +/- the standard deviation).

Therefore, in a practical application the value of j_b should be chosen not only taking into account its influence on the maximum model order, but also trying to include in the analysis correlation functions that contain a number of cycles of the structure modes varying from 1 to 10. Of course that this is just an indication, each particular application has its own particularities (percentage of noise, distribution of the modes in the frequency range under analysis, levels of damping, ...) and so several alternative identifications with different parameters should always be tried.

The processing of the simulations from the model with closely spaced modes (model CM, Figure 2.10) with the SSI-COV method showed that this method keeps its performance even in the presence of modes with similar natural frequencies (Magalhães et al. 2009f).

2.3.5 *p*-LSCF Method

The poly-reference Least Squares Complex Frequency Domain method (*p*-LSCF), also known by its commercial name PolyMAX (implemented in the software Test.Lab commercialized by LMS), is a recently created parametric frequency domain method that was firstly developed to perform the identification of modal parameters from Frequency Response Functions (Guillaume et al. 2003; Peeters et al. 2004). However, taking into account the similarities between the modal decomposition of the output half-spectrum of a system excited by white noise and its transfer function, or frequency response function (equations (2.41) and (2.58)), the adjustment of the method for Operational Modal Analysis was quite straightforward. The output-only version of the method was firstly presented by Peeters and Van Der Auweraer (2005).

The method models the half-spectrum matrix using a right matrix-fraction model in the discrete-time frequency domain, the z-domain (the variable s is replaced by $z = e^{s \cdot \Delta t}$). Therefore, considering the previously presented equation of this model (equation (2.47)), adopting polynomials of the same order for B and A , and limiting s to the imaginary axis ($s = i \cdot \omega$), the half-spectrum matrix evaluated at a given discrete frequency ω_j is modelled by:

$$S_{yy}^+(\omega_j) = B \cdot A^{-1} = \left[\sum_{r=0}^p B_r \cdot e^{i \cdot \omega_j \cdot \Delta t \cdot r} \right] \cdot \left[\sum_{r=0}^p A_r \cdot e^{i \cdot \omega_j \cdot \Delta t \cdot r} \right]^{-1} \quad (2.76)$$

where B_r and A_r are matrices with the model parameters, p is the order of the polynomials and Δt is the sampling time used to measure the structural responses. The number of lines of the half-spectrum is equal to the number of measured degrees of freedom (n_o) and it has as many columns as the number of *dof* selected for references ($n_r \leq n_o$). B_r and A_r are real-valued matrices with dimensions n_o -by- n_r and n_r -by- n_r , respectively.

The formulation of the method in the z-domain improves its numerical conditioning, because a segment of the frequency (or imaginary) axis in the s-domain is mapped to a segment of a unite circle in the z-domain, as illustrated in Figures 2.4 and 2.5 (the frequency axis establishes the limit between the stable and the unstable region). Therefore, numbers that can have a large variation, when large frequency intervals are selected, are converted to numbers that only differ on a rotation factor in the z-plane.

The goal of the identification algorithm is to find the model parameters, matrices B_r and A_r , that minimize the differences between the half-spectrum matrix estimated from the measured output time series (represented by \hat{S}_{yy}^+) and the theoretical half-spectrum matrix given by equation (2.76):

$$E^{NLS}(\omega_j) = \left[\sum_{r=0}^p B_r \cdot e^{i \cdot \omega_j \cdot \Delta t \cdot r} \right] \cdot \left[\sum_{r=0}^p A_r \cdot e^{i \cdot \omega_j \cdot \Delta t \cdot r} \right]^{-1} - \hat{S}_{yy}^+(\omega_j) \quad (2.77)$$

However, this equation for the error to be minimized leads to a nonlinear least squares (NLS) problem. In order to avoid this extra complexity, and instead obtain a linear least squares problem, an alternative error equation is formulated by right multiplying the previous equation by A (Guillaume et al. 2003), which gives:

$$E^{LS}(\omega_j) = \left[\sum_{r=0}^p B_r \cdot e^{i \cdot \omega_j \cdot \Delta t \cdot r} \right] - \hat{S}_{yy}^+(\omega_j) \cdot \left[\sum_{r=0}^p A_r \cdot e^{i \cdot \omega_j \cdot \Delta t \cdot r} \right] \quad (2.78)$$

where $E^{LS}(\omega_j)$ is a n_o -by- n_r matrix with the errors ($E_{o,r}$) to be minimized. At this stage, it is possible to give different weights to different frequency ordinates (ω_j) just by pre-multiplying the previous equation by a scalar weighting function $w(\omega_j)$. This can be useful to give less importance to spectral ordinates with less quality.

If the polynomial basis functions evaluated at ω_j are organized in one row vector with $(p + 1)$ components:

$$\Omega(\omega_j) = [\Omega_0(\omega_j) \quad \Omega_1(\omega_j) \quad \dots \quad \Omega_p(\omega_j)] = [e^{i\omega_j \Delta t \cdot 0} \quad e^{i\omega_j \Delta t \cdot 1} \quad \dots \quad e^{i\omega_j \Delta t \cdot p}] \quad (2.79)$$

then, one general line o of the error matrix is calculated with the following equation (the subscript LS was dropped to simplify the notation):

$$E_o(\omega_j) = \Omega(\omega_j) \cdot \begin{bmatrix} B_{0o} \\ B_{1o} \\ \vdots \\ B_{po} \end{bmatrix} + \begin{bmatrix} \Omega_0(\omega_j) \cdot \hat{S}_{yy_o}^+ & \Omega_1(\omega_j) \cdot \hat{S}_{yy_o}^+ & \dots & \Omega_p(\omega_j) \cdot \hat{S}_{yy_o}^+ \end{bmatrix} \cdot \begin{bmatrix} A_0 \\ A_1 \\ \vdots \\ A_p \end{bmatrix} \quad (2.80)$$

where B_{r_o} represents the o line of matrix B_r and $\hat{S}_{yy_o}^+$ represents the o line of matrix \hat{S}_{yy}^+ .

Introducing the following definitions:

$$\beta_o = \begin{bmatrix} B_{0o} \\ B_{1o} \\ \vdots \\ B_{po} \end{bmatrix} \text{ with } o = 1, 2, \dots, n_o \quad \text{and} \quad \alpha = \begin{bmatrix} A_0 \\ A_1 \\ \vdots \\ A_p \end{bmatrix} \quad (2.81)$$

equation (2.80) can be generalized to all the discrete frequencies values, ω_1 to ω_{n_f} , within a previously selected frequency interval for the analysis:

$$E_o(\beta_o, \alpha) = [X_o \quad Y_o] \cdot \begin{bmatrix} \beta_o \\ \alpha \end{bmatrix}$$

with

$$X_o = \begin{bmatrix} \Omega(\omega_1) \\ \vdots \\ \Omega(\omega_{n_f}) \end{bmatrix} \quad \text{for } o = 1, 2, \dots, n_o \quad (2.82)$$

$$Y_o = \begin{bmatrix} \Omega_0(\omega_1) \cdot \hat{S}_{yy_o}^+ & \Omega_1(\omega_1) \cdot \hat{S}_{yy_o}^+ & \dots & \Omega_p(\omega_1) \cdot \hat{S}_{yy_o}^+ \\ \vdots & \vdots & & \vdots \\ \Omega_0(\omega_{n_f}) \cdot \hat{S}_{yy_o}^+ & \Omega_1(\omega_{n_f}) \cdot \hat{S}_{yy_o}^+ & \dots & \Omega_p(\omega_{n_f}) \cdot \hat{S}_{yy_o}^+ \end{bmatrix} \quad \text{for } o = 1, 2, \dots, n_o$$

With a further step, it is possible to express the complete error matrix as a function of a matrix with all the model parameters β_o and α :

$$E(\beta_o, \alpha) = \begin{bmatrix} X_1 & 0 & \dots & 0 & Y_1 \\ 0 & X_2 & \dots & 0 & Y_2 \\ \vdots & \vdots & \ddots & \vdots & \vdots \\ 0 & 0 & \dots & X_{n_o} & Y_{n_o} \end{bmatrix} \cdot \begin{bmatrix} \beta_1 \\ \beta_2 \\ \vdots \\ \beta_{n_o} \\ \alpha \end{bmatrix} = J \cdot \theta \quad (2.83)$$

The least squares problem could be resolved by setting $J \cdot \theta = 0$ and solving this over-determined system of equations by means of the Moore-Penrose pseudo-inverse, after the introduction of a constraint to avoid the trivial solution $\theta = 0$ (like it is done later in equation (2.89)). However, due to the large dimension of J , $n_o \cdot n_f$ -by- $(p+1) \cdot (n_o + n_r)$, especially when a large frequency range is selected, this is a very demanding numerical calculation. Therefore an alternative way is followed.

The model parameters are determined using the Least Squares cost function, which is obtained by adding all the squared elements of the error matrix ($E_{o,r}$) evaluated at all the discrete frequency values, ω_1 to ω_{n_f} :

$$\varepsilon = \sum_{o=1}^{n_o} \sum_{r=1}^{n_r} \sum_{j=1}^{n_f} E_{o,r}(\omega_j) \cdot E_{o,r}(\omega_j)^* \quad (2.84)$$

Using the expressions of equation (2.82), the scalar cost function can be also calculated with the following matrix equation:

$$\begin{aligned}\varepsilon(\beta_o, \alpha) &= \sum_{o=1}^{n_o} \text{tr} \left\{ E_o(\beta_o, \alpha)^H \cdot E_o(\beta_o, \alpha) \right\} = \\ &= \sum_{o=1}^{n_o} \text{tr} \left\{ \begin{bmatrix} \beta_o^T & \alpha^T \end{bmatrix} \cdot \begin{bmatrix} R_o & S_o \\ S_o^T & T_o \end{bmatrix} \cdot \begin{bmatrix} \beta_o \\ \alpha \end{bmatrix} \right\}\end{aligned}\quad (2.85)$$

with $R_o = \text{Re}(X_o^H \cdot X_o)$; $S_o = \text{Re}(X_o^H \cdot Y_o)$; $T_o = \text{Re}(Y_o^H \cdot Y_o)$

where $\text{tr}\{\bullet\}$ means the trace, or the sum of the elements in the main diagonal, of a matrix and $\text{Re}(\bullet)$ selects the real part of a complex number. The selection of the real part is due to the base assumption that the matrices to be determined, B_r and A_r , are real-valued.

The minimum of the cost function is then determined by forcing its derivatives with respect to the unknowns (elements of the B_r and A_r matrices) to become zero:

$$\begin{aligned}\frac{\partial \varepsilon(\beta_o, \alpha)}{\partial \beta_o} &= 2 \cdot (R_o \cdot \beta_o + S_o \cdot \alpha) = 0 \quad \text{with } o = 1, 2, \dots, n_o \\ \frac{\partial \varepsilon(\beta_o, \alpha)}{\partial \alpha} &= 2 \cdot \sum_{o=1}^{n_o} (S_o^T \cdot \beta_o + T_o \cdot \alpha) = 0\end{aligned}\quad (2.86)$$

The first matrix equation with dimension $(p+1)$ -by- n_r , contains the derivatives of the cost function with respect to all the elements stored in the matrices β_o . The second is a $n_r \cdot (p+1)$ -by- n_r matrix equation that contains the derivatives of the cost function with respect to all the elements organized in the α matrix.

With the aim of reducing even more the size of the system of equations to be solved, the unknowns β_o can be eliminated:

$$2 \cdot (R_o \cdot \beta_o + S_o \cdot \alpha) = 0 \Leftrightarrow \beta_o = -R_o^{-1} \cdot S_o \cdot \alpha \quad (2.87)$$

Consequently, matrix α can be obtained by solving the following reduced system of equations:

$$2 \cdot \sum_{o=1}^{n_o} (T_o - S_o^T \cdot R_o^{-1} \cdot S_o) \cdot \alpha = 0 \Leftrightarrow M \cdot \alpha = 0 \quad (2.88)$$

where M is $n_r \cdot (p+1)$ -by- $n_r \cdot (p+1)$ matrix that can be calculated from the output half-spectrum matrix estimated from the measured time series. Comparing the dimensions of matrix M with the ones of matrix J , it is evident that this second procedure is much less computationally demanding.

In order to avoid the trivial solution of the previous equation: $\alpha = 0$; a constraint has to be imposed. This can be done, for instance, by imposing that one of the A_r matrices is equal to a non-zero constant value. This constraint also removes the parameters redundancy that exists in RMFD models (multiplying numerator and denominator with the same matrix yields different numerator and denominator polynomials, but the same transfer function or output spectrum matrix). The selection of the constraint has a huge impact on the quality of the results, as it will be illustrated afterwards with the application of the method to simulated data. The described algorithm provides better results, if A_0 is forced to be an identity matrix.

Then, the resolution of the system of equations is elementary:

$$\begin{aligned}
 M \cdot \alpha = 0 &\Leftrightarrow \left[\begin{array}{c|c} M_{aa} & M_{ab} \\ \hline M_{ba} & M_{bb} \end{array} \right] \cdot \begin{bmatrix} I \\ A_1 \\ \vdots \\ A_p \end{bmatrix} = \begin{bmatrix} 0 \\ 0 \\ \vdots \\ 0 \end{bmatrix} \Leftrightarrow \\
 &M_{bb} \cdot \alpha_b = -M_{ba} \Leftrightarrow \alpha_b = -M_{bb}^{-1} \cdot M_{ba} \\
 &\Rightarrow \alpha = \begin{bmatrix} I \\ -M_{bb}^{-1} \cdot M_{ba} \end{bmatrix}
 \end{aligned} \tag{2.89}$$

M_{ba} contains the first n_r columns and the last $p \cdot n_r$ lines of M , M_{bb} contains the last $p \cdot n_r$ columns and lines of M , and α_b contains the last $p \cdot n_r$ lines of α .

Once the A_r matrices have been determined, the B_r matrices can be calculated using the relation between the α and β_0 matrices presented in equation (2.87). With this step the identification problem is solved. It is now necessary to obtain the modal parameters of the identified model.

The standard implementation of the p-LSCF method, as described in (Peeters and Van Der Auweraer 2005), determines the operational reference vectors and the system poles, and thus the natural frequencies and the modal damping ratios, from the calculated sub-matrices of the α matrix through resolution of a general eigenvalue problem that uses an auxiliary matrix called companion matrix (Cauberghe 2004), which is constructed using the following expression:

$$Co = \begin{bmatrix} -\alpha_p^{-1} \cdot \alpha_{p-1} & -\alpha_p^{-1} \cdot \alpha_{p-2} & \dots & -\alpha_p^{-1} \cdot \alpha_1 & -\alpha_p^{-1} \cdot \alpha_0 \\ I & 0 & \dots & 0 & 0 \\ \vdots & \ddots & \dots & \vdots & \vdots \\ 0 & 0 & \dots & I & 0 \end{bmatrix} \tag{2.90}$$

The general eigenvalue problem is defined by the equation:

$$C_o \cdot V_o = \mu \cdot V_o \quad (2.91)$$

The resolution of the eigenvalue problem provides $n_r \cdot p$ eigenvalues organized in complex conjugate pairs. Firstly, these have to be converted into the continuous-time domain (equation (2.17)) and then, can be used to estimate the natural frequencies and modal damping ratios (equation (2.75)). The eigenvectors of this eigenvalue problem (columns of matrix V_o : V_{o_k}) are related with the operational reference vectors (g_k) by the expression:

$$V_{o_k} = \begin{bmatrix} \mu_k^{p-1} \cdot g_k \\ \mu_k^{p-2} \cdot g_k \\ \vdots \\ \mu_k \cdot g_k \\ g_k \end{bmatrix} \quad (2.92)$$

Consequently, the operational reference vectors coincide with the last n_r lines of the calculated eigenvectors. As already referred in section 2.2.3, these vectors depend on the modal parameters of all the structure modes and do not have any special physical meaning.

Afterwards, the mode shapes are found with another least squares problem using the following modal decomposition of the positive output spectrum matrix (an adaptation of equation (2.41)):

$$S_{yy}^+(\omega) = \sum_{k=1}^{n_m} \frac{\phi_k \cdot g_k^T}{i \cdot \omega - \lambda_k} + \frac{\phi_k^* \cdot g_k^H}{i \cdot \omega - \lambda_k^*} + i \cdot \omega \cdot UR + \frac{LR}{i \cdot \omega} \quad (2.93)$$

Note that the residual terms that take into account the influence of the modes outside the frequency interval selected for the analysis (concept illustrated with Figure 2.6) have been modified. This had to be done because the shapes of single degree of freedom positive output spectra and frequency response functions are obviously different. In the case of the output spectra, the equation of the residues does not depend on the type of measured signals, which can be either displacements, velocities or accelerations (Peeters and Van Der Auweraer 2005). Since the system poles and the operational reference vectors have already been determined, this is a linear problem because the only unknowns of the equation are the mode shape components and the residual terms.

Like in the case of the SSI-COV method, it is not possible to anticipate which model order (polynomials order, p) will provide the best results. Therefore, the same strategy has to be followed: model with orders within a previously defined interval are adjusted to the data and the corresponding

modal parameters represented in a stabilization diagram. Due to the estimation of the mode shapes in a second step, with this approach the stabilization diagrams have to be created before the determination of the modes shapes and consequently have to be only based on poles and operational reference vectors.

In the present work an alternative algorithm, also presented in (Juang 1994) and (Reynders 2009), was used for the extraction of the modal parameters from the identified RMFD models. This is based on the transformation of the RMFD model fitted to the positive output spectrum matrix into an equivalent state-space model by the use of the expressions presented in equation (2.48). After this step, the identification follows the procedure already presented while describing the SSI-COV algorithm: determination of the eigenvalues and vectors of A and subsequent calculation of the modal parameters. This model conversion has to be repeated as many times as the number of tried model orders, so that the modal parameters associated with different model orders are represented in a stabilization diagram, which facilitates the selection of the physical modes of the tested structure.

This alternative approach has the practical advantage of permitting the use of some of the routines previously developed for the SSI-COV method and of providing stabilization diagrams that also consider the mode shapes instead of the meaningless operational reference vectors. This will prove to be very advantageous for the application of the tools presented in section 2.4 that automatically interpret stabilization diagrams. Furthermore, with the firstly presented procedure, the correct identification of the modes shapes is dependent on the previous correct selection of a set of physical poles. One disadvantage of the secondly presented procedure is that the residual influence of the modes outside the frequency band under analysis is not considered. However, this drawback is common to all time domain methods.

In (De Troyer et al. 2009) it is presented an algorithm to obtain the variance of modal parameters estimated by the p-LSCF method. The comment previously made with regard to the equivalent procedure to be used together with the SSI-COV method is also valid for this approach: the obtained confidence intervals are associated with the specific conditions observed during the period of acquisition of the adopted time series.

Numerical Simulations

The numerical simulations of the responses of Model SM (Figure 2.10) to a random excitation were also used to explore the performance of the p-LSCF method. With that purpose, the identification algorithm was applied to 100 simulations of all the scenarios presented in Table 2.4. Like in the

evaluation of the other methods, the total time length of the acceleration signals varied from 5 to 80 minutes. Considering that the basis of the method is the output half-spectrum matrix, whose elements are calculated from the inverse FFT of the positive time lags of correlation functions, the parameters used for its calculation will certainly have impact on the estimated modal parameters. Therefore, different lengths for the correlation functions were tried. Different correlation lengths lead to different resolution of the spectra. In particular, the values presented in Table 2.4 led to spectra with resolutions between 0.156 Hz (2.5/16) and 0.010Hz (2.5/256). Figure 2.22 presents one element of the half-spectrum matrix of the outputs estimated from time series with 30 minutes using three different resolutions. The first spectrum is defined with only 16 points, but still the peaks associated with the two modes, around 1.3 and 1.6Hz can be observed. These spectra, as well as all the spectra derived from the simulated data, were calculated after the application of an exponential window to the correlation functions with a factor of 0.1 (its amplitude for the last correlation time lag is 0.1). This reduces the effect of noise associated with larger time lags of the correlation functions and minimizes the leakage error.

Table 2.4 – Scenarios for the application of the p-LSCF method

Number of time lags of the correlation functions	Total time length (minutes)								
	5	10	20	30	40	50	60	70	80
32 (-●-)*	1a	1b	1c	1d	1e	1f	1g	1h	1i
64 (-x-)	2a	2b	2c	2d	2e	2f	2g	2h	2i
128 (-○-)	3a	3b	3c	3d	3e	3f	3g	3h	3i
256 (-□-)	4a	4b	4c	4d	4e	4f	4g	4h	4i
512 (-◇-)	5a	5b	5c	5d	5e	5f	5g	5h	5i

* symbols used in the graphics of Figure 2.24

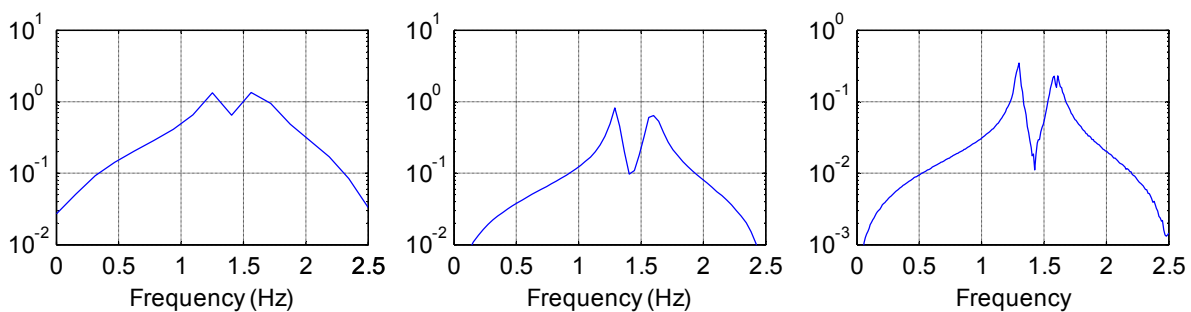


Figure 2.22 – Absolute values of element (1,1) of the positive spectrum matrix for scenarios 1d, 3d and 5d (from left to right).

Firstly, the influence of the constraint used for the resolution of equation (2.88) on the quality of the stabilization diagrams is demonstrated using a simulation from scenario 3d. Figure 2.23 shows two stabilization diagrams constructed from the same dataset with two different constraints: $A_p = I$ and $A_0 = I$, and considering polynomials with orders from 1 to 10 (model order). The meaning of the

adopted symbols has already been defined in Figure 2.19. The stabilization criteria for both diagrams were the following: stable frequencies - relative differences lower than 1% and positive damping; stable modal damping ratios - relative differences lower than 2% and positive damping; stable mode shapes - MAC higher than 0.95 and positive damping. It is evident the superior quality of the second one, in which the majority of the unstable poles can be distinguished from the stable poles due to their negative modal damping ratios. This property is the most interesting characteristic of the p-LSCF method, as it permits to obtain much clearer and therefore easier to analyse stabilization diagrams. The theoretical justification for this behaviour is presented in (Reynders 2009).

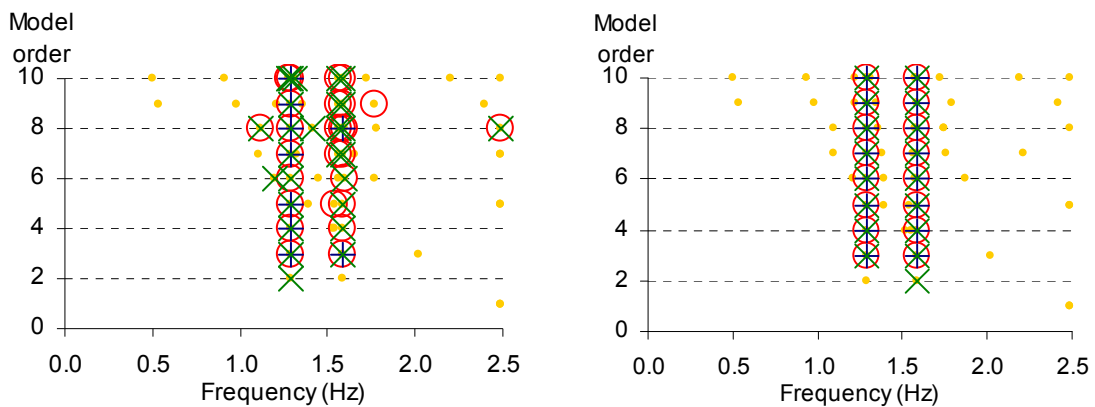


Figure 2.23 – Stabilization diagrams for scenario 3d using different constraints: $A_p = I$ (left); $A_0 = I$ (right).

The processing of 100 simulations for the 45 scenarios characterized in Table 2.4 was done with the same algorithm for automatic post-processing of the results associated with models of different orders that was used together with the SSI-COV method. Polynomials of orders between 1 and 10 were adopted for all the scenarios. As the two system outputs were assumed to be reference outputs, a model with a polynomial order of 10 is converted into a state-space model of order 20, and consequently provides estimates for 10 modes (2 physical modes plus 8 numerical modes).

As already reported for the other two methods, also with the p-LSCF method the estimates for the natural frequencies and mode shapes extracted from all the processed datasets were very close to their theoretical values. The results obtained for the modal damping ratios are systematized in Figure 2.24, which includes the mean values and the standard deviations of the estimates. The presented plots show that the use of longer correlation functions may lead to biased estimates, especially for the second mode when time series shorter than 30 minutes are used. This is justified by the fact that longer correlations contain at their latter points very few information of the modes with higher damping and an important contribution of the signal noise. This aspect as consequences on the estimated positive spectra, as it can be observed in the last spectrum of Figure 2.22 that presents a not well defined peak

for the second mode (there are several small peaks around the resonant frequency). The use of longer time series permits the development of more averages that minimize the effect of noise.

The values of the standard deviations are generally slightly lower than the ones observed for the other studied identification algorithms. They are not very sensitive to the adopted spectra resolution, but they decrease with the increase of the time series length.

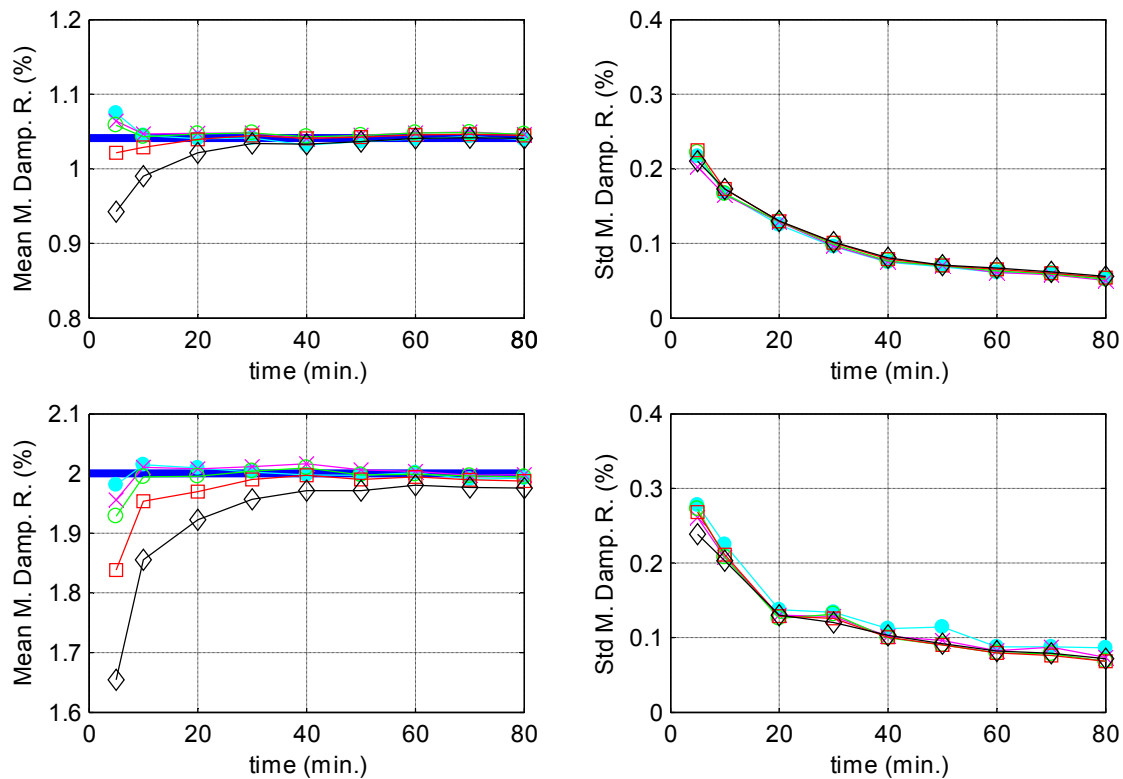


Figure 2.24 – Mean values and standard deviations of the estimates obtained with the p-LSCF method for the 2 modes of model SM using the parameters characterized in Table 2.4 (mode 1 at top, mode 2 at bottom, theoretical values represented by a horizontal solid line, symbols of the lines defined in Table 2.4).

The application of the p-LSCF algorithm to 100 simulations for outputs of model CM (see Figure 2.10) using the parameters of scenario 1d led to the following results (mean \pm standard deviation): $f_1 = 1.5720 \pm 0.0013 \text{ Hz}$; $\xi_1 = 1.0058 \pm 0.098\%$; $f_2 = 1.5914 \pm 0.0021 \text{ Hz}$; $\xi_2 = 2.0191 \pm 0.131\%$. The proximity between the estimates and the real values shows that this method is able to correctly identify closely spaced modes, even when a quite low frequency resolution (only 0.156Hz) is used.

To sum up, in practical applications the spectra resolution, conditioned by the length of the adopted correlation functions, should be high enough to well characterized all the modes within the selected frequency range and, at the same time, should be kept as low as possible to reduce the effect of noise and the calculation effort. Usually, the visual inspection of the amplitude and phase of spectra estimated with several alternative resolutions enables the selection of an adequate value.

2.4 Automated Operational Modal Analysis

2.4.1 Introduction

In the context of dynamic monitoring systems recording continuously the responses of an instrumented structure, it is very important to develop tools that can process the collected data automatically. Since the structural condition can be evaluated through the analysis of modal parameters variations, it is crucial to include in the processing the identification of these parameters. However, all the previously presented techniques to perform the identification of structural modal parameters require at some stages of the analysis human intervention. Consequently, a lot of research has been developed with the goal of achieving algorithms that can automatically extract accurate estimates of modal parameters from continuously recorded structural responses during normal operation conditions. This section is devoted to the presentation of algorithms for automated operational modal analysis. Their implementation in monitoring software is characterized in chapter 4 and then, their application in the framework of two dynamic monitoring projects is described in chapters 5 and 6.

Firstly, it is presented an implementation of an automated version of the Frequency Domain Decomposition method (FDD) that was recently developed by Brincker et al. (2007). Then, attention is placed on strategies to automate parametric identification methods.

The research efforts that have been performed to automate the identification of structural modal parameters using parametric algorithms are focused on three complementary aspects: conception of identification algorithms that can produce clearer stabilization diagrams, study of additional parameters to characterize mode estimates in order to make a more well-founded selection of the stable modes, and development of methodologies to perform an automatic analysis of the information usually presented in stabilization diagrams.

In the field of the development of new identification algorithms, an important outcome was the already presented p-LSCF method, which provides clearer stabilization diagrams that facilitate the selection of the physical mode estimates.

Concerning the definition of additional criteria to distinguish physical mode estimates from spurious ones, Verboven et al. (2002) presented one that is suitable for all system identification methods: the complexity of the modal vector (in most of the practical applications real modes are expected and so estimates with high mode shape complexity can be considered as spurious). Others are associated with

particular system identification techniques and some of them are only applicable in the context of input-output tests. The autonomous procedure developed by Pappa et al. (1998), for the Eigensystem Realization Algorithm (ERA), uses the “Consistent-Mode Indicator” (a specific indicator of this method) to analyse data provided by a hammer test. In (Verboven et al. 2001), the automated modal identification approach presented for the analysis of frequency response functions is based on a frequency-domain maximum likelihood estimator and a stochastic validation criterion: the selection of the physical modes is based on the uncertainty of the estimates, which is an additional output of the used identification algorithm. In (Deraemaeker et al. 2008), the concept of modal transfer norm is used together with a stochastic subspace identification method, for the analysis of output-only simulated data. Reference (Scionti et al. 2003) presents some additional mode selection techniques to remove spurious modes from deterministic state space models.

After the elimination of all, or at least part of the spurious mode estimates, there is still the need for a procedure to group all the estimates associated with models of different orders that are related with the same physical mode. The most simplistic approaches overcome this step with the selection of a conservative model order, instead of analysing the results of several model orders. However, this is not the most adequate procedure, because it can happen that the selected model does not contain estimates for all the modes and even if all estimates are present, there is no guarantee that the estimates provided by that model order are the best ones.

A natural way for the automatic interpretation of stabilization diagrams consists in the development of algorithms to mimic the decisions that an experienced modal analyst takes during the examination of a stabilization diagram. This is followed in reference (Scionti et al. 2003), where the suggested technique is tested with data acquired during an in-flight flutter test. This technique starts with the selection of vertical columns of stable poles, using a double set of histograms, shifted by half a bin-width.

An alternative is the use of cluster analysis. In the present work, it is proposed a new methodology for the automatic interpretation of stabilizations diagrams based on this statistical tool. Therefore, in section 2.4.3 the principal concepts involved in cluster analysis are summarized and reference is made to other works where it is applied in the context of modal analysis. Then, the new approach is detailed in section 2.4.4.

2.4.2 Automated FDD

The automated Frequency Domain Decomposition method described and implemented in this work follows the methodology presented in (Brincker et al. 2007). This is based on the spectrum of the first singular value of the output spectrum matrix and uses the concept of modal domain. The modal domain of each mode is composed by the points of the singular value spectra around the peak centred at the mode natural frequency that are dominated by that mode. This is identified by determining the singular values which are associated with singular vectors that are similar to the singular vector observed at the resonance frequency. The analysis of the modal domains around the peaks observed in the first singular value spectrum permits to distinguish peaks associated with physical modes from peaks motivated by noise or harmonic excitation. The detection of peaks due harmonic excitation will not be discussed here, because it has little importance in most of civil engineering applications. Due to the fact that, when the tested structure is excited by an harmonic excitation motivated by the operation of rotating machinery or a turbine in the case of dams, the frequency of operation of the machine or turbine is usually known, and so it is quite easy to identify the peak associated with it.

The implemented methodology consists on the repeated application of the following steps to the spectrum of the first singular value:

- identification of the maximum within the search domain; at the beginning this is equal to the frequency range defined by the user;
- selection of the points around the identified peak that are associated with similar mode shapes (identified from the first singular vectors), using the MAC coefficient (equation (2.68)) as similitude measure;
- if the number of selected points is larger than a predefined value and if there are points at both sides of the peak, the identified peak is elected as a natural frequency and the selected group of points is called modal domain; otherwise, the peak is assumed to be related to data noise;
- redefinition of the frequency search domain by removal of the previously selected group of points, either if they are associated with a mode or with noise;
- repetition of these steps in the reduced search domain, until a specified number of identified natural frequencies has been achieved, the search set is empty or the maximum spectrum amplitude is lower than a predefined noise level.

This procedure provides a set of natural frequencies and mode shapes (given by the singular vectors evaluated inside the modal domains).

It is possible to extend the algorithm to provide also modal damping ratios. This could be done following the procedure described in section 2.3.3, using the inverse FFT of the spectrum segments contained in the modal domains. However, the analysis of data collected in real structures shows that the fitting of an exponential function to the obtained modal decay needs some judgment, so that an adequate segment of the decay is selected. Therefore, the automation of this step does not provide very reliable results. Still, it is an approach that demonstrated to be efficient in the processing of simulated data.

The most critical step of this algorithm is the classification of a group of points selected around a relative maximum as a modal domain or as noise. The simple criterion used here, just based on the number of points and on the existence of points at both sides of the peak, worked very well in the application presented in chapter 5. However, the processing of lower quality data may require a more robust criterion, implying for instance the analysis of the “bell” shape or of its transformation to the time domain, which should be close to a modal decay.

The application of the method requires the definition of some parameters. These include the frequency resolution, the frequency interval under analysis, the MAC value limit of the points in the same modal domain and the minimum number of points of the modal domains. The number of expected natural frequencies and the noise level are optional parameters that can be used to shorten the number of searches for maxima.

The specification of the frequency resolution is critical. If the value is too small (the used segments are longer, the number of averages is lower), the amount of noise is higher and so, the automatic identification becomes more difficult. On the other hand, higher values limit the accuracy on the identification of natural frequencies. The MAC limit used for the definition of the modal domain is dependent on the number of measured points because the ability of the MAC to distinguish two similar mode shapes increases with the number of used components. The value set for the minimum number of points of the modal domains obviously depends on the adopted MAC limit and on the level of noise present in the data.

Ultimately, it is important to stress that the correct selection of the method parameters for the automatic processing of a large number of datasets should result from previous sensitivity tests performed on a small group of typical datasets.

In chapter 5, it is shown that the application of this approach to data collected by the monitoring system installed in the Infante D. Henrique Bridge provided good results in terms of natural frequency and mode shape estimates. The most relevant drawbacks of this methodology are the dependency of the accuracy of the natural frequency estimates on the used frequency resolution, its inability to identify coincident or very close natural frequencies and the lack of robustness for the estimation of modal damping ratios. Anyway, it is a method that still has some margin for improvements.

2.4.3 Cluster Analysis for Automated OMA

Cluster analysis is the name for a group of multivariate techniques whose primary purpose is to group objects based on the characteristics they possess. The resulting groups, or clusters, of objects should then exhibit high internal (within-cluster) homogeneity and high external (between cluster) heterogeneity (Hair et al. 1998). In the context of the analysis of results provided by the application of parametric identification techniques that use models of several orders, the goal is to group the mode estimates that represent the same physical mode. This can be done, for instance, representing all the estimates by the corresponding natural frequency and modal damping ratio, like it is exemplified in Figure 2.25 for a structure with four modes and considering the results provided by five model orders. In order to make the figure simpler, only the physical modes are represented, in a real application some further points more or less randomly distributed would be present. The cluster analysis groups the points that are close to each other (circles of the figure). The concept graphically illustrated for a case where only two variables are considered can also be applied when a higher number of variables are involved. However, when more than three characteristics are used the graphical interpretation becomes impossible.

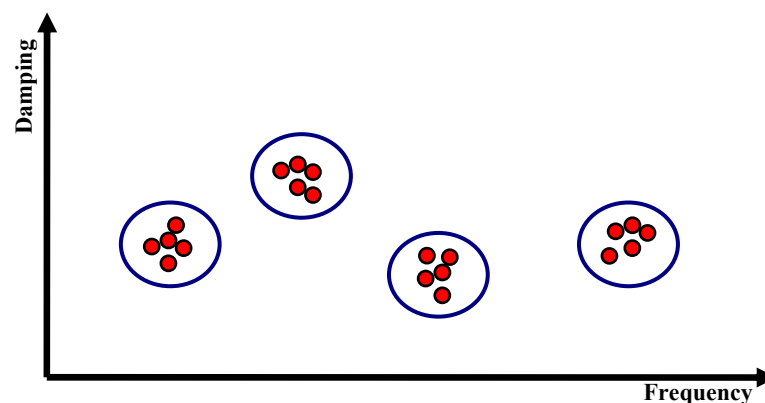


Figure 2.25 – Scheme to illustrate the application of clustering algorithms.

Most commonly used clustering algorithms can be classified into two general categories: hierarchical and non-hierarchical.

Non-hierarchical clustering procedures, frequently referred to as K-means clustering, assign objects into a previously specified number of clusters (K) using the following procedure. Firstly, cluster seeds are selected as the initial cluster centres, and all objects within a previously specified threshold distance are included in the resulting clusters. Then, an iterative algorithm is used to minimize the sum of distances from each object to its cluster centroid, over all clusters. This algorithm moves objects between clusters until the sum cannot be decreased further. The result is a set of clusters that are as compact and well-separated as possible. The major problems faced by all non-hierarchical clustering procedures are the need to previously define the number of clusters and the requirement to select the clusters seeds. The second drawback is usually overcome by a random selection of the seeds. However, this leads to another problem that is the not deterministic nature of the solution, as different runs can produce different solutions.

In references (Verboven et al. 2002), (Goethals et al. 2004) and (Carden and Brownjohn 2008), non-hierarchical algorithms are used for the automatic interpretation of data contained in stabilization diagrams. In the first reference, the estimated modes are represented in a damping vs frequency diagram (like in the scheme presented in Figure 2.25) and a clustering technique is combined with self-learning algorithms which permit a better choice of the algorithm parameters and the assessment of the nature (physical or numerical) of the obtained clusters. In the second one, a Fuzzy C-mean clustering algorithm (an improvement of the described K-mean algorithm, which instead of associating an object to a certain group, gives it a membership grade) is used to distinguish physical poles from computational modes resulting from a maximum likelihood estimator applied to input-output tests data. The distinction is based on a total of six characteristics that include, for instance, the standard deviation of the pole estimate, which is an output of the adopted identification algorithm, and indices that evaluate the complexity of the mode shape estimates. In the third reference, a Fuzzy C-mean clustering algorithm is also used, but in this case to group mode estimates provided by the processing of several datasets using the representation of their poles in the z-plane (as exemplified in Figure 2.5), rather than the more classical representation on a damping vs frequency diagram.

Hierarchical clustering algorithms are based on the construction of a hierarchy of a treelike structure. At the beginning, each object is considered a cluster. In subsequent steps, the two closest clusters (or individuals) are combined into a new aggregate cluster, thus reducing the number of clusters by one in each step. Eventually, all individuals are grouped into one large cluster (Figure 2.26). The implementation of the hierarchical algorithms is composed of the following main steps: calculation of the similarity between every pair of objects in the dataset, linking of the objects in a hierarchical tree and, finally, the definition of a rule to cut the hierarchical tree at a certain level, assigning all the

objects of each branch to a single cluster. Depending how the distance between clusters is calculated, there are different hierarchical algorithms: single linkage, complete linkage, average linkage, Ward's method and centroid method (Hair et al. 1998).

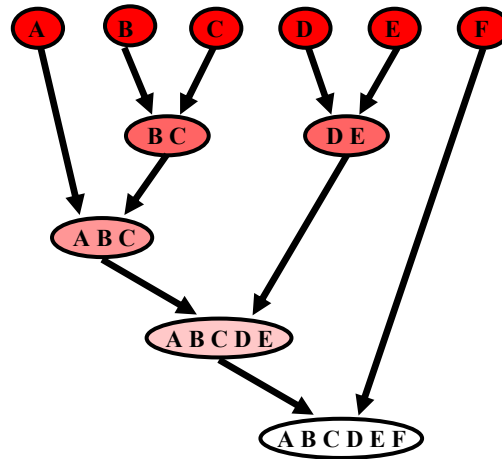


Figure 2.26 – Hierarchical clustering.

The hierarchical algorithms have the advantage of being deterministic and of permitting a well-founded selection of the final number of clusters, based on the previously constructed hierarchical tree. On the other hand, they have the drawback of being computationally demanding in the presence of a large number of individuals, as the similitude between every pair has to be computed. Verboven et al. (2003) uses hierarchical clustering for the analysis of stabilization diagrams produced by the application of the LSCF method (Least Squares Complex Frequency Domain) to datasets collected in an input-output experiment. In the proposed methodology, the grouping is only based on the pole estimates and therefore not considering the mode shapes, which are only used in a second phase to evaluate the quality of the formed groups.

2.4.4 Proposed Methodology for Automated OMA

The proposed methodology for automatic identification of modal parameters, using parametric identification methods, is based on a hierarchical clustering algorithm. The method is suitable for the analysis of the outputs produced by any parametric identification technique that provides estimates of natural frequencies, modal damping ratios and mode shapes for models of several orders. It groups the mode estimates associated with the same physical mode and permits the separation of the numerical or noisy estimates (Magalhães et al. 2009e).

In a first step, the similarity between all the pairs of estimated modes is calculated. The most common procedure for the evaluation of this parameter is to calculate the Euclidian distance between the

objects to be clustered, considering for ordinates the values of the variables that characterize each individual. In the context of operational modal analysis, the most straightforward procedure is to measure the distance between mode estimates in diagrams of the type of the one presented in Figure 2.25 or in representations of the poles in the s or z -plans and therefore, considering directly or indirectly the natural frequencies and the modal damping ratios as distinguishing factors. However, the modal damping ratios are not very suitable to distinguish modes, owing to the fact that different modes can have the same modal damping ratios and because their estimates present a high scatter.

Therefore, the proposed methodology relies on a similarity measure that is based on the estimates of natural frequencies and mode shapes, the modal parameters that can really distinguish two modes. In this way, the distance between two modes (i and j) is calculated with the following formula:

$$d_{i-j} = \left| \frac{f_i - f_j}{f_j} \right| + (1 - MAC_{i,j}) \quad (2.94)$$

where f_i is the natural frequency of the mode estimate i and $MAC_{i,j}$ is the Modal Assurance Criterion between the mode shapes of the estimates i and j . If the distance between two mode estimates is short, that means both estimates present similar natural frequencies and mode shapes. Therefore, they are probably representing the same physical mode, and so they should be included in the same cluster.

In some applications, it can be convenient to give more importance to the relative differences of the natural frequencies than to the mode shape differences or vice versa. This can be achieved with the multiplication of each difference by different weighting factors. In the applications presented in chapters 3, 5 and 6, good results were achieved without weighting factors.

As already mentioned, alternative hierarchical algorithms differ in the way the distance between already formed clusters is calculated. In the proposed methodology, the single linkage is used. With this option, the distance between two clusters is equal to the smallest distance between objects inside the two clusters (this distance is also calculated with equation (2.94)).

The above defined rules permit the construction of the hierarchical tree. The next step is the selection of the tree cut level. This is usually dependent on the expected number of clusters. However, in the present application it is impossible to estimate that number. It is feasible to have an estimate of the number of physical modes, but in the application of the method, it will be observed that some clusters are used to group spurious mode estimates, whose quantity is impossible to predict. Therefore, the criterion used to prune the branches of the hierarchical tree consists of imposing a maximum limit for the distance between any point and its closest point of the same cluster.

The lower is the limit the higher is the number of resulting clusters. As a consequence, if the distance is too small, estimates associated with the same physical mode might be split in several clusters. Generally, distances lower than one avoid the inclusion of estimates for different physical modes in the same cluster, as the MAC between the corresponding mode shapes should be close to zero (assuming that the number of measured points is not very limited).

After this step, several groups of modal estimates are obtained. It is now important to distinguish the groups that contain estimates associated with physical modes from the ones that contain numerical or spurious estimates. This separation is usually easy, because the estimates associated with physical modes are very consistent for models with different orders. Therefore, the groups that contain estimates of physical modes present a much higher number of members than the groups that contain numerical estimates, which present a higher scatter between models of different orders. Normally, the number of physical modes (n_m) expected in the frequency range of analysis can be anticipated (for instance by a simple preliminary frequency domain analysis), thus the n_m groups with more elements are selected.

Until now, the modal damping estimates were not taken into account. As a consequence, in the modal estimates stored in the groups associated with physical modes, we may expect to find some extreme values of modal damping ratios. These are removed by an outlier analysis (Johnson and Wichern 1992) performed within all selected clusters, which eliminates the mode estimates with modal damping ratios below the lower quartile limit minus 1.5 times the interquartile range or above the upper quartile limit plus 1.5 times the interquartile range (25 % of the values are below the lower quartile limit, 25 % of the values are above the upper quartile limit and the interquartile range is the distance between the upper and lower quartile limits).

The final outputs of the proposed methodology are the average values of the modal parameters (natural frequency, modal damping ratio and mode shape) corresponding to the estimates that belong to the same selected cluster.

As it was presented, this method does not require the previous construction of a stabilization diagram, because all mode estimates, stable or unstable, are considered. In chapters 5 and 6, it will be shown that this version performs very well in real applications. It has the great advantage of requiring only two user-defined parameters, which are the maximum limit for the distance between any point and its closest point of the same cluster and the number of expected modes (if this number is not known it can be defined in a conservative way).

However, it can also be applied after the construction of a stabilization diagram, considering as inputs for the cluster analysis only the stable poles. This might increase the quality of the results in more demanding applications with, for instance, higher levels of noise, especially if some additional criteria, besides the relative variations of the modal parameters, are used in the classification of the stable poles (some possibilities are referred in section 2.4.1). This alternative approach has the disadvantage of requiring much more user-defined parameters: all the criteria adopted for the selection of stable poles.

At the end of this section, it has to be pointed out that all the methodologies that automate the identification of modal parameters need some tuning that depends on the particular characteristics of the tested structure and consequently it is unrealistic to think that it is possible to process a new dataset from an unknown structure without any first human judgment. However, once the algorithm has been trained for a typical dataset of a particular dynamic system, it can be successfully applied on similar datasets of the same system.

Then, the proposed methodology is illustrated with simulated data; its capabilities to deal with real data are proven with the applications presented in chapters 3, 5 and 6.

Illustration with simulated data

The evaluation of the performance of the SSI-COV and p-LSCF methods (sections 2.3.4 and 2.3.5) was based on the automatic processing of several simulated datasets. This was done using the previously presented methodology. Here, its application to a dataset of model SM (see Figure 2.10) processed by the SSI-COV method is illustrated.

Figure 2.27 presents the most relevant steps. The stabilization diagram represents the natural frequencies values of all mode estimates (stable and unstable) provided by models with even orders between 2 and 20. These are the inputs for the application of the clusters algorithm. The groups created by the cluster analysis are characterized by the mean natural frequencies of the mode estimates inside each group and the number of elements of the group (second plot). Two groups stand out; these contain the poles that are associated with physical modes (the two modes of the two degree of freedom model with natural frequencies around 1.3 and 1.5 Hz). The elements inside the two selected groups are represented in a natural frequency vs modal damping ratio diagram. In this particular case, the damping values of the elements inside the same group are very consistent (around 1 and 2%), so the elimination of outliers is not necessary.

In all the processed simulated datasets the distance between any point and its closest point of the same cluster, calculated with equation (2.94), was limited to 0.001. Such a low value is only possible with simulated data. In the applications to real data it is demonstrated that this parameter has to be higher.

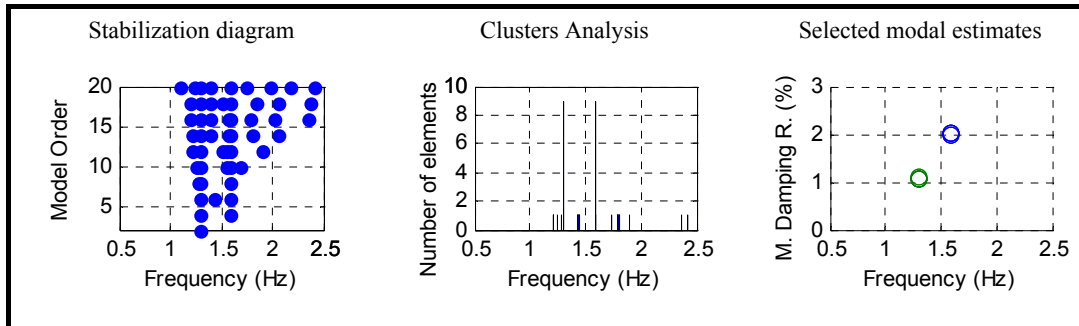


Figure 2.27 – Steps of the proposed methodology for automated OMA.

The application of this methodology together with the p-LSCF method leads to similar plots. The major difference is that the majority of the numerical poles are eliminated before the application of the cluster analysis due to their negative damping.

2.5 Merging Strategies for Multiple Setup Tests

2.5.1 Introduction

Ambient vibration tests of civil engineering structures usually involve the need to measure the structure response to ambient excitation at a large number of points so that the mode shapes can be characterized with enough spatial resolution. The limited number of available sensors or acquisition channels imposes the development of several setups with the sensors in different positions. Because in this type of test the excitation is not controlled, and it can vary in intensity or frequency content from one setup to the other, it is necessary to keep some sensors in the same positions during the entire test. As already referred in section 2.3.2, these are designated reference sensors and cannot be placed at the nodes of the mode shapes to be estimated. In short, during an ambient vibration test, a group of sensors (reference sensors) is permanently placed in the same positions, while the remaining sensors (moving sensors) are moved until the whole defined measurement grid is covered.

The classical strategy to deal with data collected during ambient vibration tests composed by several setups consists in processing the signals of each setup separately, therefore obtaining a set of modal parameters for each setup. The mode shape components identified in each setup are then ‘glued’ back together using the mode shape components at the reference sections identified in all the performed setups. When a large number of setups is involved, as it is the case of the applications presented in chapter 3, this approach becomes very time consuming because of the number of analyses that have to be performed, one for each setup, and due to the need to pair the results obtained in each individual analysis. This last step is not always evident because in some setups some modes may be missing.

Therefore, with the goal of developing techniques to make the processing of data collected during ambient vibration tests of large structures based on a significant number of setups more efficient, an increasing interest on procedures that permit the processing of all collected datasets with just one analysis has been observed during the last few years.

This section starts with the description of the classical approach, designated Post Separate Estimation Re-scaling (PoSER), and then characterizes two alternatives methodologies to process data from several setups together: Post Global Estimation Re-scaling (PoGER) and Pre Global Estimation Re-scaling (PreGER). These three approaches are also systematized in (Parloo 2003). Finally, a new combined methodology is presented.

2.5.2 Post Separate Estimation Re-scaling

The Post Separate Estimation Re-scaling (PoSER) strategy, whose principles have been used in the context of ambient vibration tests of civil engineering structures for a long time (Felber 1993), is schematically described in Figure 2.28 (adapted from (Parloo 2003)). This is the methodology that is available in well known software packages for operational modal analysis (e.g. Artemis commercialized by SVS, MACEC developed in K. U. Leuven and Test.Lab commercialized by LMS).

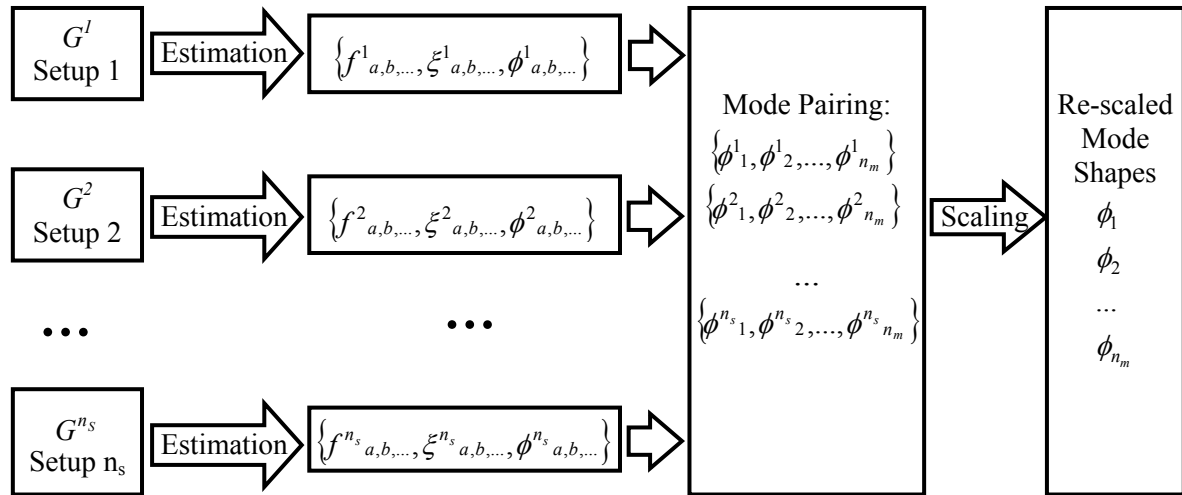


Figure 2.28 – Classical re-scaling procedure (PoSER).

The symbols G^j , with $j = 1, \dots, n_s$, where n_s is the total number of setups, represent the inputs of the algorithm used in the identification of the modal parameters, which can be correlation matrices or (positive) spectrum matrices. $\{f^j_{a,b,\dots}, \xi^j_{a,b,\dots}, \phi^j_{a,b,\dots}\}$ represent the modal parameters (natural frequencies: f ; modal damping ratios: ξ , and mode shape segments: ϕ) identified in setup j .

The development of n_s analyses provides n_s sets of modal parameters. Theoretically, even assuming variations in the intensity and frequency content of the excitation, the natural frequencies and modal damping ratios identified from data of different setups should coincide. However, in real applications some variations are noticed. These are explained by a not perfect linear behaviour of the structure, by the influence of environmental factors, like the temperature, or by extra masses, for instance due to varying traffic intensity in the case of a bridge test. Furthermore, it may happen that not all the modes are identified in all setups. Therefore, a procedure has to be adopted to map the mode estimates of each setup (a, b, \dots in Figure 2.28) to the physical modes of the tested structure ($1, 2, \dots, n_m$ in Figure 2.28). Usually, the results of one setup k , where all the relevant modes of the structure have been successfully identified, are used as reference and then, the estimates of the remaining setups are mapped with these reference results. This mode pairing should take into account the natural frequencies and also the mode shape components at the reference outputs.

Finally, for each mode, it is obtained a set of mode shape segments with some common components. Thus, for each mode, the mode shape segments have to be scaled by a factor that minimizes the differences between the common components of all the segments. If the scale of the modes of setup k is used as reference, then the following expression can be used:

$$\phi_i^{j \rightarrow k} = \alpha_i^{j \rightarrow k} \cdot \phi_i^j$$

with
$$\alpha_i^{j \rightarrow k} = \frac{(\phi_i^{j,ref})^H \cdot (\phi_i^{k,ref})}{(\phi_i^{j,ref})^H \cdot (\phi_i^{j,ref})} \quad (2.95)$$

where the vector $\phi_i^{j,ref}$ contains the mode shape components of mode i at the reference outputs evaluated in setup j .

At the end, for each mode i ($i = 1, \dots, n_m$) it is obtained a complete mode shape according to the expression:

$$\phi_i = \begin{bmatrix} \phi_i^{k,ref} \\ \phi_i^{1 \rightarrow k,mov} \\ \phi_i^{2 \rightarrow k,mov} \\ \vdots \\ \phi_i^{n_s \rightarrow k,mov} \end{bmatrix} \quad (2.96)$$

where $\phi_i^{j \rightarrow k,mov}$ is a vector with the scaled mode shape components of mode i at the points where the moving sensors were placed during setup j .

The estimates of natural frequencies and modal damping ratios associated with the different setups can be used to obtain average values and to quantify the scattering of these modal parameters during the test period.

This methodology has the disadvantage of requiring a very heavy analysis effort when a large number of setups is processed, which, in the case of a parametric method, involve the tedious task of interpreting many stabilization diagrams. However, it has the advantage of characterizing the scattering of natural frequency and modal damping ratio estimates during the period of the ambient vibration test. The observed variations are due to the uncertainty of the estimates and also to the influence on modal parameters of environmental (e.g. temperature) or operational factors (e.g. traffic intensity over a bridge) that may vary during the dynamic test.

2.5.3 Post Global Estimation Re-scaling

The Post Global Estimation Re-scaling (PoGER) procedure, characterized in Figure 2.29, is the simplest approach that permits to process data collected during several setups with just one analysis.

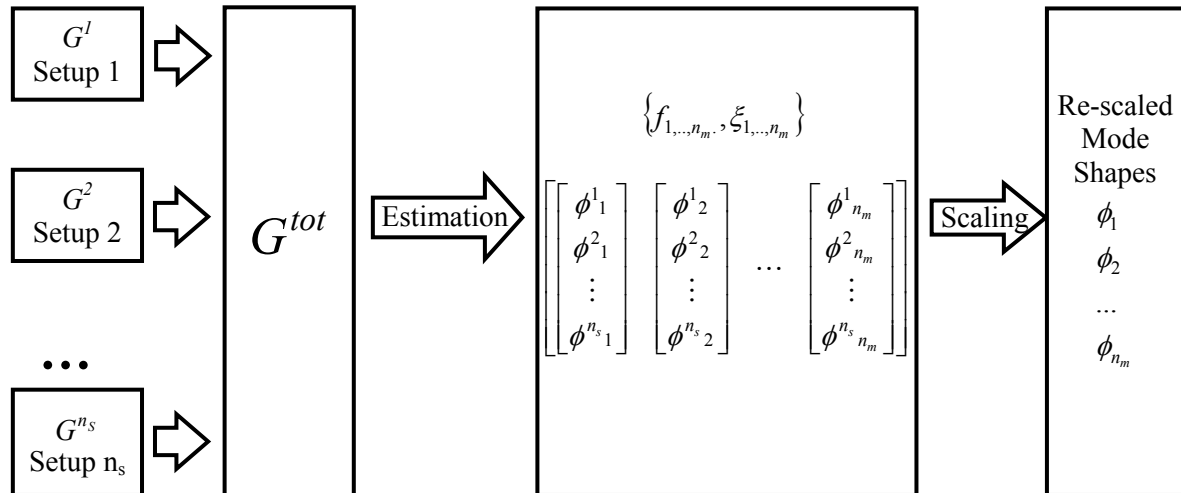


Figure 2.29 – Post Global Estimation Re-scaling (PoGER).

In a first step, the matrices G^1 to G^{n_s} , which can be correlation or (positive) spectrum matrices with n_o lines and n_r columns, are stored in a global matrix:

$$G^{tot} = \begin{bmatrix} G^1 \\ G^2 \\ \vdots \\ G^{n_s} \end{bmatrix} \quad (2.97)$$

This large matrix ($n_o \cdot n_s$ -by- n_r) is used as input for the estimation algorithm. The identification provides natural frequencies, modal damping ratios and modes shapes of n_m modes. However, each obtained mode shape is composed by n_s blocks that contain the mode shape segments measured in each setup, comprehending the components associated with both the reference sensors and the moving sensors. Thus, the components at the reference outputs are repeated n_s times. Because no previous scaling was applied, the segments are not at the same scale. But, again the mode shape components at the reference outputs can be used to re-scale all the segments to a common level. This is done using the same procedure that is adopted in the previously described strategy, with equation (2.95). Final complete mode shapes estimates are also given by equation (2.96).

This methodology makes the identification of modal parameters much more straightforward, because only one stabilization diagram has to be analysed and the mode pairing procedure is avoided. Practical applications show that the stabilization diagram provided this single analysis present clearer vertical

alignments of stable poles than the ones observed is stabilization diagrams associated with just one setup (see chapter 3). Therefore, its interpretation is facilitated.

Nevertheless, the use of large matrices makes this method more computationally demanding, especially in terms of memory requirements. Moreover, as only one set of modal parameters is obtained, the variation or uncertainty of the natural frequency and modal damping ratio estimates during the ambient vibration test is not characterized.

2.5.4 Pre Global Estimation Re-scaling

The Pre Global Estimation Re-scaling (PreGER) approach is another alternative based on a global estimation of modal parameters. In this case, the correlation or the (positive) spectrum matrices, estimated from the signals collected during the developed setups, are scaled before the identification. Consequently, the obtained mode shapes do not need any further post-processing; the results of the identification are the final modal parameter estimates. The algorithm steps are represented in Figure 2.30.

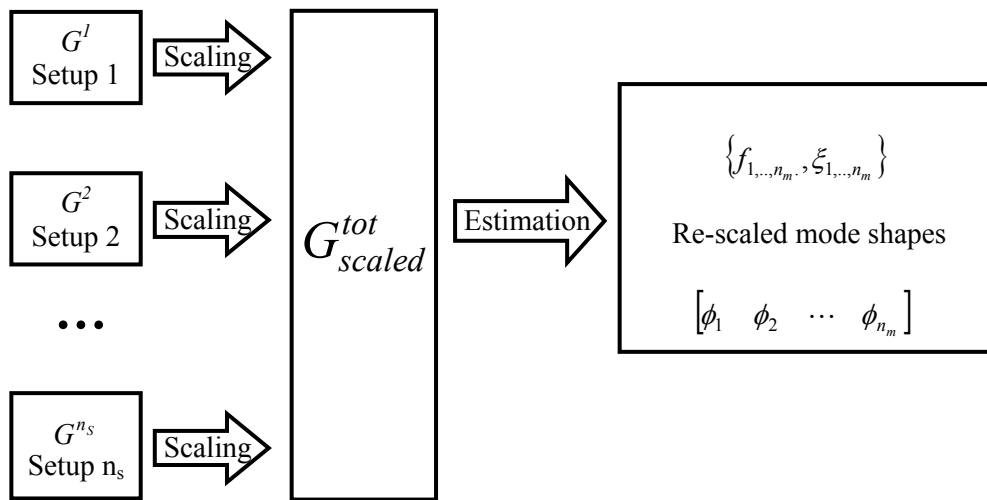


Figure 2.30 – Pre Global Estimation Re-scaling (PreGER).

In the case of the frequency domain methods the scaling of the (positive) spectrum matrices is quite simple. Placing the reference outputs in the first lines of the output spectrum matrix, the spectrum matrices of all the setups S^j can be divided in two blocks: $S^{j,ref}$ with the auto and cross-spectra between the reference outputs and $S^{j,mov}$ with the cross-spectra between the other outputs (not reference) and the reference outputs.

Then, the scaling of the $S^{j,mov}$ matrices is performed with the following operation (Parloo 2003):

$$S_{scaled}^{j,mov} = S^{j,mov} \cdot (S^{j,ref})^{-1} \cdot \left(\frac{1}{n_s} \cdot \sum_{k=1}^{n_s} S^{k,ref} \right) \quad (2.98)$$

The first multiplication of the previous equation eliminates the poles of the system. These are then recovered through the multiplication of the result by an average output spectrum matrix that contains the contributions of the spectra between the reference outputs of all the setups. The total spectrum matrix used in the identification contains the average spectrum matrix of the reference outputs and the scaled spectrum matrices with the cross-spectra of the outputs measured by the moving sensors:

$$S_{scaled}^{tot} = \begin{bmatrix} \frac{1}{n_s} \cdot \sum_{k=1}^{n_s} S^{k,ref} \\ S_{scaled}^{1,mov} \\ \vdots \\ S_{scaled}^{n_s,mov} \end{bmatrix} \quad (2.99)$$

If correlation matrices are used, the strategy described in (Dohler et al. 2010; Mevel et al. 2002) can be adopted. The correlation matrices calculated from time series collected in different setups are scaled to a common excitation level through the use of controllability matrices (see equation (2.71)), which can be derived from the decomposition of a Toeplitz matrix filled with correlation functions between the reference outputs calculated from the time series collected at the reference *dof* during all the developed setups.

In the PreGER approach the lines of the correlation or spectrum matrices with the reference outputs are not repeated n_s times, as it happens in the PoGER approach, so it has the advantage of using a smaller matrix in the identification, which significantly reduces the amount of memory required for the data processing.

2.5.5 A Combined Methodology

Considering the advantages and disadvantages of the separated and global estimation approaches and taking profit from the algorithm presented in section 2.4.4, a new methodology that combines both strategies is proposed.

Firstly, a global estimation approach is applied to the collected data. This provides a single estimate for each natural frequency and corresponding modal damping ratio and complete mode shapes. Then,

with the goal of characterizing the variation of the modal parameters during the ambient vibration test period, each setup is analysed separately using the algorithm previously presented to automatically process the information stored in stabilization diagrams. The algorithm parameters are tuned with one typical setup and then applied to the remaining setups. Because a set of reference modal parameters is already available, only the clusters that contain mode estimates that are close to the reference values (close means similar natural frequencies and mode shape components at the reference *dofs*) are selected.

With this combined methodology, global mode shapes are obtained without having to go through a mode paring procedure and the scattering of the natural frequencies and modal damping ratios is characterized without requiring the manual analysis of several stabilization diagrams. This last information is also very important to roughly characterize the level of uncertainty associated with the global estimates.

In chapter 3 this methodology is applied in the processing of a large database collected at the Humber Bridge.

2.6 Final Considerations

This chapter starts with a brief presentation of the mathematical formulations that can be used to model linear time-invariant dynamic systems excited by deterministic or stochastic forces. These constitute the theoretical background of the identification algorithms that are then presented. Three algorithms commonly used for operational modal analysis are described with some detail: a non-parametric method (FDD), a parametric method in the time domain (SSI-COV) and a parametric method in the frequency domain (p-LSCF). The description of the identification methodologies is followed by numerical studies based on simulated data that permitted the evaluation of the performance of the methods and of the influence of the user-defined parameters on the quality of the results. From the analysis of the obtained results it was possible to establish some rules that facilitate the selection of the parameters to be defined by the analyst during the application of the identification algorithms.

Afterwards, it is presented a new methodology to perform the identification of modal parameters automatically, so that operational modal analysis can be used in the context of continuous dynamic monitoring systems. This is described after a review of the previously available approaches and the explanation of the adopted statistical tool: Clustering Analysis. The proposed methodology is adequate to be used together with any parametric identification technique that bases the identification of the modal parameters on several models with different orders, being therefore an alternative to the manual interpretation of stabilization diagrams.

Finally, different strategies to merge data from multiple setups are presented. More efficient alternatives than the traditional procedure based on the separated analysis of each setup are described. These are especially relevant to process data collected during ambient vibration tests of large civil engineering structures that usually involve the development of a considerable number of setups. A new methodology that permits an efficient global processing and, at the same time, the characterization of the modal parameters scatter during the test is proposed.

In short, this chapter presents the most important processing tools that are then extensively used in the applications described in the following chapters.

Chapter 3

AMBIENT VIBRATION TESTS



3. AMBIENT VIBRATION TESTS

3.1 Introduction

Ambient vibration tests are practical and economical dynamic tests that permit an accurate identification of modal parameters of civil engineering structures without disturbing their normal operation. Therefore, nowadays, these tests are usually performed after the construction of important infrastructures for finite element model validation, before rehabilitation works to better characterize the structure and tune its numerical model or in the context of inspection programs to evaluate the safety of existing structures. Beyond that, they provide experimental information that can be used for the design and tuning of vibration control devices, for the configuration of dynamic monitoring systems and for the definition of a set of dynamic properties of the initially non-damaged structure at the commissioning stage, which may then be used for the application of vibration-based damage detection techniques.

The identification of modal properties of civil engineering structures from ambient vibration has already been used for a long time. The following pioneering applications are documented on the available bibliography: identification of the natural frequencies of a 14-storey building (Crawford and Ward 1964); evaluation of natural frequencies, mode shapes and modal damping ratios from the analysis of spectra derived from ambient measurements performed on two suspension bridges (MacLamore et al. 1971); and comparison of the results provided by ambient and forced vibration tests on two buildings (Trifunac 1972). Since these first applications, very complete ambient vibration tests have been performed worldwide on several outstanding bridges, as for instance the Golden Gate Bridge (Abdel-Ghaffar and Scanlan 1985), after the very innovative ambient vibration measurements performed by Carter (1937) on the same structure, the Humber Bridge in the U.K. (Brownjohn et al. 1986), both Bosphorus Bridges (Brownjohn et al. 1989; Brownjohn et al. 1992), the Ganter Bridge in Switzerland (Felber and Cantieni 1996) or the Tsing Ma suspension bridge in Hong Kong (Xu et al. 1997), just to mention some of the studies performed at the end of the last century.

In Portugal, the first experimental studies developed with the aim of identifying structural dynamic characteristics were performed by the National Laboratory of Civil Engineering (LNEC) and date back to 1954, when the first natural frequency of a bridge was derived from strains measured after the passage of a truck over a bump (Marecos 1954). The early tests of the Tagus Suspension Bridge (Marecos et al. 1967) and the first dynamic test on a Portuguese Dam (Pereira 1962) are also of special historical relevance. The ambient vibration tests more recently performed by LNEC on several Portuguese structures (including bridges, dams and buildings) are reported in (Rodrigues 2004). The

Faculty of Engineering of the University of Porto (FEUP), in the context of the research and consultancy activities of the Laboratory of Vibrations and Monitoring (ViBest), has also been involved in the performance of ambient vibration tests on several outstanding Portuguese structures, as for instance, the Vasco da Gama cable-stayed Bridge (Cunha et al. 2001), the Luiz I Bridge before and after rehabilitation works (Cunha and Calçada 2000; Cunha et al. 2006), the Guadiana cable-stayed Bridge (Magalhães et al. 2007a) and the suspended roof of the Braga Stadium (Magalhães et al. 2008c).

Despite the already long history of ambient vibration tests, there are still several issues that need further research. The use of sophisticated parametric system identification algorithms in civil engineering structures is recent and still needs to become more mature throughout the performance of more practical applications. Furthermore, the developments of the acquisition hardware have permitted to obtain with little effort large databases that have to be processed in an efficient way. Therefore, there is the need to develop and test processing methodologies suitable to deal with large quantities of data.

Taking this in mind, in section 3.3 and 3.4 of this chapter, databases recently collected during the ambient vibration tests of two large structures, the Millau Viaduct and the Humber Bridge, are processed with the identification algorithms presented in chapter 2 and previously implemented in Matlab routines. Special emphasis is given to the evaluation of procedures that process several datasets together, as these permit a much more efficient analysis of large databases. The description of the two applications is preceded by a synthesis of the experimental procedure usually followed in ambient vibration tests and by a brief description of the more commonly adopted equipment.

Although modern output-only modal identification techniques, in conjunction with the use of appropriate state-of-the-art vibration measurement equipment, can provide very accurate estimates of natural frequencies and mode shapes, it is usually observed that the corresponding damping estimates present a significant scatter. Therefore, more research studies are needed to better evaluate the quality of the modal damping ratio estimates that is possible to achieve with ambient vibration tests, in particular through the comparison of the obtained values with the ones provided by the less practical but more precise free vibration tests.

As a consequence, the last section of this chapter (3.5) compares modal damping ratio estimates based on ambient and free vibration tests using data collected on large civil engineering structures where both tests were performed. The analysis involves the processing of data collected on two cable-stayed bridges, on a steel roadway bridge, on a footbridge and on the suspended roof of a stadium.

3.2 Experimental Procedure and Equipment

The experimental procedure followed in ambient vibration tests is quite simple. The ambient response of the structure under study is captured by one or more reference sensors, at fixed positions, together with a set of moving sensors, placed at different measurement points along the structure, in different setups. The number of instrumented points is conditioned by the spatial resolution needed to appropriately characterize the shape of the most relevant modes of vibration (according to preliminary finite element modelling), while the reference points must be conveniently far from the corresponding nodal points.

The selected sampling frequency is usually conditioned by characteristics of the adopted equipment. In order to avoid aliasing errors (Maia and Silva 1997), it should be higher than at least two times the highest frequency captured by the sensors or the cutting frequency of analog low pass filters that might be included in the measuring chain. The chosen sampling frequency also limits the number of modes that can be identified, as only the modes with a frequency lower than one half of the sampling frequency are observable.

Finally, the length of the time series collected in each setup has to be chosen. The numerical simulations performed in chapter 2 showed that this parameter has an important influence on the estimates of modal parameters, especially relevant on the random error of modal damping ratio estimates. The numerical simulations also demonstrated that the optimal length depends on the lowest natural frequency, on the modal damping ratios, on the signal-to-noise ratio and also on the adopted identification algorithm (parametric methods can provide better results with shorter time series than for instance the FDD method). Therefore, it is very difficult to establish a universal rule. Furthermore, in most of the cases, the adopted time length is conditioned by the time available to perform the test. A rule of thumb suggested by experienced researchers (Cantieni 2005) states that the length of the acquired time windows should be 1000 to 2000 times the period of the fundamental natural frequency of the tested structure. However, the extremely low natural frequencies of the applications presented in this chapter and constraints on the time available for the performance of the ambient test forced the adoption of time series with a length of about 180 times the period of the mode with the lowest frequency. Still, it will be shown that good results could be obtained.

With regard to the necessary equipment, the most important components are the sensors. The structure vibration can be measured in displacements, velocities, accelerations or even strains, but accelerations are usually preferred. Despite the large variety of acceleration sensors based on different working principles (piezoelectric, capacitive or force-balance) with adequate characteristics to measure ambient

vibrations (Maia and Silva 1997; Rodrigues 2004), the most appropriate sensors for ambient vibration tests in civil engineering structures are the force-balance accelerometers. These sensors present a measuring range that starts at DC, which means that they are sensitive to the very low natural frequencies found in flexible structures (in the application that is presented in section 3.3, a frequency of 0.05Hz is identified), are conceived to be insensitive to high-frequency vibrations and their high sensitivity and low noise make them appropriate to measure the low levels of vibration usually observed during dynamic tests where no kind of external artificial excitation is used.

In traditional measuring chains, the continuous electrical signal produced by each sensor is transported by electrical cables to a central acquisition system (Figure 3.1). The central acquisition system comprehends one or several analog-to-digital converters that transform the continuous signals into discrete sequences of numbers, which may then be processed in any computer. The most important characteristic of the analog-to-digital converter is its number of bits, as it is directly related with the measurement resolution (the resolution is approximately equal to the measuring range divided by two to the power of the number of bits). The acquisition system may also contain electric circuits to pre-process the analog signals before digitization, as for instance low pass filters or signal amplifiers. If force-balance sensors are adopted, the central system or some distributed batteries should also provide the power necessary for the correct functioning of this type of sensors.

Although most of the ambient tests performed worldwide in large civil engineering structures have been based on the use of long electrical cables connecting the sensors to a central acquisition system, the implementation of this type of solution is rather cumbersome and time consuming. Therefore, there is presently a natural tendency to develop wireless architectures or at least reduce drastically the cables length by introducing local digitization and single cable signal transmission.

A very efficient and comfortable alternative has been intensively used by FEUP (Cunha et al. 2007) and LNEC (Rodrigues 2004). This solution is based on a set of portable autonomous recorders (Figure 3.2) that avoid the use of cables and minimize the labour associated with the preparation and execution of the dynamic test. These devices are constituted by a very sensitive internal or external tri-axial force balance accelerometer, a 18 or 24 bit analog-to-digital converter (to guarantee high sensitivity), a rechargeable battery that enables autonomy for one day of tests, a removable Compact Flash card where the acceleration time series are recorded that permits a fast download of the acquired data, and an external GPS sensor to ensure an accurate time, so that several units can work independently and synchronously. At the beginning of the test, the recorders are programmed to record a certain number of time series (equal to the number of planned setups) with a defined length and time interval between successive acquisitions. During the test, the time gap between successive acquisitions is used to

change the position of the moving recorders. At the end of the test, the files stored in the memory cards (one file per setup and recorder) are transferred to a computer and after being converted to ASCII files are ready to be processed. The two ambient vibration tests that will be described in sections 3.3 and 3.4 as well as most of the applications presented in section 3.5 were performed with this equipment.



Figure 3.1 – Equipment for ambient vibration tests based on a central acquisition system (Wenzel and Pichler 2005).

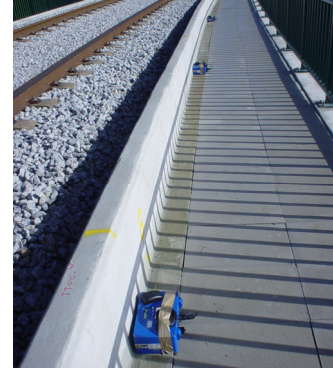


Figure 3.2 – Three portable autonomous recorders from Geosig (www.geosig.com) during the ambient vibration test of a railway viaduct.

Other practical solutions for the performance of ambient vibration tests are documented in references (Pakzad and Fences 2009; Whelan et al. 2009) and (Gentile and Bernardini 2008). The first two report the use of networks of wireless sensors based on MEMS accelerometers, whereas the last one describes a non-contact measuring system based on a radar sensor adequate to simultaneously measure the dynamic displacement of several points of a structure with high sensitivity.

The data collected during ambient vibration tests is then processed by the output only identification algorithms presented in chapter 2. In spite of the existence of commercial software where some of the described algorithms are implemented, as Macec (Reynders et al. 2008b), Artemis (www.svibs.com) or Test.Lab (www.lmsintl.com), in this work all the identification techniques introduced in the previous chapter were implemented in Matlab. This permitted to obtain a deeper knowledge of the standard algorithms, to develop alternative algorithms and at the end to obtain a set of tools that are more complete than the ones available in commercial software. For instance, the global estimation procedures are not implemented in the mentioned software packages. Therefore, the majority of the results presented throughout this work derived from the use of the programmed Matlab routines.

3.3 Millau Viaduct

3.3.1 Introduction

The Millau Viaduct (Figure 3.3) is an outstanding multi-span cable-stayed bridge located in southern France that opened to traffic in 2004. It integrates a new highway connection between Northern Europe and East Spain providing a link between Clermont-Ferrand and Béziers over the valley of River Tarn near Millau. The concept of this unique structure was first proposed by the bridge designer Michel Virlogeux. The final project was then developed by a multidisciplinary team that included the architect Norman Foster.

Due to the necessity of achieving very accurate estimates for the dynamic properties of this exceptional structure (natural frequencies, mode shapes and modal damping ratios), in order to experimentally validate the finite element modelling developed at the design stage and have a good baseline structural characterization, dynamic tests were performed at the commissioning phase, under the coordination of the Centre Scientifique et Technique du Bâtiment (CSTB). The Laboratory of Vibrations and Monitoring (ViBest) of FEUP was invited to collaborate in these dynamic tests and performed an independent ambient vibration test that complemented the free vibration tests previously planned by the French laboratory.

This section (3.3) is mainly focused on the application of output-only modal identification methodologies to the database collected during the ambient vibration test of this structure. Therefore, after a brief description of the structure and of the performed dynamic tests, the results obtained by the independent processing of the data collected in each setup of the AVT are compared with the estimates provided by two alternative methodologies to process all setups together. The experimentally identified modal parameters are also correlated with their numerical counterparts extracted from a finite element model developed at the design stage. In section 3.5.3, data collected during free vibration tests is processed and the obtained modal damping ratios are compared with the estimates achieved with the ambient vibration test.



Figure 3.3 – General view of the Millau Viaduct (from www.eiffage.fr).

3.3.2 Bridge Description

The Millau Viaduct is the tallest vehicular bridge in the world, with the top of a pylon rising at 343m above the river level (Figure 3.4). It comprehends seven concrete piers that range in height from 77 to 245m (Figure 3.5). In order to resist the high bending moments, these extremely high elements were designed as wide strong box-sections (27 by 17 meters at the base of the tallest pier) that split into two flexible shafts in the upper last 90m (Figure 2.2). Each pier supports a steel pylon with a height of about 90 meters.

This viaduct with a total length of 2460m is also the longest cable-stayed bridge in the world. It comprehends eight spans: two side spans 204m long and six intermediate spans of 342m (Figure 3.5). The deck is an orthotropic steel box-girder with constant dimensions: 32m wide and 4.2m thick. It carries two lanes of traffic in each direction and is equipped with wind screens designed to limit the wind action over the vehicles and to improve the aerodynamic behavior of the structure (Virlogeux et al. 2005). The box girder is vertically supported by the stay-cables anchored in its center and is tied down to the piers by vertical prestressing tendons in line with the two fixed bearings on each shaft.



Figure 3.4 – Millau Viaduct over the valley of river Tarn; views of the tallest pier.

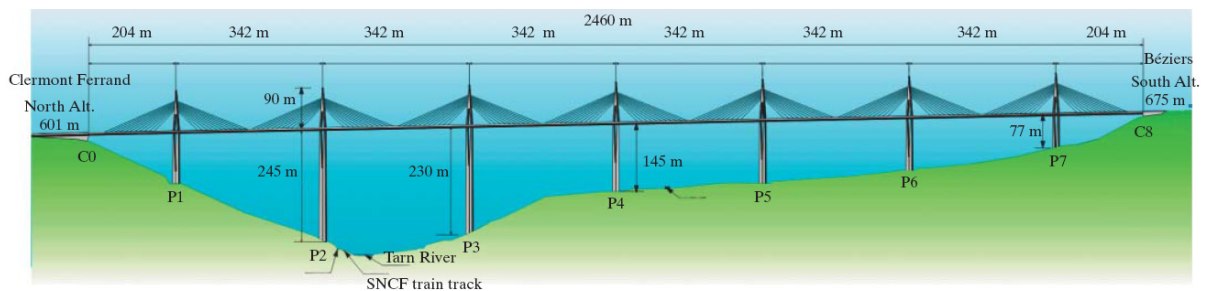


Figure 3.5 – Millau Viaduct elevation (Virlogeux et al. 2005)

3.3.3 Dynamic Tests

The dynamic tests of the Millau Viaduct started with the development of an ambient vibration test. This test took place on the 24th of November 2004 and was based on the use of four GSR-18 recorders from Geosig equipped with internal tri-axial force-balance accelerometers. With the purpose of identifying as many modes of vibration as possible, essentially of vertical and transversal bending nature, with just one day available for this test, the measurement grid was restricted to the bridge longitudinal axis. This time constrain precluded the identification of torsion modes. Two recorders were used as references and therefore were permanently placed at sections R1 and R2 (Figure 3.6), while the other two were successively moved to measure the remaining 26 sections schematically indicated in Figure 3.6. The recorders were programmed to acquire with a sampling rate of 100Hz during periods of 960s in intervals of 20 minutes. The last 4 minutes were used to change the position of the moving sensors. The test lasted approximately 5h, including programming of the equipment and the development of 13 setups. So, it is very relevant to realize that, with the adopted equipment, it took less than one day to perform measurements along the entire length of this large structure. During the test the wind speed was always very low and the traffic very sporadic, as the bridge had not been open to traffic yet.

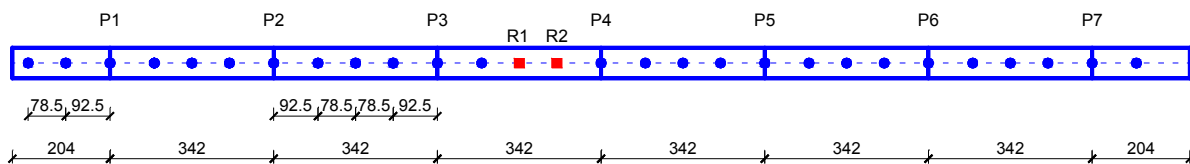


Figure 3.6 – Points of the deck instrumented during the ambient vibration test (top view with indication of the piers position: P1 to P7).

The ambient vibration test was followed by free vibration tests, which were planned and coordinated by CSTB (Flamand and Grillaud 2005). In order to record the free vibration of the structure at as many points as possible three complementary groups of sensors were used (see Figure 3.7): 12 accelerometers from the bridge permanent monitoring system (S1 to S12), 8 accelerometers from CSTB and FEUP (C1 to C8) connected to the acquisition system of CSTB, and three of the recorders used in the ambient vibration test (G1 to G3). The two pairs of accelerometers C2, C4 and G2, G3 were located at the lateral edges of the structure, with the purpose of identifying torsion modes; the remaining sensors were installed along the longitudinal axis of the viaduct.

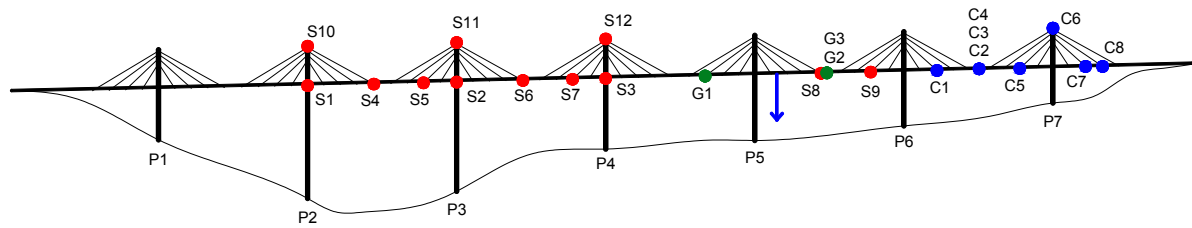


Figure 3.7 – Points instrumented during the free vibration test and point of application of the load (blue arrow).

The free vibration test consisted in the sudden rupture of a cable linking the deck to a counterweight with a mass of 110ton erected on the ground 120m below the deck. This operation was firstly conducted after tensioning the cable with a force of 600kN, using a hydraulic jack installed inside the bridge deck, and then repeated after increasing the force to 1000kN. In both cases, the wind speed was low, oscillating between 2 and 5m/s. The structural response was measured during 960s. Figure 3.7 indicates the point of the deck chosen to hang the cable, which is located at about 1/3 of the P5-P6 span and not centred in the longitudinal axis, so as to excite symmetric and anti-symmetric vertical bending modes and also torsion modes. The data collected during these free vibration tests is processed in section 3.5.3.

3.3.4 Preliminary Analysis

First of all, a preliminary frequency domain analysis was carried out to identify the most relevant natural frequencies and to analyse the variation of the frequency content of the time series collected during 13 setups.

For each setup, two spectrum matrices were calculated, one with the spectra of the collected vertical acceleration time series and another for lateral accelerations. Then, the singular value decomposition of these 4-by-4 spectrum matrices was performed. Figure 3.8 shows for both directions the average singular values spectra and colour maps with the variation of the 1st singular value spectra during the 13 setups of the ambient vibration test. The colour maps are a top view of 13 spectra placed side-by-side where the colour is a function of the spectra amplitude (increasing amplitudes from blue to red). These plots show the existence of a large number of modes in the frequency range 0.1-1.0Hz. Inspection of the colour maps also evidences that not all the modes are clearly present in all the setups. This last fact is important to interpret some of the results presented in the following sections.

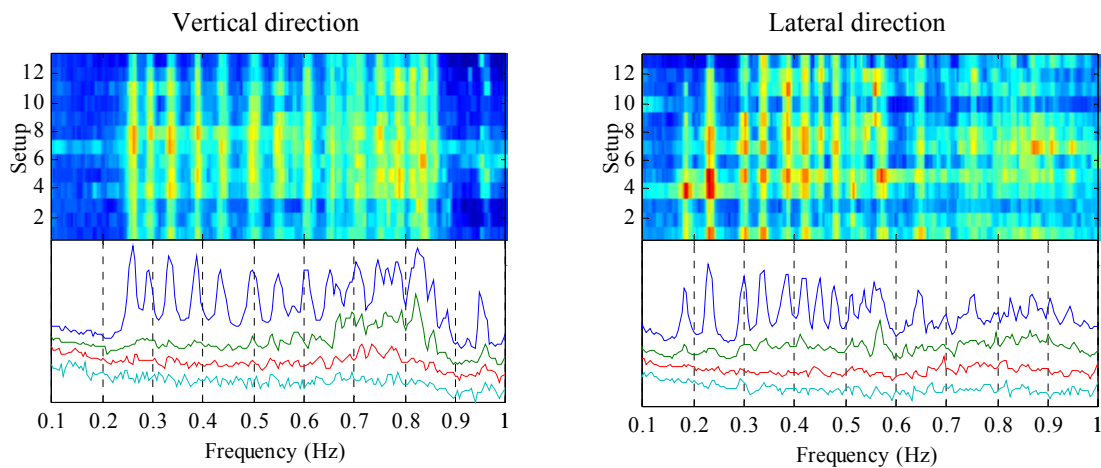


Figure 3.8 – Average singular values of the spectrum matrices and colour maps with the variation of the 1st singular values during the ambient vibration test.

Considering the large number of modes with natural frequencies lower than 1Hz, the application of the identification algorithms was concentrated in the frequency band 0-0.8Hz. Therefore, the acceleration time series originally recorded with a sampling frequency of 100Hz were filtered by an 8th order Butterworth low-pass filter with a cut-off frequency of 0.8Hz and re-sampled with a sampling frequency of 2Hz.

3.3.5 Modal Parameters Identification

The database collected during the ambient vibration test of the Millau viaduct was processed with three different identification algorithms using Matlab routines implemented during the development of the present work. In a first instance, the classical Peak Picking method was used to have quick and rough estimates of the most relevant natural frequencies and mode shapes (Caetano et al. 2004). Then, two parametric identification algorithms were applied: the SSI-COV and the p-LSCF. The results provided by the application of the SSI-COV method are presented in (Caetano et al. 2007). This work details the application of the p-LSCF method using different processing strategies: individual analysis of each setup (PoSER approach) and global analysis of all setups adopting two different scaling procedures (PoGER and PreGER approaches).

The p-LSCF method starts with the calculation of positive spectrum matrices from the sets of acceleration time series measured simultaneously at different locations during each setup. In this application, the elements of these matrices were estimated with the correlogram approach and using the high-speed FFT-based algorithm for the calculation of correlation functions mentioned in section 2.3.2. The transformation of the correlation functions into spectra is preceded by the application of an exponential window to reduce the leakage and the effect of the noisier terms of the tails of the

correlation functions. In the current analysis, exponential windows that reduce the amplitude of the last term of the correlation functions to 1/10 were adopted. Their effect is exemplified in Figure 3.9 with positive auto-spectra estimated from acceleration time series collected at the reference section R2. These spectra were calculated from correlation functions with 256 points, which proved to be a good value for this parameter of the identification algorithm after some preliminary trials with alternative lengths for the correlation functions.

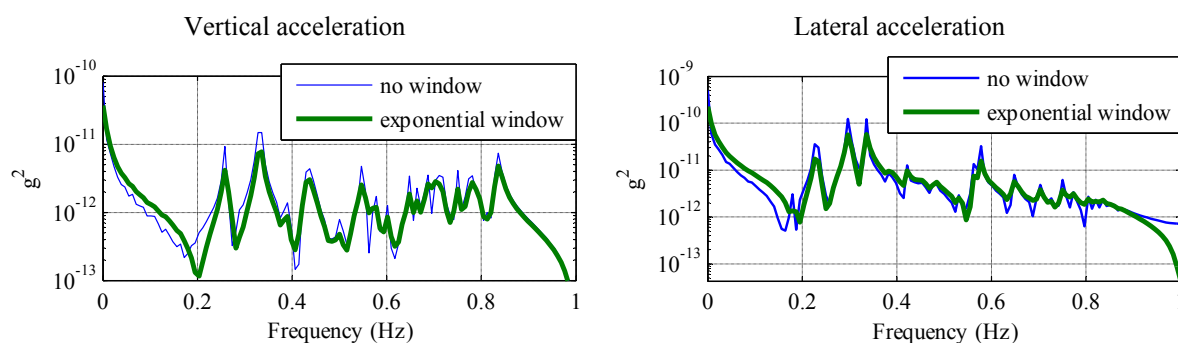


Figure 3.9 – Positive auto-spectra at the reference section R2 estimated from auto-correlation functions with and without the application of an exponential window.

p-LSCF, PoSER

Initially, the p-LSCF method was applied following the traditional methodology, which means that an independent identification was performed with the data collected in each setup. Therefore, the identification algorithm was applied to 13 output positive spectrum matrices. Since only the lateral and vertical accelerations measured at each instrumented section were considered and because the lateral and vertical accelerations at the two reference sections were adopted for reference outputs of the identification algorithm, these matrices have dimensions 8-by-4. Consequently, 13 stabilization diagrams, like the one presented in Figure 3.10, were manually analysed for the selection of a stable pole for each physical mode. As it can be observed in the vertical scale of the stabilization diagram, the polynomial order of the adopted models varied from 1 to 50.

Inspection of this particular stabilization diagram shows that this method was able to identify more than 20 modes in the frequency range between 0.1 and 0.8Hz, where 3 pairs of closely spaced modes are included (with frequencies around 0.30, 0.33 and 0.38Hz).

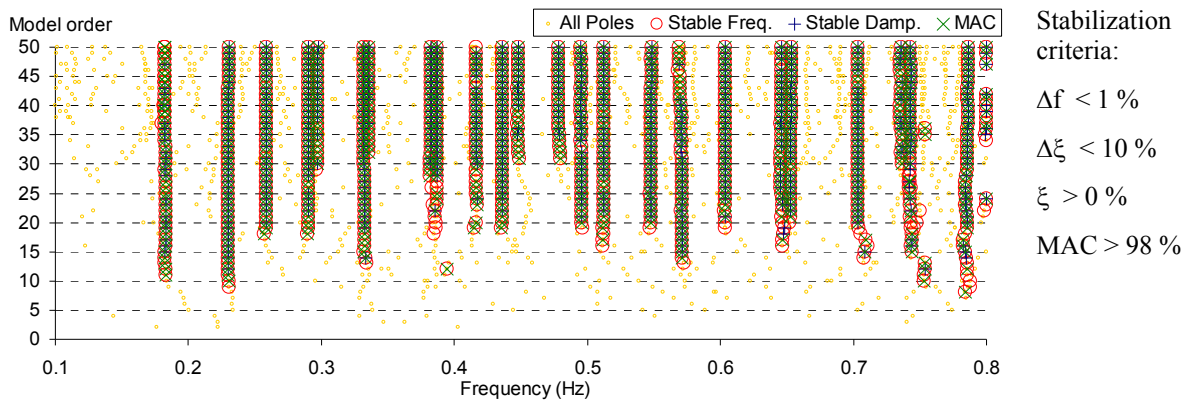


Figure 3.10 – Stabilization diagram of setup 4 with the estimates given by the p-LSCF method.

The analysis of the stabilization diagrams associated to each setup originates 13 sets of modal parameters. In order to have the global picture of the mode shapes, a procedure has to be adopted to find the correspondence between the modal parameters identified in the different setups. This is not straightforward, since not all the modes are identified in all the setups and because the natural frequencies can change their relative order during the test, especially because closely spaced modes are present.

In the present application, the pairing of the modal parameters identified in the 13 setups was done considering the modal parameters identified in one representative setup (setup 4) as target values. Then, for all the other setups the poles with natural frequencies in the vicinity of the target values that presented higher MAC values were chosen. The MAC coefficients were calculated using the reference degrees of freedom.

Figure 3.11 presents all pairs of identified natural frequencies and modal damping ratios. The final estimates of the natural frequencies and modal damping coefficients (values also presented in Figure 3.11) are the averages of the values provided by each setup that were grouped using the previously described procedure. The estimates of the natural frequencies are very similar in all the setups, whereas the modal damping ratios present a significant scatter, expressed by standard deviations around 0.20% (see Table 3.1). This scatter is justified not only by the higher uncertainty associated with the estimates of this parameter (as demonstrated with the simulations presented in chapter 2) but also due to the influence on the modal damping ratios of environmental or operational factors that changed during the ambient vibration test, as for instance the wind characteristics (aerodynamic damping) or the level of vertical excitation.

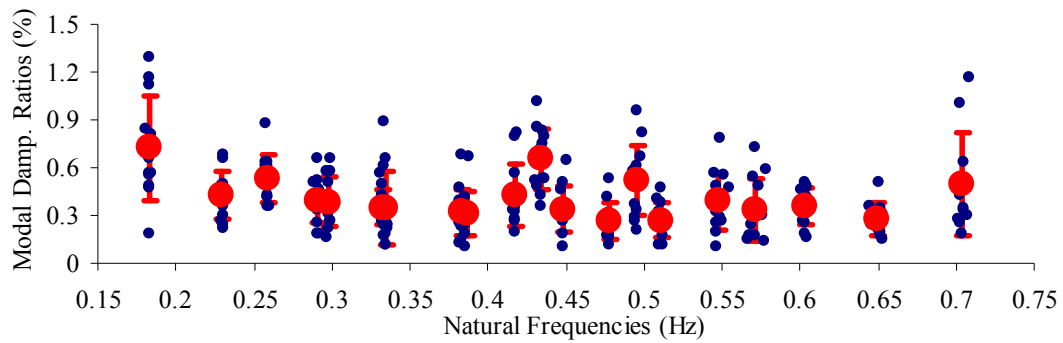


Figure 3.11 – Identified natural frequencies and modal damping ratios: values estimated in each setup (smaller blue dots) and final results represented by the average values (larger red dots) and by an interval of variation for the modal damping ratios based on the standard deviation (average \pm standard deviation).

The global configurations of the mode shapes are obtained after concatenating the components identified in each setup, which are scaled through the ordinates at the reference degrees of freedom (equation (2.95)). Figures 3.12 and 3.13 show some of the identified mode shapes. In particular, the mode shapes of the pairs with closely spaced frequencies are represented to show that this identification technique was able to completely separate the modes. Apart from the 4th vertical bending mode (f_{V4}), all the other vertical and lateral bending modes are of very good quality. In the representation of the 4th vertical mode two mode shape components are missing because this mode was not identified in one of the setups. The colour maps presented in Figure 3.8 had already shown that during some setups the level of excitation was not high enough to efficiently excite some modes.

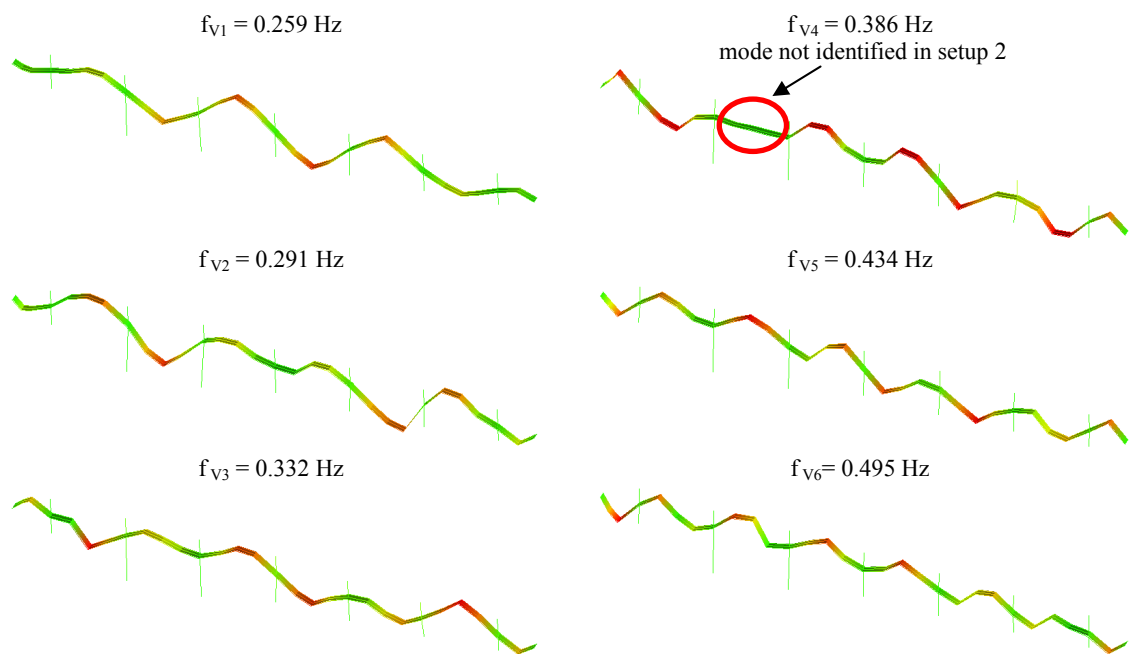


Figure 3.12 – First six vertical mode shapes identified with the PoSER approach (plotted with the Tesl.Lab software)

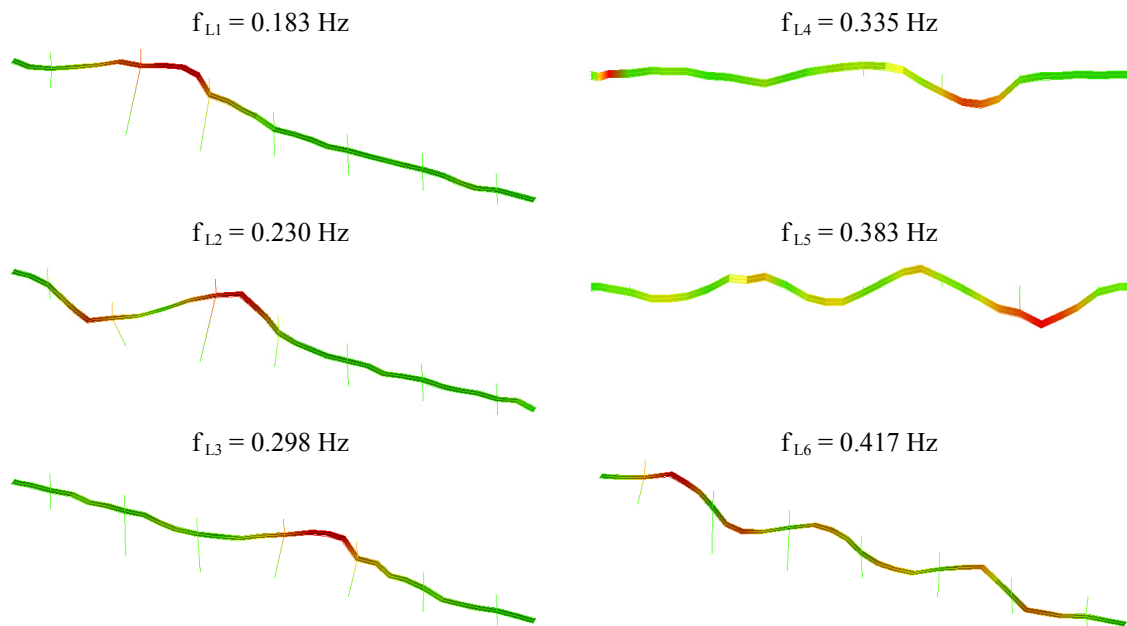


Figure 3.13 – First six lateral mode shapes identified with the PoSER approach (plotted with the Tesl.Lab software)

The existence of setups where some modes are not identified is one of the pitfalls of processing the data collected in each setup separately. Another disadvantage is that the identification is very time consuming, as for instance in this application 13 stabilization diagrams had to be analyzed. In order to try to overcome these drawbacks, the collected database was also processed with global estimation procedures. The obtained results are presented in the following paragraphs.

p-LSCF, PoGER

The most straightforward strategy to simultaneously process data collected during several setups with common reference outputs is the PoGER. According to the explanation presented in section 2.5.3, when this approach is followed together with the p-LSCF method, the output positive spectrum matrices of each setup are placed on the top of each other to form a global matrix, which in the case of the present application has $8 \times 13 = 104$ lines and 4 columns (8 - number of *dof* instrumented in each setup; 13 - number of setups; 4 - number of outputs elected for reference). The elements of this global matrix were calculated using the same parameters that were adopted in the previous analysis (same exponential window and same length of the correlation functions).

The application of the identification algorithm to the global output positive spectrum matrix produced the stabilization diagram presented in Figure 3.14. This very ‘clean’ stabilization diagram permits the identification of 24 alignments of stable poles in the frequency range 0.1-0.8 Hz, which are associated with 24 structural modes. The final modal parameter estimates, presented in Table 3.1, were selected from the results of a model of order 42.

The mode shapes associated to each pole contain 104 components, or 13 groups with 8 components, due to the repetition of the mode shape components at the reference outputs. These repeated values were then used to scale each segment and obtain the scaled 56 mode shape components associated with the vertical and lateral direction of the 28 instrumented sections.

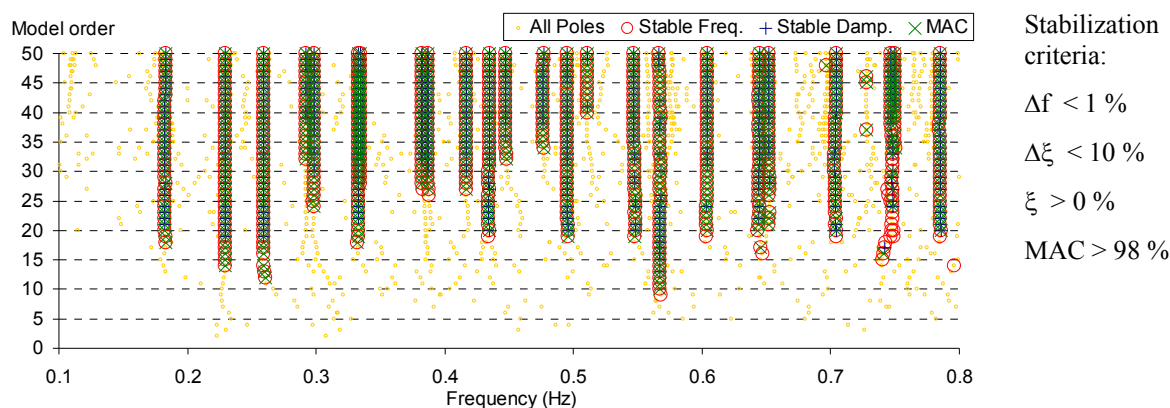


Figure 3.14 – Stabilization diagram with the estimates given by the p-LSCF method using the PoGER approach.

The natural frequencies and the mode shapes given by this analysis are presented in Figures 3.15 and 3.16 together with the results provided by a numerical model developed by the design office Greisch (Flamand and Grillaud 2006). This model was used all along the construction process up to the completion of the bridge and therefore it represented the state of the bridge at the date of the test, but did not suffer any updating after the execution of the dynamic tests.

It is remarkable the correlation achieved between the numerical and experimental results both in terms of natural frequencies and mode shapes. These experimental results are an excellent validation for the developed numerical model and at the same time permit some fine tuning, especially concerning the piers-foundation interaction, as the larger discrepancies (still quite small) are observed in the natural frequencies of the lateral modes that mobilize the shortest piers.

The experimentally estimated mode shapes also demonstrate the capability of the PoGER approach to provide conveniently scaled mode shapes. The natural frequencies and modal damping ratios given by the applied global estimation methodology are compared with the ones provided by the setup-by-setup analysis in Table 3.1 and Figure 3.17. The graphic shows all individual estimates of the PoSER analysis and compares the mean values of this approach with the results of the PoGER approach. The table presents the statistical characterization (mean and standard deviation) of the PoSER estimates and the single estimates of the global analysis for each mode. With the global analysis, it was possible to identify an extra mode because in the separated analysis of each setup, it was not possible to correctly individualize the two closely spaced modes with frequencies around 0.64-0.65Hz in all the setups.

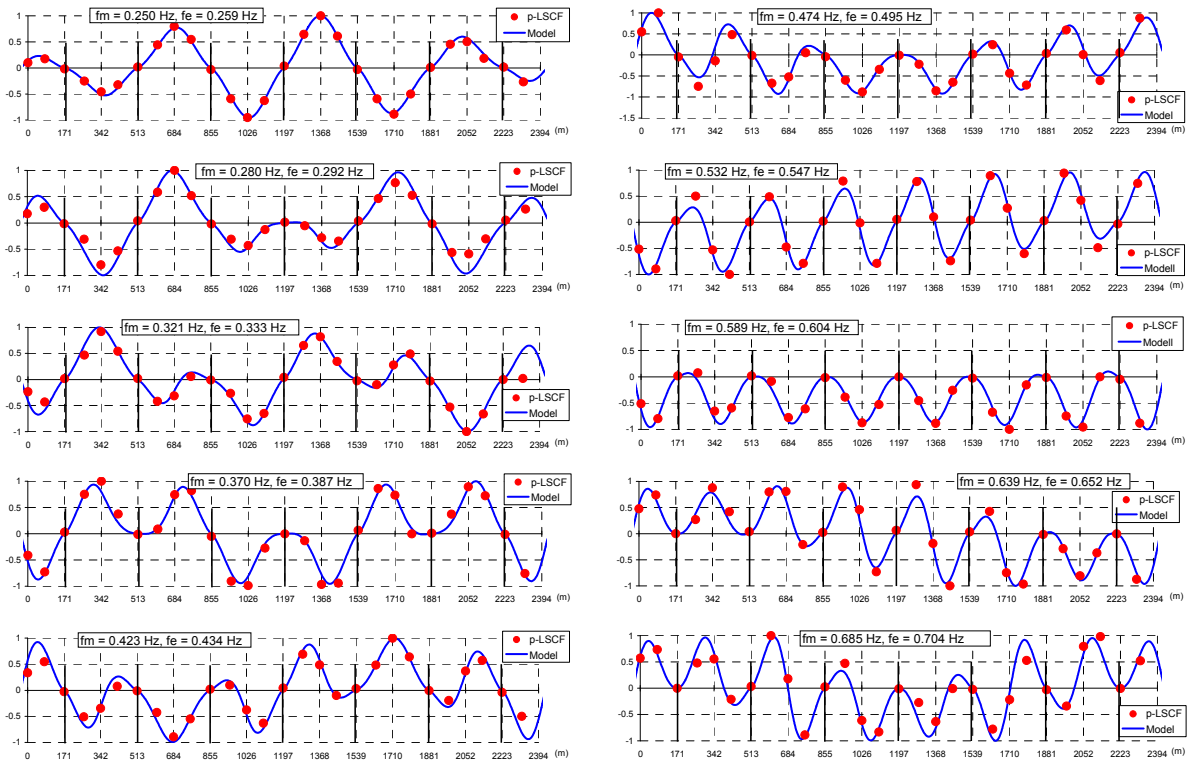


Figure 3.15 – Results of the PoGER/p-LSCF analysis for the vertical bending modes (frequencies f_e) compared with the numerical results (frequencies f_m).

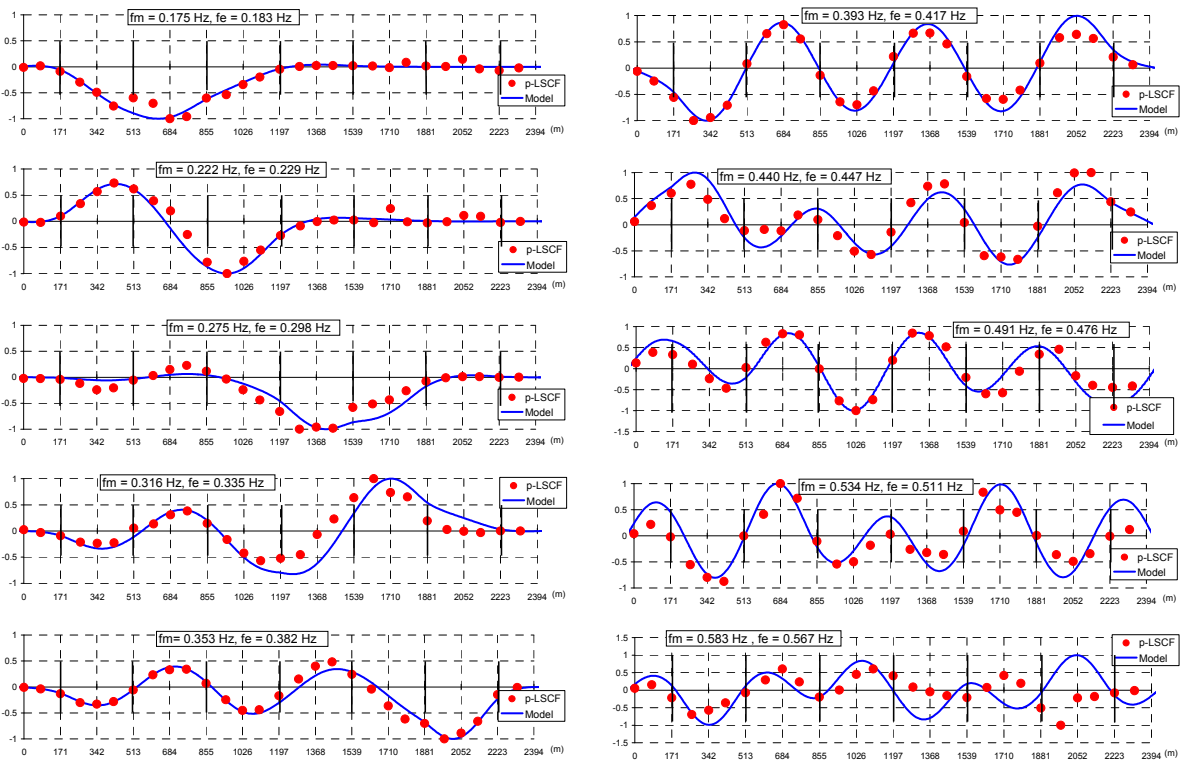


Figure 3.16 – Results of the PoGER/p-LSCF analysis for the lateral bending modes (frequencies f_e) compared with the numerical results (frequencies f_m).

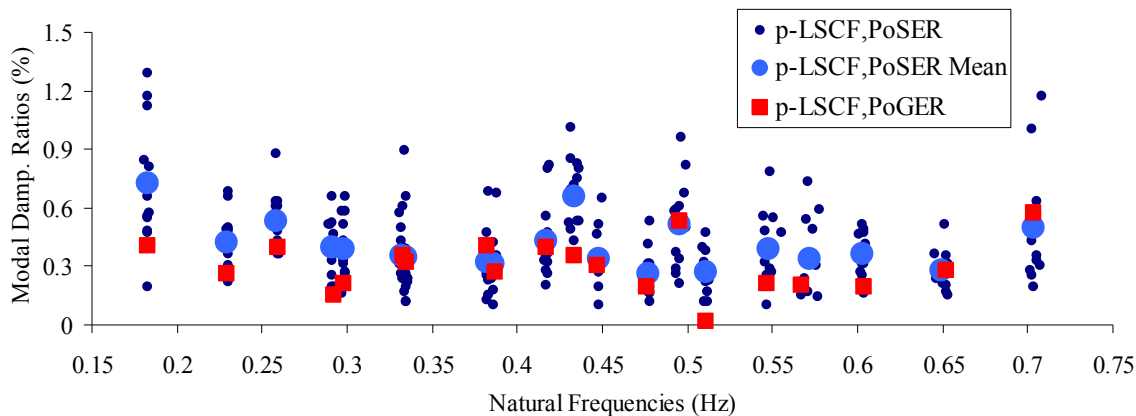


Figure 3.17 – Comparison of the natural frequencies and modal damping estimates obtained with the PoSER/p-LSCF and PoGER/p-LSCF analyses.

Table 3.1 – Comparison of the results provided by PoSER/p-LSCF and PoGER/p-LSCF (σ denotes standard deviation)

Mode Type* ¹	PoSER				PoGER	
	f (Hz)	σ (f) (Hz)	ξ (%)	σ (ξ) (%)	f (Hz)	ξ (%)
L	0.183	0.0007	0.73	0.33	0.183	0.40
L	0.230	0.0004	0.42	0.15	0.229	0.26
V	0.259	0.0006	0.53	0.15	0.259	0.40
V	0.291	0.0008	0.40	0.14	0.292	0.15
L	0.298	0.0007	0.39	0.15	0.298	0.21
V	0.332	0.0013	0.35	0.11	0.333	0.36
L	0.335	0.0008	0.35	0.23	0.335	0.32
L	0.383	0.0006	0.32	0.14	0.382	0.41
V	0.386	0.0009	0.32	0.14	0.387	0.27
L	0.417	0.0009	0.43	0.19	0.417	0.40
V	0.434	0.0017	0.65	0.19	0.434	0.36
L	0.448	0.0008	0.34	0.14	0.447	0.30
L	0.477	0.0007	0.26	0.11	0.476	0.19
V	0.495	0.0020	0.52	0.22	0.495	0.53
L	0.511	0.0011	0.27	0.11	0.511	0.02* ²
V	0.548	0.0028	0.39	0.18	0.547	0.21
L	0.572	0.0035	0.34	0.19	0.567	0.20
V	0.603	0.0010	0.36	0.12	0.604	0.20
L	-	-	-	-	0.644	0.39
V	0.650	0.0036	0.28	0.10	0.652	0.28

*¹ V – vertical bending mode; L – lateral bending mode

*² not reliable estimate; the stabilization diagram (Figure 3.14) presents very few stable poles for this mode

This synopsis of the results shows that the mean natural frequencies estimated by the PoSER analysis and the corresponding values given by the PoGER analysis are almost coincident. For the modal damping ratios the results are not so coherent for all the modes. Still, for the majority of the modes the global analysis provided values that are within the interval of variation of the PoSER analysis estimates. Nevertheless, when a global identification is performed some care has to be taken in the interpretation of the obtained modal damping ratios. As only one value is obtained for each mode, the results do not express the large uncertainty always associated with the estimation of this parameter.

p-LSCF, PreGER

In section 2.5.4, it is presented a global estimation procedure called PreGER that can be an alternative to the previously applied methodology. As explained in chapter 2, the use of this approach together with the p-LSCF method implies the scaling of the spectrum matrices associated with each setup before the creation of a global spectrum matrix. In opposition to the PoGER approach, with this methodology the spectra associated with the reference outputs are not repeated on the global spectrum matrix and therefore, in the present application, this is a 56-by-4 matrix.

The application of the identification algorithm to this global spectrum matrix, using the same parameters that were adopted in the previous analyses (correlations with 256 points, same exponential window and polynomial orders between 1 and 50), provided a stabilization diagram with very few alignments of stable poles. Consequently, the majority of the modes could not be identified.

Then, in order to try to improve the results, the vertical and lateral acceleration time series were processed separately. The processing of the global spectrum matrix of the vertical *dof* (28-by-2 matrix) provided the stabilization diagram presented in Figure 3.18. Despite being a stabilization diagram which is less clear than the one produced by the PoGER approach, it permitted the identification of all the vertical modes within the frequency band under analysis. These are characterized in Figure 3.19. It can be observed that the natural frequencies almost coincide with the previously estimated and that the modal damping ratios are consistent with values presented in Figure 3.17. As the spectra were previously scaled, no post-scaling of the mode shape components is needed with this methodology. So, the presented mode shapes were directly provided by the identification algorithm. These are similar to the ones given by the PoGER approach, but some less accurate mode shape components can be detected by the lack of symmetry or anti-symmetry of some mode shapes that was not observed in the results provided by the PoGER approach.

The processing of a global spectrum matrix with the lateral *dof* did not provide a stabilization diagram with clear alignments of stable poles, as several vertical alignments of poles presented negative damping. So, an accurate identification of the modal parameters of the lateral modes could not be done with this approach.

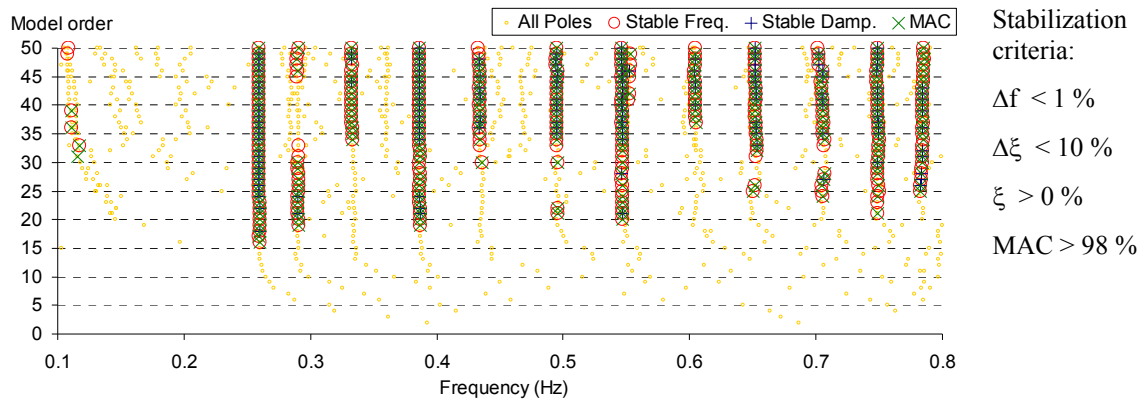


Figure 3.18 – Stabilization diagram with the estimates given by the p-LSCF method for the vertical modes using the PreGER approach

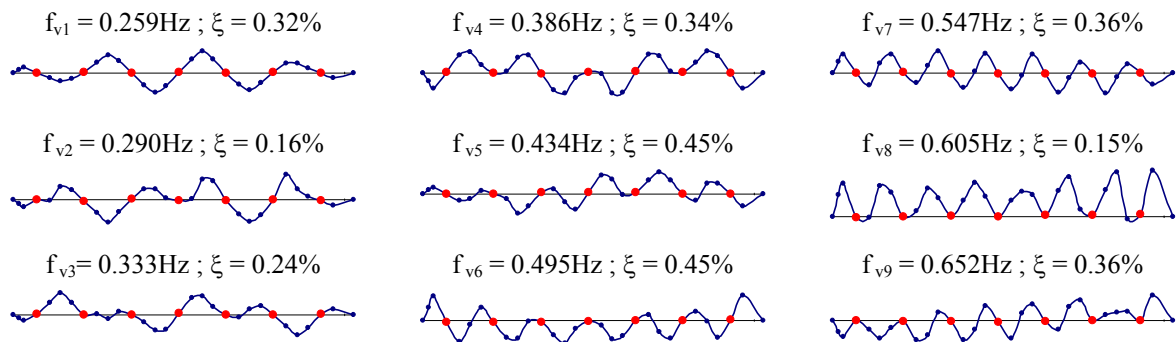


Figure 3.19 – Modal parameters of the first 9 vertical modes provided by the application of the p-LSCF method using the PreGER approach (red dots at the positions of the piers).

All the available approaches to process several setups together are based on the assumption that the modal properties of the structure under analysis are constant during the test. However, in real applications this is only approximately true, because natural frequencies present small variations motivated for instance by variations on the structure temperature and the modal damping ratios can be influenced by the vibration amplitude or by the wind intensity. Apparently, in the present application of the p-LSCF method, the PoGER approach was more robust with respect to these small non-stationarities of the structure properties and so permitted the estimation of high quality modal parameters.

The incapability of the PreGER approach to provide accurate estimates for the lateral modes is certainly due to the lack of robustness of the methodology adopted to scale the spectra (equation 2.98) against small variations of the modal parameters and also against the measurement noise. The colour

maps presented in Figure 3.8 shows that the spectra of the vertical accelerations present less variations during the test than the ones associated with the lateral accelerations.

3.3.6 Conclusions

The outstanding characteristics of the Millau Viaduct justified the performance of very complete dynamic tests at the commissioning stage, with the purpose of validating the numerical studies developed during design. In particular, this section demonstrates that it was possible to extract a lot of useful information from data collected during the ambient vibration test.

First of all, it is relevant to mention that the adopted equipment, which avoids the use of cables, permitted to cover the full length of this very large structure in few hours and so, with a test that took less than one day, including preparation and measurements, it was possible to collect data that enabled an adequate characterization of the most relevant modes. Thus, the efficiency of ambient vibration tests performed with adequate equipment was clearly proven.

The acceleration time series recorded during the ambient vibration test were processed with several alternative output-only modal identification techniques. In this work, the application of the p-LSCF method is explored adopting three alternative strategies: PoSER, PoGER and PreGER.

The traditional approach (PoSER), based on separated analyses of each setup, made possible the identification of all the relevant modes and also the characterization of the scatter of their natural frequencies and modal damping ratios during the test. However, its application is very time consuming and some modal components could not be determined. On the other hand, the PoGER approach proved to be able to provide very accurate estimates of natural frequencies and mode shapes with little effort, as only one very clear stabilization diagram had to be interpreted. In particular, very good results were also achieved for three pairs of closely spaced modes.

Furthermore, the application of the p-LSCF method following the PoGER approach enabled the estimation of 20 modes of vibration in the frequency range 0.1-0.7Hz, which exhibit an excellent correlation with the modal properties previously calculated from a finite element model. This fact shows, on the one hand, an adequate numerical characterization of the bridge and, on the other hand, the excellent performance and high accuracy of the employed output-only modal identification technique. It is of special importance the demonstration that it was possible to obtain well scaled mode shapes with the global processing of all the setups.

Finally, the PreGER approach was tested. In this particular application, it was not possible to obtain with this technique a complete characterization of all the modes identified with the other two methodologies. Only the vertical modes could be correctly identified. This less good performance of the PreGER approach with regard to the PoGER, when combined with the p-LSCF method, was also observed in the processing of data collected at a steel arch bridge over the Douro River, in Portugal (Reynders et al. 2009). Nevertheless, it is still worth testing both approaches in other applications in order to confirm if the PoGER approach is definitively more robust against small variations of the modal parameters during the ambient vibration test and less sensitive to the always present measurement noise.

For the modes estimated with the three tested approaches, the agreement between results is good. The natural frequencies almost coincide and the mode shapes are very similar. The largest discrepancies are observed in the modal damping ratios. However, the results of both global estimation approaches are coherent and within the interval of variation of the estimates provided by the PoSER approach. Nevertheless, it has to be pointed out that the global estimation approaches have the disadvantage of not characterizing, at least approximately, the uncertainty associated with the estimation of the modal parameters, which is especially relevant in the case of the modal damping ratios.

As there is still some lack of confidence on the modal damping ratios derived from ambient vibration measurements, these will be validated in section 3.5.3 with the values estimated from the recorded free decays.

3.4 Humber Bridge

3.4.1 Introduction

The Humber Bridge (Figure 3.20), in operation since 1981, is the largest suspension bridge of the United Kingdom. A first ambient vibration test of this outstanding structure was performed in July 1985 by the University of Bristol (Brownjohn et al. 1986), with the main goal of validating finite element modelling procedures for suspension bridges. Twenty three years later, in July 2008, a new ambient vibration test was performed at the Humber Bridge, this time under the leadership of the University of Sheffield (Professor James Brownjohn), with the collaboration of the Faculty of Engineering of the University of Porto (FEUP) and of Professors Ivan Au and Paul Lam from the City University of Hong Kong. In particular, the team from FEUP provided 6 of the 10 used recorders, contributed to the test planning, helped in the configuration and calibration of the measuring equipment, was deeply involved in the field test and in the in-situ validation of the acquired database and developed an independent processing of the collected data.



Figure 3.20 – Humber Bridge view from the South side.

This last test, performed in the context of a research project on Structural Health Monitoring (Brownjohn and Worden 2008), prepares for the installation of a dynamic monitoring system in the bridge, and aimed essentially to obtain a set of vibration modes with enough resolution to capture dynamic effects that could be affected by structural changes of interest to the bridge operator. As a complementary objective, the test of this large structure was also an interesting challenge that permitted to test recent developments both in terms of measuring equipment and techniques for data processing (Brownjohn et al. 2010). In particular, the present work is focused on the use of the

collected database to evaluate the identification procedures presented in chapter 2, giving special emphasis to their suitability to deal with large amounts of data.

3.4.2 Bridge Description

The Humber Bridge, with a main span of 1.410 meters, had from the end of construction, at 1981, to 1998 the world longest span. Nowadays, it is at 5th position in the ranking of world longest spans. The bridge superstructure was erected from 1976 to 1981 by a partnership of several British companies (British Bridge Builders) following the design developed by Freeman Fox and Partners, which had previously designed the Severn Bridge (UK, main span - 988m) and the Bosphorus Bridge (Turkey, main span -1074m).

The bridge deck is divided in three segments with lengths of 280m (north side span), 1410m (main span) and 530m (south side span) (see Figure 3.21). Its section is a trapezoidal hollow box 22m wide and 4.5m deep with 3m wide panels cantilevering from each side of the box to carry the walkways (see Figures 3.22 and 3.23). It is built up from welded stiffened steel plate panels, generally 18.1m long. The connection between the three decks and the towers or abutments is provided by pairs of steel A-frame rockers that were designed to permit longitudinal motion and rotation about transversal and vertical axes. Between the adjacent ends of the main and the side span sections of the deck there is an expansion joint (one at each tower) that was designed to accommodate relative longitudinal displacements of 2.9 metres.

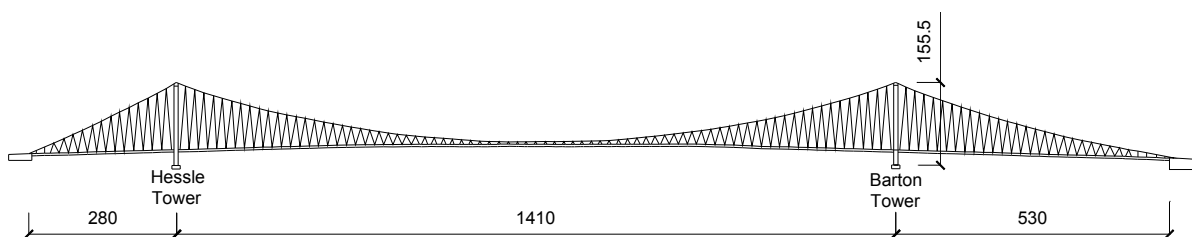


Figure 3.21 – Elevation of the Humber Bridge (distances in meters).

The two towers consist of two hollow reinforced concrete legs, 155.5m high, braced by four horizontal beams; the lowest one accommodates the supports for the bridge decks (see Figure 3.20). The Barton tower (south side) is founded on clays. Therefore, it is supported by two 24m diameter concrete caissons sunk 8m into the clay. The Hesse tower is founded on chalk, 8m below the ground level, by a massive reinforced concrete slab 44m long, 16m wide and 11.5m high.

The main cables are made of 14 948 parallel galvanised draw wires 5mm in diameter which, for ease of erection control and anchoring, were grouped in 37 strands. The deck is suspended from the two

main cables by high tensile steel hangers, which are inclined to provide some longitudinal stiffness to deck.

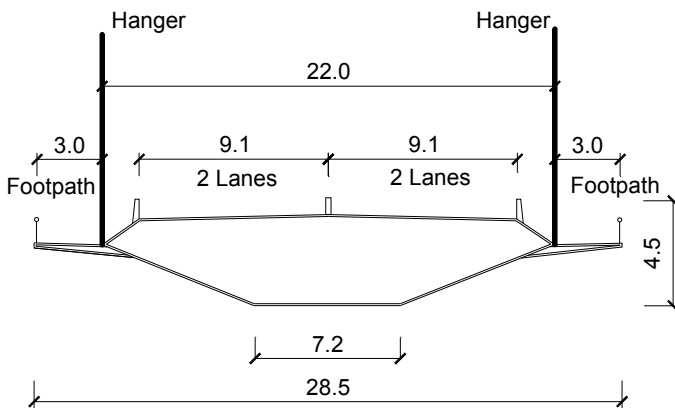


Figure 3.22 – Humber Bridge cross section (distances in meters).



Figure 3.23 – Humber Bridge deck, view from underneath.

3.4.3 Ambient Vibration Test

The bridge size imposed several technical and logistical difficulties, partially overcome by the use of a data acquisition system that avoids electrical cables between the measuring units. The test was conducted using 10 triaxial Geosig recorders, model GSR-24, which were previously tested in the laboratory to ensure that the different types of used acceleration sensors (force balance sensors from different manufactures: RefTek, Guralp and QA) were well calibrated and that the time synchronization between measuring units, achieved with external GPS sensors, was accurate. Figure 3.24 shows the used equipment during an initial setup with all the recorders placed at the same section (5 at each side of the deck) to check their synchronization.

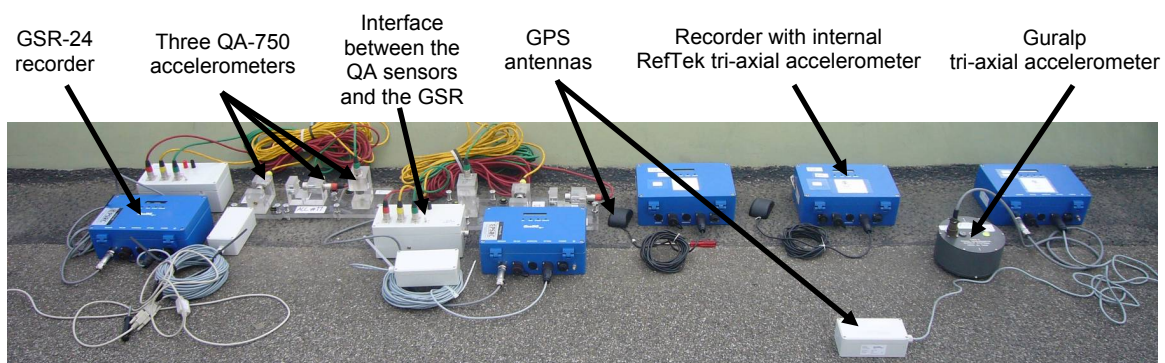


Figure 3.24 – Equipment used in the Ambient Vibration Test of the Humber Bridge

During the test of the main span, two pairs of recorders were permanently located at two reference sections (R1 and R2, marked with red squares in Figure 3.25), while the other six worked as moving

sensors, three at each side of the bridge deck, covering the remaining instrumented points (blue circles in Figure 3.25) in different test setups. Each section was instrumented at both upstream and downstream deck sides at the footpaths as close as possible to the connection of the cantilever to the main box beam (see bridge top view presented in Figure 3.25).

The side spans are not monolithically connected to the main span; as already mentioned, they have independent supports at the towers provided by pairs of A-frames. Therefore, the existence of local modes involving only the side spans is expected. Thus, for the setups that include sections of the side spans, an additional reference section was adopted (RH and RB marked with green triangles in Figure 3.25), which reduced the number of moving recorders from six to four.

The choice of the reference points stemmed from inspection of the set of experimental and calculated mode shapes of the bridge presented in the report of the ambient vibration test performed in 1985 (Brownjohn et al. 1986), trying to guarantee that the reference points were not close to nodal points of the most significant modes of vibration.

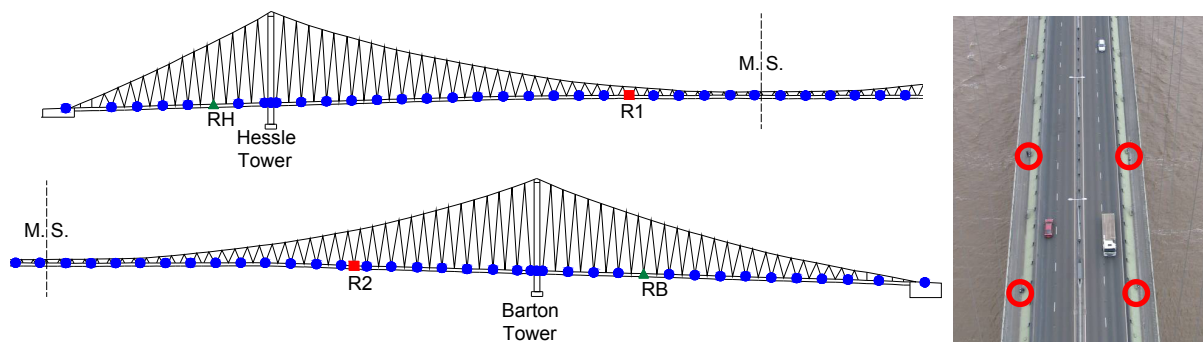


Figure 3.25 – Instrumented sections with indication of the reference sections (R1, R2, RH and RB) and top view of the bridge deck with the position of four seismographs.

During the last day of tests, measurements were performed also at both towers. One of the reference sections located at the main span was kept (the one between the Hessle tower and the mid span) and four additional reference points were adopted, two at the top of each tower (represented in red at Figure 3.26). The remaining 4 stations, two for each tower, covered the points represented in blue in Figure 3.26 with three setups.

The time signal acquisition was performed with a sampling frequency of 100Hz (imposed by the filters of the acquisition equipment) and for each sensors layout, 4 time segments with 895 seconds (aprox. 15 minutes) were recorded, which corresponds to a total acquisition time of almost one hour. Such long acquisition periods were necessary because very low natural frequencies were expected. The fragmentation in four time segments was imposed by a limitation of the software to program the recorders.

3.4.4 Preliminary Analysis

Before performing the identification of modal parameters with parametric methods, the collected time series were analysed both in time and frequency domain. Figure 3.27 presents a sample of acceleration time series collected by one of the stations placed at a reference section, showing that the level of vertical vibrations is much higher than the observed along the lateral and longitudinal directions. The lateral acceleration time series present a significant quasi-static component with high frequency content in the range 0-0.04Hz, which is certainly induced by the wind action and by the asymmetrical loads due to the passage of heavy vehicles that originate deck rotations.

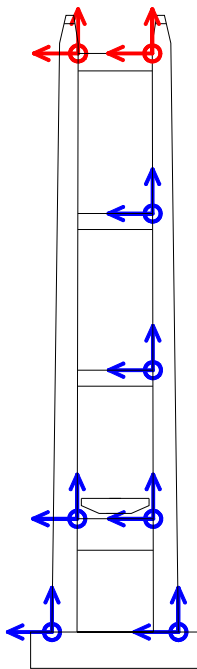


Figure 3.26 – Degrees of freedom measured at the towers

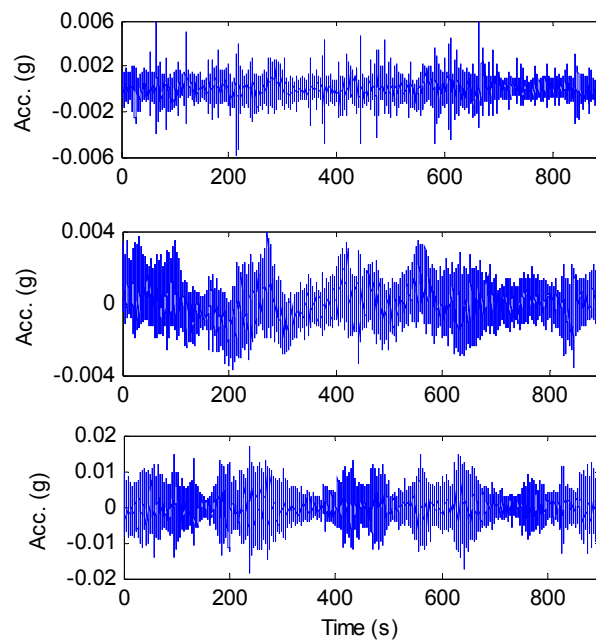


Figure 3.27 – Sample of measured acceleration time series (longitudinal, transversal and vertical from top to bottom).

The time evolution of the energy content of the time series measured at the reference sections, during the ambient vibration test (5 days, 29 setups), is characterized in Figure 3.28. This is quantified by the root mean square (RMS) value evaluated using the power spectral density ordinates within the frequency range from 0.04 to 1Hz (frequency band selected for modal analysis and that excludes the quasi-static component).

In order to obtain a first overview of the resonant frequencies of the Humber Bridge, an independent analysis was performed for the frequency content associated with three fundamental deck movements: vertical displacements (vertical bending modes), lateral displacement (lateral bending modes) and rotations about the longitudinal axis (torsion modes). So, from the acceleration time series collected at each deck section, the following combined signals were calculated: half-sum (or average) and half-

difference of the vertical accelerations and average of the lateral accelerations. Considering the possible independent behaviour of the three segments of the bridge deck, average auto-spectra involving the combined signals of all the instrumented sections of each deck segment were calculated. Because the averaged auto-spectra are associated with setups that may present different vibration levels, the spectra are normalized before being averaged. These averaged normalized auto-spectra are presented in Figure 3.29, together with the averaged normalized auto-spectra of the lateral and longitudinal acceleration time series recorded at the towers. The analysis is concentrated on the frequency range 0-1Hz, which already permits the identification of more than 30 natural frequencies. The values of frequencies associated with the most prominent peaks are annotated. These are rough estimates of the bridge natural frequencies.

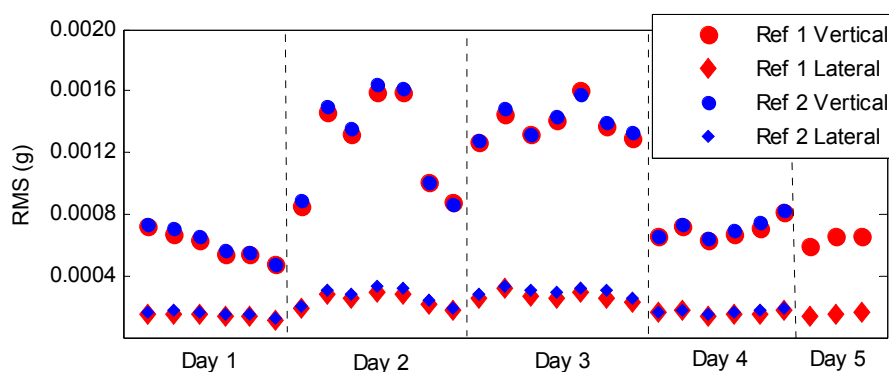


Figure 3.28 – Evolution of the RMS values during the five days of test (frequency range: 0.04 to 1Hz).

The presented plots prove the independent behaviour of the three spans, evidenced by the existence of independent peaks for each span (only few peaks are common to the three spans), as it was anticipated considering the type of connections between the deck segments and the towers. The observation of the spectra also shows a high density of modes in the frequency range 0-1Hz and the existence of groups of closely spaced modes, as for instance around 0.31Hz, where there are three vertical bending modes (peaks in the spectra of the half-sum of the deck vertical accelerations) and a torsion mode (peak in the spectra of the half-difference of the deck vertical accelerations). The identification of a resonant frequency of 0.056Hz (a period of 18 seconds) in the spectra associated with the lateral direction proves that the used accelerometers are sensitive to such low frequency vibrations.

As expected, the spectra of the longitudinal accelerations recorded at the towers present some peaks which are also associated with vertical bending modes. On the other hand, some of the lateral modes are also observable on the spectra of the lateral accelerations measured at the towers. However, the levels of vibration observed at the towers are much lower than the ones recorded at the deck level (the amplitude of the longitudinal accelerations at the top of the towers is about 1/10 of the amplitude of the deck vertical accelerations).

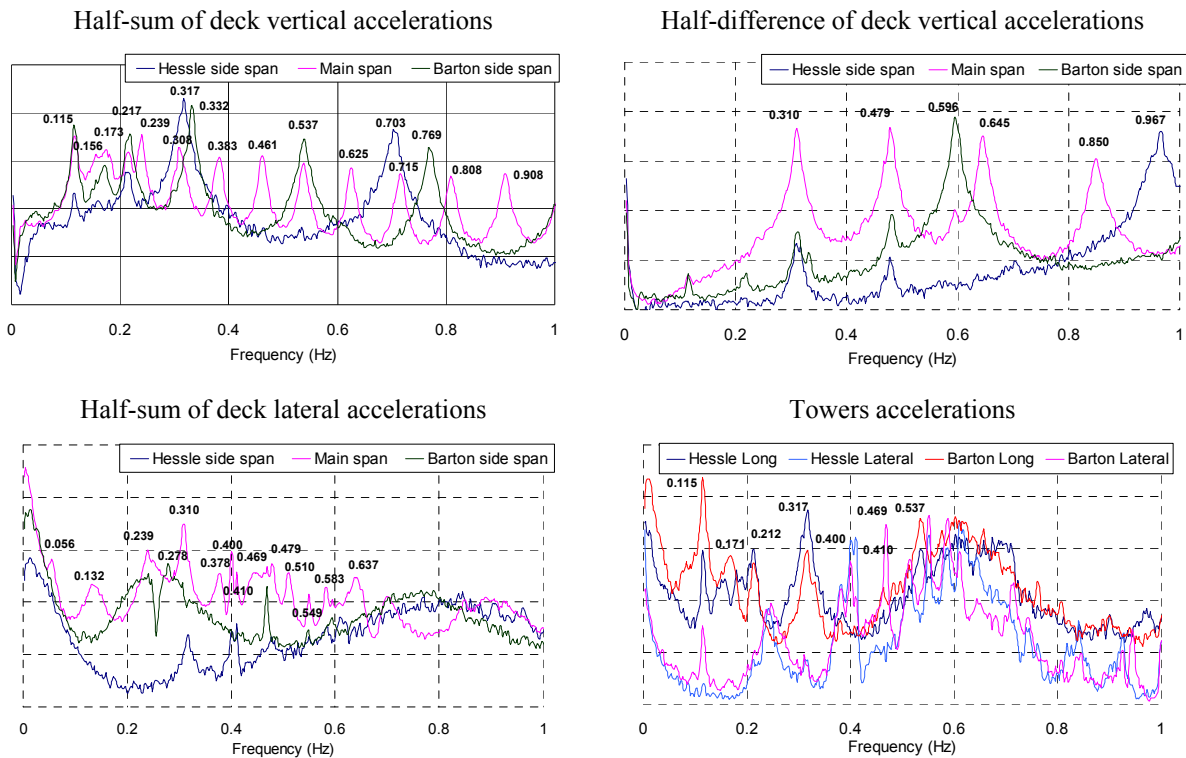


Figure 3.29 – Averaged normalized auto-spectra (y in logarithmic scale).

During the performance of the dynamic test, at the end of each day, plots similar to the ones previously presented were created and then, the mode shapes associated with each identified peak were calculated from the cross-spectra between the reference sections and the remaining instrumented sections, following the classical Peak-Picking methodology. This very fast and simple processing permitted to validate the collected data in situ and find out possible problems that could be subsequently recovered with the development of additional setups during the following days. As a consequence, right after the end of the test, quite reasonable estimates of natural frequencies and mode shapes of the most relevant modes were available (Magalhães et al. 2008a).

After this preliminary analysis, the already validated database was processed by parametric identification methods in order to obtain a more complete set of more accurate modal parameters. This was preceded by pre-processing operations of trend removal, low-pass filtering and re-sampling. Considering the large number of modes with natural frequencies lower than 1Hz, the time signals were re-sampled with a sampling frequency of 5Hz, after the application of a low-pass filter with a cut-off frequency of 1.2Hz.

The identification algorithms presented in the next section are based on correlation or half-spectrum matrices estimated from the time series collected during each setup. As in each setup, four time segments were collected instead of a continuous time signal; the final correlations and spectra

estimates resulted from the average of four intermediate estimates derived from the recorded time segments.

3.4.5 Modal Parameters Identification

In this work, the identification of the modal parameters was based on the application of three alternative methodologies: a global processing with the SSI-COV method, a global processing with the p-LSCF method and an automated separated processing of all the setups with the SSI-COV method taking profit from the results provided by the previous global analysis. The large number of setups (29) precludes a separated analysis of all the setups based on a manual interpretation of stabilization diagrams.

Normally, when parametric identification methods are used, the time series collected in each setup are processed all together without any previous combination of the signals to separate the different types of modes, because these methods have the ability to identify closely spaced modes. However, an initial analysis of some setups showed that the large difference between the vibration amplitudes for vertical and lateral directions, as evidenced in Figure 3.27, together with the existence of modes with almost coincident natural frequencies (e.g. 0.310 and 0.308Hz) makes this joint analysis inefficient (the vertical modes with more energy hide the lateral modes and it is not possible to obtain a perfect separation between the vertical bending mode and the torsion mode with frequencies 0.310 and 0.308Hz). Furthermore, the simultaneous processing of all the collected time series using global estimation approaches (PoGER) leads to very large matrices that make the processing very demanding, especially in terms of computer memory.

Consequently, the processing of the data collected at the bridge deck was based on the independent analysis of the same three combined signals that were used to make the plots presented in Figure 3.29, which permit a separate identification of the three fundamental types of modes: vertical bending, torsion and lateral bending. This procedure is adequate for this bridge, because it does not present mode shapes with complex geometry (a mixture of lateral and vertical displacements with deck rotations), as previously demonstrated by the results given by its numerical modelling (Brownjohn et al. 1986).

SSI-COV, PoGER

The SSI-COV method was applied following the PoGER approach (see section 2.5.3). Three global analyses, one for each set of pre-combined signals, involving all the 26 setups developed along the bridge deck were performed. Therefore, in each analysis a total of 26 correlation matrices were stacked on the top of each other. After some trials, it was concluded that good results could be obtained using correlations with 199 points (number of blocks of the Toeplitz matrix $j_b = 100$), which contain $199/5 \times 0.056 = 2.23$ cycles of the mode with the lowest natural frequency. In order to reduce the calculation effort and the computer memory requirements, only two outputs were selected for reference, these coincide with the test reference sections of the main deck (R1 and R2 in Figure 3.25). Thus, the correlation matrices of each setup present 5 lines (number of instrumented sections) and 2 columns (number of outputs elected for reference). As a result, the global correlation matrix is 130-by-2 and the Toeplitz matrix to which the SVD is applied is 13000-by-200.

Figure 3.30 presents the stabilization diagram associated with the half-sum of the vertical accelerations. In the analysed frequency band, there are 14 alignments of stable poles. As only the reference sections of the main span were considered, the local mode shapes of the lateral spans are not correctly identified with this analysis. A supplementary study, just concentrated on the lateral spans, was performed for the identification of these local modes. Taking profit from the additional references RB and RH (see Figure 3.25), it was possible to identify five further vertical bending modes in the frequency range under study.

In order to avoid the subjective task of manually selecting one stable pole for each mode, the algorithm for automated identification presented in section 2.4.4 was applied to all the poles, stable and unstable, represented in the stabilization diagram. Figure 3.31 characterizes the groups achieved with the cluster analysis imposing a limit for the distance between elements of the same group (calculated with equation (2.94)) of 0.05. There are 14 groups that clearly stand out, these are the ones associated with physical modes. The natural frequencies, modal damping ratios and mode shapes of the selected mode estimates are presented in Figure 3.32. It can be observed that mode shapes of very good quality were obtained. Only one of the selected groups is not represented ($f \approx 0.32\text{Hz}$), this is associated with a mode that mainly involves the Barton side span and so its mode shape could not be well characterized with the reference sections of the main deck.

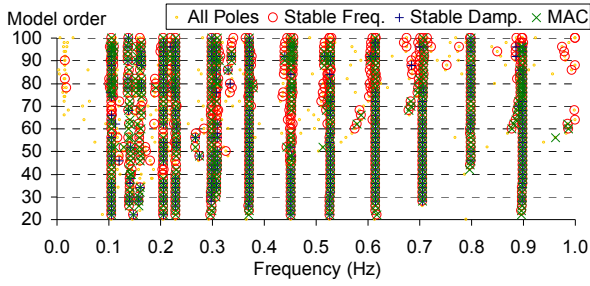


Figure 3.30 – SSI-COV global analysis stabilization diagram for the half-sum of the vertical accelerations.

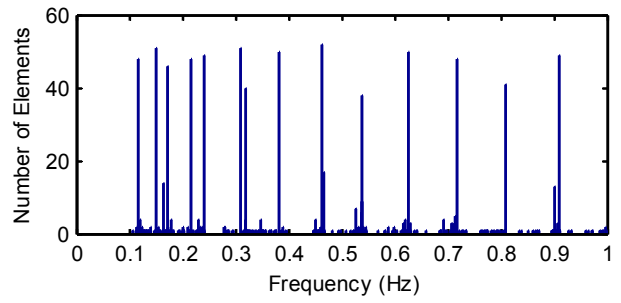


Figure 3.31 – Clusters formed from the poles presented in the stabilization diagram of Figure 3.30.

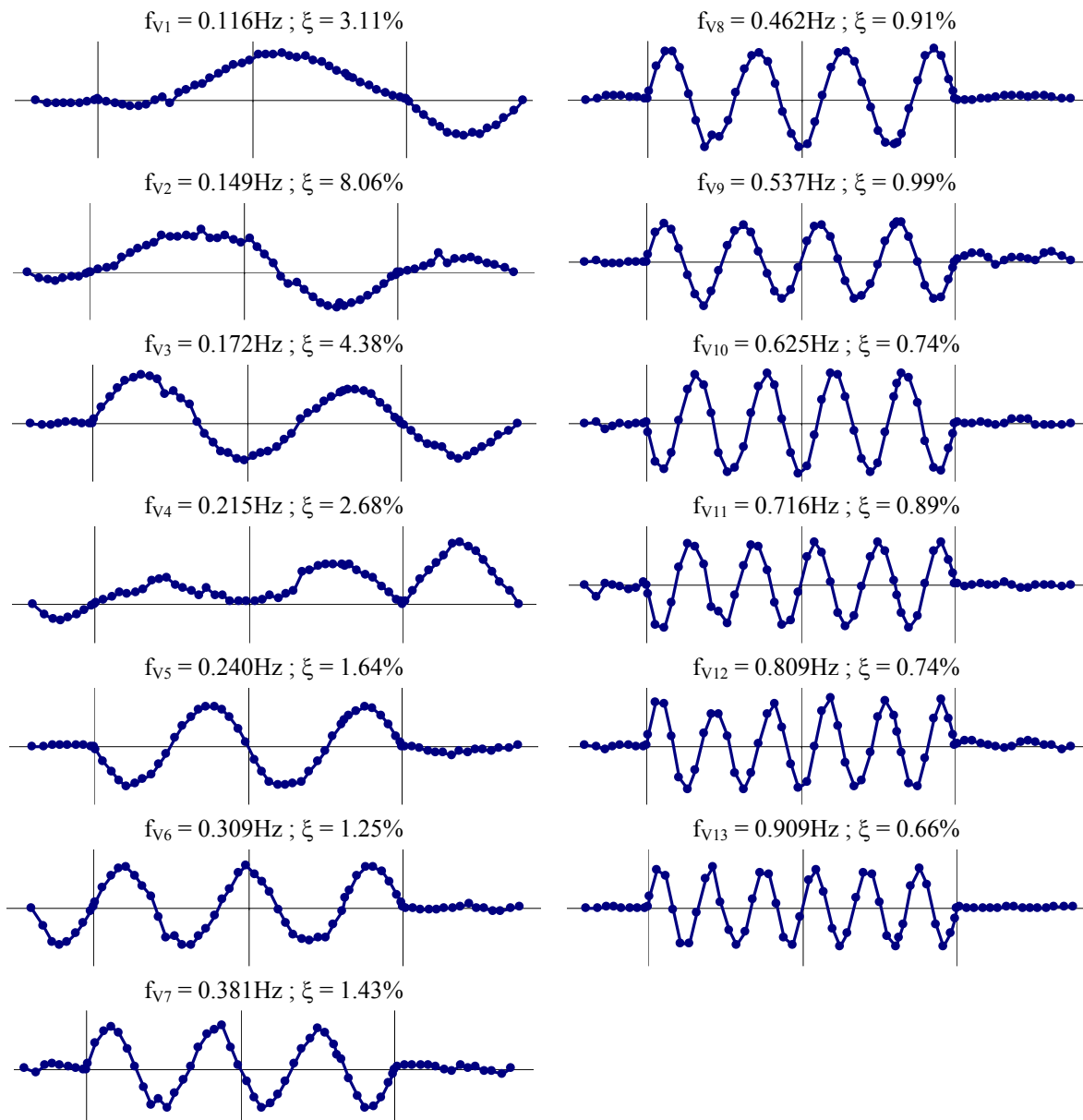


Figure 3.32 – Modal parameters of the vertical modes in the frequency range 0-1Hz (vertical lines at the position of the towers and at mid-span; each dot represents an estimated mode shape component).

The setups performed at the towers only include one of the main span references, so these were processed separately and then the obtained mode shape components were glued with the deck mode shapes using the common reference. However, the tower movements were not perceptible in the global figures. So, Figure 3.33 presents the mode shape components along the longitudinal direction of the bridge estimated at the towers for the first four vertical modes. These were scaled to present a unitary value at the deck reference section R1 in order to prove that the tower movements are negligible when compared to the amplitude of the mode shapes at the deck level. This was also observed for the remaining vertical bending modes.

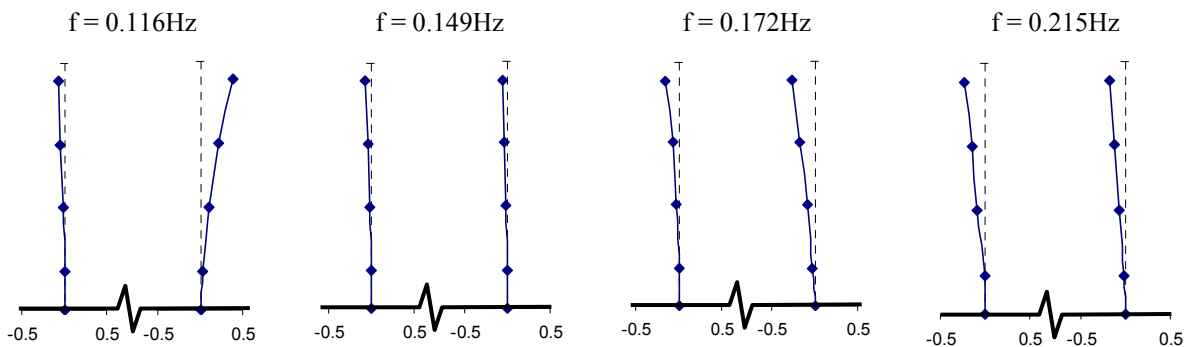


Figure 3.33 – Tower mode shape components in the longitudinal direction for the first four vertical modes (scaled to present a unitary value at the reference section R1; Hessle tower at the left and Barton tower at the right).

Figure 3.34 presents the stabilization diagram obtained after the processing of the semi-difference of the vertical acceleration. Five clear alignments of stable poles correspond to five torsion modes. One of these is a local mode of the Barton side span ($f = 0.592\text{Hz}$), the other four are characterized in Figure 3.36.

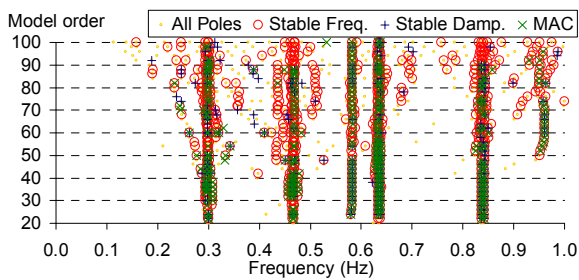


Figure 3.34 – SSI-COV global analysis stabilization diagram for the half-difference of the vertical accelerations.

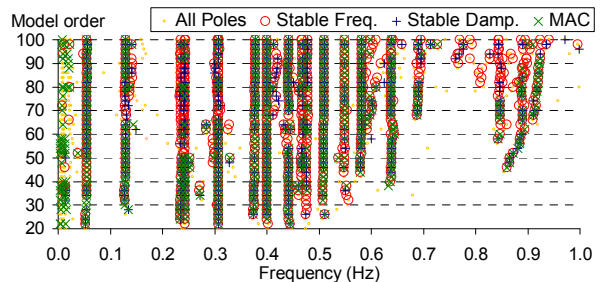


Figure 3.35 – SSI-COV global analysis stabilization diagram for the lateral accelerations.

The global processing of all the lateral acceleration time series collected at the deck level led to the stabilization diagram presented in Figure 3.35. Several vertical alignments of stable poles can be easily identified. In particular, the one associated with the first lateral mode with a natural frequency of 0.056Hz is evident. The application of the algorithm for automated modal analysis permitted an

objective analysis of the mode estimates contained in the stabilization diagram and the subsequent identification of the modes characterized in Figure 3.37.

The majority of the mode shapes are of good quality. However, there are some that do not present very smooth shapes. In the case of the first lateral mode, the inferior quality of the mode shape is probably due to its exceptionally low natural frequency, which is within a frequency range already influenced by the quasi-static components (see bottom left plot of Figure 3.29). Furthermore, as proven by the numerical results (Brownjohn et al. 1989), there are different types of lateral modes: ones where both deck and main suspension cables move in phase with the same shape, others that involve essentially oscillations of the main suspension cables and others composed by oscillations of deck and main cables with different configurations. This fact justifies the existence of modes with different natural frequencies but similar mode shapes at the deck level, as for instance modes L4 and L6. Additionally, the modes of the main suspension cables with residual components at the deck level were still identified with the developed ambient vibration test, but the obtained results are of inferior quality. Because no measurements were performed at the main cables, it is not possible to distinguish the different types of lateral modes. Still, the modes with modal components at the main cables higher than the ones observed at the deck are expected to present lower values for the modal damping ratios, as it is, for instance, the case of modes L5, L8 and L9.

The modal damping ratios estimated for some modes are quite high, in some cases (first vertical mode and first three lateral modes) higher than 5%. This is a surprising result especially taking into account that they are associated with low vibration levels. Therefore, the same signals were also processed with a parametric frequency domain method. The results of this analysis are presented in the following paragraphs.

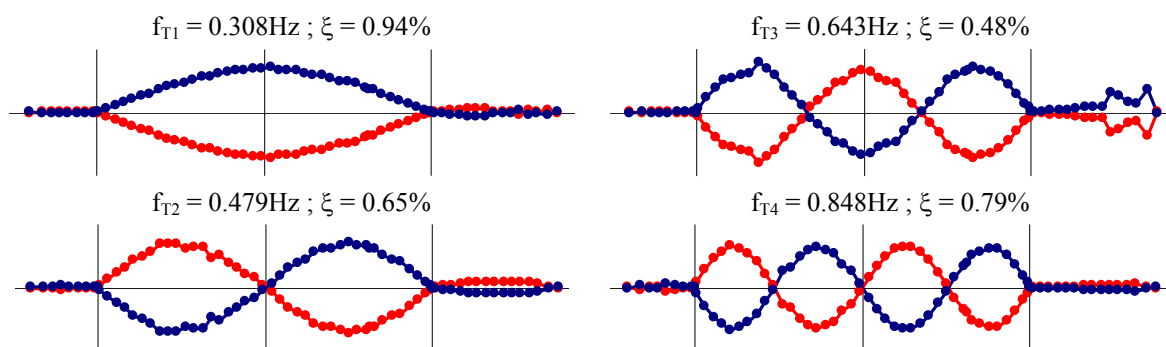
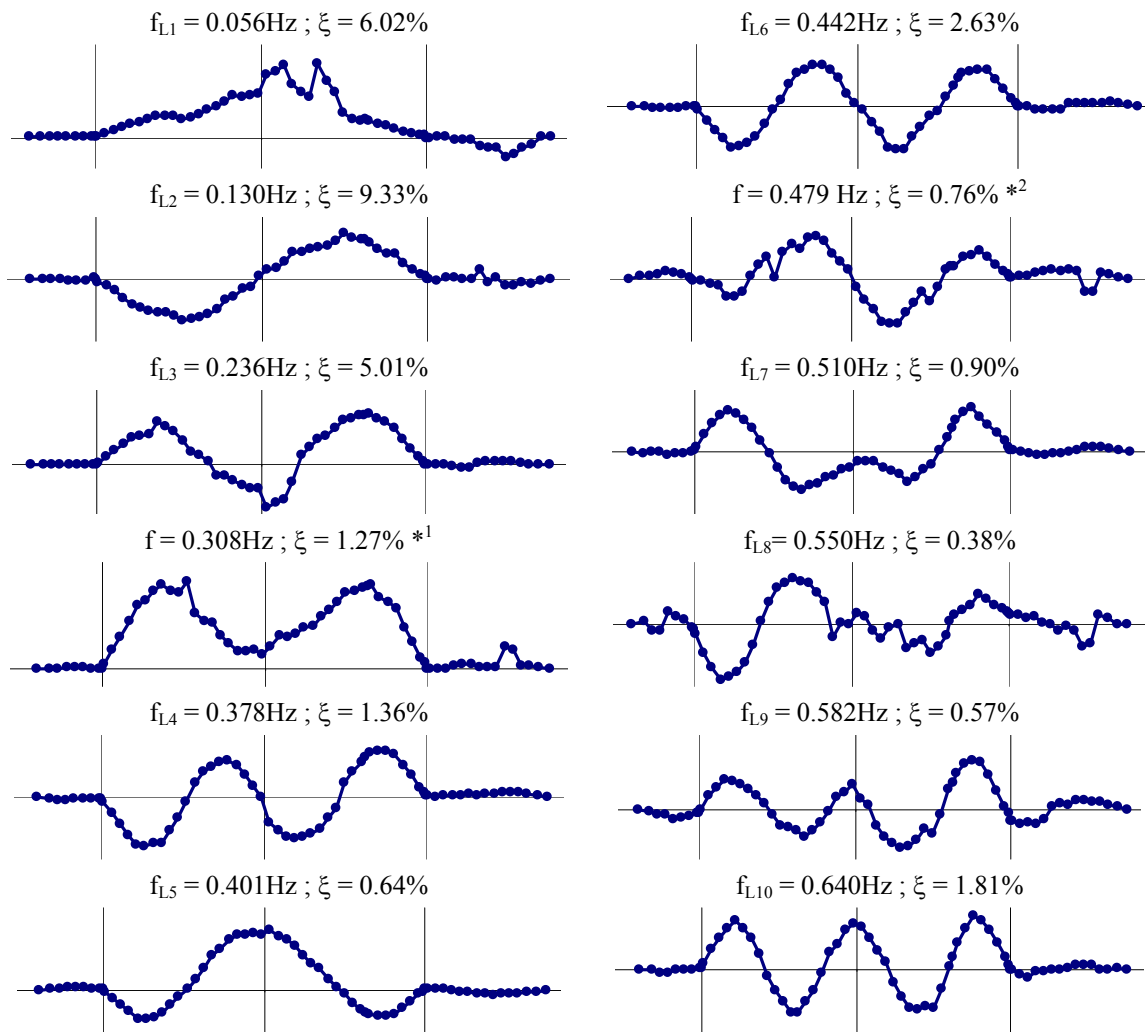


Figure 3.36 – Modal parameters of the torsion modes in the frequency range 0-1Hz (it is assumed that the modes are symmetric with respect to the deck longitudinal axis).



*1 *2 lateral components of the first and second torsion modes

Figure 3.37 – Modal parameters of the lateral bending modes in the frequency range 0-1Hz.

p-LSCF, PoGER

The application of the p-LSCF method also followed the PoGER methodology and was also based on the separated processing of the same three pre-combined signals that were adopted in the application of the SSI-COV method. The analysis was only concentrated on the global modes of the deck. In this case, global half-spectrum matrices were constructed from the half-spectrum matrices associated with each setup. These are 5-by-2 matrices because in each setup 5 sections were instrumented (5 pre-combined signals) and 2 outputs were selected for references (combined signals associated with the two reference sections of the central span). The elements of these matrices were estimated from the inverse Fourier transform of the positive time lags of correlation functions with a maximum time lag of 256 points, after the application of an exponential window with a factor of 0.1 (the amplitude of the last element of the correlation function is reduced 10%). Complementary analyses using longer

correlation functions and a higher number of references outputs demonstrated that the increase of the calculation effort is not compensated by an improvement on the quality of the results.

The processing of the three global half-spectrum matrices (one for each set of pre-combined signals) led to the stabilization diagrams presented in Figures 3.38, 3.39 and 3.40, which contain the estimates provided by models with orders between 10 and 50. The stabilization diagram associated with the half-sum of the vertical accelerations presents 12 very clear alignments. These are associated with 12 vertical bending modes that are characterized in the last two columns of the first section of Table 3.2 by their natural frequencies and modal damping ratios. The comparison with the results provided by the SSI-COV method shows that the mode with frequency 0.172Hz is missing. Several alternative analyses with different parameters were tested to try to identify this mode, but none of them was successful. Regarding the remaining vertical bending modes, the estimates provided by both methods present almost coincident mode shapes, similar natural frequencies and quite consistent modal damping ratios.

With respect to the processing of the lateral accelerations, surprisingly, the stabilization diagram of the p-LSCF method (Figure 3.39) is quite different from the one provided by the SSI-COV method (Figure 3.35). There are much less alignments of stable poles and even the presented diagram was only possible after the application of a high pass filter with a cutting frequency of 0.05Hz that reduces the influence of the quasi-static component (very relevant in the lateral direction, as illustrated with the spectra presented in Figure 3.29). Still, it was possible to identify the most relevant lateral bending modes. The results of the p-LSCF method are compared with ones from the SSI-COV method in the second section of Table 3.2. The natural frequencies are similar but considerable differences are observed on the modal damping ratios. All the mode shapes, except the first one, are analogous; the first lateral mode shape estimated with the p-LSCF method is represented in Figure 3.41.

Finally, the processing of the half-difference of the vertical acceleration time series with the p-LSCF method provided the very clear stabilization diagram represented in Figure 3.40. From this diagram, it was possible to obtain the modal parameters presented in the last section of Table 3.2. A very good correlation is observed between all the characteristics of the torsion modes estimated by the two applied methods.

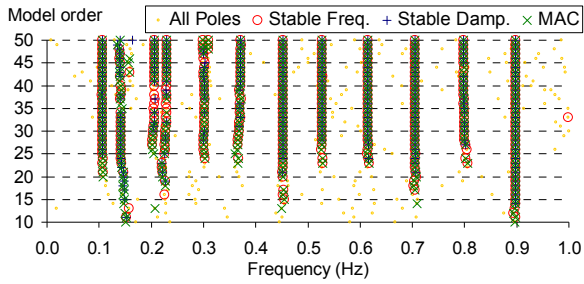


Figure 3.38 – p-LSCF global analysis stabilization diagram for the half-sum of vertical accelerations.

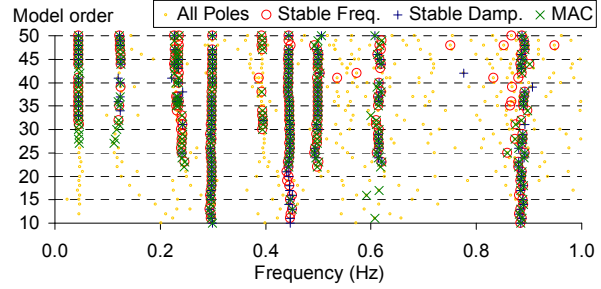


Figure 3.39 – p-LSCF global analysis stabilization diagram for lateral accelerations.

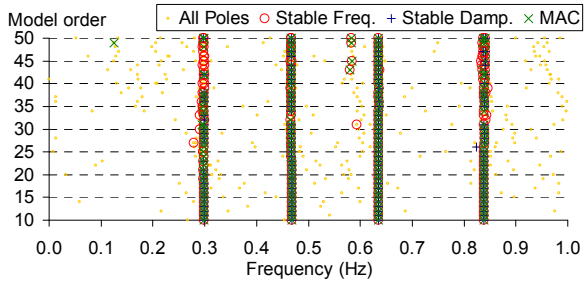


Figure 3.40 – p-LSCF global analysis stabilization diagram for the half-difference of vertical accelerations.

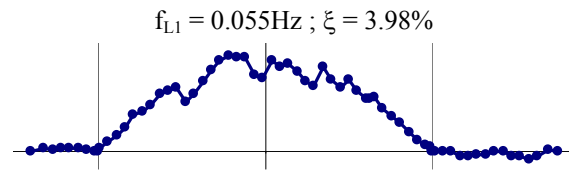


Figure 3.41 – First lateral mode shape identified with the p-LSCF method.

Table 3.2 – Comparison of results provided by the SSI-COV and p-LSCF methods

Vertical bending modes				Lateral bending modes				Torsion modes			
SSI-COV		p-LSCF		SSI-COV		p-LSCF		SSI-COV		p-LSCF	
f (Hz)	ξ (%)	f (Hz)	ξ (%)	f (Hz)	ξ (%)	f (Hz)	ξ (%)	f (Hz)	ξ (%)	f (Hz)	ξ (%)
0.116	3.11	0.116	3.27	0.056	6.02	0.055	3.98	0.308	0.94	0.308	0.97
0.149	8.06	0.153	6.56	0.130	9.33	0.134	7.37	0.479	0.65	0.477	0.72
0.172	4.38	-	-	0.236	5.01	0.238	2.69	0.643	0.48	0.645	0.60
0.215	2.68	0.215	2.21	0.378	1.36	-	-	0.848	0.79	0.849	0.64
0.240	1.64	0.239	1.24	0.401	0.64	0.404	0.21				
0.309	1.25	0.311	1.12	0.442	2.63	0.455	4.29				
0.381	1.43	0.380	1.15	0.510	0.90	0.508	2.47				
0.462	0.91	0.462	1.02	0.550	0.38	-	-				
0.537	0.99	0.557	0.91	0.582	0.57	-	-				
0.625	0.74	0.625	0.83	0.640	1.81	0.625	1.83				
0.716	0.89	0.716	0.83								
0.809	0.74	0.809	0.56								
0.909	0.66	0.908	0.69								

SSI-COV, Combined Procedure

The main disadvantage of the previously applied methodology, based on the global analysis of all datasets, is its inability to characterize the modal parameters variability during the ambient vibration test. However, as already explained in section 2.5.5, once a set of reference modal parameters is available and an algorithm for the automatic analysis of the data presented in stabilization diagrams is also accessible, in a second step, each dataset can be automatically processed to obtain the scatter of the estimates that are consistent with the previously identified reference modal parameters.

This approach was followed using all the datasets collected at the deck of Humber Bridge (Magalhães et al. 2009a). Therefore, the SSI-COV identification algorithm was applied 26x3 times (number of setups x number of pre-combined signals). For each dataset of pre-combined signals, the estimates provided by models of orders varying from 20 to 120 were post-processed by the algorithm for automatic identification presented in section 2.4.4. In the application of the clustering algorithm, the limit for the distance between elements of the same group was set at 0.02 (the distance between estimates is calculated with equation (2.94)). In order to increase the chance of obtaining estimates for low excited modes, conservative values for the number of expected modes (selected clusters) were adopted for each mode type: 16 for vertical bending modes, 18 for the lateral bending modes and 10 for the torsion modes. Afterwards, average modal parameters of the estimates grouped in the same cluster were calculated after the elimination of the estimates with extreme values for the modal damping ratios (outliers analysis). These mean values were then compared with the reference modal parameters, which are the values that resulted from the application of the SSI-COV, PoGER approach. For each reference mode and for each setup, the candidate with the maximum MAC (considering the modal components at the reference sections) was selected from the estimates with natural frequencies within the interval defined by the reference natural frequency $\pm 5\%$. Only the candidates with MAC values higher than 0.8 were accepted.

Figures 3.42 and 3.43 show the results associated with the processing of the half-sum of vertical accelerations measured at 63 sections of the deck during 26 setups. Figure 3.42 depicts the time evolution of the first 13 natural frequencies of vertical bending modes. It can be observed that some natural frequencies are missing in some setups, especially the estimates of the third mode. This means that the algorithm used for the automatic selection of poles was not able to identify, in that specific datasets, a group of mode estimates with an average natural frequency close (difference less than 5%) to one of the reference values and with similar modal components at the reference sections (MAC higher than 0.8). Note that the third vertical mode was also the mode that was not identified by the p-LSCF method.

Figure 3.43 presents all the pairs of natural frequencies and modal damping ratios estimated from the data collected in each setup. This clearly shows a considerable dispersion of the modal estimates of modes with frequencies lower than 0.3Hz, which is due to the damping dependence on operational and environmental factors (like the level of vibration and the wind characteristics) and also to the uncertainties of the identification technique.

Figures 3.44 and 3.45 characterize the scatter of the modal parameters associated with the lateral bending and torsion modes. The first three lateral modes present a very large dispersion, whereas the torsion modes present quite consistent modal damping ratios during the testing period.

Table 3.3 compares the results obtained with the combined procedure (designated by APoSER-Automatic Post Separate Estimation Re-scaling) with the ones obtained with the PoGER approach. For the APoSER methodology the final values of the modal parameters are given by the average of the estimates associated to each of the 26 setups. It can be verified that these average values are consistent with the estimates provided by the PoGER approach.

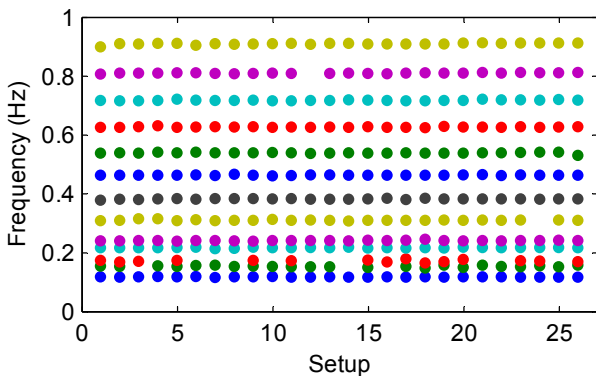


Figure 3.42 – Variation of the first 13 natural frequencies of vertical bending modes during the ambient vibration test.

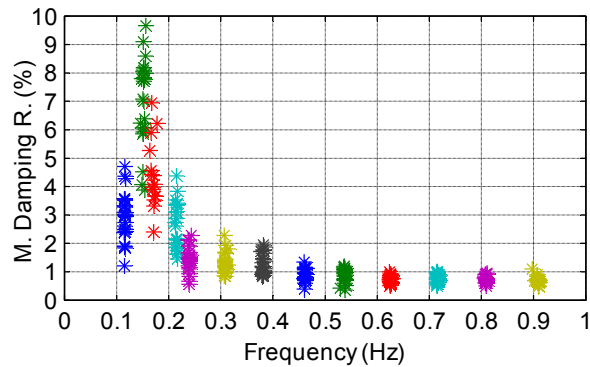


Figure 3.43 – Estimates of the natural frequencies and modal damping ratios of the vertical bending modes given by the independent processing of 26 setups.

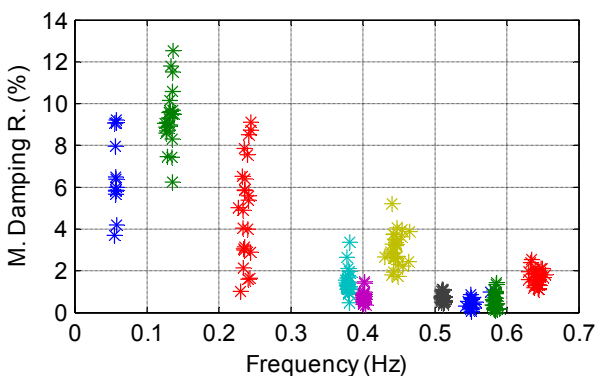


Figure 3.44 – Estimates of the natural frequencies and modal damping ratios of the lateral bending modes given by the independent processing of 26 setups.

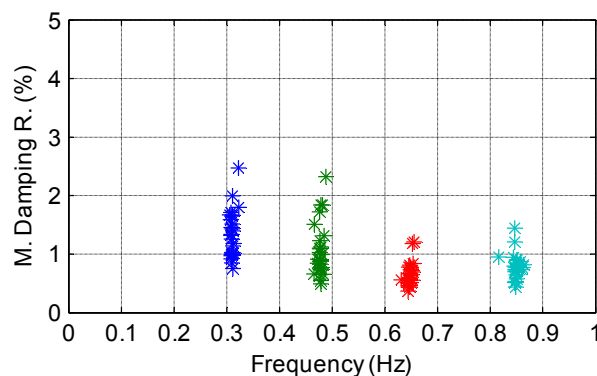


Figure 3.45 – Estimates of the natural frequencies and modal damping ratios of the torsion modes given by the independent processing of 26 setups.

Table 3.3 – Comparison of results provided by SSI-COV, PoGER and APoSER (σ denotes standard deviation)

Vertical bending modes						Lateral bending modes					
PoGER		APoSER				PoGER		APoSER			
f (Hz)	ξ (%)	f (Hz)	σ (f) (Hz)	ξ (%)	σ (ξ) (%)	f (Hz)	ξ (%)	f (Hz)	σ (f) (Hz)	ξ (%)	σ (ξ) (%)
0.116	3.11	0.116	0.0008	2.98	0.81	0.056	6.02	0.057	0.0009	6.62	1.85
0.149	8.06	0.152	0.0026	7.04	1.54	0.130	9.33	0.132	0.0037	9.34	1.43
0.172	4.38	0.170	0.0036	4.42	1.20	0.236	5.01	0.237	0.0047	4.95	2.42
0.215	2.68	0.215	0.0012	2.59	0.79	0.378	1.36	0.379	0.0017	1.46	0.59
0.240	1.64	0.239	0.0012	1.47	0.45	0.401	0.64	0.401	0.0009	0.76	0.26
0.309	1.25	0.309	0.0018	1.30	0.37	0.442	2.63	0.446	0.0075	3.06	0.80
0.381	1.43	0.381	0.0014	1.27	0.34	0.510	0.90	0.511	0.0015	0.72	0.19
0.462	0.91	0.462	0.0010	0.88	0.21	0.550	0.38	0.552	0.0075	0.46	0.26
0.537	0.99	0.537	0.0020	0.87	0.23	0.582	0.57	0.584	0.0023	0.58	0.38
0.625	0.74	0.625	0.0014	0.73	0.13	0.640	1.81	0.642	0.0058	1.71	0.38
0.716	0.89	0.716	0.0016	0.78	0.15						
0.809	0.74	0.809	0.0013	0.74	0.11						
0.909	0.66	0.908	0.0030	0.70	0.12						
Torsion modes											
PoGER		APoSER				PoGER		APoSER			
f (Hz)	ξ (%)	f (Hz)	σ (f) (Hz)	ξ (%)	σ (ξ) (%)	f (Hz)	ξ (%)	f (Hz)	σ (f) (Hz)	ξ (%)	σ (ξ) (%)
0.308	0.94	0.311	0.0039	1.35	0.40						
0.479	0.65	0.478	0.0048	1.06	0.45						
0.643	0.48	0.648	0.0048	0.66	0.20						
0.848	0.79	0.849	0.0083	0.79	0.21						

3.4.6 Conclusions

This section presents the processing of a very complete ambient vibration test database collected during 5 days at the Humber Suspension Bridge. This processing included a first simple and fast analysis with the Peak-Picking method, essential to obtain an in-situ confirmation of the quality of the acquired data, and then the application of the parametric methods SSI-COV and p-LSCF, to achieve more reliable estimates of the modal parameters of the modes in the frequency range 0-1Hz.

The large number of setups forced the application of procedures based on the global processing of all datasets. In this case, the PoGER approach was followed together with both identification methods. The SSI-COV method permitted to obtain a more complete set of modal parameters. The p-LSCF method confirmed most of the results of the SSI-COV method but failed the identification of some

modes. The larger discrepancies in the results of both methods were observed for the modal damping ratios of the lateral modes, which indicate a lower level of confidence on these parameters, probably due to the lower level of the accelerations measured in the lateral direction. Still, both methods were able to clearly identify the most relevant modes, including the lowest lateral mode with a frequency of about 0.05Hz.

The new approach presented in section 2.5.5, which is based on the separated automatic processing of each setup using as reference the estimates provided by the global analysis, was applied for the first time in this section and proved to be a very easy to apply procedure that complements the results of the global analysis with the characterization of the modal parameter estimates variability.

The estimated modal damping ratios of some modes are quite high, especially taking into account that these are associated with low vibration levels. The setup-by-setup analysis confirmed the average values of the global analyses and showed that there is a great variability of the higher modal damping ratios, associated with modes with frequencies lower than 0.3Hz. This variability is partially due to the uncertainty of the estimates and may also stem from the contribution of aerodynamic damping, which depends on the wind speed, and also from the damping dependency on the vibration amplitude. The dynamic monitoring system planned for this structure (Brownjohn and Worden 2008) will certainly contribute for a better understanding of these phenomena.

3.5 Damping estimation with Ambient Vibration and Free Vibration Tests

3.5.1 Introduction

Modal damping ratios are very difficult to predict at design stage, but they have a strong influence on the dynamic structural behaviour, because the amplitude of vibrations at resonance is inversely proportional to these coefficients. Therefore, in structures subjected to relevant dynamic excitations it is important to perform dynamic tests after construction with the specific goal of identifying accurate modal damping ratios, to check the assumptions adopted during design and if necessary implement solutions to increase the damping and consequently reduce vibrations.

Like for other modal parameters, experimental identification of modal damping ratios can be based on forced vibration, free vibration or ambient vibration tests. As the results presented in the previous section demonstrate, the estimates of modal damping ratios obtained with ambient vibration tests are not as accurate as the ones provided for natural frequencies and mode shapes. The correlation between different methods is always lower for this parameter and the scatter of the estimates extracted from different datasets is quite high. That is why it is still very common to perform complementary free vibration tests, when the accurate identification of modal damping ratios is required.

During the last years, the Laboratory of Vibrations and Monitoring of FEUP has been involved in the execution and/or signal processing of a significant number of dynamic tests that comprehended both ambient and free vibration tests. Therefore, in this section, the results achieved with these two types of tests in five relevant structures are compared, in order to evaluate the level of accuracy that modern output-only modal identification techniques can provide for damping ratio estimates.

3.5.2 Free vibration tests: testing and processing procedures

Free vibration tests performed on civil engineering structures for identification of modal damping ratios can be of two types: (i) measurement of the free response after application of a sinusoidal load with an excitation frequency coincident with one of the structure natural frequencies or (ii) measurement of the free structural response after the application of an impulse or imposed displacement.

The first type of tests is less practical, since the application of a sinusoidal load requires the use of special equipment, it takes long time, as a separate test has to be done for each mode, and previous knowledge of the natural frequencies and mode shapes is needed, because each sinusoidal load must be applied with the correct frequency at the anti-node of the mode to be excited. Even so, these tests

were recently performed for instance on a steel roadway bridge (La Grand Ravine Bridge) and on the suspended roof of the Braga Stadium (the results are presented in section 3.5.6 and 3.5.7)

On the other hand, the impulse tests are more convenient, because they can rely on the sudden release of a mass previously suspended from the structure (no special mechanical equipment is needed) and with just one test it is possible to identify the modal damping ratio of several modes. Of course that, the prior identification of mode shapes is useful, as the mass must be hanged from a point where the most important modes have significant modal components.

In (Rodrigues and Ledesma 2009) an alternative free vibration test is presented for the case of railway bridges. It is demonstrated, with results from three bridges, that free decays measured after the passage of trains can be successfully used to identify the structure modal parameters.

The traditional procedure to analyse free decays recorded after the application of an impulse consists of applying several band-pass filters to isolate the contributions of the most important modes. As the resulting sets of filtered data should only contain the contribution of a single mode, the modal damping ratio is directly estimated by fitting exponential functions to the relative maxima of these free decays. In the case of decays measured after application of resonant sinusoidal loads, they should only contain the contribution of a single mode, so the exponential functions can be directly fitted to the recorded time series. This classical approach faces difficulties to isolate the contribution of modes with close natural frequencies.

As alternative to this rather simple procedure, the output-only SSI-COV method can be adapted to extract modal parameters from free decays measured after the application of an impulse, imposed displacements or sinusoidal loads. The observed free decays are closely related with the correlations of the responses associated with a white noise excitation. Consequently, these measured free decays can be used as input of the SSI-COV method, taking the place of the correlation functions calculated from the ambient responses. However, in this case, instead of basing the identification on the correlations between all the measured responses and some responses elected as references, evaluated at predefined time lags, the algorithm is applied to a time dependent matrix with a single column containing the free decays measured at the instrumented points (yd_i , where i represents the time instant, yd is a n_o -by-1 matrix and n_o is the number of measured responses).

This approach overcomes the limitations of the traditional procedure, as with this method the model that is fitted to the data permits the identification of closely spaced modes. Furthermore, with this technique, after the identification of the modal properties, it is possible to decompose the measured

free decays in modal decays using the well-known decomposition of the output correlation matrix (already presented in chapter 2):

$$R_i = C \cdot A^{i-1} \cdot G \quad (3.1)$$

If the correlation matrix is replaced by the measured free decays (yd_i) and A substituted by its modal decomposition, the following expression is obtained:

$$yd_i = C \cdot \Psi \cdot \Lambda^{i-1} \cdot \Psi^{-1} \cdot G \quad (3.2)$$

where Ψ contains in its columns the mode shapes, Λ is a diagonal matrix, whose elements are equal to $e^{\lambda_k \cdot \Delta t}$, Δt is the time interval between each sample and λ_k ($k = 1, \dots$, model order), are the eigenvalues of the state-space model that are related with the natural frequencies and modal damping ratios of the tested structure. The contribution of a specific mode for the measured decays can be obtained with equation (3.2), considering in the diagonal matrix only the two eigenvalues (complex conjugate pairs) that are associated with that mode. This post-processing is very important to check the results and to evaluate the importance of each mode in the measured response. The damping estimates of the less excited modes are expected to be less reliable.

3.5.3 Millau Viaduct

A detailed description of the dynamic tests performed on this structure and of the results provided by the processing of the data recorded during the ambient vibration test has already been presented in section 3.3. Now, the analysis is focused on the identification of modal damping ratios from the measured free decays and on the comparison of these results with the ones provided by the ambient vibration test.

The data recorded by the three adopted data acquisition systems (see Figure 3.7) during the free vibration tests was processed by the SSI-COV method adapted to deal with free decays, and by the application of band-pass filters (Caetano et al. 2004). A good agreement was found between results obtained from the different data sets and identification methods. Here, only two sets of results are presented: the ones provided by the application of the SSI-COV method to the decays collected by the permanent monitoring system of the bridge (sensors S1 to S12 in Figure 3.7) and by the application of band pass-filters to the data collected by the recorders G1 to G3 (Figure 3.7).

The free vibration tests comprehended the application of impulsive loads, which stemmed from the sudden rupture of a cable tensioned with 600kN in a first test, and with 1000kN in a second one. The

first impulse produced a maximum acceleration at the mid-span of the span where the load was applied of 77mg, whereas the second impulse produced at the same point an acceleration of 106mg.

Figure 3.46 compares the estimates given by the p-LSCF method applied independently to the data of the 13 setups of the ambient vibration test (represented by the average values and by error bars with an amplitude equal to the standard deviations) with three results of the free vibration tests: the estimates provided by the SSI-COV method applied to the two free decays measured by sensors S1 to S12 and produced by the two applied impulsive loads (Imp1: 600kN, Imp2: 1000kN), and the estimates given by the use of band pass filters on the decays recorded by sensors G1 to G3 after the application of the higher load. As expected, the parametric identification algorithm confirmed all the modal damping coefficients identified by application of band-pass filters and made possible the identification of damping ratios for a higher number of modes.

The stabilization diagram associated with the application of the SSI-COV method to the decay with higher amplitude (Figure 3.47) shows that it was not possible to identify all the modes that were previously characterized with the ambient vibration test (Figure 3.10). This happens because the impulsive load only excited the vertical modes with non-zero modal components at its point of application.

The comparison between the results associated with the AVT and the FVT shows very small differences in the two modes with frequencies between 0.2 and 0.3Hz. But, significant differences are observed for the third mode represented in the graphic. These might be explained by the dependence of the corresponding modal damping ratio with the amplitude of oscillations, as it is observed a coherent increase of the damping ratio with the amplitudes of vibration of the used time segments. For the other modes the results present a reasonable consistency, except for the last mode. The presented stabilization diagram shows a less clear alignment of stable poles for this mode, and so, less reliable results were obtained.

The application of the SSI-COV method permitted also, by use of equation (3.2), to decompose the measured decay in modal decays of the modes excited by the applied impulses. Figure 3.48 shows that decomposition for one segment of the decay produced by the application of Imp2. This permits to clearly identify the modes with higher contributions to the measured structural response.

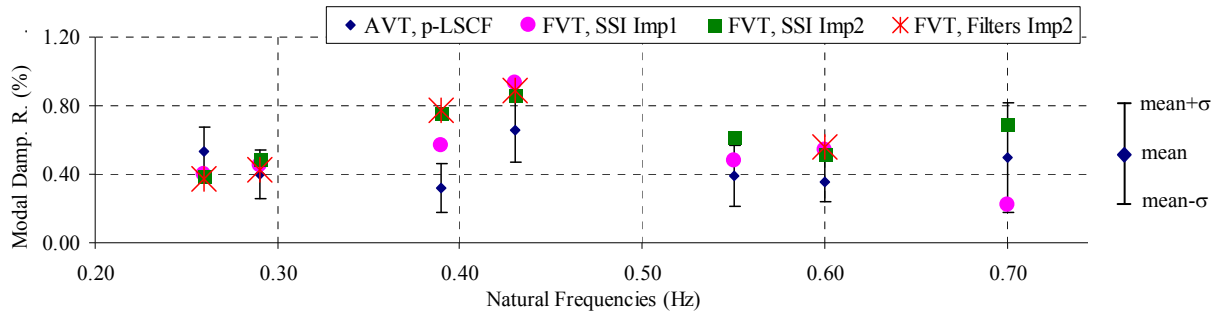


Figure 3.46 – Modal damping ratios obtained from the Ambient Vibration Test (AVT) and from the Free Vibration test (FVT). Imp1: 600kN; Imp2: 1000kN.

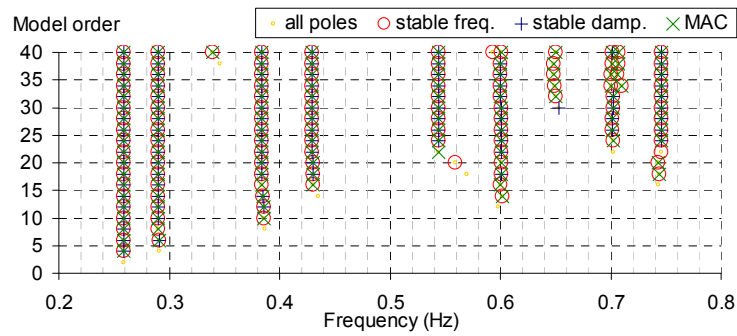


Figure 3.47 – Stabilization diagram associated with the application of the SSI-COV method to the free decay measured after the application of impulse Imp2.

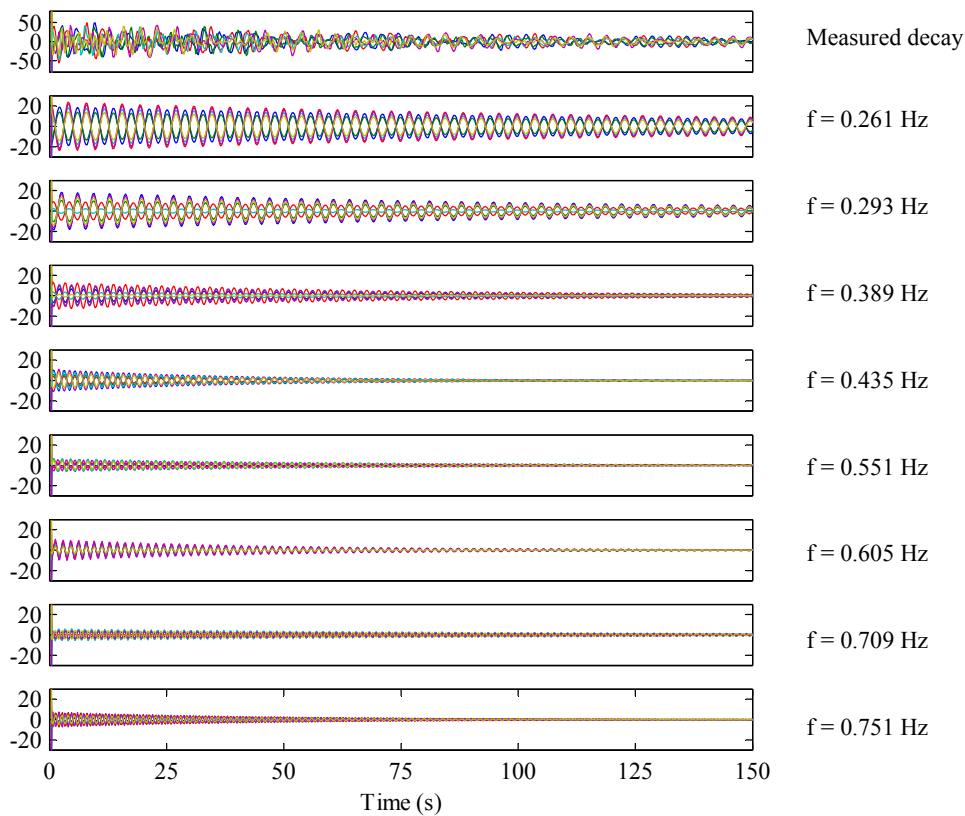


Figure 3.48 – Free decay measured at Millau Viaduct decomposed in modal decays.

3.5.4 Vasco da Gama Cable-stayed Bridge

The Vasco da Gama Bridge, in Lisbon, crosses the Tagus River over a total length of about 12km. This large structure includes a cable-stayed bridge (Figure 3.49) with a main span of 420m and 3 lateral spans on each side (62m + 70.6m + 72m), resulting in a total length of 829.2m. The height of the two H-shaped towers is 147m.



Figure 3.49 – Vasco da Gama Bridge (general view and barge suspended for application of the impulse)

At the end of construction, an ambient vibration test and a free vibration test were performed. During the ambient vibration test, the main excitation source was wind, which suffered speed fluctuations between 1m/s and 22m/s. A total of 58 points were instrumented during 25 setups of 16 minutes. The free vibration test consisted in the measurement of the bridge response at 3 sections after the sudden release of a barge with 60ton (Figure 3.49, left) previously suspended from the bridge deck. To minimize the effect of undesired aerodynamic damping, this test was performed on a day with low wind velocities (<2.5m/s).

The modal parameters identified with the ambient vibration test showed that the first mode shape is transversal (BT1) and has a natural frequency of 0.30Hz. The first vertical bending mode (BV1) has a natural frequency of 0.34Hz, whereas the first torsion mode (T1) has a natural frequency of 0.47Hz. Further information about the dynamic tests, the procedures used to process the collected data and the obtained results are presented in references (Caetano 2000; Cunha et al. 2001) and (Peeters et al. 2002).

Here, only the results related with the modal damping ratio estimates are detailed. Figure 3.50 shows the modal damping ratios estimated using the data collected during the ambient vibration test (AVT) and during the free vibration test (FVT). Like in the Millau viaduct, the results of the AVT have a significant dispersion (average standard deviation of 0.36%, average relative standard deviation of 52%). The estimates of both procedures of analysis applied to the free decays (filters and SSI-COV) are close to the average values of the AVT.

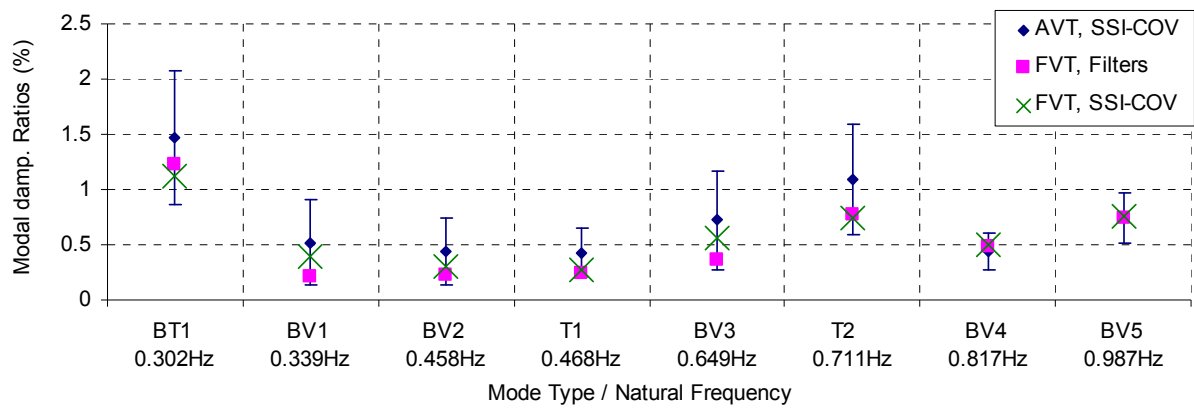


Figure 3.50 – Modal damping ratios obtained from the Ambient Vibration Test (AVT, mean values and standard deviations) and from the Free Vibration Test (FVT) of Vasco da Gama Cable-stayed Bridge.

3.5.5 Pedro e Inês Footbridge

The Pedro e Inês Footbridge is a new landmark that links both banks of Mondego River at the city of Coimbra, in Portugal. The bridge has a total length of 275m and is formed by a central parabolic arch, which spans 110m and rises 9m, and two half parabolic arches in steel supporting with total continuity a composite steel-concrete deck (Figure 3.51).



Figure 3.51 – Pedro e Inês Footbridge (general view and hanging of a mass for application of an impulse)

The preliminary dynamic studies of this bridge indicated that it would be prone to vibrations induced by pedestrians, requiring control devices. For the correct final design of the Tuned Mass Dampers (TMDs) it was crucial to have a good characterization of the dynamic behaviour of the bridge. Therefore, after bridge construction and before installation of the control devices, dynamic tests were performed. These included an ambient vibration test and several free vibration tests. A detailed description of all the tests, processing procedures and results can be found in (Magalhães et al. 2007b). Further details about the design of the tuned mass dampers, of their test and calibration and of the permanent monitoring system installed to observe the level of vibration of the bridge are reported in (Caetano et al. 2010a; Caetano et al. 2010b).

The ambient vibration test comprehended 19 setups that allowed the measurement of acceleration time series with 16 minutes at 20 sections. The collected data was processed by the Enhanced Frequency Domain Decomposition method and by the Data driven Stochastic Subspace Identification (SSI-DATA) method. Both methods provided estimates of natural frequencies and modal damping ratios for 13 modes in the frequency range 0-5Hz. In Figure 3.53, the results of the SSI-DATA method for the modal damping ratios are summarized by the average value and by an interval of variation defined by the standard deviation (average standard deviation of 0.45%, average relative standard deviation of 46.5%).

As the accurate identification of modal damping ratios was of utmost importance for the correct design of the control devices, a total of 10 free vibration tests were performed: 3 vertical and 3 lateral impulses applied at mid-span (Figure 3.52), 2 vertical impulses applied in the deck span over one of the supports inside the river (Figure 3.51, left) and 2 vertical impulses in a lateral span.

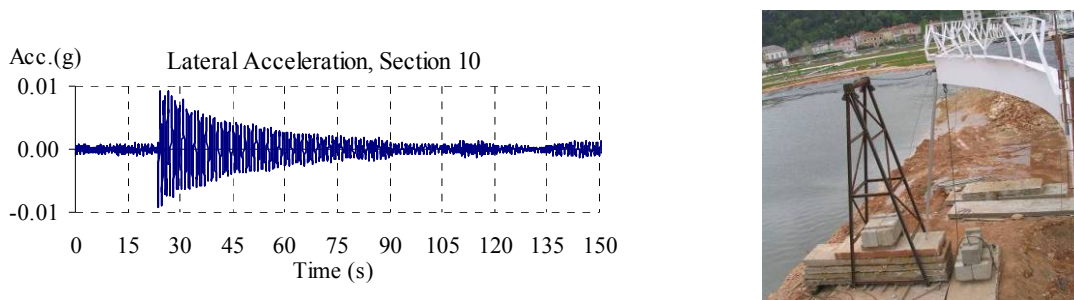


Figure 3.52 – Free vibration response measured at Pedro e Inês Footbridge after the application of a lateral impulse and auxiliary structure used for its application.

The first eight impulses were applied to excite specific modes (the mass was suspended at the anti-node of the mode). So, it was possible to isolate the contribution of each of those modes in the measured free decays, by application of low-order band-pass filters. The results of this procedure are represented in Figure 3.53 by the marks ●. A total of 8 values are represented: three estimates for the first and second modes and two estimates for the 10th mode. It is evident the good agreement between these estimates and the average values provided by the ambient vibration test.

The last two impulses, applied in a lateral span, excited several modes and so the use of filters became inappropriate. Thus, the collected decays were processed by the SSI-COV method, providing the two groups of estimates represented also in Figure 3.53 by the marks x. These estimates confirmed the ones provided by the other free decays for the 2nd and 10th modes and it was possible to obtain estimates for more 5 modes that agree quite well with the results of the ambient vibration test.

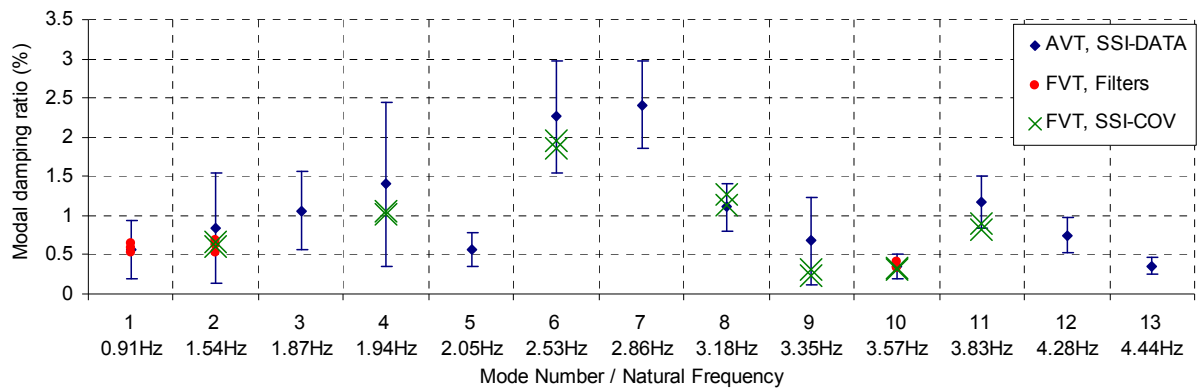


Figure 3.53 – Modal damping ratios of Pedro e Inês Footbridge obtained from the Ambient Vibration Test (AVT) and from the Free Vibration Tests (FVT).

3.5.6 La Grande Ravine Bridge

La Grande Ravine Bridge integrates a new road (“Route de Tamarins”) that was recently constructed in La Réunion, an island in the Indian ocean, which is a French overseas department. This bridge, with a span of 288m, crosses over an exceptional 170m deep breach (Figure 3.54). Its deck is a steel box girder, which was launched from both sides and connected at midspan. Intermediate supports are provided by two high-performance prestressed concrete braces inclined at 20° to the horizontal. These braces are rigidly fixed into the abutments at the base and equilibrated at the other end by external prestressing cables, which go inside the deck and are anchored in counterweights at the back of the abutments (Croiset et al. 2006).



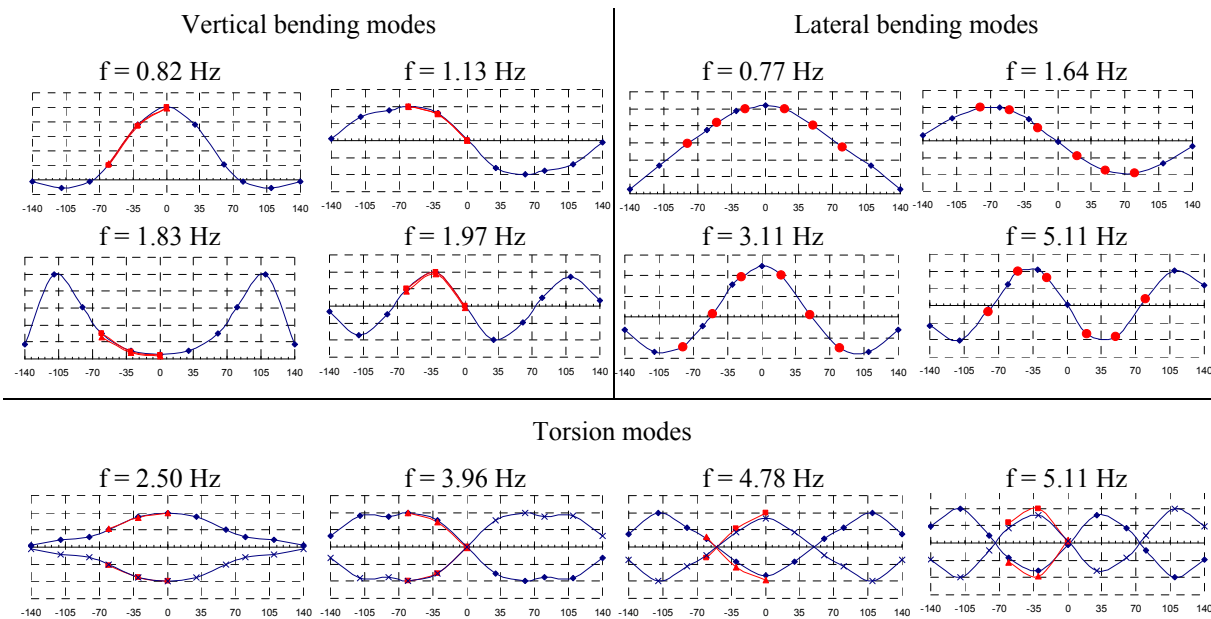
Figure 3.54 – La Grande Ravine Bridge, during construction (photo from www.greisch.com) and after completion.

As this structure is located in a region with a high risk of cyclonic winds, special numerical studies were developed by Setec TPI (www.tpi.setec.fr) using data derived from wind tunnel tests performed at CSTB. In order to validate the numerical models adopted in these studies, after the bridge construction and before its opening to traffic, a series of dynamic field tests were performed. These

were coordinated by CSTB and aimed the accurate identification of the most relevant modal parameters of the bridge by performing forced vibration tests and collecting acceleration time series of the bridge response to ambient excitation. ViBest/FEUP was responsible for the processing of the ambient vibration measurements.

The bridge response to ambient excitation was measured during 5 setups of 30 minutes with 6 uni-axial force-balance sensors, which were placed in a total of 11 sections of the bridge, either measuring along the vertical or lateral directions. Firstly, it was performed an independent analysis of each dataset with the SSI-COV algorithm, and then the resulting mode shape components were “glued” to obtain a global picture of the mode shapes. Figure 3.55 shows some of the identified mode shapes (Magalhães et al. 2009b). As some sections were measured in more than one setup, the mode shape components provided by the analysis of different datasets are represented with different symbols.

Figure 3.57 characterizes the limits of the interval of variation of the modal damping ratio estimates for the first 14 modes of the bridge given by the application of the SSI-COV method to the 5 collected datasets.



As the ground under the bridge was inaccessible, it was not possible to suspend masses at the deck to produce free decays. Therefore, forced vibration tests were carried out in this case through the use of an exciter developed in CSTB (Figure 3.56), which permits the application of both horizontal and vertical sinusoidal loads. After tuning the frequency of excitation with one of the bridge frequencies, it

was possible to obtain modal decays like the one represented in Figure 3.56, from which the modal damping ratios could then be extracted.

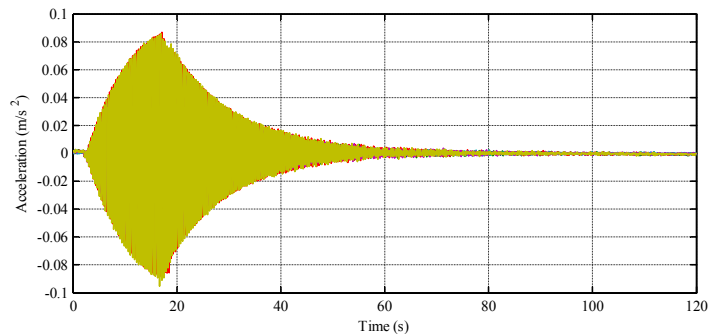


Figure 3.56 – Excitation device developed by CSTB with two steel profiles to increase its mass, and one of the measured free decays.

After performing a considerable number of forced vibration tests (during 4 days) with different excitation frequencies and different positions of the exciter and of the sensors, it was possible to obtain modal damping estimates for 14 modes (Flamand 2009). As it was observed that damping depends on vibration amplitude for most of the modes, the fitting of exponential functions to the recorded decays at different amplitude levels provided an interval of variation for the majority of the modal damping ratios. The limits of these intervals are graphically characterized in Figure 3.57.

Taking into account that the ambient vibration and the free vibration tests were not performed under the same conditions (different vibration levels, different masses over the bridge, different wind action,...) the results are reasonably coherent.

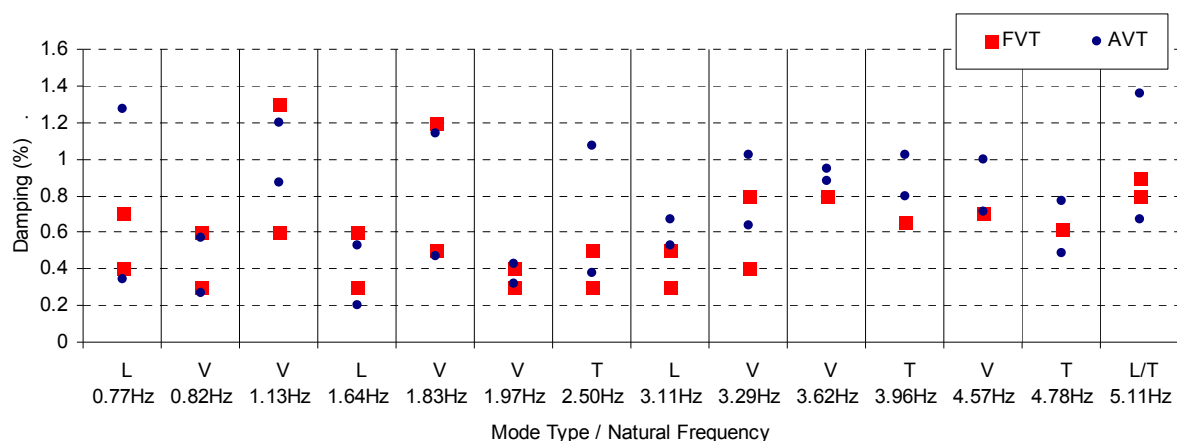


Figure 3.57 – Modal damping ratios of La Grande Ravine Bridge obtained from the Ambient Vibration Tests (AVT) and from the Free Vibration Tests (FVT). Mode type: L – lateral bending; V – vertical bending; T – torsion.

3.5.7 Braga Stadium Suspended Roof

The Braga Stadium was one of the stadia constructed in Portugal for the 2004 European Football Championship (Figure 3.58). The most outstanding element of the structure is its very flexible suspended roof, which is essentially formed by cables with a span of 202m that support two concrete slabs over the stands of the stadium with a length of 57.3m and a thickness of 0.245m. As chapter 6 is dedicated to the continuous dynamic monitoring of this roof, it is presented there a more detailed characterization of the structure and of the experimental work developed to prepare the installation of the monitoring system. This section is only focused on the comparison of the modal damping estimates provided by the AVT and FVT performed on this unique roof after its construction.

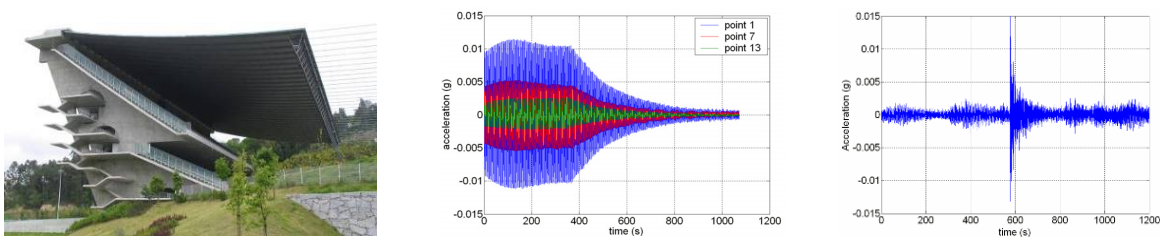


Figure 3.58 – Braga Stadium (view of the east side and records of the decays measured in the roof after the application of a sinusoidal load in resonance and after the application of an impulse).

The necessity of analysing the susceptibility of the suspended roof to wind excitation required the accurate experimental identification of modal damping ratios. Taking that in mind, three different types of dynamic tests were performed: an ambient vibration test that allowed the identification of natural frequencies, mode shapes and modal damping ratios; forced vibration tests with the application of sinusoidal loads and free vibration tests after the application of an impulse for the identification of modal damping ratios. These dynamic tests and the obtained results are described in (Magalhães et al. 2008c). To better interpret the results subsequently presented, it is import to refer that the roof structure is characterized by low natural frequencies (the first ten modes have natural frequencies between 0.28Hz and 0.74Hz) and presents some closely spaced modes (see chapter 6, Figure 6.6).

Figure 3.59 summarizes the results of all used methodologies in terms of modal damping ratios. The ambient vibration test comprehended the performance of 28 setups with duration of 16 minutes. Each setup was processed independently, and therefore, besides the average values, it was possible to obtain a rough characterization of the estimates variability. The presented plot characterizes the results provided by the SSI-COV method by means of the average values of the modal damping ratios and the corresponding standard deviations, quantified with the error bars. The standard deviations present an average value (involving the first 10 modes) of 0.21%, which corresponds to a mean relative standard deviation of 52.6%.

The decays measured after the application of an impulse were processed using the procedure based on band pass-filtering and subsequent fitting of exponential functions and by means of the SSI-COV method. The use of filters allowed the identification of the modal damping ratios of modes 3, 4, 6 and 10 (FVT, Filters). For the others, it was not possible to get results owing to the closeness of the natural frequencies or due to lack of excitation. The application of the SSI-COV method to the same data (FVT, SSI-COV) made possible the identification of additional damping ratios by the analysis of the stabilization diagram presented in Figure 3.60, which contains 10 clear vertical alignments of stable mode estimates. When the comparison is possible, the results of both techniques (FVT, Filters and FVT, SSI-COV) are almost coincident (Figure 3.59).

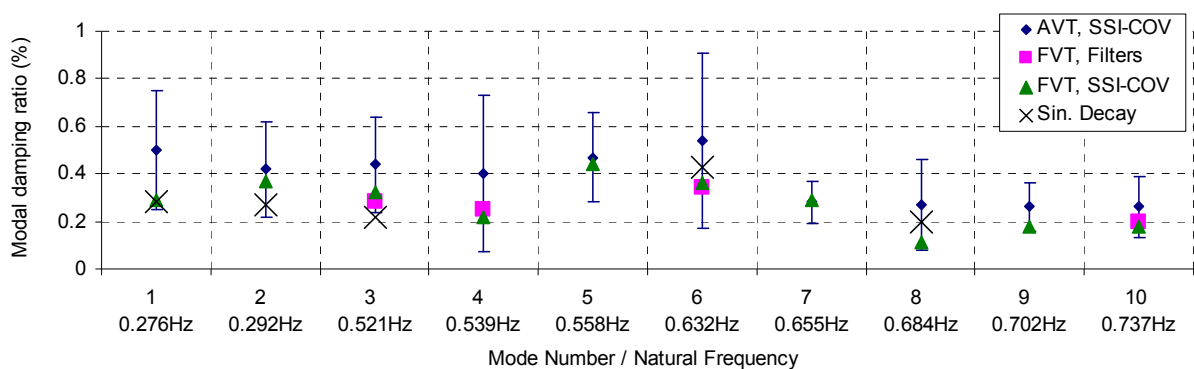


Figure 3.59 – Modal damping ratios of the stadium suspended roof obtained from the Ambient Vibration Test (AVT), from the Free Vibration Test (FVT) and from the tests with sinusoidal excitation (Sin. Decay).

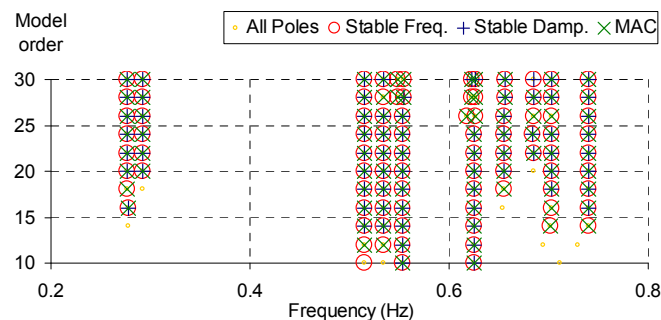


Figure 3.60 – Stabilization diagram associated with the application of the SSI-COV method to the free decays measured after the application of an impulse.

Furthermore, the SSI-COV method provided the modal decays of the first 10 modes represented in Figure 3.61. These characterize the responses of the 5 points of the roof measured during the free vibration test. It is very interesting to observe that the sum of the calculated modal decays almost coincides with the measured ones. This comparison is shown in Figure 3.62 for one of the measured degrees of freedom (located at one corner of the roof).

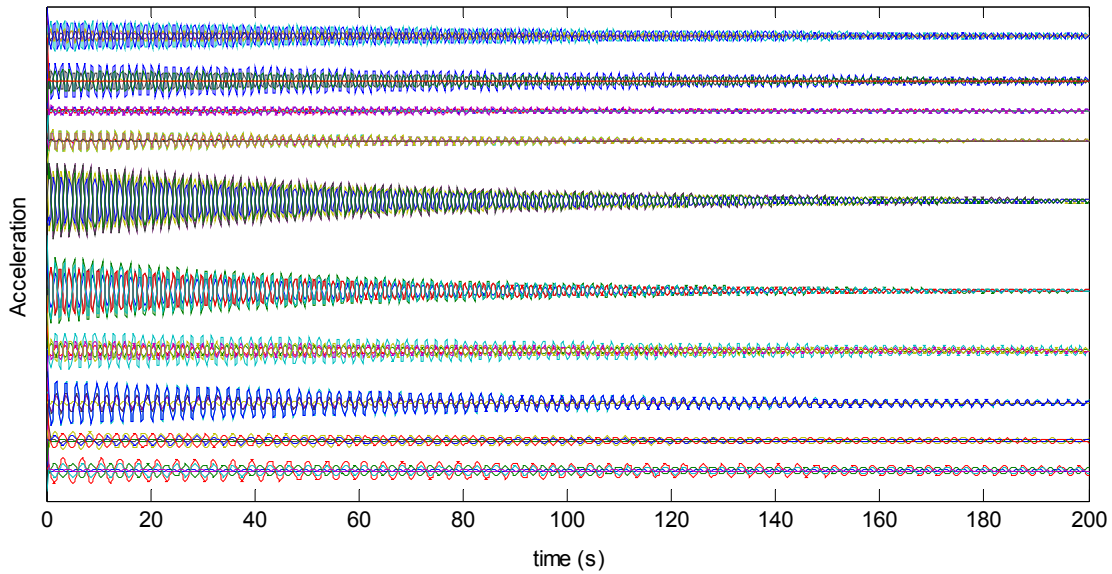


Figure 3.61 – Decomposition of the measured free decays, after application of the impulse, in the modal decays of the first 10 modes of the stadium suspended roof.

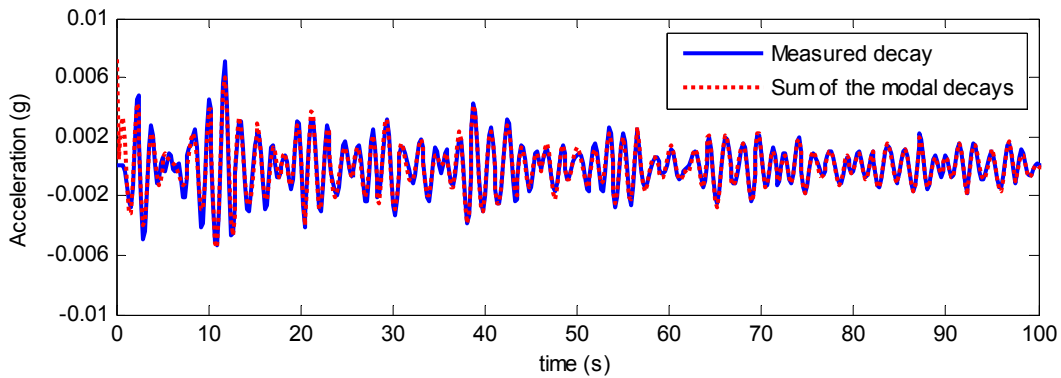


Figure 3.62 – Comparison between measured free decay and sum of calculated modal decays for one of the instrumented degree of freedom of the stadium suspended roof.

The forced vibration tests based on the application of sinusoidal loads were performed to specifically excite five modes. As the measured response only contained the contribution of one mode the modal damping ratio estimates were obtained by the more traditional procedure (fitting of exponential function). Figure 3.59 shows that the identified modal damping ratios are similar to the ones provided by the impulsive tests. Therefore, the significant amount of work associated with these tests could have been avoided.

The comparison between modal damping ratios identified using artificial and ambient excitation shows some differences, quite relevant in the case of the first mode. However, the intervals of variations (defined by the standard deviation) presented for the AVT estimates contain all the values derived from the FVT.

3.5.8 Conclusions

The processing of data collected during the ambient vibration tests and free vibration tests of five relevant civil engineering structures permitted to compare the quality of the modal damping estimates provided by the two types of tests.

The estimates extracted from artificially imposed free decays are more reliable because the input is controlled, the effect of the aerodynamic damping can be minimized, since these tests are carried out under very low wind velocities, the signal to noise ratios are higher than in ambient vibration tests and the interference of the mass and suspension of vehicles over the bridge or other operational factors can be avoided, as these tests should be performed with the structure closed. Beyond that, forced vibration tests also permit to study the variation of the modal damping ratios with the level of vibration. However, they are not as practical and economical as the ambient vibration tests and the estimates of the modal damping ratios are associated with excitation levels that are different from the ones observed during normal operation conditions.

In the analyses of the free decays, the SSI-COV method and the exponential decay fitting provided similar results when it was possible to individualize the modes by the use of filters, but the former was able to provide accurate estimates for a higher number of modes. Furthermore, the decomposition of the free decays in modal decays showed very good results also in applications with closely spaced modes.

The results obtained with the presented full scale applications demonstrated that the damping estimates provided by ambient vibration tests showed a fairly high scatter, expressed by relative standard deviations around 50%. This stems mainly from two reasons. One is the use of relatively short time series (between 16 and 30 minutes) to study structures with fundamental natural frequencies around 0.3Hz and small modal damping ratios, as it was the case of the two cable-stayed bridges and of the suspended roof. The relative standard deviations observed in the numerical studies presented in chapter 2, when the SSI-COV method was applied to time segments of 20 minutes, were around 20%. The other main reason is the non-stationarity of the excitation, not reproduced in the simulations presented in chapter 2. During the ambient vibration tests, sometimes performed during more than one day, significant variations of the intensity and frequency content of the excitation can occur, which can lead to variations of the structural damping, that is commonly dependent on the amplitude of structural oscillations (e.g. existence of friction forces that are only mobilized for certain vibration levels). The variation of wind characteristics during ambient vibration tests can also induce damping variations

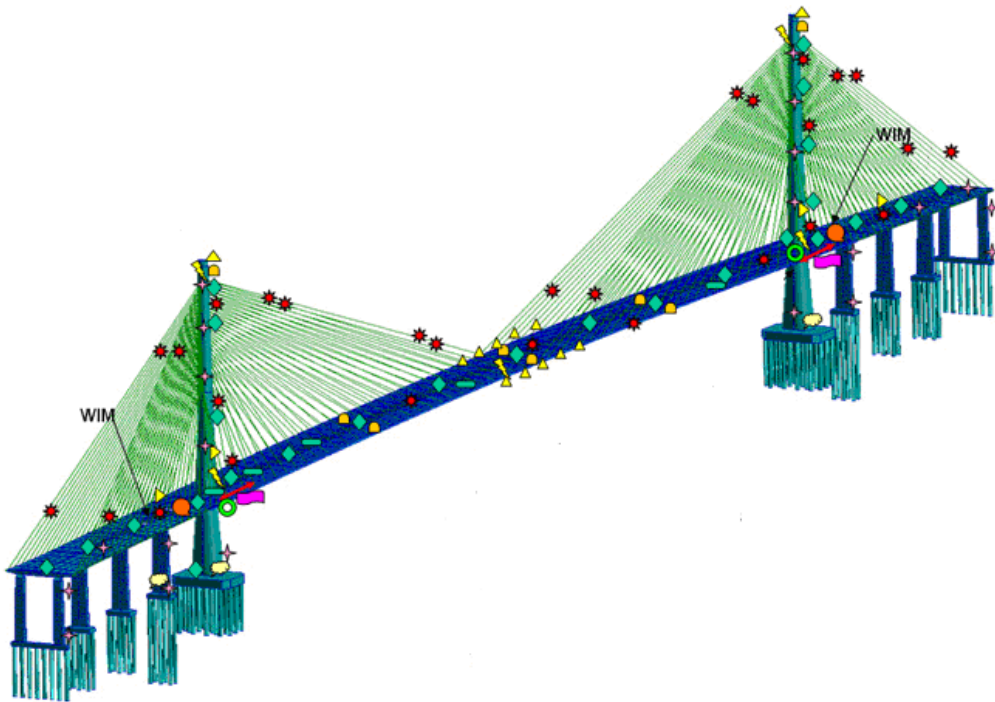
motivated by the existence of aerodynamic damping components, as already observed during the ambient vibration test of a cable-stayed bridge (Magalhães et al. 2007a).

Besides that, in all the analysed databases, the majority of the modal damping ratio estimates obtained from the free decays is within the interval defined by the average values +/- the standard deviation of the estimates given by ambient vibration tests. This conclusion is very important to increase the confidence in the results provided by ambient vibration testing.

To sum up, ambient vibration tests are very economical and practical, and, if properly performed, can provide reasonable estimates of modal damping ratios. Still, it is important to develop further research in order to better understand all the reasons behind the observed dispersion and find procedures to reduce it. Data collected by permanent dynamic monitoring systems that allow the tracking of the damping evolution during long periods under different ambient conditions can be very useful in this context. Some interesting results are presented in chapters 5 and 6.

Chapter 4

CONTINUOUS DYNAMIC MONITORING



4. CONTINUOUS DYNAMIC MONITORING

4.1 Introduction

A Structural Health Monitoring (SHM) system for a civil engineering structure is the combination of equipment adequate to permanently characterize the structure actions and responses (or just the responses) with processing tools that transform the acquired data into information, which permits to assess the structural performance of the instrumented elements. Actually, the concept of SHM has been used in a broader sense also to designate sporadic static or dynamic field tests or period monitoring installations (Bisby 2004), but the aim of the current research is the development of systems based on the permanent acquisition of data and on its online automatic processing to provide valuable information to operators and owners of important infrastructures.

Nowadays, an increasing interest in permanent monitoring of the structural behaviour of important civil infrastructures, such as bridges, has been observed. This is due to the need of controlling a huge number of structures that are reaching their critical age and also to the necessity of validating the performance of new structures with high levels of complexity. Moreover, recent technological advances have contributed to make the installation and operation of permanent monitoring systems more practical and economical and permit a very efficient transmission and processing of the recorded data.

All over the world there are already several advanced applications of SHM systems on bridges. Trying to cover emblematic examples from different countries documented in available bibliography, the following applications can be mentioned: Tsing Ma Bridge in Hong Kong (Wong 2004), Akashi Kaikyo Bridge in Japan (Abe and Fujino 2009), Seohae Bridge in Korea (Koh et al. 2009), Confederation Bridge in Canada (Londono 2006), Commodore Barry Bridge in the United States (Aktan et al. 2003) and Oresund Bridge in Denmark (Peeters et al. 2003). A large number of other bridge monitoring systems are described in (Boller et al. 2009) and Ko and Ni (2005) present a brief synthesis of the monitoring systems installed in twenty Chinese bridges. Despite the greater attention devoted to bridge applications, SHM systems have also been implemented in other civil engineering structures. Brownjohn (2007) describes relevant SHM applications in dams, offshore structures, buildings, towers, nuclear installations and tunnels. Descriptions of further examples are also available in the databases of SAMCO (www.samco.org) and SHMII (www.ishmii.org) associations.

In Portugal, it is of historical relevance the pioneering monitoring system installed by the National Laboratory LNEC in the 25 de Abril Suspension Bridge over the Tagus River in Lisbon. This was

installed in 1970 and already included a dynamic monitoring component (Marecos and Castanheta 1970) that permitted the identification of the lateral and vertical fundamental frequencies. Nowadays, the main Portuguese bridges and dams are equipped with monitoring systems. But the majority of them only comprehend static measurements sometimes complemented by a dynamic component which is generally only configured for the recording of the structure response during the occurrence of earthquakes. There are some exceptions, as for instance the Pedro e Inês Footbridge, which has a dynamic system in permanent operation to monitor its levels of vibrations, and that is also suitable to track the evolution of its modal properties (Caetano et al. 2010b). Two other recent and quite complete installations will be presented in chapters 5 and 6.

The implementation of well designed structural health monitoring systems permits to: (1) check design assumptions, specially when novel materials or structural systems are adopted; (2) verify serviceability limits and provide alerts when pre-defined thresholds are overcome (for instance the occurrence of strong winds may impose the closure of a bridge); (3) evaluate the structural condition and detect possible damages at an early stage; (4) provide information for safety assessment immediately after extreme events such as earthquakes; (5) provide useful data for the planning of inspections and rehabilitation or maintenance operations; (6) evaluate the effectiveness of maintenance, retrofit or repair works; and (7) obtain large amounts of in-situ data useful to better understand load-response mechanisms and consequently improve the design codes.

Despite the already considerable number of practical applications, a large research effort is still needed to improve the present management and processing capabilities in order to conveniently explore the data collected by the instrumentation and accomplish all the mentioned potential capabilities.

The achievement of the previously presented goals imposes also the integration of several types of sensors to measure diverse phenomena using different working principals and adopting different sampling rates. The most commonly implemented SHM systems can be divided in the following three main components: (1) static monitoring, characterized by the adoption of sampling rates of the order of 1 sample/hour, which aims the characterization of phenomena with a low rate of variation, as for instance the temperature at several points of the structure, the relative displacements at the joints and the evolution of displacements, rotations and strains motivated by concrete creep and shrinkage or settlements at the supports; (2) dynamic monitoring, which encompasses the characterization of the structural response to dynamic loads, such as wind, traffic (trucks, trains or pedestrians in footbridges) or earthquakes, the evaluation of the levels of vibration for verification of serviceability limit states, the characterization of the time evolution of the structure modal parameters, the characterization of the level of cable vibrations and of the corresponding axial forces through the use of the vibration chord

theory; and (3) durability monitoring, which aims the evaluation of the corrosion of steel elements or of the reinforcement of concrete structures due to chloride contamination or carbonation (FIB 2003). Some monitoring systems are also complemented by weather stations for characterization of the environmental factors (temperature, humidity and wind), weigh-in-motion systems to measure traffic loads and video cameras. A very recent application where all these components are being integrated is the monitoring system of the Stonecutters Bridge, in Hong Kong. Figure 4.1 shows the distribution of the different types of adopted sensors. However, after presenting this quite complex monitoring system, it is important to refer that it is also possible to extract very relevant information from much more modest systems, provided that the sensors and the elements to be monitored are carefully selected.

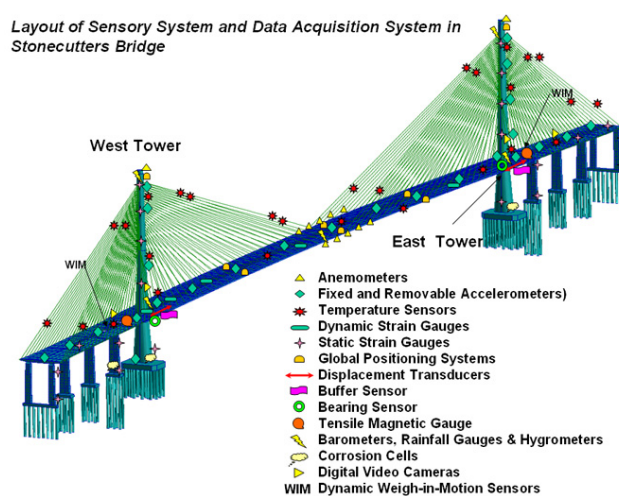


Figure 4.1 – Monitoring system of the Stonecutters Bridge (from www.stonecuttersbridge.net).

The data collected by each monitoring component has to be processed by specific algorithms, but then it is very important to analyse and correlate the achieved results in order to provide to operators and owners only a synthesis of the most relevant outputs from the structural behaviour point of view.

The present work, and in particular this chapter, is focused on the use of the operational modal analysis algorithms presented in chapter 2 to process time series collected by permanent dynamic monitoring systems, so that the recorded data is transformed into information from which the structural performance of the instrumented system can be inferred. The followed procedure is described in the next section (4.2). Then, section 4.3 presents the tools available to post-process the modal parameters identified with the algorithms already described in chapter 2 with the aim of detecting structural anomalies. Finally, section 4.4 describes a software package that integrates most of the presented algorithms and that was developed for the management and processing of the large amounts of data collected by permanent dynamic monitoring systems.

4.2 Structural Health Monitoring based on Modal Parameters

The goal of all vibration-based health monitoring procedures is to extract features from periodically sampled dynamic responses that can serve as indicators of the structural condition of the system under observation. The continuous statistical analysis of the time evolution of these features should permit to evaluate the ability of the structure to perform its intended function despite its inevitable ageing and degradation.

As reported in (Sohn et al. 2002), there exist several alternatives for the features to be extracted from dynamic measurements. However, in the case of civil structures monitored under normal operation, only the features that can be extracted from the responses of the dynamic system to ambient excitation are adequate. Output-only modal analysis techniques permit the identification of the structure modal parameters under operational conditions and therefore, the estimated natural frequencies, mode shapes and modal damping ratios can be adopted as “fitness for purpose” or damage indicators. Alternatively, features extracted from the use of ARMA models (Sohn et al. 2002), spatial filters (Deraemaeker et al. 2008), robust singular value decomposition directly applied to the collected time series (Vanlanduit et al. 2005), principal components analysis of the collected time series (De Boe and Golinval 2003) or Kalman models fitted to the structural responses (Yan et al. 2004) may also be adopted.

For the post-processing of the identified features, a large number of damage detection algorithms are mentioned in the literature reviews (Doebeling et al. 1996; Sohn et al. 2002). These are organized in four levels: (1) detection of damage, (2) localization of damage, (3) quantification of damage, and (4) prediction of the remaining life of the structure. With a permanent dynamic monitoring system it is difficult to go beyond level 1, because only a limited number of points are usually measured. Still, usually the main goal of a monitoring system is to give an alert that should then trigger more detailed investigations that may then reach level 4. For the purpose of damage detection, one of the important advantages of using modal parameters is their global nature, which means that damage can be detected (but not localized or quantified) without measuring points in the vicinity of the damaged zone.

The present work is focused on the analysis of the time evolution of modal parameters with the goal of detecting anomalous variations that might be caused by the occurrence of damage. The characterization of the time evolution of modal parameters is only possible with algorithms capable of automatically estimate these parameters from acceleration time series continuously acquired by permanent dynamic monitoring systems. Therefore, the algorithms previously presented in section 2.4, which allow a very accurate automatic identification of natural frequencies, modal damping ratios and mode shapes, are crucial in this context.

As damages are normally associated with a stiffness reduction, this necessarily implies abnormal reductions of the natural frequencies and therefore this is the modal parameter more commonly used for damage detection. Accurately identified mode shapes can be adopted for the localization of damage only if a quite dense measuring grid is used. The modal damping ratios might be also sensitive to damage but the higher uncertainty usually associated with their estimates makes more difficult the identification of small variations. Besides the detection/localization of damage, modal parameters estimated during normal operation can be also used to better understand some phenomena such as the influence of the wind characteristics on natural frequencies and modal damping ratios or the dependency of modal damping ratios with vibration levels.

However, natural frequencies are also influenced by environmental effects (temperature, humidity, wind,...) and by operational factors, as for instance the traffic intensity in the case of bridges. Therefore, it is very important to eliminate the influence of these factors, so that small changes due to damages can be detected.

The temperature is the factor with the larger influence on natural frequencies. Thus, there are several references that report variations of natural frequencies that are correlated with measured temperatures. A variation of 5% of the first natural frequency was observed at the Alamosa Canyon Bridge, located in New Mexico, during a period of 24 hours (Farrar et al. 1997); whereas frequencies variations around 15% were observed at the Z24 bridge, in Switzerland, during one year of observation (Peeters and De Roeck 2001). Larger variations, of the order of 50%, observed in a bridge with a span of 6.76m, are attributed to the freezing of the supports (Alampalli 1998). In more recent continuous monitoring programs, annual variations of the natural frequencies between 5 and 13% have been observed on two box girder concrete bridges (Fraser et al. 2007; Liu and DeWolf 2007), while fluctuations of 0.2 and 1.5% have been quantified in the Ting Kau cable stayed bridge (Ni et al. 2005).

The influence of other factors has also been documented. For instance, in (Macdonald and Daniell 2005), a study based on the monitoring of a cable-stayed bridge reports the influence of the wind speed on the natural frequencies, with velocities of 15m/s leading to frequency decreases of 1%, and states that the variable traffic caused also frequency reductions of 1%. In (Siringoringo and Fujino 2008) variations on the natural frequencies and modal damping ratios of the Hakucho Bridge (a suspension bridge in Japan) are correlated with the wind speed and partially justified by the stick-slip behaviour of the bearings.

The following section of this chapter is dedicated to the methods available to remove the influence on natural frequencies of all the mentioned factors and then provided indexes suitable for the detection of

abnormal structural changes. Alternatively, it is also possible to extract from the structural response features that are sensitive to damage but not sensitive to the environmental influence. Possible candidates are the mode shapes and peaks of the outputs of modal filters (Deraemaeker et al. 2008). However, the use of mode shapes for damage detection imposes the adoption of a measuring grid with a high spatial resolution which makes the monitoring system more complex and expensive. The efficiency of modal filters has not yet been proven in full scale civil engineering applications, which present challenges that cannot be completely tested with numerical simulations or with laboratory experiments.

A very complete proof-of-concept of structural health monitoring based on modal parameters was achieved in the context of the SIMCES research project (Peeters 2000), using as demonstrator the Z24 Bridge in Switzerland, which was a post-tensioned concrete box girder bridge with a main span of 30m. This project included two major phases: one that lasted approximately one year, during which the dynamic response of the bridge was monitored, and a second phase, in which damages were artificially applied to the structure. The first phase permitted to obtain models for the elimination of environmental effects on the estimated natural frequencies and the second step permitted to demonstrate that the imposed damages were detectable from the analysis of the time evolution of the identified natural frequencies corrected by the previously established model.

4.3 Removing environmental and operation effects on natural frequencies

4.3.1 Introduction

One possible approach to remove the effects of environmental and operational factors on natural frequencies consists on the establishment of models capable of representing the physical phenomena behind the frequency changes.

The references mentioned in the previous section related with the study of the effects of temperature on modal parameters, and particularly the work of Rohrmann et al. (2000), which includes the development of a finite element model that incorporates the modelling of the materials thermal behaviour, show that the following physical mechanisms can contribute for the correlation between observed temperatures and frequency changes: dependency of structural materials elasticity modulus on temperature, which is relevant for concrete and very significant for the asphalt commonly used in bridge pavements (the elasticity modulus of asphalt can vary from zero, during the summer when its temperature reaches 50°C, to values similar to the ones of concrete specimens, during winters with negative temperatures); influence of the expansion or contraction movements driven by temperature on the support conditions; opening and closing of cracks that may exist in concrete elements motivated by curvature variations due to differential temperatures; and freezing of the soil around the structure supports, which has consequences on the stiffness of the boundary conditions. This incomplete list already shows that even if just the effect of temperature is considered, the number of phenomena to be modelled is quite large and their effects very complex.

Therefore, this approach is interesting to better understand the major factors with influence on the observed structural dynamic behaviour, but not adequate in the context of structural health monitoring programs, because for each new practical application a very complex model would have to be developed and even so some effects would not be correctly represented.

As a consequence, instead of trying to understand the physics of the problem, it is possible to rely on black-box models, whose parameters are tuned using a large number of observations, to establish relations between the natural frequencies and the factors that may influence them.

However, this approach imposes the measurement of the factors that may influence natural frequencies. As the selection of these factors is not always straightforward, it is possible to follow a third approach, based on statistical tools that allow the correction of natural frequencies without the need to measure environmental and operational factors.

The present work only covers the last two approaches. Both use experimental data to identify a system able to quantify the relation between known or unknown environmental and operational factors (inputs of the system) and the estimated natural frequencies (outputs of the system). In this chapter it is used an analogy with the system identification methods presented in chapter 2 and therefore, the methods that assume that the factors that influence the modal parameters are measured are designated input-output methods, whereas the ones that consider only the time evolution of the natural frequencies are entitled output-only methods.

4.3.2 Input-Output methods

The input-output methods presented here are essentially based on the development of linear regression analyses between estimated natural frequencies and environmental or operational factors measured by the monitoring system. Classical statistical methods with different level of complexity will be presented, starting with static linear regression models and ending with ARX models. Non-linear methods and methods based on the statistic learning theory (Vapnik 1999), such as the support vector machine (SVM) or neural networks (NN) will not be covered. Ni et al. (2005) presents a brief description of the SVM algorithm and demonstrates its application in the context of the structural health monitoring of the Ting Kau cable-stayed bridge. The use of non-linear regression models for the elimination of the temperature effects on natural frequencies is illustrated in (Steenackers and Guillaume 2005) using the database collected at the Z24 Bridge.

Multiple Linear Regression

The simplest method available to establish a model relating observed environmental or operational factors with estimated natural frequencies is the Multiple Linear Regression. Multiple Linear Regression is a statistical technique that can be used to analyse the relation between a single dependent variable and several independent (predictor) variables (Hair et al. 1998). The established relation (model) can be useful, in an initial phase, for understanding the influence of each predictor (input of the model) on the dependent variable (output of the model) and then to predict future values of the dependent variable when only the predictors are known. In the context of Structural Health Monitoring, a first set of data is used to obtain the model and then, in a second step, the model is used to predict the natural frequencies taking into account the measured independent variables. The predicted natural frequencies are subsequently compared with the values directly estimated from the collected acceleration time series.

The underlying linear model is characterised by the equation (Johnson and Wichern 1992):

$$\mathbf{y} = \mathbf{Z} \cdot \boldsymbol{\beta} + \boldsymbol{\varepsilon} \quad (4.1)$$

where \mathbf{y} is a n -by-1 column vector with n observations (y_k) of the dependent variable (y), \mathbf{Z} is a n -by- p matrix with the corresponding n values of p selected independent variables, $\boldsymbol{\beta}$ is a p -by-1 vector with the parameters to be determined that weight the contribution of each independent variable, and $\boldsymbol{\varepsilon}$ is a n -by-1 column vector that contains the values of the random error (ε), which accounts for measurement errors of the elements of \mathbf{y} and for the effects of other variables not explicitly considered in the model. This last term is assumed to have the following properties:

$$\begin{aligned} E[\boldsymbol{\varepsilon}] &= 0 \\ \text{Cov}[\boldsymbol{\varepsilon}] &= E[\boldsymbol{\varepsilon} \cdot \boldsymbol{\varepsilon}^T] = \sigma_\varepsilon^2 \cdot \mathbf{I} \end{aligned} \quad (4.2)$$

where $E[\bullet]$ is the expected value operator, \bullet^T means transpose and \mathbf{I} represents an identity matrix n -by- n . The presented equations state that the mean of the error is assumed to be zero, that the errors are independent and also that their variance (σ_ε^2) is constant.

The first column of \mathbf{Z} is usually composed by ones and the remaining columns contain the independent variables, which are often normalized (subtracting the variable mean from each observation and then dividing the difference by the variable standard deviation). In this way, the mean of the independent variable is given by the first element of vector $\boldsymbol{\beta}$.

The first step of a regression analysis is the selection of independent variables that can contribute to explain the variations observed on the dependent variable. In the context of analysis of the time evolution of modal parameters, the first candidates are temperatures measured in the structure. However, even if just temperatures are used, from all the available temperature measurements, the more relevant to explain the variations of the natural frequencies have to be selected. In a preliminary phase, a set of predictors with high correlations with the dependent variable and low correlations between themselves should be selected. The correlation between two variables x and y , with n observations x_k and y_k , is defined as:

$$r_{xy} = \frac{\sum_{k=1}^n (x_k - \bar{x}) \cdot (y_k - \bar{y})}{\sqrt{\sum_{k=1}^n (x_k - \bar{x})^2} \cdot \sqrt{\sum_{k=1}^n (y_k - \bar{y})^2}}, \text{ with } \bar{x} = \frac{1}{n} \cdot \sum_{k=1}^n x_k ; \bar{y} = \frac{1}{n} \cdot \sum_{k=1}^n y_k \quad (4.3)$$

This index varies from -1 to 1. Absolute values close to one indicate a high linear association (or correlation) between the two variables.

The main objective of regression analysis is then to estimate the parameters (vector β) that provide a good fit between the observations and the values of the independent variable provided by the model. These are usually obtained through the least squares method, which minimizes the sum of the squared errors. Following this approach, the estimates of the model parameters ($\hat{\beta}$) are given by equation:

$$\hat{\beta} = (Z^T \cdot Z)^{-1} \cdot Z^T \cdot \mathbf{y} \quad (4.4)$$

It should be noted that, this expression is adequate for mathematical derivations but has poor numerical properties, being therefore its practical implementation based on the QR decomposition of Z (Mathworks 2009).

After the estimation of the model parameters, the quality of the obtained model has to be evaluated, in particular to check if the predictors were well chosen. As the least squares method minimizes the sum of the squared errors, an obvious indicator of the fitting quality is the value of the loss function, defined as:

$$\hat{\sigma}_\varepsilon^2 = \frac{1}{n} \cdot \sum_{k=1}^n \varepsilon_k^2 \quad (4.5)$$

with the estimated equation errors (also called residuals) defined as the difference between the observed (\mathbf{y}) and estimated ($\hat{\mathbf{y}}$) values of the dependent variable:

$$\hat{\varepsilon} = \mathbf{y} - \hat{\mathbf{y}} = \left(I - Z \cdot (Z^T \cdot Z)^{-1} \cdot Z^T \right) \cdot \mathbf{y} \quad (4.6)$$

The loss function is also an estimate of the error variance (σ_ε^2 defined in equation (4.2)). The major disadvantage of this quality criterion is its dependence on the absolute values of the y variable. This can be avoided using a normalized y or, alternatively, adopting the coefficient of determination defined by equation (Johnson and Wichern 1992):

$$R^2 = 1 - \frac{\sum_{k=1}^n \hat{\varepsilon}_k^2}{\sum_{k=1}^n (y_k - \bar{y})^2} = \frac{\sum_{k=1}^n (\hat{y}_k - \bar{y})^2}{\sum_{k=1}^n (y_k - \bar{y})^2} \quad (4.7)$$

The second equality shows that the coefficient of determination is a ratio between two variances. Therefore, it quantifies the percentage of the total variation in the y_k 's "explained" by the predictor variables. It varies from one, when the fitted equation passes through all data points, to zero, when the predictor variables have no influence on the dependent variable.

Once a good model has been obtained, it can be applied to calculate predictions of the dependent variable (\hat{y}_0) associated with values of the predictors not considered in the construction of the model (denoted by z_0). These are designated forecasts and are given by equation (4.1) without the error term:

$$\hat{y}_0 = z_0 \cdot \hat{\beta} \quad (4.8)$$

As a perfect match between forecasted and observed values is not expected, it is fundamental to compute confidence intervals to account for the inherent uncertainties. If it is assumed that the errors (ε) have a normal distribution, the upper and lower bounds of a $100 \cdot (1-\alpha)$ per cent confidence interval for the forecasted value (\hat{y}_0) are computed as (Johnson and Wichern 1992):

$$\hat{y}_0 \pm t_{n-p, \alpha/2} \cdot \sqrt{\hat{\sigma}_\varepsilon^2 \cdot \left[1 + z_0^T \cdot (Z^T \cdot Z)^{-1} \cdot z_0 \right]} \rightarrow \hat{y}_0 \pm I(z_0) \quad (4.9)$$

The term $t_{n-p, \alpha/2}$ represents the upper $100 \cdot (\alpha/2)$ percentile of a t -distribution (or Student's t -distribution) with $n-p$ degrees of freedom. It should be noted that when $n-p$ is greater than 30 (which easily occurs in the context of continuous monitoring) the t -distribution almost coincides with the normal distribution. As an example, if a 95% confidence interval is pretended and if the number of observation (n) used to establish the model is higher than 30 plus the number of predictors (p), the term $t_{n-p, \alpha/2}$ assumes a value around 2.

Particularising to the monitoring application, the natural frequencies directly estimated from the collected acceleration time series (\tilde{y}_o) should lay within the confidence intervals of the frequency forecasts derived from the established regression model:

$$\hat{y}_0 - I(z_0) < \tilde{y}_o < \hat{y}_0 + I(z_0) \quad (4.10)$$

with $I(z_0)$ defined in equation (4.9). If the first columns of Z is filled with ones and the remaining columns with normalized values of the predictors, then, as already referred, the first model parameter (β_1) coincides with the average value of the depend variable (\bar{y}) and equation (4.10) can be rewritten in the following form:

$$\bar{y} - I(z_0) < \tilde{y}_0 - \sum_{j=2}^p \beta_j \cdot z_{0j} < \bar{y} + I(z_0) \quad (4.11)$$

The previous equation states that each new natural frequency estimate can be corrected using the previously identified regression model and the corresponding values of the predictors (z_{0j}), so that the effects of the environmental and operational factors are minimized. The corrected values should be within a confidence interval around the mean. Values outside the interval can be justified by an incorrect identification of the frequency or by the influence of other factors not explained by regression model, as it is the case of a structural damage.

In the framework of a Dynamic Monitoring project, the multiple regression models should be constructed using data collected during at least an entire year, so that the influence of environmental factors in the natural frequencies is well characterized by considering a large range of variation, with data from summer and winter periods. This is quite relevant because regression models are only adequate to forecast values associated with input variables inside the region of the data used to construct the model. In other words, they are not valid for extrapolations.

Multivariate Linear Regression

In the analysis of the effects of environmental or operational factors on natural frequencies instead of only one dependent variable (output), there exist as many independent variables as the number of estimated modes, which are explained by the same predictors. Therefore, in this case, a multivariate multiple regression analysis has to be applied. This might be solved with the application of the above described procedure as many times as the number of outputs. Alternatively, it is possible to formulate this problem with just one equation:

$$Y = Z \cdot B + E \quad (4.12)$$

where Y is a n -by- m matrix with the time evolution of the m identified natural frequencies in each column, Z is a n -by- p matrix with the corresponding n values of p selected predictors (eg. temperatures), B is a p -by- m matrix with the parameters of the models to be determined and E is a n -by- m matrix that contains in each column the errors associated with the modelling of each natural frequency. All the presented equations for the predictions and confidence intervals remain valid for the multivariate case.

Dynamic regression models

Regression models applied to observations that characterize the time evolution of a certain variable can be classified as static or dynamic. Static models explain the values of the output variables at a certain time instant $y_k = y(t_k)$ using only the observations of the predictors associated with the same time instant $x_k = x(t_k)$. Dynamic models assume that the values of the dependent variables at a certain time instant can also be influenced by the values of the model inputs at previous time instants. In the characterization of the temperature influence on natural frequencies, the adoption of a dynamic model is justified by the dynamics of the heating up and cooling down processes.

The formulation just described for static models can also be followed in the case of dynamic models, by adding predictors composed by observations with a predefined time lag with respect to the observations of the dependent variables.

The ARX model

The dynamic regression model can be further generalized in order to calculate predictions considering also previous values of the dependent variables. This can be dealt using dynamic models described in system identification literature (Ljung 1999), as the ARX model that comprehends an Auto-Regressive output and an eXogeneous input part. If only one input and output is considered, the model is characterized by the following equation:

$$y_k = -a_1 \cdot y_{k-1} - \dots - a_{p_a} \cdot y_{k-p_a} + b_1 \cdot z_{k-p_k} + b_2 \cdot z_{k-p_k-1} + \dots + b_{p_b} \cdot z_{k-p_k-p_b+1} + \varepsilon_k \quad (4.13)$$

where y_k is the value of the dependent variable (output) at instant k , z_k is the value of the predictor (input variable) at instant k , a_k and b_k are the model parameters to be determined and ε_k the model error at instant k . The ARX model is characterized by three parameters: the auto-regressive order p_a (number of past observations of the output variable considered in the model), the exogeneous order p_b (number of adopted values of the input variable) and the pure time delay between input and output p_k .

The presented equation can be easily adapted to consider several input variables, just by replacing z_k and b_k by column and row vectors. Estimates of the model parameters can be obtained by the Least Squares method using the same expression that was presented for the linear regression model (equation (4.4)), after grouping a_k and b_k in one vector (β) and assembling the past observations of the output and the inputs in matrix Z :

$$\begin{aligned}
 \beta^T &= [a_i (i = 1, \dots, p_a) \quad b_i (i = 1, \dots, p_b)] \\
 \varphi_k^T &= [-y_{k-1} \quad \dots \quad -y_{k-p_a} \quad z_{k-p_k} \quad \dots \quad z_{k-p_k-p_b+1}] \\
 Z^T &= [\varphi_1 \quad \varphi_2 \quad \dots \quad \varphi_n]
 \end{aligned} \tag{4.14}$$

After the identification of the model parameters, it can also be used to obtain forecasts. Expressions for confidence intervals of forecasts provided by ARX models are presented in (Peeters 2000).

4.3.3 Output only methods

The present section is focused on a set of methods that eliminate the effects of environmental and operational factors on features extracted from data collected by a dynamic monitoring system through the decomposition of a correlation or covariance matrix of the time variation of the structural features over a reference period of time. These are described and applied for instance in (Kullaa 2004; Yan et al. 2005a) and (Deraemaeker et al. 2008). Alternatively, it is also possible to achieve the same goal by the direct decomposition of time series with the extracted features (Vanlanduit et al. 2005) or through the use of neural networks (Sohn et al. 2003).

Principal Components Analysis

Principal Component Analysis (PCA) is a multivariate statistical tool concerned with explaining the variance or covariance structure of a set of variables through a few linear combinations of these variables (Johnson and Wichern 1992). It is commonly used to reduce the dimension of the problem, by substituting a group of correlated variables by a new smaller group of independent variables, which are designated principal components.

The original variables stored in a vector y with m components (note that in the presentation of the regression analysis y represented a vector with the values of a single variable at different time instants, whereas here y represents a generic sample of m different variables) can be transformed into another set of m variables z by the application of the following equation:

$$z = T \cdot y \tag{4.15}$$

where T is a m -by- m orthonormal matrix (its inverse coincides with its transpose) that applies a rotation to the original coordinate system. The goal of PCA is to find a transformation that leads to a set of variables (z – the principal components) with the following properties: all the variables are independent between each other, so the covariance matrix of z is diagonal, and the variance of the

variables z_1 to z_m decreases from z_1 to z_m . In this way, the first principal component (z_1) explains the major proportion of the variance of the original variables, whereas the last components of z present smaller variances and so some of them can be neglected because they are not relevant to explain the variability of the original variables.

Considering the relation between y and z , the covariance matrix of y (coincident with the correlation matrix of y when the mean of the variables is zero), designated by Σ , may be related with the covariance matrix of z , a diagonal matrix represented by A , through the following expression (because T is an orthonormal matrix $y = T^T \cdot z$):

$$\Sigma = E[y \cdot y^T] = E[T^T \cdot z \cdot z^T \cdot T] = T^T \cdot A \cdot T \quad (4.16)$$

As the singular value decomposition of the covariance matrix of the original variables gives:

$$\Sigma = U \cdot S \cdot U^T \quad (4.17)$$

its outputs can be used to obtain the transformation matrix ($T = U^T$) and the variances of the components of z (elements in the diagonal of S). Since the algorithms for singular value decomposition provide the singular values in descending order, the first element of the diagonal of S coincides with the variance of z_1 . Furthermore, matrix S can be split in two parts: $S_1 = \text{diag}(s_1, s_2, \dots, s_p)$ a diagonal matrix with the first m singular values on the diagonal, and $S_2 = \text{diag}(s_{p+1}, s_{p+2}, \dots, s_m)$ a diagonal matrix with the remaining singular values, which are not relevant to explain the variability of the components of y . The value of p can be found looking for a gap in the plot of all the singular values in descending order. However, in practical applications, a clear drop rarely occurs. So, it is better to rely on the following ratio:

$$I = \frac{\sum_{i=1}^p S_i}{\sum_{i=1}^m S_i} \quad (4.18)$$

This ratio determines the percentage of the variance of the observed data (sum of the variance of each component of y) that is explained by the first p components of z . So, p can be chosen with the goal of achieving a certain value for I , for instance 0.95.

Once p has been chosen, the set of variables z_1 to z_p can be calculated with equation (4.15) using a matrix \hat{T} built from the first p columns of U (note that $T = U^T$). In current statistical applications the analysis ends at this point, as the reduction of the dimension of the problem has already been achieved.

However, it is possible to make a further step to re-map the selected z components (\hat{z}) to the original space, by means of the reduced T matrix (\hat{T}):

$$\hat{y} = \hat{T}^T \cdot \hat{z} = \hat{T}^T \cdot \hat{T} \cdot y \quad (4.19)$$

The differences between the re-mapped values and the original values are quantified by the residual error:

$$\varepsilon = y - \hat{y} \quad (4.20)$$

In the context of eliminating the effects of environmental and operational factors on natural frequencies estimated from data continuously collected by a dynamic monitoring system, vector y has as many components as the number of estimated frequencies. The covariance or the correlation matrix to which the singular values decomposition is applied is estimated from the time evolution of the natural frequency estimates during a period that should be sufficiently large to contain the full range of environmental and operational variations (typically one year) and associated with a “healthy” state of the structure.

In a first instance, the dimension reduction achieved with the application of the Principal Components Analysis forces the system to keep the effects due to relevant factors (as for example the temperature) and to eliminate secondary effects, as for instance the ones due to random errors in the identification of the natural frequencies. Then, the differences between the observed values and the re-mapped values (equation (4.20)) lead to features that are insensitive to the factors modelled by the principal components. Therefore, the application of the transformation expressed by equation (4.19), using a \hat{T} matrix obtained from a dataset associated with a reference state, to new observations and the subsequent calculation of the residues following equation (4.20) produces features (the components of ε) that enhance the effects that are present in the observations, but were not observed in the reference datasets. Consequently, these residues can be used to detect abnormal values that might be justified by the existence of damaged zones. The post processing of these residues will be presented in sub-section 4.3.4 (Control Charts).

The efficiency of this methodology is proven in (Yan et al. 2005a) using data produced by numerical simulations and also collected in a model of a wooden bridge excited by a electro-dynamic shaker. Its application to data continuously collected by a dynamic monitoring system installed in a footbridge is documented in (Hu et al. 2009). An extension of PCA to non-linear cases is proposed and applied to data collected in concrete box-girder bridge (the Z-24 bridge in Switzerland) by Yan et al. (2005b).

In chapter 5 it will be illustrated the importance of PCA in the context of the data processing performed in the presented monitoring application.

Factor Analysis

Factor Analysis (FA) is a multivariate statistical tool whose essential purpose is to describe the covariance relationships among many variables in terms of a few underlying, but unobservable, random quantities called factors (Johnson and Wichern 1992). It can be considered an extension of PCA, as both are based on the decomposition of a covariance matrix, that uses a more elaborate model.

In the context of dynamic monitoring, the estimated features (normally natural frequencies) can be expressed as the sum of two components:

$$y = f(te, hu, wi, tr, \dots) + \varepsilon \quad (4.21)$$

where y is a vector with m components (e.g. first m identified natural frequencies), f is a function of the environmental and operational parameters (temperature, humidity, wind, traffic, ...) and ε is a vector that quantifies the influence of abnormal occurrences, such as a stiffness reduction, on each component of y . Instead of trying to identify the function f , using for instance a regression analysis, it can be decomposed in two mappings (Deraemaeker et al. 2008):

$$f(te, hu, wi, tr, \dots) = L(NL(te, hu, wi, tr, \dots)) \quad (4.22)$$

a first general mapping that might be non-linear (NL) that transforms the environmental and operational factors into a set of so-called unobservable factors (represented by z), which are then related to the estimated features by a linear mapping. The relation between m observable features (the natural frequencies) and p unobserved factors is expressed by the following equation:

$$y = L \cdot z + \varepsilon \quad (4.23)$$

where L is a m -by- p matrix. This equation defines the model adopted for factor analysis. It is similar to the expression used for multivariate linear regression (equation (4.12)), but in factor analysis the z components are not measured. In the framework of factor analysis, the elements of matrix L are designated factor loadings, the components of z are named common factors and the ε_1 to ε_m are called specific factors, since they are a combination of the error in the identification of the y components with the factors that are uniquely associated with each y component.

Furthermore, the factor model assumes the following properties:

$$\begin{aligned}
 E[y] &= E[z] = E[\varepsilon] = 0_{(m \times 1)} \\
 E[z \cdot z^T] &= I_{(p \times p)} \\
 E[\varepsilon \cdot \varepsilon^T] &= \Psi_{(m \times m)} = \begin{bmatrix} \psi_1 & 0 & \cdots & 0 \\ 0 & \psi_2 & \cdots & 0 \\ \vdots & \vdots & \ddots & \vdots \\ 0 & 0 & \cdots & \psi_m \end{bmatrix} \\
 E[\varepsilon \cdot z^T] &= 0_{(m \times p)}
 \end{aligned} \tag{4.24}$$

First of all, as the expected values of the y components are assumed to be zero, the means of the random processes associated with the observed variables have to be subtracted to each new observation. The structure of the covariance matrix of z (coincident with the correlation matrix of z) implies that the common factors are independent and possess a unitary variance. The specific factors are also assumed to be independent between each other and not correlated with the common factors.

Taking into account the previous properties, the following equation for the covariance matrix of the observations can be established:

$$\begin{aligned}
 \Sigma &= E[y \cdot y^T] = E[(L \cdot z + \varepsilon) \cdot (L \cdot z + \varepsilon)^T] = \\
 &= E[L \cdot z \cdot z^T \cdot L^T + L \cdot z \cdot \varepsilon^T + \varepsilon \cdot z^T \cdot L^T + \varepsilon \cdot \varepsilon^T] = \\
 &= L \cdot E[z \cdot z^T] \cdot L^T + E[\varepsilon \cdot \varepsilon^T] \Leftrightarrow \\
 \Sigma &= L \cdot L^T + \Psi
 \end{aligned} \tag{4.25}$$

Factor analysis seeks the determination of matrices L and Ψ that fit a set of n observations of y . There are two algorithms to achieve this: the principal factors method and the maximum likelihood method. Here, only the first one is going to be presented. The description of the other can be found in any classical book of multivariate statistical analysis, as for instance (Johnson and Wichern 1992).

The most simplistic version of the principal factors method assumes that the specific factors are of minor importance and estimates the L matrix from the outputs of the singular values decomposition of the covariance matrix of the observations:

$$\begin{aligned}
 \Sigma &= U \cdot S \cdot U^T = [U_1 \quad U_2] \cdot \begin{bmatrix} S_1 & 0 \\ 0 & S_2 \end{bmatrix} \cdot \begin{bmatrix} U_1^T \\ U_2^T \end{bmatrix} \approx U_1 \cdot S_1 \cdot U_1^T \\
 \hat{L} &= U_1 \cdot \sqrt{S_1}
 \end{aligned} \tag{4.26}$$

In the first expression, like in the application of the Principal Components Analysis, the covariance matrix of the observable variables is approximated neglecting the contribution of its last $m - p$ singular values, which may be selected using the index presented in equation (4.18). Apart from the scale factor $\sqrt{s_i}$ (s_i represents a element in the diagonal of S_1), the factor loadings of the i th common factor coincide with the coefficients for the i th principal component of the data. Therefore, this simple version of the Factor Analysis is equivalent to the application of the Principal Components Analysis.

A more complete factor model is obtained with the inclusion of the specific factors. These may be taken to be the diagonal elements of $\Sigma - L \cdot L^T$ ($\hat{\Psi} = \text{diag}(\Sigma - \hat{L} \cdot \hat{L}^T)$), where L is estimated with equation (4.26). Furthermore, it is still possible to improve the model if the following iterative procedure is followed:

- 1 – singular value decomposition of the correlation matrix estimated from the data:

$$\Sigma = U \cdot S \cdot U^T$$

- 2 – selection of the first p singular values and estimation of matrix L :

$$\hat{L} = U_1 \cdot \sqrt{S_1}$$

- 3 – estimation of the correlation matrix of the specific factor:

$$\hat{\Psi} = \text{diag}(\Sigma - \hat{L} \cdot \hat{L}^T)$$

- 4 – new estimate for matrix $\hat{L} \cdot \hat{L}^T$:

$$\hat{L} \cdot \hat{L}^T = \Sigma - \hat{\Psi}$$

- 5 – singular values decomposition using the new estimate for $\hat{L} \cdot \hat{L}^T$:

$$\hat{L} \cdot \hat{L}^T = U \cdot S \cdot U^T$$

- 6 – go back to step 2 and repeat until the estimates for L converge.

Alternative procedures can be pursued using different strategies to define the initial guesses for the specific factors (Johnson and Wichern 1992).

Given L and Ψ , the estimates of the common factors (z), called factor scores, can be easily obtained. Different formulas are available, which differ on the way the specific factors (in this step regarded as errors) are minimized (Johnson and Wichern 1992). A simple least squares procedure leads to the following equation:

$$\hat{z} = (\hat{L}^T \cdot \hat{L})^{-1} \cdot \hat{L}^T \cdot y = (S_1)^{-1/2} \cdot U_1^T \cdot y \quad (4.27)$$

The resolution of a least squares problem in which the squared errors (ε_i^2) are weighted by the inverse of their variances ($1/\psi_i$) produces the following factor scores:

$$\hat{z} = \left(\hat{L}^T \cdot \hat{\Psi}^{-1} \cdot \hat{L} \right)^{-1} \cdot \hat{L}^T \cdot \hat{\Psi}^{-1} y \quad (4.28)$$

Alternatively, the adoption of the regression method detailed in (Johnson and Wichern 1992), leads to the equation:

$$\hat{z} = \left(I + \hat{L}^T \cdot \hat{\Psi}^{-1} \cdot \hat{L} \right)^{-1} \cdot \hat{L}^T \cdot \hat{\Psi}^{-1} y \quad (4.29)$$

After the estimation of L and z , going back to equation (4.23), it is possible to obtain the residuals ε_i . As explained in the introduction to factor analysis (equation (4.21)), in the context of a dynamic monitoring project, these should be variables that are insensitive to the operational and environmental conditions that can then be used for damage detection. If the structure suffers deterioration with impact on the modal parameters, the factor model established using data from the reference stage cannot explain the changes of the observed variables (usually natural frequencies). Therefore, these changes remain in the specific factors (ε_i), which can then be used to trigger alarms. Like for all the other methods, the factor model should be constructed using data from a full range of operational and environmental conditions.

In (Kullaa 2004) and (Deraemaeker et al. 2008) the use of factor analysis for structural health monitoring is demonstrated using data generated by numerical models. The first reference demonstrates its ability to detected damage under different operational conditions using the model of a crane, and comprehends also the analysis of alternative equations for the estimation of the factor scores (eq. (4.28) and (4.29)). In the second paper, the capability of factor analysis to eliminate the effects of temperature on the modal parameters of a numerically simulated bridge is explored.

4.3.4 Control Charts

After obtaining features that are insensitive to operational and environmental factors, a procedure has to be used to monitor the values of those features in order to detect abnormal occurrences. The control charts are statistical tools that can be used for that purpose. A control chart typically consists of data plotted in time order and horizontal lines, designated control limits, that indicate the amount of variation due to common causes. Therefore, an observation outside the control region is considered to be an out-of-control observation, or in other words, an observation suggesting a special cause of

variation. In the context of structural health monitoring, this cause of variation may be associated with the occurrence of damage.

The simplest control chart, only suitable to control one characteristic, is the \bar{X} -chart (or X -bar chart). This chart is constructed by plotting the individual observations or the mean of groups of observations in time order and by drawing three lines: a centre line (CL) and two additional horizontal lines corresponding to the upper and lower control limits, labelled UCL and LCL, respectively. The centre line is positioned at the mean of the sample with all the observations, designated by $\bar{\bar{x}}$ (it is used the symbol $\bar{\bar{x}}$ for the sample mean because the symbol \bar{x} is reserved for the mean of subsamples). The control limits are given by:

$$\begin{aligned} UCL &= \bar{\bar{x}} + 3 \cdot \sigma \\ LCL &= \bar{\bar{x}} - 3 \cdot \sigma \end{aligned} \tag{4.30}$$

where σ is the sample standard deviation when single observations are controlled. If the mean of subsamples of size r is controlled, then, σ is equal to the sample standard deviation divided by \sqrt{r} . The multiplication of σ by 3 together with the assumption of a normal distribution for the feature that is being controlled corresponds to a confidence interval of 99.7%.

When this control chart is integrated in a dynamic monitoring system, x designates a generic observation of a one-dimensional feature that is insensitive to the operational and environmental effects, which can be, for instance, the Euclidian norm of the residues (ε) obtained after the application of PCA or FA.

However, in the presence of a process characterized by more than one feature multivariate control charts can be applied. In (Johnson and Wichern 1992; Montgomery 2005) and (Kullaa 2003) several alternative multivariate control charts are detailed and applied. Here, only a commonly used chart designated Shewhart or T^2 is presented.

In practical applications two types of control can be followed. Control charts can be used to monitor the stability of a sample of multivariate observations, which means that several observations are available and the goal is to check if all the samples respect the control limits. Or, control charts can be used to set a control region for future observations, taking into account the properties of data collected during a reference period. The second approach is the one that is adequate for implementation in a permanent monitoring system that should check if each new observation lies within a previously defined “safety” region.

The verification of future observations can be done following two methodologies: each new observation can be checked or the verification can be done only when a set of new observations is available.

If each future individual observation x (a vector with m components) is verified the so-called T^2 -statistic is calculated with the expression:

$$T^2 = \frac{n}{n+1} \cdot (x - \bar{\bar{x}})^T \cdot S^{-1} \cdot (x - \bar{\bar{x}}) \quad (4.31)$$

where n is the number of observations collected during the reference period, which are used to obtain the process average ($\bar{\bar{x}}$) and the covariance matrix (S). The lower control limit (LCL) is equal to zero and the upper control limit is equal to:

$$UCL = \frac{(n-1) \cdot m}{n-m} \cdot F_{m,n-m}(\alpha) \quad (4.32)$$

where $F_{m,n-m}(\alpha)$ denotes the α percentage point (e.g. 0.95 or 0.99) of the F distribution with m and $n-m$ degrees of freedom.

If the verification of new occurrences is done using subgroups with r observations of x , the T^2 -statistic is calculated with the expression:

$$T^2 = r \cdot (\bar{x} - \bar{\bar{x}})^T \cdot S^{-1} \cdot (\bar{x} - \bar{\bar{x}}) \quad (4.33)$$

where \bar{x} is the subgroup average and $\bar{\bar{x}}$ is the process average, which is estimated by the mean of the subgroup averages (subsamples mean) when the process is in control (the reference stage). The lower control limit (LCL) is equal to zero and the upper control limit is equal to:

$$UCL = \frac{m \cdot (s+1) \cdot (r-1)}{s \cdot r - s - m + 1} \cdot F_{m,s \cdot r - s - m + 1}(\alpha) \quad (4.34)$$

where s represents the number of groups collected during the reference period, which are used to obtain the process average ($\bar{\bar{x}}$) and the covariance matrix (S).

The practical use of these control charts is illustrated in the monitoring application presented in chapter 5.

4.3.5 Conclusions

Section 4.3 was devoted to the description of two alternative approaches to eliminate the effects of environmental and operational variables on natural frequencies estimated from the responses of the monitored structure measured during normal operation.

The first one assumes that all the variables with relevant influence on natural frequencies can be measured. In this case, it is possible to establish regression models between the estimated natural frequencies and the measured environmental and operational factors using data collected in a reference period during which the structure is considered to be undamaged. This methodology fails to provide good results when a factor with an important impact on the natural frequencies is not measurable. It also has the disadvantages of requiring more experimental resources and of requiring a larger analysis effort to select the predictors.

On the other hand, the secondly presented methodology, through the use of the statistical tools Principal Components Analysis (PCA) or Factor Analysis (FA), implicitly models the underlying relationship between environmental and operational variables and natural frequencies. Following this approach the measurement of environmental or operational parameters is avoided. However, because less information is available, not all the damages that can be detected with the regression analysis are detectable with this alternative methodology.

Figure 4.2 presents a simple example that permits to illustrate the types of damages that are not identified with the output-only methods. In this example it is assumed that only two natural frequencies are monitored and that they only depend on an environmental variable designated by T . The application of the PCA to the blue points (values measured during the reference period) represented in Figure 4.2 a) leads to only one non-zero singular value that is associated with a principal component that coincides with the represented dashed line. In this ideal situation the vector with the errors or unique factors (ε) is null and therefore the results of FA coincide with the ones delivered by PCA. The model constructed with the undamaged points would provide a large error when applied to the red point represent in Figure 4.2 a) and consequently would identify the existence of damage. However, this model would provide a null error for the red point represented in Figure 4.2 b), despite the existence of damage. On the contrary, the measurement of T would permit to detect that this red point does not respect the regression model constructed with the blue points.

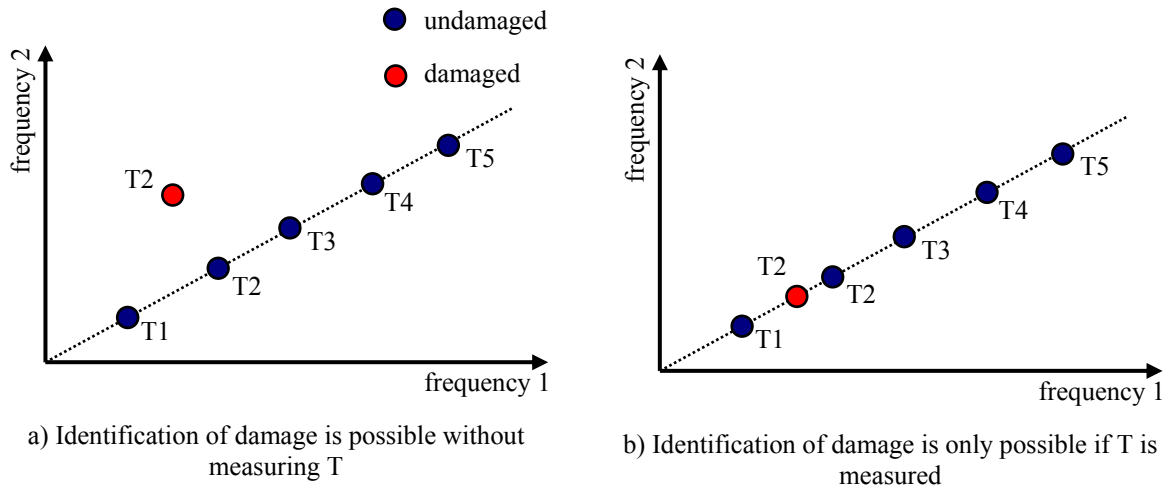


Figure 4.2 – Identification of damage with and without measuring the factors that influence the estimated natural frequencies.

The concept illustrated in this simple example remains valid when the number of natural frequencies and influence factors increases. The geometric interpretation becomes more difficult, but it can be said that, with the PCA or FA it is only possible to detect damages that produce changes on the natural frequencies which are ‘orthogonal’ to the changes caused by environmental or operational factors.

Taking in mind the advantages and drawbacks of the two approaches, the best solution is to base the damage identification on the application of both. In a first step, the input-output methods can be used to eliminate the influence of the factors that can be easily measured, as for instance the temperatures on some structural members. Then, the output-only methods can be applied to minimize the influence of the factors that were not measured and so increase the chances of identifying small damages. Finally, control charts can be applied to synthesise the results on a simple to interpret chart.

4.4 A Dynamic Monitoring Software – DynaMo

The need for the development of software to efficiently extract useful information from data collected by Dynamic Monitoring Systems is evidenced by the huge difference between the number of bridges with Monitoring Systems and the number of publications showing a clear and useful interpretation of the results provided by those systems.

In particular, Structural Health Monitoring based on modal parameters depends on the successful application of two crucial tools: algorithms for the automatic identification of modal parameters and algorithms for the elimination of environmental and operational effects on modal parameters. The first algorithms have already been described in section 2.4, whereas the latter were presented in the previous section. This section explains how both algorithms were integrated in a monitoring software package, which also includes tools for data transference and management. The developed monitoring software was named DynaMo, which stands for DYNAmic MOnitoring. Its main goal is to transform the collected acceleration time series into meaningful information from the structural behaviour point of view.

The DynaMo software was programmed in Matlab and then compiled to become a standalone application that can be deployed in any computer with any operating system without the need to pre-install Matlab.

The data processing can be done at the instrumented structure by the same computer that is responsible by the data collection or the raw data can be transferred to another computer placed in a different location, where then the data processing is developed. In any case, the data has to be processed right after being acquired or transferred, so that timely alerts can be provided to the infrastructure owner or operator.

The first architecture is more adequate when the internet connection available at the instrumented structure is of poor quality, since the size of the files with the outputs of the processing is much smaller than the size of the files with the raw data. However, the quality of nowadays internet services makes feasible the second solution, which permits to adopt a simpler and more robust computer, and therefore less prone to problems, at the remote site. This was the strategy adopted in the applications that will be presented in chapters 5 and 6. Consequently, the monitoring software was developed according to this scheme for the data flow. Nevertheless, it can be easily adapted to be integrated in monitoring systems with different architectures.

Accordingly, in the development of the dynamic monitoring software, it was assumed that in the instrumented structure there is a computer with a folder accessible by FTP (File Transfer Protocol) where files with the collected data are created by the acquisition software at a certain predefined rate. Some simple routines were developed to be used in this computer, which is called server. These include one routine to compress the files before being transferred and another one to delete the files older than a predefined age to limit the memory space used by the data files.

The DynaMo software is continuously running in a computer, designated client, that can be placed in any location with an internet connection. After the creation of each new data file on the server and its subsequent compression, DynaMo executes the following tasks:

- download of the most recent data file;
- archive of the original data in a database, so that it can be later used to test alternative processing methodologies;
- pre-processing of data to eliminate the offset and, if necessary, apply filters and reduce the sampling frequency;
- characterization of the signal amplitude by its maxima and root mean square values;
- processing of data for automatic identification of modal parameters using three different identification algorithms: Frequency Domain Decomposition (FDD), Covariance driven Stochastic Subspace Identification (SSI-COV) and poly-Least Squares Complex Frequency Domain (p-LSCF);
- post-processing of the identified natural frequencies to minimize the effects of the measured and not measured environmental and operational factors.
- construction of control charts for the identification of abnormal values;
- creation of a database with all the results.

The database with the original files is only useful to permit future research studies. As it consumes a large amount of memory, in the context of long term applications it has to be discarded. In Figure 4.3 it is illustrated how this database is organized using as example the data collected in the application that is presented in chapter 5, the Infante D. Henrique Bridge. In this application a new file is generated every 30 minutes, so in the folder associated with each day there are 48 files. The extensions *.txt.gz means that the data files are text files (txt) that have been compressed (gz).

The pre-processing tools include several alternative filters (low-pass, high-pass or band-pass) to select the frequency range of interest for the subsequent analysis. This can be followed by a re-sampling in order to reduce the number of points of the time series and so make the subsequent processing more efficient. After this, the maxima and the root mean square values of all the collected time series are characterized. This permits the continuous verification of serviceability limit states, especially relevant for instance in footbridges, and in chapter 5 it will be shown that the signal amplitude is also important to explain variations of modal parameters.

The automatic identification of modal parameters is the most important task of the DynaMo software. Three different state-of-the-art algorithms were implemented, which gives to the user the freedom to apply just one or to simultaneously use the three and then select the results with higher quality. As explained in chapter 2 (section 2.4), these algorithms present some parameters that have to be tuned for each new application. Therefore, the software contains routines to perform some preliminary offline processing with several intermediate results that facilitate the adjustment of the parameters of the algorithms for automatic identification. In chapters 5 and 6 the selection of these parameters is illustrated. The identification of modal parameters is followed by a procedure that links the new set of modes with the ones identified in previous setups. This is also explained in chapter 5.

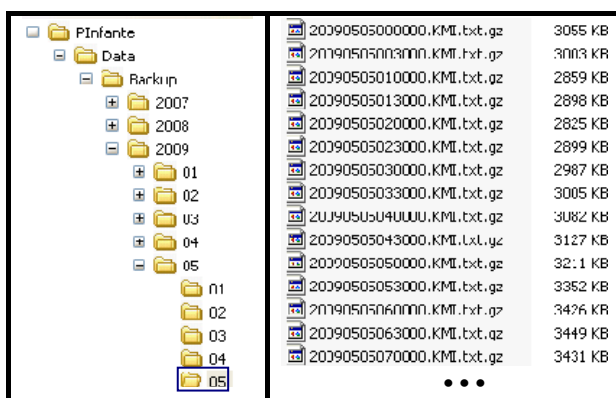


Figure 4.3 – Organization of the database with the original data files.

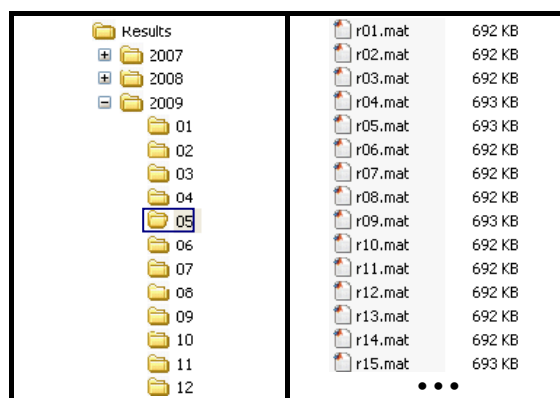


Figure 4.4 – Organization of the database with the files that contain the outputs of the processing.

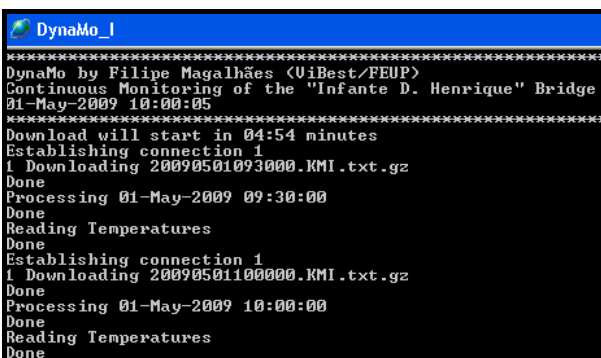
The identified modal parameters can then be post-processed by routines that minimize the effect of the environmental and operational factors. The DynaMo permits the use of multivariate regression models or/and the adoption of models derived from principal components analyses. As explained in section 4.3, these models should be established using the time evolution of natural frequencies under a significant range of variation of environmental and operational factors. Therefore, their application only starts one year after the beginning of the monitoring program. After each complete year, the models can be improved to incorporate a larger range of variation of the factors that influence the modal parameters.

Afterwards, the outputs of the previous post-processing are synthesized in control charts that permit the detection of abnormal values that may then trigger alarms.

All the important results of the data processing are stored in a database that follows the organization illustrated in Figure 4.4. There is a folder for each month that contains one file for each day. These daily files (with the extension *.mat) contain matrices with different sets of results: maxima, root mean square values, modal parameters identified by all the applied identification techniques, etc. Adopting as example the data of the Infante D. Henrique Bridge, it is interesting to observe that the 48 files associated with each day, with more than 144MB, are transformed into information that can be stored in a file with less than 700KB.

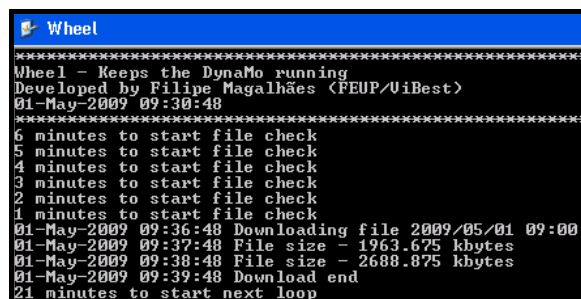
The DynaMo has the status window presented in Figure 4.5 that displays the operations that are being performed by the software. Besides the data download and processing, for the case of the Infante D. Henrique Bridge, there is an extra operation that is needed to obtain the temperature readings. As the temperature at several structural elements is measured by a different monitoring system, the temperature values are not included in the downloaded data files and therefore, it was necessary to develop an extra routine to continuously extract the temperature values stored in the database of the static monitoring system.

As it is very important to guarantee that the monitoring software is always ‘alive’, a complementary program called Wheel (Figure 4.6) was developed, whose function is to keep the DynaMo running. This software verifies if the DynaMo is downloading the files at the time it is programmed to, and monitors the downloading process. If the Wheel finds fails (these sometimes occur due to sporadic problems in the internet connection), then it means that the DynaMo is not working properly and consequently it is restarted.



```
DynaMo_1
*****
DynaMo by Filipe Magalhães (UiBest/FEUP)
Continuous Monitoring of the "Infante D. Henrique" Bridge
01-May-2009 10:00:05
*****
Download will start in 04:54 minutes
Establishing connection 1
| Downloading 20090501093000.KMI.txt.gz
Done
Processing 01-May-2009 09:30:00
Done
Reading Temperatures
Done
Establishing connection 1
| Downloading 20090501100000.KMI.txt.gz
Done
Processing 01-May-2009 10:00:00
Done
Reading Temperatures
Done
```

Figure 4.5 – Status window of the DynaMo software.



```
Wheel
*****
Wheel - Keeps the DynaMo running
Developed by Filipe Magalhães (FEUP/UiBest)
01-May-2009 09:30:48
*****
6 minutes to start file check
5 minutes to start file check
4 minutes to start file check
3 minutes to start file check
2 minutes to start file check
1 minutes to start file check
01-May-2009 09:36:48 Downloading file 2009/05/01 09:00
01-May-2009 09:37:48 File size - 1963.675 kbytes
01-May-2009 09:38:48 File size - 2688.875 kbytes
01-May-2009 09:39:48 Download end
21 minutes to start next loop
```

Figure 4.6 – Status window of the Wheel software.

With regard to the time used by DynaMo for data retrieving and processing, in the case of the application on the Infante D. Henrique Bridge, the download of each data file takes approximately 3 minutes (due to limitations of the upload velocity of the internet connection), while the processing, which includes the automatic identification of 12 natural frequencies with the three implemented techniques, takes about one minute in a regular computer.

In order to facilitate the access to the database with the results, several routines were implemented to create various types of graphics. Later, these were integrated in a Graphic User Interface (GUI), named DynaMo Viewer, that was developed by another PhD student at ViBest (Diord et al. 2009). These was also programmed in Matlab and then compiled to become a windows standalone application. Figure 4.7 presents the main windows of this GUI customized for the application in the Infante D. Henrique Bridge. It is essentially composed by a table in the form of a calendar that displays all the available setups. After the selection of a time period, which can vary from one day to several months, it is possible to obtain plots with the time evolution of the modal parameters estimated with the selected identification algorithm (as presented in Figure 4.8) or, for instance, to plot the time evolution of the maxima of the vertical accelerations.

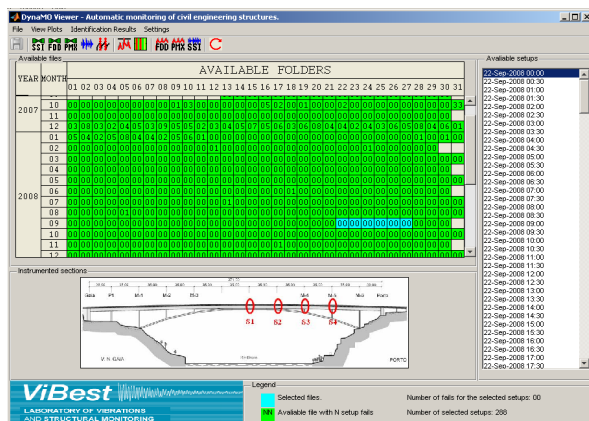


Figure 4.7 – Main window of the DynaMo Viewer software.

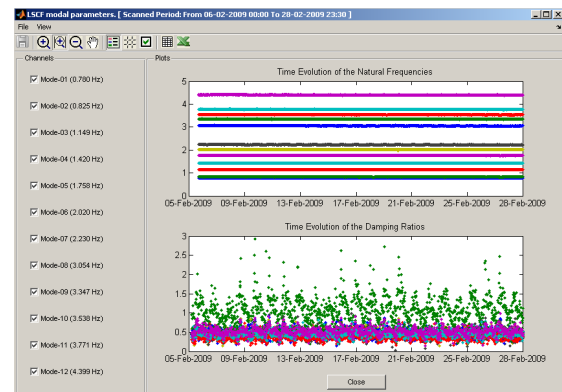


Figure 4.8 – Plots produced by the DynaMo Viewer software.

In the next chapter, results provided by more than two years of continuous operation of the DynaMo software, processing the data collected at the Infante D. Henrique Bridge, will be presented.

Chapter 5

DYNAMIC MONITORING OF THE INFANTE D. HENRIQUE BRIDGE



5. DYNAMIC MONITORING OF THE INFANTE D. HENRIQUE BRIDGE

5.1 Introduction

Bearing in mind the recent developments of monitoring hardware and the advances in data processing capabilities, it is opportune to perform practical applications on full-scale bridges with the most advanced commercially available dynamic monitoring hardware and taking profit from processing routines based on the latest theoretical developments of Operational Modal Analysis.

Therefore, with the main goal of demonstrating the potential of structural health monitoring systems based on dynamic measurements, a monitoring project of a long span concrete arch bridge was started. This project comprehended five main phases: (i) numerical modelling and ambient vibration test to characterize the dynamic behaviour of the bridge and better design the monitoring system, (ii) installation of the monitoring equipment, (iii) development of software to retrieve the continuously collected time series from the bridge to FEUP and to perform the on-line automatic identification of the bridge modal parameters, (iv) study of the modal parameters variations during one year to obtain numerical models to eliminate the effects of environmental and operational factors, and finally, (v) evaluation of the capability of the installed monitoring system to detect small damages.

Similar monitoring experiments are being pursued in other structures, as for instance in the Tamar Bridge (Brownjohn and Carden 2008), in a highway overpass in San Diego (Fraser et al. 2007) or in the Coimbra Footbridge (Hu et al. 2009). The outcomes of all these research studies will certainly contribute to obtain more arguments to convince the owners of important infrastructures about the benefits of vibration based health monitoring.

This chapter starts with a brief description of the bridge that is followed by the presentation of the main outcomes of the preliminary numerical and experimental studies. Then, the installed monitoring equipment is described. Afterwards, the application of the algorithm for automatic identification of modal parameters, introduced in chapter 2 and implemented in the monitoring software presented in chapter 4, is described with detail. After this, the use of regression models for the elimination of environmental and operational effects on the estimated natural frequencies is explored using a two years database (first year to define the model, second year for validation). Finally, it is evaluated the ability of control charts applied together with Principal Components Analysis to detected small simulated damages.

5.2 Bridge Description

The Douro River is crossed by several outstanding bridges linking the cities of Porto and Gaia, located at the north of Portugal. At the beginning of the 21st Century the Infante D. Henrique Bridge, a concrete arch bridge, joined the 19th Century metallic Maria Pia and Luiz I Bridges and the 20th Century concrete Arrábida and S. João Bridges. The aerial photo in the chapter cover page shows the new bridge in the middle of the two centenary bridges (Maria Pia Bridge at the bottom, downstream).

The Infante D. Henrique Bridge is composed of two mutually interacting fundamental elements: a very rigid prestressed reinforced concrete box girder, 4.50m deep, supported by an extremely shallow and thin reinforced concrete arch, 1.50m thick, as shown in the elevation and cross-sections represented in Figure 5.1. The arch spans 280m between abutments and rises 25m until the crown, thus exhibiting a shallowness ratio greater than 11/1. In the 70m central segment, arch and deck meet to define a box-beam 6m deep. The arch has constant thickness and its width increases linearly from 10m in the central span up to 20m at the springs (Adão da Fonseca and Millanes Mato 2005). Owing to the high stiffness of the deck with respect to the slenderness of the arch, the structure behaves as a beam bridge defined between abutments and with intermediate elastic supports 35m apart.

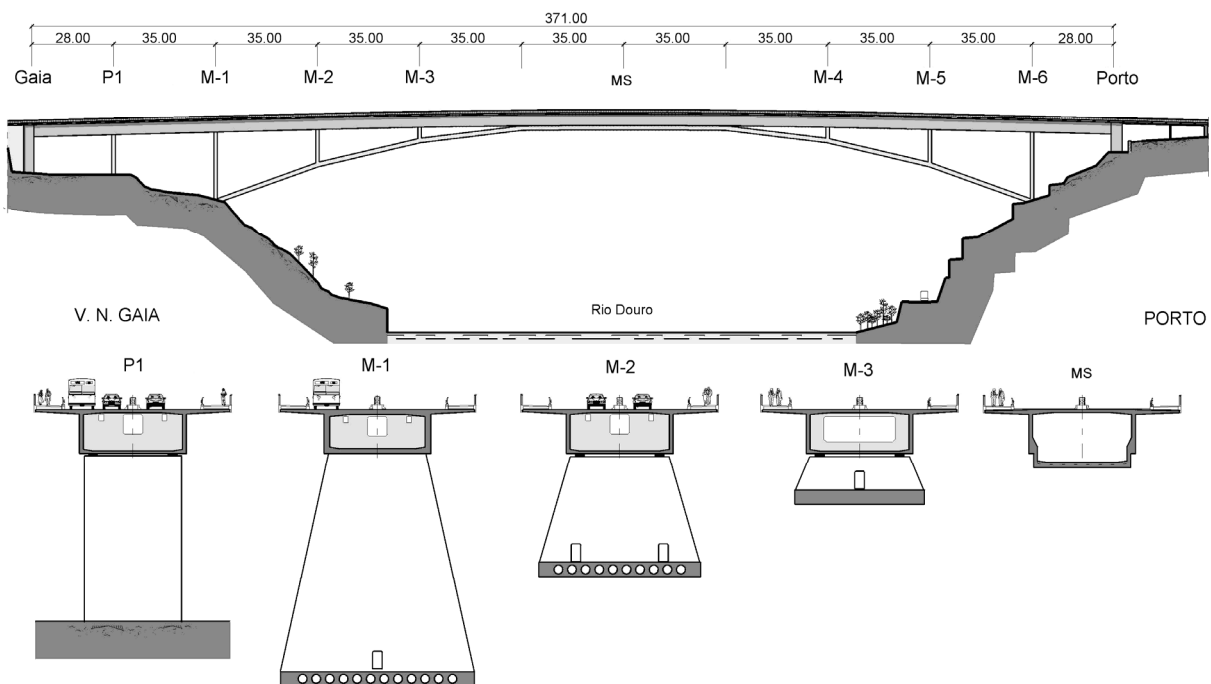


Figure 5.1 - Elevation and cross-sections of the bridge.



Figure 5.2 – Bridge during construction.

The extreme shallowness and flexibility of the arch implied significant complexity of construction (Figure 5.2) and required a very accurate control of geometry, deformations and forces. This control was performed by three separate instrumentation systems: one for concrete elements (comprising strain gauges, clinometers and temperature sensors); another for temporary stay cables; and another one for the granite rocky slopes. ViBest/FEUP was contracted to measure on a regular basis the tension forces installed in the provisional stay cables using vibration chord theory (Adão da Fonseca et al. 2002). Those three instrumentation systems provided an accurate understanding of the structural behaviour, and supported important decisions of the designer and the constructor at several critical moments of construction. Owing to the evident usefulness of the monitoring activity during this phase, the owner decided to keep the static monitoring system working after the bridge opening to traffic, and agreed to install a new long term dynamic monitoring system, suggested by ViBest/FEUP with the support of the designer.

It is also relevant to point out that the bridge is one of the main entrances into the Porto city centre. Therefore, it is crossed by a large number of vehicles, especially during the morning rush hours, as it can be observed by the pictures taken by a traffic camera pointed to the bridge (Figure 5.3).

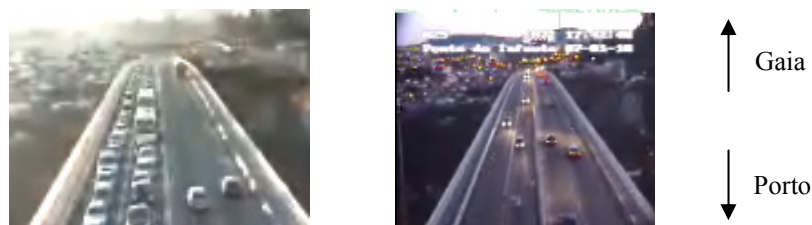


Figure 5.3 – Traffic over the Infante D. Henrique Bridge at 9:00 and at 17:30 of 07/01/2010.

5.3 Preliminary Experimental and Numerical Studies

5.3.1 Ambient Vibration Test

The correct design of a dynamic monitoring system requires previous knowledge of the structural modal parameters. Therefore, it is very important to conduct an ambient vibration test before the installation of the monitoring equipment. The ambient vibration test of the Infante D. Henrique Bridge was developed without disturbing its normal use, taking profit from the vibrations induced by traffic and wind, using the procedure and equipment already described in Chapter 3.

During the ambient vibration test, two recorders were permanently located at the cross-section of the deck selected for reference (section 8 in Figure 5.4), at both sides of the deck (upstream and downstream). Two other recorders scanned the bridge deck measuring accelerations along three orthogonal directions at both sides of the remaining 15 cross-sections represented in Figure 5.4.

For each sensor layout, time series with 16 minutes were collected with a sampling frequency of 100 Hz. However, before the use of the identification tools, a decimation was applied to reduce the sampling frequency from 100Hz to 20Hz.

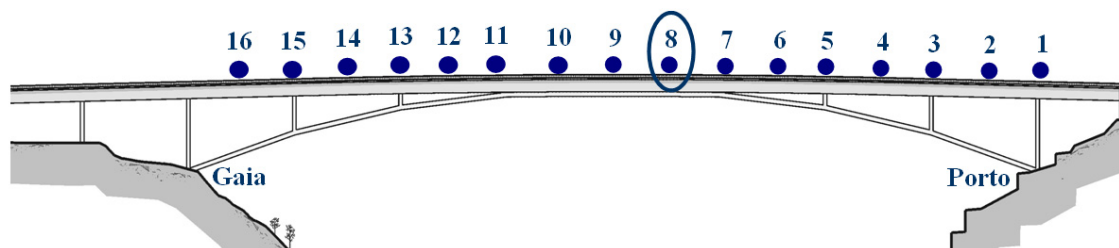


Figure 5.4 - Instrumented cross-sections; the ellipse indicates the reference cross-section.

Identification of modal parameters from the data collected during the ambient vibration test was achieved with two output-only identification methods with different theoretical bases: the Frequency Domain Decomposition and the Data-driven Stochastic Subspace Identification. A detailed description of the results provided by both methods is presented in (Magalhães et al. 2006b), where it is also shown that the estimates provided by the two approaches are very consistent. Here, only the results of the FDD method are characterized.

The first step of the FDD method is the construction of a spectrum matrix from the ambient responses collected in each test setup. In the present application, four time series were considered for each instrumented section: upstream and downstream vertical accelerations, mean values of the two measured lateral accelerations and mean values of the two measured longitudinal accelerations. Hence, spectrum matrices with 8 rows and 4 columns were organized for each setup. The elements of these matrices were estimated using the Welch procedure (Welch 1967) by dividing the available time series in segments of 102.4 seconds (2048 points), considering an overlap of 66% between segments and adopting a Hanning window to reduce the leakage. The selected parameters allowed the calculation of averages over 26 time segments and produced spectra with a frequency resolution of 0.00977Hz.

Figure 5.5 presents the average of normalized singular values spectra covering all setups. This graphic is a synthesis of the frequency content present in each setup and allowed the identification of 13 resonant frequencies (marked with dashed vertical lines) within the frequency range of analysis (0 - 5Hz).

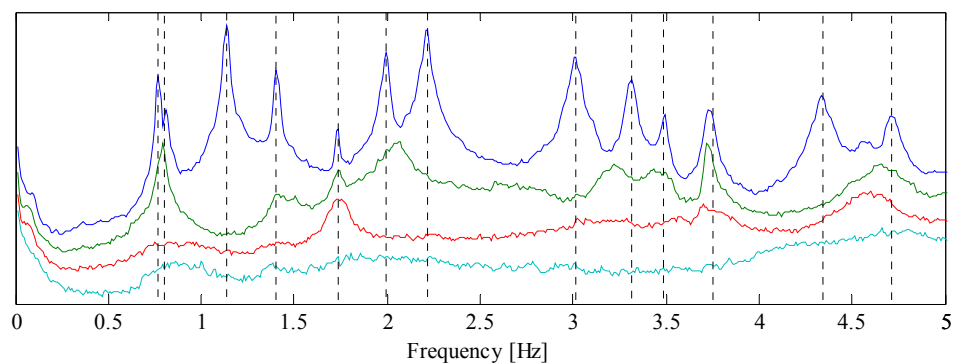


Figure 5.5 - Average Normalized Singular Values.

With each setup, eight modal components are calculated. These are then grouped together using the components at the reference section to correctly scale the segments identified in each setup. Figures 5.6, 5.7 and 5.8 show some of the identified modes of vibration plotted with the Artemis software (SVS 1999-2004). These are compared with the ones provided by the numerical model that is described in the next sub-section. The correlation between the experimental and numerical mode shapes is remarkable.

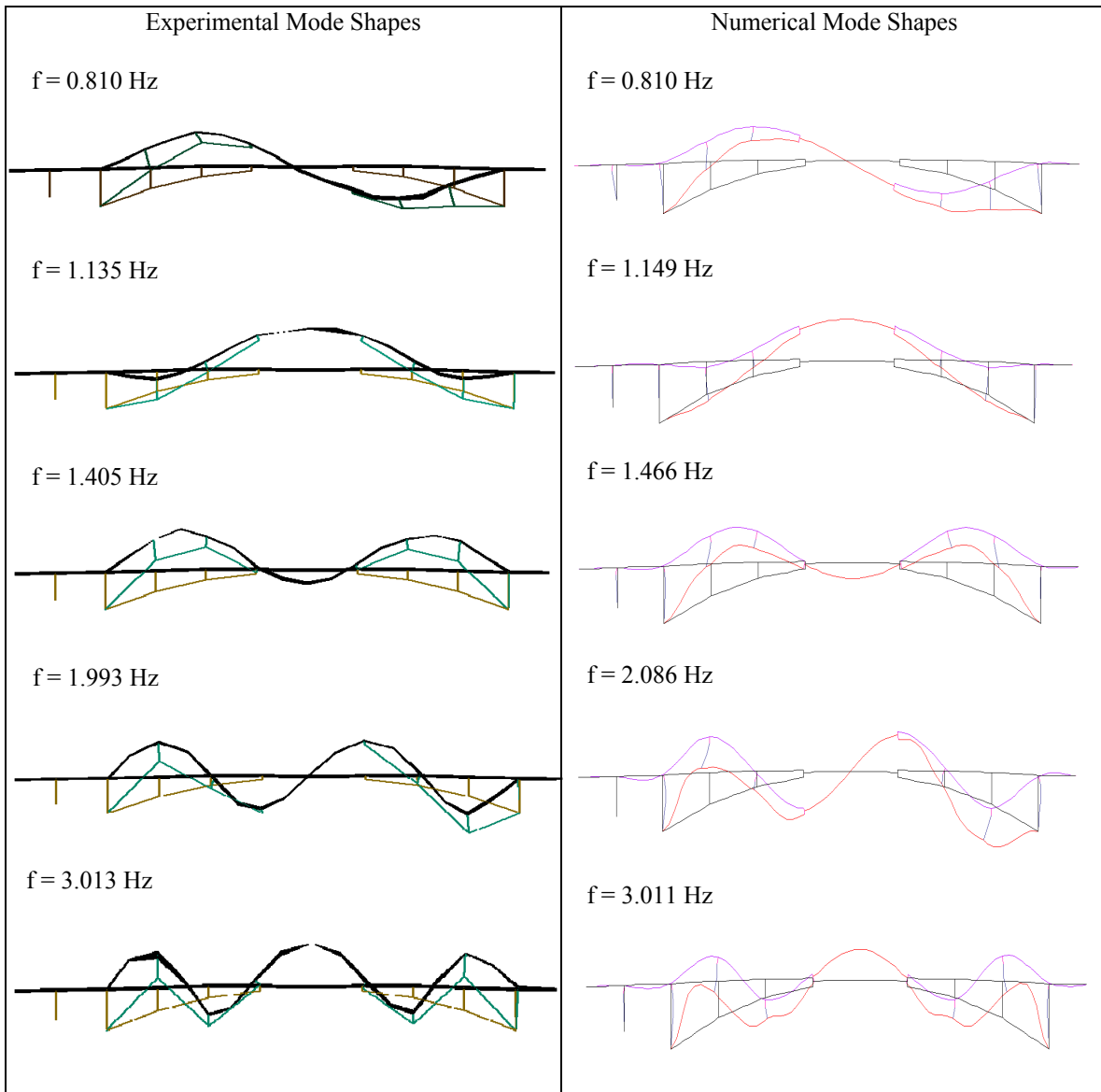


Figure 5.6 - Lateral view of the first 5 vertical bending modes.

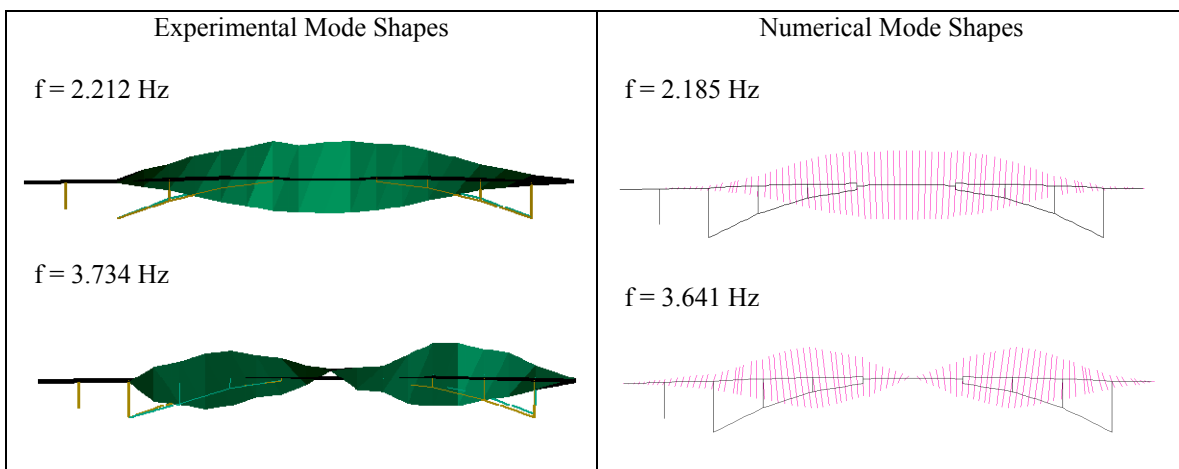


Figure 5.7 - Lateral view of the first and second torsion modes.

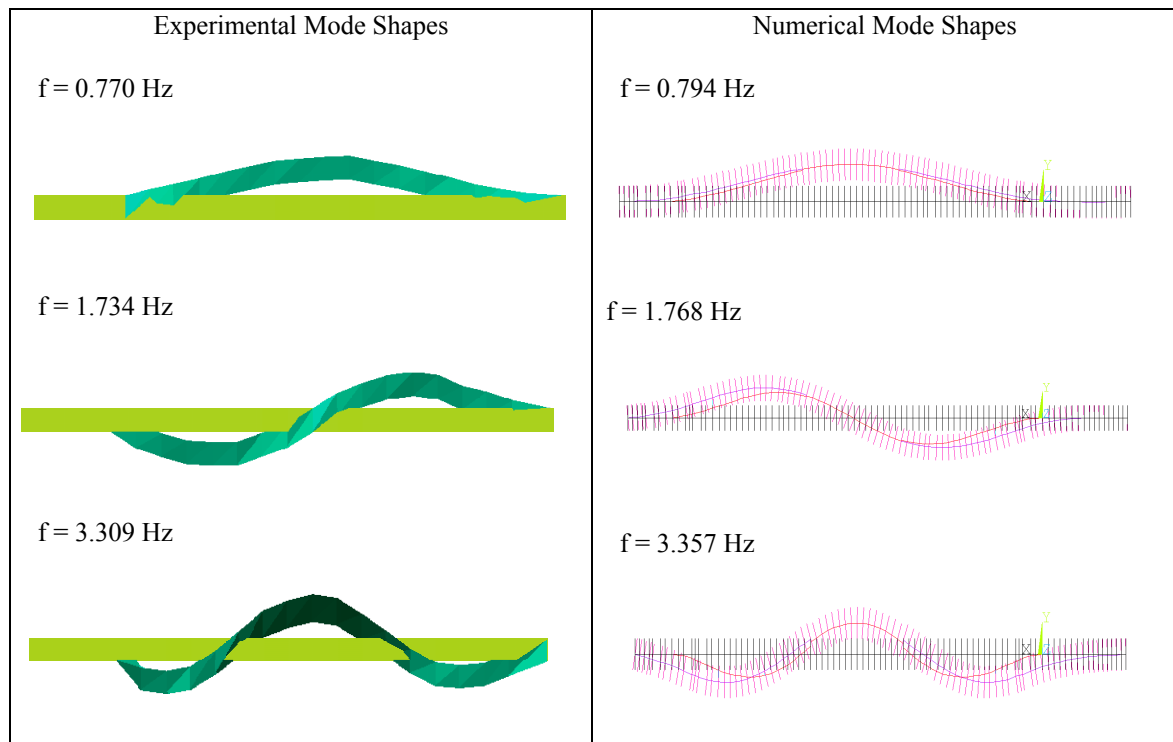


Figure 5.8 - Top view of the first, second and third lateral bending modes.

5.3.2 Numerical modelling

In order to better understand the dynamic behaviour of the bridge and interpret the modal parameters estimated by the ambient vibration test, the structural behaviour of the bridge was modelled with the ANSYS software using 3D bar finite elements. Cross section properties (area, moments of inertia, torsion moment of inertia and shear deflection constants) were defined according to the geometry of the deck, arch and columns. The same elasticity modulus of 37GPa (value provided by tests performed during the bridge construction) was adopted for the deck and arch concrete and an elasticity modulus of 34GPa (value defined by EC2 (CEN 2004) for a C35/45 concrete) was considered for the concrete of the columns.

Connection between deck and the highest columns (M1 and M6, Figure 5.1) are monolithic, whereas connections with other columns and abutments are provided by two unidirectional sliding pot bearings. These bearings allow movements along the longitudinal direction of the bridge and rotation in all directions. However, for low levels of excitation, as it is the case during normal operation, and also during ambient vibration tests, the behaviour of these connections may be different. For low levels of vibration, friction forces can prevent displacement or rotation.

To analyse the influence of the behaviour of these connections on modal parameters, three alternative models were developed:

- Model 1 (M1): longitudinal displacement and rotations free in all pot bearings;
- Model 2 (M2): longitudinal displacement and rotations fixed in all pot bearings;
- Model 3 (M3): longitudinal displacement and rotations fixed in the pot bearings of the columns but free in the pot bearings of the abutments.

Natural frequencies of the most relevant modes provided by the three models are presented in Table 3.1. Models 1 and 2 establish the lower and upper bounds of the numerical natural frequencies calculated using the material properties previously defined. A significant variation of the natural frequencies of vertical modes is noted (especially the associated with the first mode).

Modes identified experimentally show that the deck undergoes longitudinal movements. Therefore, the hypothesis of fixing longitudinal movements in the abutments is not correct. On the other hand, model M3 shows that, even fixing the relative movements and rotation in all columns, the numerical frequency of the first mode is considerably lower than the experimental one.

In order to better understand the longitudinal behaviour of the bridge, two additional measurements were performed: longitudinal acceleration at the deck near the expansion joint in the Gaia bank and longitudinal acceleration of the Gaia abutment. Spectra of the collected time series are represented in Figure 5.9. These graphics show the existence of some of the natural frequencies of the bridge in the response of the abutment and, in particular, the presence of the natural frequency of the first vertical mode. This means that the abutment is mobilized in the movements associated with the first vertical bending mode, due to the existence of friction forces. Therefore, the appropriate modelling of the behaviour of the bridge requires the inclusion in Model 3 of horizontal springs to simulate the additional stiffness provided by the abutments.

This last conclusion led to the development of a “more correct” model of the bridge: Model 4. This model is similar to Model 3 but includes a horizontal spring at each abutment with a stiffness constant that was adjusted in order to obtain a good matching between numerical and experimental frequencies. Table 3.1 shows that the correlation between modal parameters of the final numerical model and the experimental ones is very good, with relative errors in natural frequencies lower than 5% and MAC values always greater than 0.95.

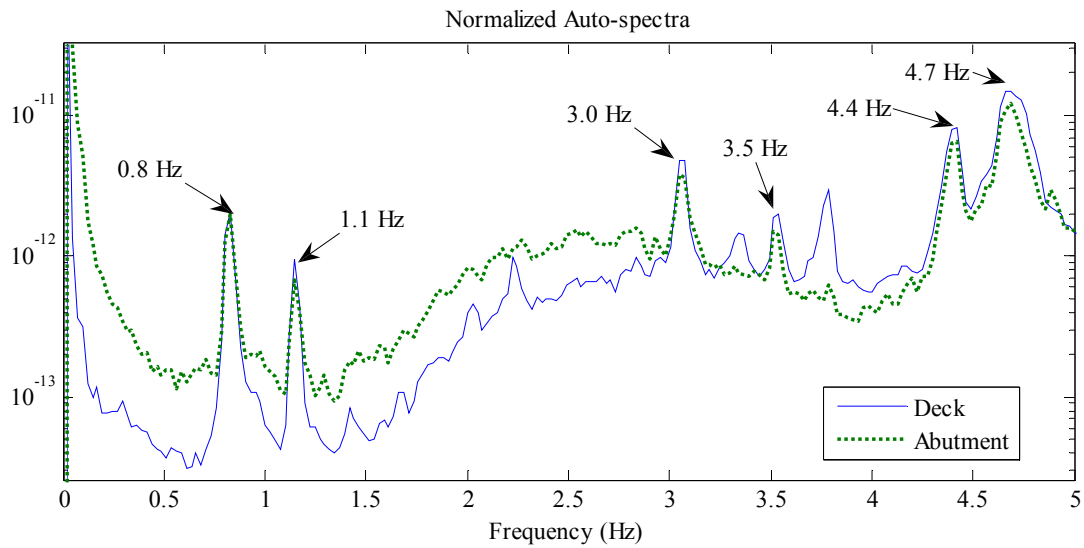


Figure 5.9 - Normalized auto-spectra of longitudinal accelerations measured simultaneously at the deck and at the Gaia abutment.

Table 5.1 – Modal parameters obtained with the considered numerical models compared with the experimental values.

Mode*	Exp.	Model 1		Model 2		Model 3		Model 4		MAC
	Freq. (Hz)	Freq. (Hz)	Error (%)	Freq. (Hz)	Error (%)	Freq. (Hz)	Error (%)	Freq. (Hz)	Error (%)	
V1	0.810	0.541	-33.29	1.054	29.96	0.701	-13.56	0.810	-0.12	0.995
V2	1.135	1.081	-4.76	1.164	2.56	1.144	0.79	1.149	1.23	0.994
V3	1.405	1.244	-11.46	1.473	4.84	1.465	4.27	1.466	4.34	0.992
V4	1.993	1.766	-11.35	2.088	4.82	2.086	4.72	2.086	4.72	0.994
L1	0.770	0.794	3.12	0.799	3.77	0.794	3.12	0.794	3.12	0.996
L2	1.734	1.767	1.90	1.788	3.11	1.768	1.96	1.768	1.96	0.989
L3	3.309	3.353	1.30	3.394	2.54	3.357	1.42	3.357	1.42	0.965
T1	2.212	2.169	-1.90	2.211	0.00	2.185	-1.18	2.185	-1.18	0.956
T2	3.734	3.632	-2.73	3.724	-0.27	3.641	-2.49	3.641	-2.49	0.952

* Mode type, defined considering the most relevant components (L – lateral bending; V – vertical bending; T – torsion).

5.4 Monitoring System Description

Traditional monitoring systems are based on one central acquisition system to which all the sensors are connected. However, it is more convenient to have the digitizers distributed along the monitored structure, in order to reduce the length of the sensor cables, as these are sensitive to electrical interferences that can corrupt the electrical signals generated by the sensors. Additionally, after digitization, the information collected by several sensors can be transmitted through a single ethernet cable or even using wireless devices. Therefore, with this alternative solution, the installation becomes simpler and noise is minimized. These advantages are enhanced when large civil structures are involved. Whenever the distance between digitizers is longer than 90 m, it is necessary to replace the ethernet cable by a fibre optical cable, which can span long distances without signal interference, making this arrangement even more flexible. As perfect signal synchronization is essential for modal analysis, this type of architecture requires a solution to guarantee a good synchronization of the clocks of the digitizers. This can be achieved with a synchronization cable connecting the distributed digitizers or with one GPS antenna and receiver for each digitizer to tune their internal clocks using the information provided by the observable satellites.

The monitoring system installed in Infante D. Henrique Bridge is a decentralized system, which is essentially composed by 12 accelerometers and 2 digitizers distributed along the bridge according to the schemes presented in Figures 5.10 and 5.11 (Magalhães et al. 2008d). All the equipment is located inside the deck box girder, being therefore well protected from the environmental threats.

The bridge is almost symmetric and the previously performed ambient vibration test has proven that the mode shapes are also approximately symmetric or anti-symmetric. Therefore, as the number of available accelerometers was limited, it was decided to instrument just one half of the bridge instead of smearing the sensors along the whole bridge, in order to obtain a good spatial characterization of as many modes as possible. Consequently, those accelerometers were distributed along four sections between the mid-span and the abutment at the Porto bank. Three sensors equip each section: one to measure the lateral acceleration and two for the vertical acceleration at the downstream and upstream sides. These enable the characterization of lateral and vertical movements and rotations associated with torsion modes.

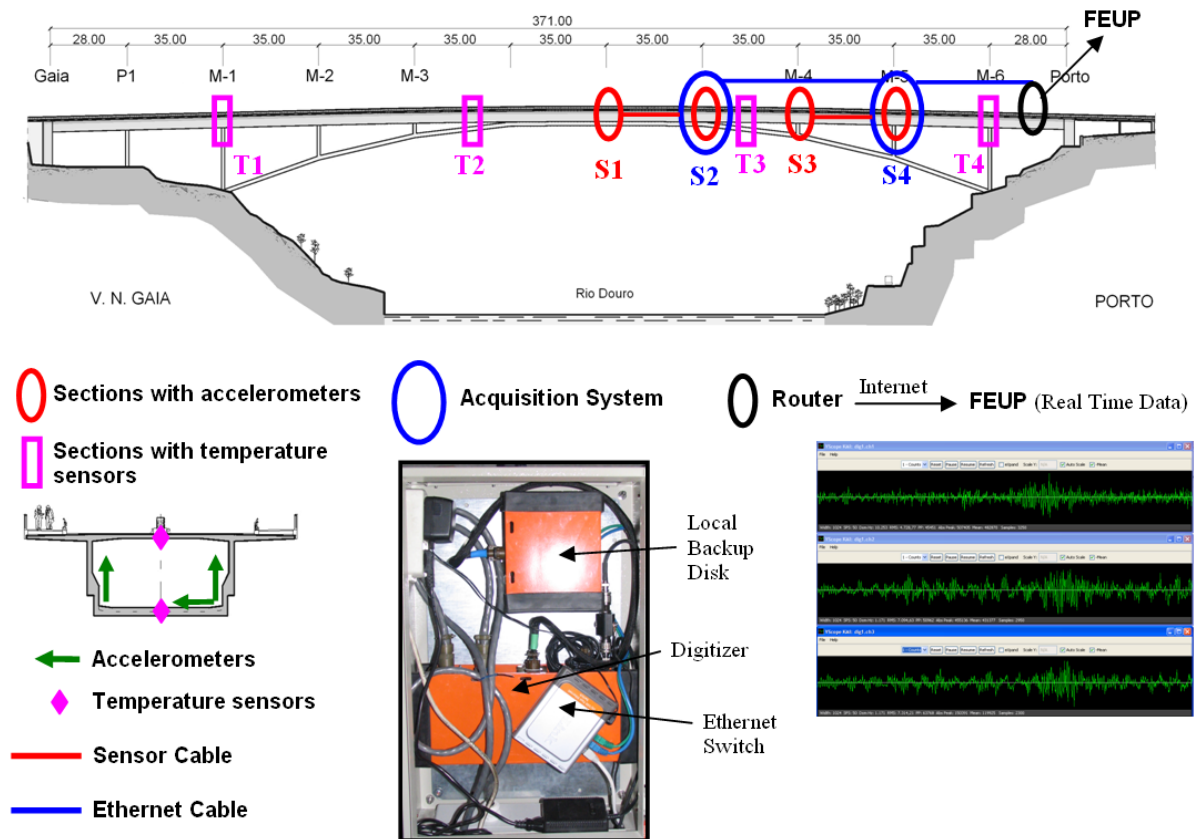


Figure 5.10 - Scheme of the monitoring system installed in the Infante D. Henrique Bridge.

In the context of continuous dynamic monitoring of civil engineering structures, in order to be able to accurately characterize the structure response during extreme events (like earthquakes or strong storms) and also during quiet periods with very low levels of accelerations, it is very important to use sensors with a high dynamic range, defined by the ratio of the largest to the smallest signals that can be measured, usually expressed in $\text{dB} - 20 \cdot \log_{10}(\text{largest signal}/\text{smallest signal})$. Furthermore, the sensors should have the capability to cover low frequencies, to permit a good characterization of the lower modes of the structure under observation, or even present the ability to measure the DC response, which means the possibility of measuring the gravity and therefore allows simple field calibration and validation, reducing the configuration errors.

Taking this into account, the selected accelerometers are force balance accelerometers, model FBA ES-U2 (Figure 5.12) produced by Kinemetrics Inc. (www.kmi.com), and present a dynamic range of 145 dB, a frequency range from DC to 200 Hz, a user-selectable measuring range that can vary from $\pm 0.25\text{g}$ to $\pm 4\text{g}$ and extremely low levels of noise (around $2 \mu\text{g}$). In the present installation, the measuring range was fixed to $\pm 0.25\text{g}$, with the goal of optimize the sensitivity (80 V/g for the used configuration) of the sensors and consequently reduce the effect of the noise introduced by the measuring chain, while keeping a conservative acceleration range, as the maximum observed acceleration is lower than 12mg .

The adopted digitizers are Q330 (www.Q330.com) developed by Quanterra Inc., a subsidiary of Kinemetrics Inc. These allow the connection of six dynamic channels and 4 auxiliary static channels, comprehend 4 data ports that permit simultaneous real-time telemetry of the acquired data to a central site and transference to local recording units, and are equipped with a 24-bit analog-to-digital converter, to take profit from the large dynamic range of the accelerometers.

The two digitizers were placed at sections S2 and S4 (Figure 5.10) of the bridge deck and connected by a single ethernet cable. Another ethernet cable links section S4 with a router that is the interface between the local network and the internet. The synchronization of the digitizers is achieved with two GPS antennas, placed outside the bridge deck and connected to each of the units, which allow the continuous update of the internal clocks of the digitizers.

In an initial phase, the digitizers were connected to the router and to local recording units especially designed to work together with the Q330 (Baler PB14F). The continuously produced data was simultaneously recorded in the local backup units and directly transmitted through the internet to the Faculty of Engineering of the University of Porto (FEUP). At FEUP, a data integrator software was responsible to collect the data packets delivered by the two digitizers and create text files with the 12 measured acceleration time series. This architecture had the advantage of avoiding the use of a computer in the remote site, but it was not robust against interruptions of the internet connection. During connection breakdowns, some data packets were not transmitted and the corresponding data files were left incomplete. It was possible to recover the missed data using the local recording units, but this had to be done using a manual procedure and therefore the desired autonomy of the monitoring system had not yet been reached.

In order to overcome this issue, the creation of the text files was moved to the bridge side using a rugged, ultra-low power, multi-purpose processor designed for field deployments in extreme operating conditions – the Slate from Kinemetrics (see Figure 5.12c). This field processor, connected to the local network using the router (Figure 5.11), gathers the data packets produced by the digitizers to create text files with the acceleration time series of all the sensors. In order to allow the creation of a local data backup, the used unit has a storage capacity of 15Gbytes, materialized by Compact Flash cards, accessible from FEUP using a FTP (File Transfer Protocol) connection. The Slate has embedded applications running over Linux to monitor the processor activity, to recover the system after possible crashes and to make the maintenance of its memory. A new routine to continuously compact the created text files was implemented to increase its backup capability and to shorten the time needed to transfer the files to FEUP.

Once some confidence was gained in the backup capabilities of the Slate, the Balers became redundant and therefore were removed. However, it is important to state that, if a very robust system is desired, these are very relevant components, as they are directly connected to the digitizer and therefore less susceptible to possible communication problems and not dependent on the reliability of a computer.

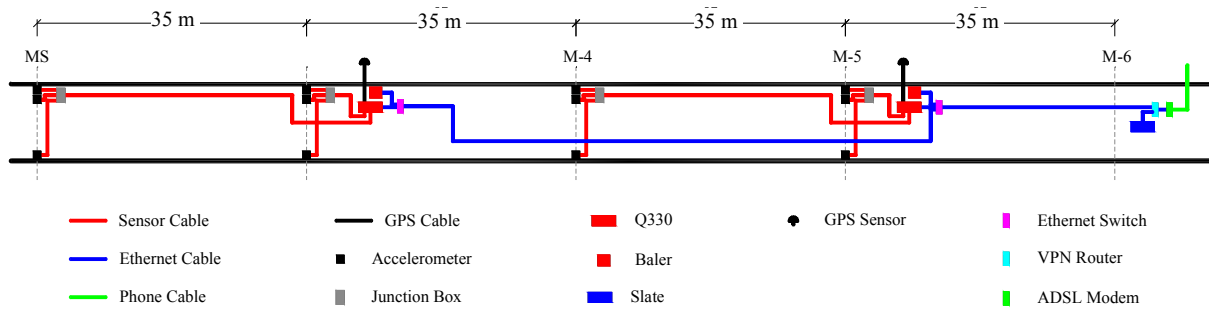
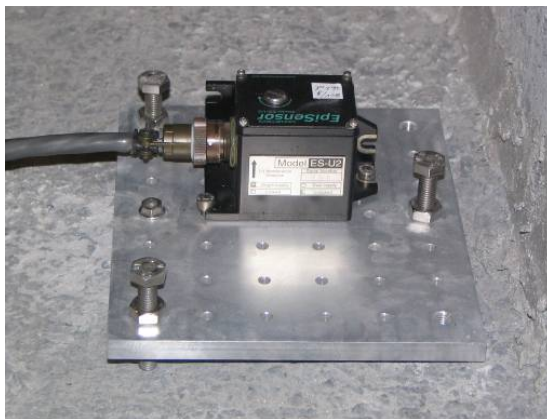


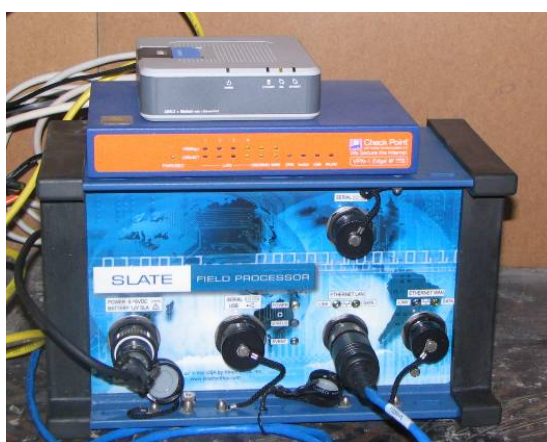
Figure 5.11 – Detailed characterization of the Monitoring System (top view of the deck).



a)



b)



c)

a) accelerometer attached to a levelling plate;

b) junction box to group the signals of three accelerometers in a single cable and two accelerometers (one measuring vertical accelerations and another measuring lateral accelerations);

c) field processor (Slate), VPN router and ADSL Modem, from bottom to top;

Figure 5.12 – Installation details.

All the components of the monitoring system (digitizers, local recording units and field processor) can be remotely accessed, as each of them has a unique IP address and specific software for remote control. Therefore, the configuration of the system (e.g. sampling frequency and length of the time segments) and the analysis of parameters used to check the system condition (e.g. quality of the GPS signals, digitizer internal temperature and input voltage) can be performed remotely.

For the monitoring of this bridge, a sampling frequency of 50 Hz and a length of 30 minutes were selected. Consequently, each half an hour a new text file with 12 columns (number of accelerometers) and $30 \times 60 \times 50 = 90\,000$ lines is available. These files are then transferred and processed by the Dynamic Monitoring software already described in chapter 4.

In the selection of the time series length, priority was given to the quality of the modal parameter estimates in order to obtain a system that is able to detect small stiffness changes. If the purpose was to have a rapid alarm at the occurrence of an anomaly, the length of the files could be reduced, but the accuracy of the estimates would decrease. A good compromise could be then to present less accurate natural frequency estimates using shorter time periods, to rapidly detect important and sudden anomalies, and obtain more accurate estimates at the end of each 30 minutes.

As already mentioned, this dynamic monitoring system is complemented by an independent static monitoring system (performing acquisitions every 10 minutes) that was installed in the bridge during the construction and comprises strain gauges, clinometers and temperature sensors. Measurements of the temperature sensors embedded in the concrete (also marked in Figure 5.10) are essential for the development of numerical models that extract the effect of temperature from the identified natural frequencies, these will be explored in section 5.6. Furthermore, a weather station that integrates the national meteorological network exists close to the bridge. It records the air temperature, humidity and wind velocity and direction, which can be used to investigate the possible effects of these variables on the identified modal parameters. However, this study has to be limited to six months, because it was decommissioned after the first six months of operation of the dynamic monitoring system.

5.5 Monitoring Results

The Dynamic Monitoring system of the Infante D. Henrique Bridge has been in continuous operation since the 13th of September of 2007. Therefore, a large database of acceleration time series and identified modal parameters is already available. In the present section, the results obtained during the first year of operation, from September 2007 to September 2008, are explored. In the following sections, the complete database is used firstly to study methods to remove the effects of environmental and operational factors on the identified modal parameters and then to evaluate the ability of the installed monitoring system and developed routines for damage detection.

In order to characterize the reliability of the installed Dynamic Monitoring system, Figure 5.13 shows the setups missed during the first 445 days of operation (from 13/09/2007 to 30/11/2008). The fails are concentrated in the month of December and first half of January. In this period the Balers had already been removed and the Slate was not working with the optimal configuration. After 12/01/2008 the number of fails is very limited, since these are only justified by very sporadic small interventions that forced a reboot of the system. Considering the first year of operation, from the total number of datasets: $48 \times 366 = 17568$ (number of datasets per day \times number of days), only 243 were missed.

YEAR	MONTH	MISSING SETUPS																														
		01	02	03	04	05	06	07	08	09	10	11	12	13	14	15	16	17	18	19	20	21	22	23	24	25	26	27	28	29	30	31
2007	09																															
	10	00	00	00	00	00	00	00	00	01	03	00	00	00	00	00	05	02	00	01	00	00	02	00	00	00	00	00	00	00	00	33
	11	00	00	00	00	00	00	00	00	00	00	00	00	00	00	00	00	00	00	00	00	00	00	00	00	00	00	00	00	00	00	00
	12	03	08	03	02	04	05	03	09	05	05	02	03	04	05	07	05	06	03	06	08	04	04	02	04	03	06	05	08	04	06	01
2008	01	05	04	02	05	08	04	04	02	05	06	01	00	00	00	00	00	00	00	00	00	00	00	00	00	00	00	00	01	00	01	00
	02	00	00	00	00	00	00	00	00	00	00	01	00	00	00	00	00	00	00	00	00	00	00	00	01	00	00	00	00	00	00	
	03	00	00	00	00	00	00	00	00	00	00	00	00	00	00	00	00	00	00	00	00	00	00	00	00	00	00	00	00	00	00	00
	04	00	00	00	00	00	00	00	00	00	00	00	00	00	00	00	00	00	00	00	00	00	00	00	00	00	00	00	00	00	00	00
	05	00	00	00	00	00	00	00	00	00	00	00	00	00	00	00	00	00	00	00	00	00	00	00	00	00	00	00	00	00	00	00
	06	00	00	00	00	00	00	00	00	00	00	00	00	00	00	00	00	00	01	00	00	00	00	00	00	00	00	00	00	00	00	00
	07	00	00	00	00	00	00	00	00	00	00	00	01	00	00	00	00	00	00	00	00	00	00	00	00	00	00	00	00	00	00	00
	08	00	00	00	00	01	00	00	00	00	00	00	00	00	00	00	00	00	00	00	00	00	00	00	00	00	00	00	00	00	00	00
	09	00	00	00	00	00	00	00	00	00	00	00	00	00	00	00	00	00	00	00	00	00	00	00	00	00	00	00	00	00	00	00
	10	00	00	00	00	00	00	00	00	00	00	00	00	00	00	00	00	00	00	00	00	00	00	00	00	00	00	00	00	00	00	00
	11	00	00	00	00	00	00	00	00	00	00	00	00	00	00	00	00	01	00	00	00	00	00	00	00	00	00	00	00	00	00	00

Figure 5.13 – Screen shot of DynaMo Viewer illustrating the missing setups in the period: 13/09/2007 – 30/11/2008

5.5.1 Characterization of the measured signals

The acceleration time series collected by the Dynamic Monitoring system of the Infante D. Henrique Bridge, with a length of 30 minutes and a sampling frequency of 50 Hz, are pre-processed after being stored in the backup at FEUP. The pre-processing includes the elimination of offsets, application of a eighth-order low-pass Chebyshev Type I filter (MatLab 2000a) with a cut-off frequency of 5Hz and

re-sampling with a sampling frequency of 12.5 Hz. Figure 5.14 presents two examples of acceleration time series after being pre-processed to give an idea of the level of acceleration observed during the night and during a period with intensive traffic.

The variation of the vibration levels during a regular week is characterized in Figure 5.15 using the maxima and the root mean square (RMS) values of all the acceleration time series collected during a week of November. The RMS plot is particularly interesting, as it evidences the variation of the traffic intensity, which is higher from 7 o'clock in the morning to 8 o'clock in the evening and clearly lower during the weekend (10 and 11 of November of 2007). This behaviour is comprehensible, since this bridge is one of the main entrances in the city centre, being therefore its traffic intensity correlated with the city activity.

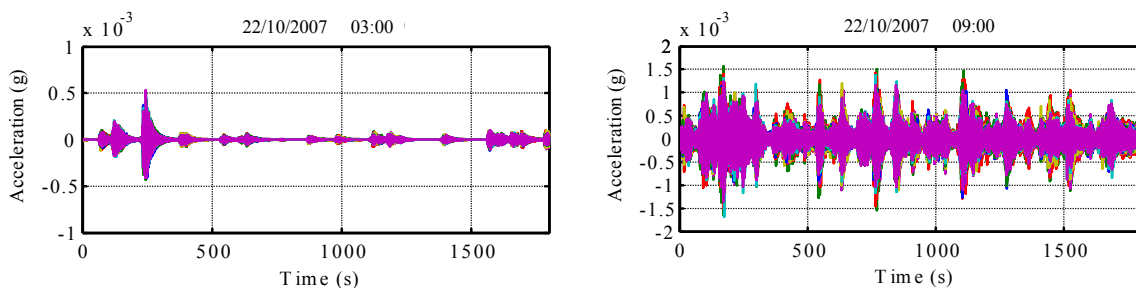


Figure 5.14 – Acceleration time series collected during the night (left) and during the morning rush hour (right).

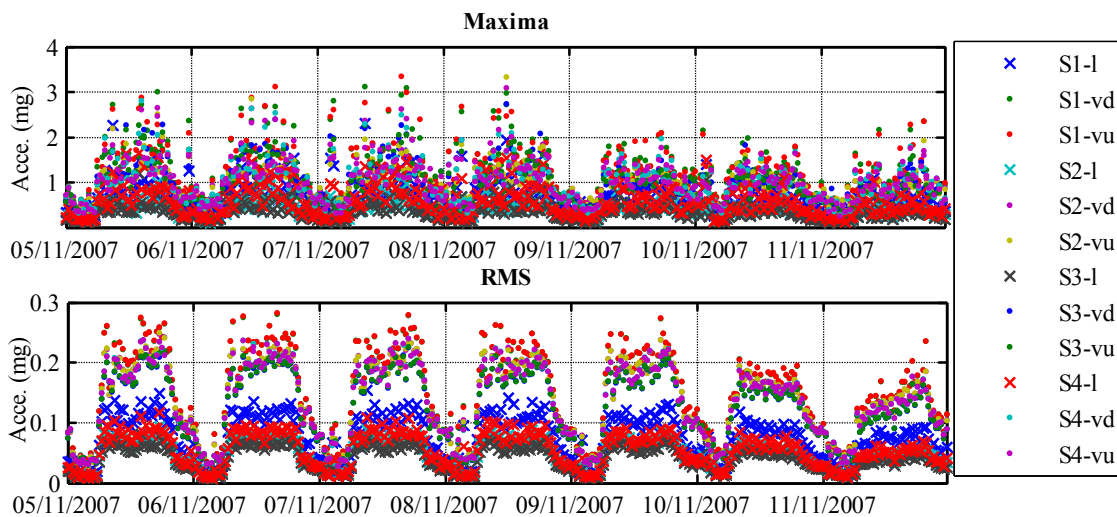


Figure 5.15 – Time evolution of the maxima and RMS values of the acceleration time series collected during the week: 05/11/2007 to 11/11/2007.

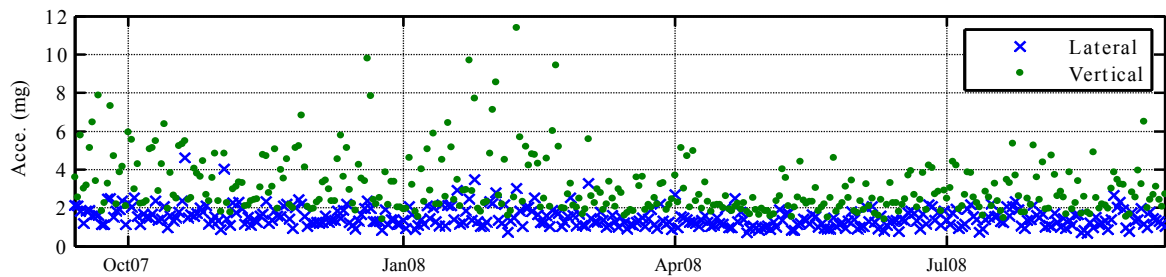


Figure 5.16 – Time evolution of the maxima of the acceleration time series collected from September 2007 to September 2008.

Figure 5.16 represents the lateral and vertical acceleration maxima observed during each day of the year under analysis. The vertical accelerations reached a maximum of 11.4mg, whereas the lateral accelerations were always lower than 5mg. The previous plot with the variation of the RMS also shows that the lateral acceleration is in average roughly equal to one half of the vertical acceleration.

The colour map presented at Figure 5.17 characterizes the frequency content of the acceleration signals collected during one month. This is a top view of the spectra of the first singular value of spectrum matrices derived from the time series collected in each 30 minutes setup placed side by side (in this case a total of $48 \times 31 = 1488$ spectra). The hotter colours mean more energy and therefore the vertical alignments in red/yellow characterize the time evolution of the excited natural frequencies. The comparison of the mean natural frequencies of these vertical alignments with the natural frequencies estimated from the data collected during the ambient vibration test (Figure 5.5) shows, as expected, a good agreement. The fact that there are thirteen natural frequencies appearing coherently in all the setups gives already good perspectives for the application of algorithms for the automatic identification of modal parameters. Still, some challenges can also be anticipated, for instance due to the existence of two closely spaced modes (first and second mode), the not so clear vertical alignment associated with the second mode and the existence of a mode with lower energy (around 3.5Hz).

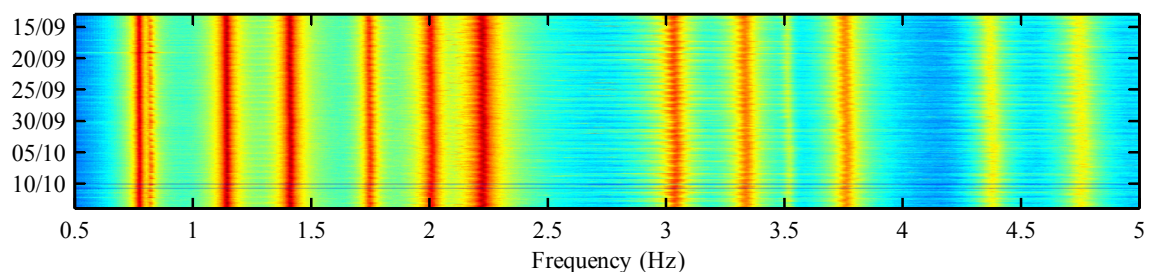


Figure 5.17 – Colour map with the variation of the signals frequency content from 13/09/2007 to 13/10/2007.

5.5.2 Automatic modal parameters identification

The algorithms developed to perform the automatic identification of modal parameters on an on-line basis integrated in the DynaMo software, presented in Chapter 4, are now explored using data collected at the Infante D. Henrique Bridge. In this application, the three algorithms: FDD, SSI-COV and p-LSCF, already described in Chapter 2, are tested with the goal of understanding the limitations and advantages of each approach.

The DynaMo software was developed in close relation with the application on this bridge, several improvements have been implemented in order to overcome difficulties encountered during its daily use. In particular, the algorithms for automatic identification of modal parameters were tuned using data collected during the first weeks after the installation of the monitoring equipment. Therefore, their online implementation only became operational on the 24th of November of 2007. Data collected before this date was processed offline using the files stored in the backup. This justifies the selection of the modal parameters extracted from the time series collected during this day (24/11/2007) as references for the tracking of modal parameters.

In the following paragraphs the practical application of each identification technique is described in detail, giving special attention to the selection of the user-defined parameters associated with each algorithm. For all the approaches, the choice of these parameters was based on parametric tests performed over a minimum of 48 datasets (a complete day). The aim of this effort was to guarantee that the three methods are applied in optimal conditions (or at least very close to them), so that a conclusive comparison between different approaches can be made.

This optimization exercise also showed that in every new monitoring project it is essential to spend some time with the tuning of the parameters of the algorithms for automatic modal analysis, as these can have an important influence on the quality of the results.

Automated Frequency Domain Decomposition

The first step of the FDD method consists of the calculation of a spectrum matrix for each data set. In the present application, all the outputs were elected as references and so this is a 12-by-12 matrix (the number of acceleration channels is equal to 12). Therefore, the singular value decomposition of this matrix produces, for each frequency, 12 singular values and vectors. The spectra of the first singular values were used to construct colour maps like the one presented in the previous section (Figure 5.17).

The auto and cross spectra of the spectrum matrices were calculated with a resolution of 0.0061Hz (0.8% of the lowest natural frequency), using segments from the time series with a total length of 30 minutes, adopting a Hanning window and an overlap of 50%. A lower value for the frequency resolution would improve the accuracy of the natural frequency estimates. However, the higher noise level of the spectra would make the procedure for automatic identification less efficient.

Besides the elements needed for calculation of the spectrum matrices, the user-defined parameters of this methodology include the frequency interval under analysis, the MAC value limit of the points in the same modal domain and the minimum number of points of the modal domains. The number of expected natural frequencies and the noise level are optional parameters that can be used to shorten the number of searches for maxima. In the present application, the analysis was performed over the frequency range from 0.5 to 4.5 Hz. A total of 14 natural frequencies were specified for the automatic identification, a limit value of 0.4 was selected for the MAC and only modal domains with more than 7 points were considered. In the selected frequency range only 12 modes are expected, however, two extra modes are considered in order to increase the chances of not missing low excited modes.

Experience gained in the analysis of data from this bridge showed that it is better to select low values for the MAC (0.4). In this way, the number of points in the search domain is reduced more rapidly and the number of false identifications is minimized. However, it should be pointed out that this strategy is not adequate if the number of sensors is small (the ability of the MAC to distinguish mode shapes increases with the number of sensors) and if similar modes shapes for adjacent natural frequencies are expected. The minimum number of points in the modal domains has to be tuned in articulation with the selected MAC limit (the number of points in the modal domains decreases when the MAC limit is increased).

Figures 5.18 and 5.19 illustrate the output of the implemented algorithm for automatic identification applied to the time series presented in Figure 5.14, which are associated with two completely different load scenarios. The graphics show the first two singular value spectra and the modal domain associated to each peak. The colour of the modal domains is dependent on the order of the natural frequencies identification (from red to yellow) and the corresponding ordinates are the MAC values. In both cases the modal domains of the 12 firstly identified modes cover all the selected frequency range. Therefore, the search for new modes is stopped because the search domain becomes empty. The second plot shows that the algorithm is able to identify the second mode, even when its peak on the first singular value spectrum is not very clear due to its proximity with regard to the frequency of the first mode.

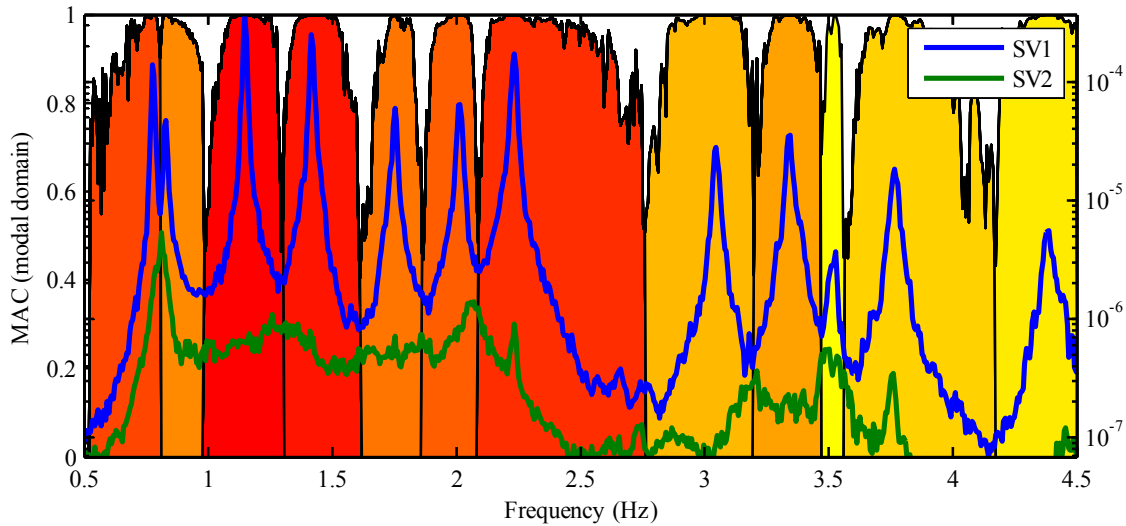


Figure 5.18 – Automatic modal analysis with FDD in the setup: 22/10/2007 03:00.

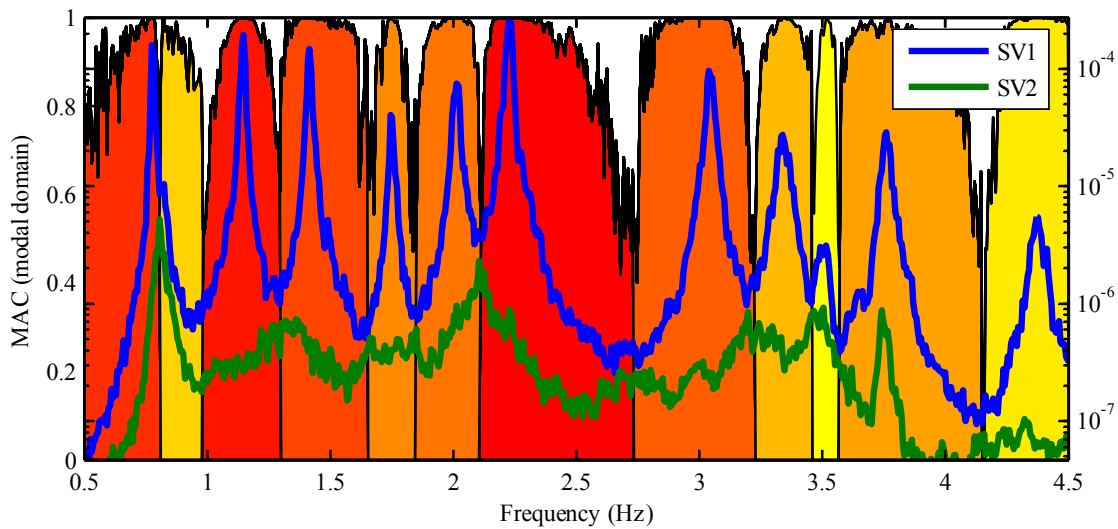


Figure 5.19 – Automatic modal analysis with FDD in the setup: 22/10/2007 09:00.

The results provided by the application of the automated version of the FDD method to the data collected during the first days of operation of the monitoring system are presented in Figure 5.20. As the number of modes identified from each dataset is not always equal to the number of physical modes within the frequency range under analysis, due to fails in the identification of some mode or to the erroneous interpretation of a noisy peak as a mode, the graphic presents points that are outside the horizontal alignments associated with the 12 bridge modes and the order of the identified modes does not always coincide with the mode number (the colour of the points belonging to each horizontal alignment is not constant).

Therefore, it is needed a procedure to link the modal parameters associated with the same physical mode and clean the false estimates. In the present application, this was achieved by comparing each new group of estimates with a set of reference values, using as references the averages of the modal

parameters of the 12 modes identified from all datasets measured during the 24th of November of 2007 (beginning of the online processing). The new estimates for each reference mode are chosen, using the MAC ratio as selection criterion, from a group composed by all the estimates provided by the independent analysis of each setup that have a natural frequency not differing more than 15 % from the reference values. Only estimates with a MAC ratio higher than 0.8 with regard to the reference mode shapes are accepted. In this way, the link between estimates of the same physical mode is achieved and simultaneously possible frequency shifts lower than 15%, motivated by the environmental variables or possible damages, are allowed. In Figure 5.21, it is shown the efficiency of the adopted procedure, by presenting the same estimates that were displayed in Figure 5.20 after the grouping.

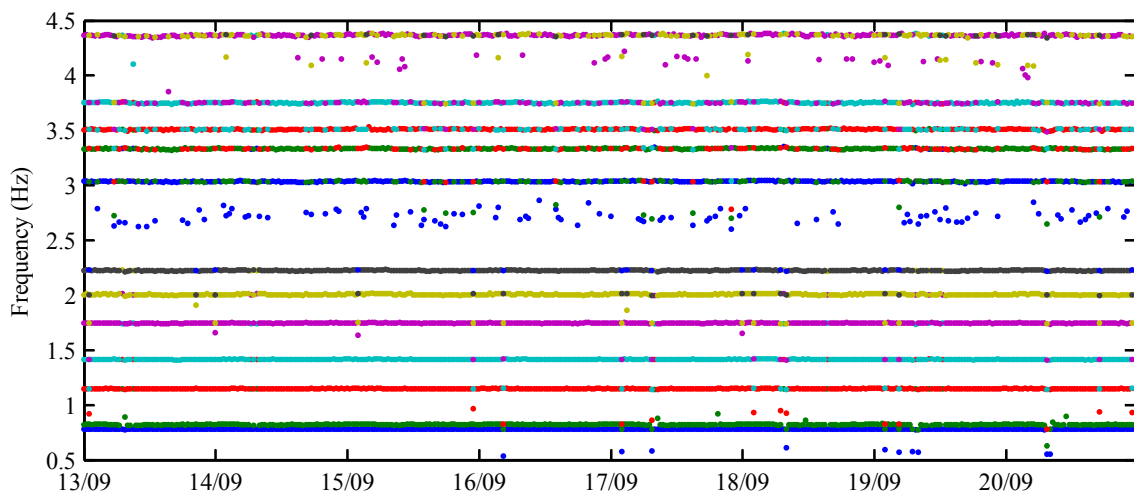


Figure 5.20 – Natural frequencies identified by the FDD method in the period 13/09/2007 – 20/09/2007.

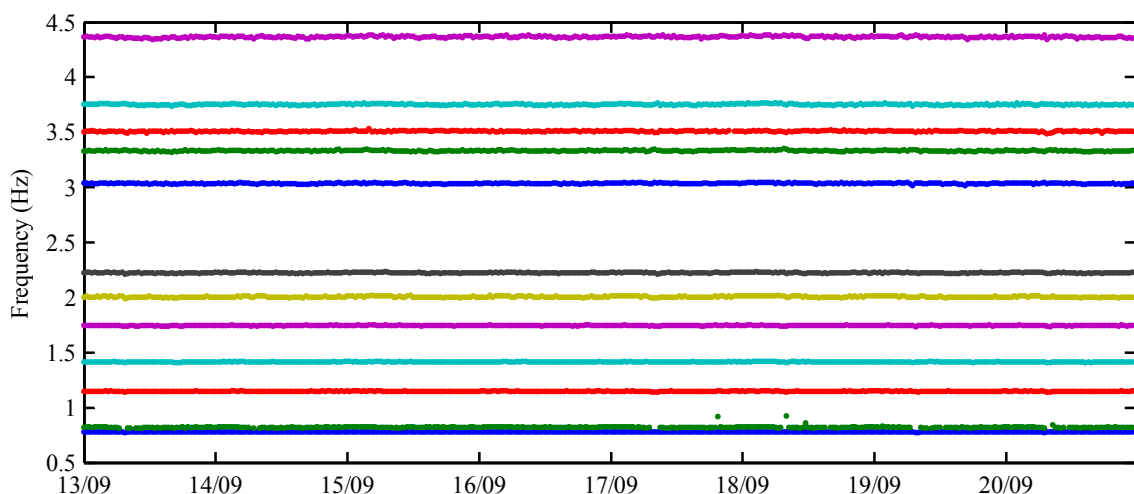


Figure 5.21 – Natural frequencies identified by the FDD method in the period 13/09/2007 – 20/09/2007 grouped using the reference modal parameters.

The reference modes coincide with the modes that had been previously identified with the ambient vibration test. The natural frequencies are not exactly the same because of several factors that are detailed in section 5.6. Direct comparison between the mode shapes provided by the ambient vibration test (represented in Figures 5.6, 5.7 and 5.8) and the ones estimated by the monitoring system is not possible, because the measured degrees of freedom are not exactly the same. However, the overlay of both estimates shows that they are very similar. Figure 5.22 presents such comparison for the first four mode shapes.

Figure 5.23 presents a zoom with the variation of the bridge first two natural frequencies during one month. This enhances one of the limitations of the adopted FDD method implementation, which is its inability to well characterize frequency variations that are of the order of magnitude of the adopted frequency resolution. Of course that, this is less relevant for higher natural frequencies, because the same relative differences are associated with higher frequency shifts.

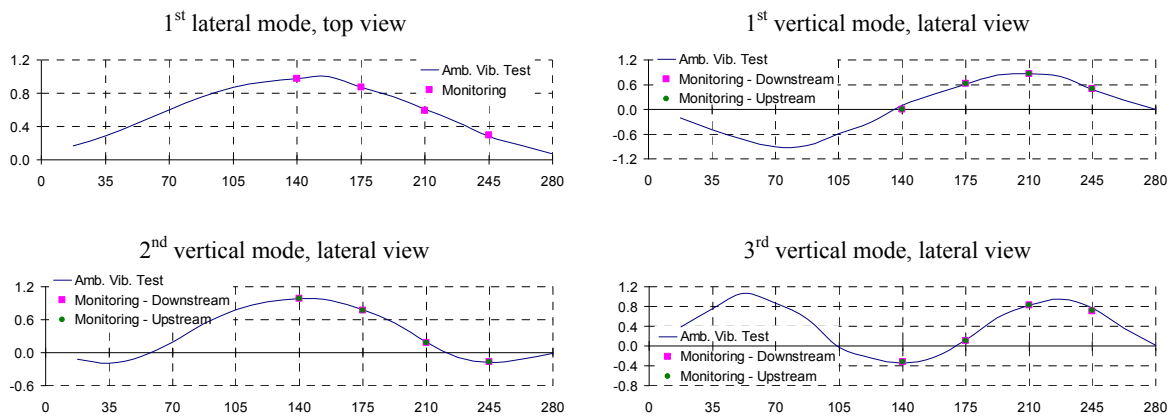


Figure 5.22 – Comparison between the first four mode shapes identified with the ambient vibration test and the reference mode shapes of the FDD method.

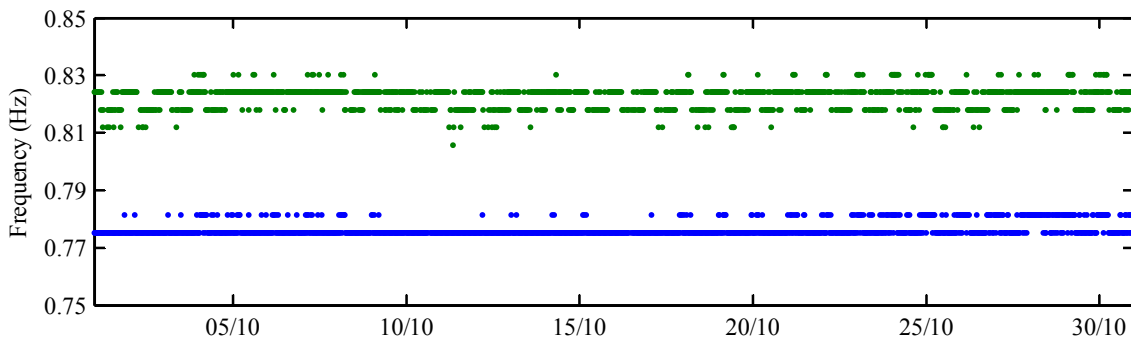


Figure 5.23 – First two natural frequencies identified with the FDD method during October 2007.

Table 5.2 synthesises the results of the application of the FDD method to all datasets collected during one year. In the second column, the success rate of the algorithm in the identification of the bridge first 12 modes is quantified. This is the ratio between the number of setups where a certain mode was


identified and the total number of processed setups. It is impressive the fact that most of the modes are automatically identified in all the 17 325 processed setups. As one would expect, the algorithm is slightly less efficient in the identification of the second mode due to its proximity with regard to the first mode. Columns 3 and 4 present the mean values and the standard deviation values (std) of the natural frequencies (f). The low values of the standard deviations already show that, in the case of this bridge, the influence of environmental and operational variables on this modal parameter is relatively small (relative standard deviation lower than 0.5%) and that it is not uniform for all the modes (relative standard deviation varying from 0.14% to 0.44%). These effects are studied in section 5.6. Columns 5 and 6 characterize the MAC coefficients between the mode shape estimates in each dataset and the corresponding reference mode shapes. Their mean values are quite high (always higher than 0.99), which means that they are not very sensitive to environmental changes and that the adopted identification procedure provided always high quality estimates. The minimum (min) MAC values of the modes that were not identified in all the datasets (success rate lower than 100%) are close to 0.80, as this was the minimum value to accept a candidate estimate for a certain reference mode.

Table 5.2 – Results of the FDD method for the period: 13/09/2007 – 12/09/2008
(total number of processed setups – 17325)

Mode	Success Rate (%)	f_{mean} (Hz)	f_{std} (Hz)	MAC_{mean}	MAC_{min}
1	100	0.7777	0.0030	0.9977	0.9660
2	98.009	0.8224	0.0068	0.9953	0.8071
3	100	1.1461	0.0029	0.9999	0.9985
4	100	1.4153	0.0047	0.9997	0.9959
5	100	1.7510	0.0054	0.9944	0.9485
6	100	2.0119	0.0076	0.9997	0.8500
7	100	2.2255	0.0062	0.9997	0.9807
8	100	3.0416	0.0110	0.9999	0.9540
9	100	3.3376	0.0092	0.9978	0.9462
10	99.965	3.5231	0.0097	0.9938	0.8428
11	99.994	3.7610	0.0106	0.9926	0.8048
12	100	4.3807	0.0155	0.9994	0.9095

Automated Covariance driven Stochastic Subspace Identification

The SSI-COV method is based on correlation matrices of the measured acceleration time series. For their calculation two parameters have to be defined: the reference outputs and the maximum time lag. After some preliminary experiments, it was concluded that stabilization diagrams with good quality were obtained considering all the outputs as references and adopting correlation functions with 100 points ($100/12.5 = 8$ seconds $\rightarrow 8 \times 0.78 = 6.2$ periods of the lower frequency). In the selection of the parameters, the time of calculation was not a constraint, since the data is being processed on-line and therefore there is a time interval of 30 minutes between each dataset that is more than enough to perform all the necessary calculations. The chosen parameters produce stabilization diagrams similar to the one presented in Figure 5.24, which is associated with one of the datasets collected during the 22nd of October of 2007. The presented diagram contains mode estimates provided by models with even orders between 20 and 100, interval that was found to provide a sufficient amount of stable estimates for the expected physical modes.

In this case, the modes classified as stable (represented by ) respected the following limits for variations between models of consecutive orders: natural frequency variation $< 1\%$; modal damping ratio variation $< 2\%$; minimum MAC coefficient between mode shape estimates > 0.99 . These limits proved to permit the clearly distinction of 12 vertical alignments of stable modes that represent the bridge first 12 modes of vibration.

Therefore, in a first attempt, the hierarchical algorithm for automatic interpretation of stabilization diagrams was applied to the stable modes of stabilization diagrams constructed with the criteria defined in the previous paragraph, using a limit for the distance between modes of the same cluster equal to 0.02 (calculated with equation (2.94)). The results illustrated in Figure 5.25 show that the poles belonging to the 12 physical modes within the analysed frequency range are grouped together.

In order to reduce the number of user-defined parameters, the algorithm was tried over all the mode estimates (stable and unstable) with positive natural frequencies and modal damping ratios provided by the considered model orders. The formed groups, considering the same distance limit, are characterised in Figure 5.26. Again, 12 clusters clearly stand out. However, in this case there are several clusters with very few elements that absorbed the spurious modes. With this more direct procedure, the definition of limits for the classification of the stable poles is avoided and thus the number of input parameters of the method is drastically reduced, while the efficiency is maintained (Magalhães et al. 2009e).

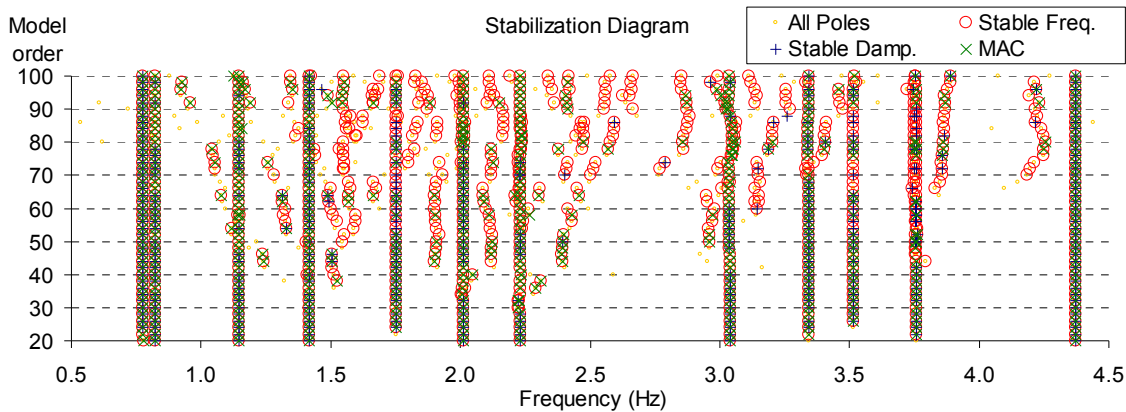


Figure 5.24 – Stabilization diagram associated with the time series collected on 22/10/2007 23:00.

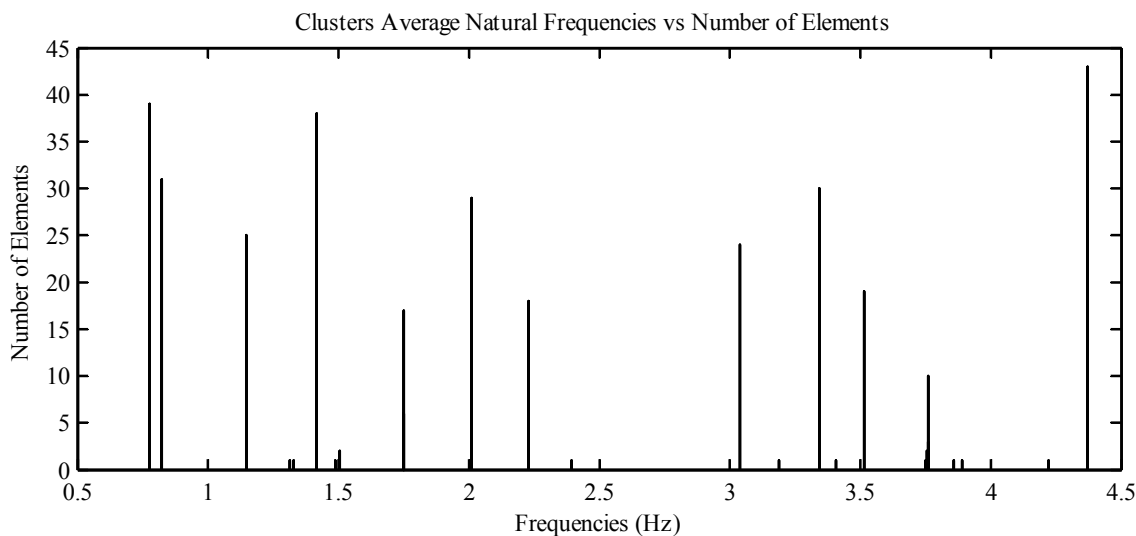


Figure 5.25 – Number of elements of the clusters formed with the stable poles represented in Figure 5.24.

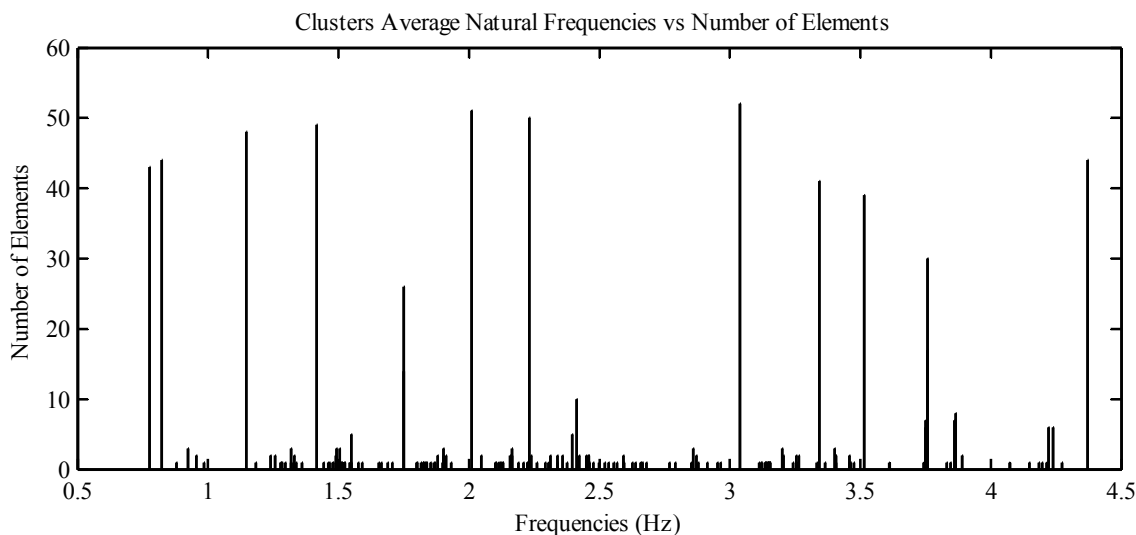


Figure 5.26 – Number of elements of the clusters formed with all the poles represented in Figure 5.24.

In Figure 5.27a the estimates that belong to the 12 clusters from Figure 5.26 with more elements are represented in a damping vs frequency diagram. As the grouping of all the poles did not take into account the damping values, a considerable dispersion is observed. Therefore, the extreme values that distort the mean values were eliminated with an outliers analysis (detailed in section 2.4.4). The effect of this operation can be evaluated with the comparison of the two graphics presented in Figure 5.27.

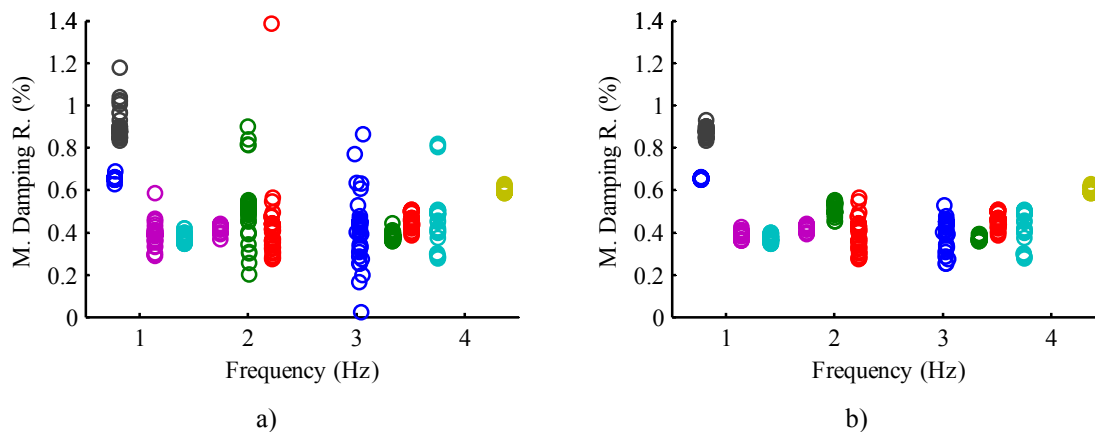


Figure 5.27 –Damping vs frequency diagrams of the mode estimates that belong to the 12 clusters with more elements, before (a) and after (b) the outliers elimination.

The final outputs of the proposed methodology are the average values of the modal parameters (natural frequency, modal damping ratio and mode shape) of the estimates belonging to the selected clusters.

The procedure previously illustrated in one setup was tried on several setups and proved to provide consistently good results. Therefore, adequate parameters had be found to use this method to process on an on-line basis the data continuously collected by the monitoring system installed in the Infante D. Henrique Bridge.

For the matching of the estimates from consecutive setups, the same parameters that were adopted for the FDD method were used (frequency variation $< 15\%$ and $MAC > 0.8$). In each setup, two extra clusters are always selected, which makes a total of 14 selected clusters, and compared with reference modal parameters given by the application of the SSI-COV method to all the setups collected during the 24th of November of 2007. The reference modal parameters are characterized in Figure 5.28, using for the description of the mode shapes a polar plot, which evidences that the imaginary components are negligible. These results prove the quality of the identified modal parameters and show good synchronization of the two digitizers provided by the GPS sensors (an imperfect synchronization would lead to phase angles different from 0 or 180 between the degrees of freedom measured by different digitizers).

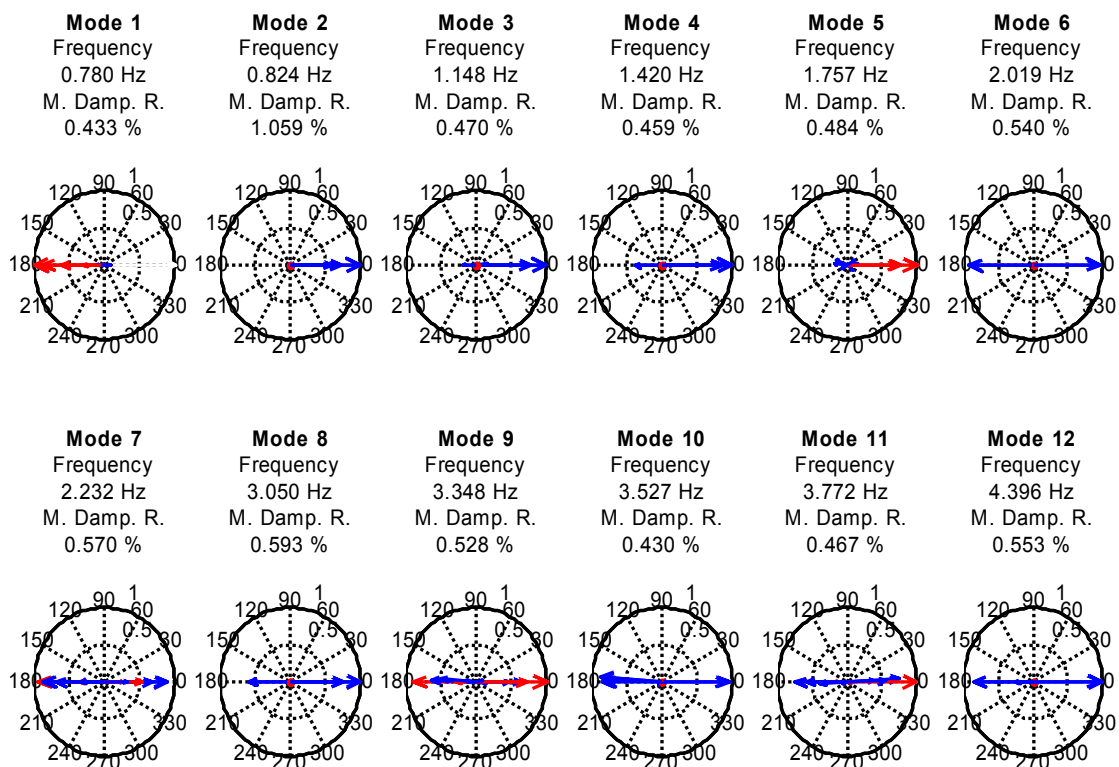


Figure 5.28 – Reference modal parameters of the SSI-COV method: natural frequencies, modal damping ratios and mode shapes represented in a polar plot (lateral components in red and vertical components in blue).

Figure 5.29 shows the evolution of the natural frequencies of the first two modes during one month identified with the SSI-COV method. The comparison of this plot with the one presented in Figure 5.23 shows that this method permits a much better characterization of small daily variations, especially relevant in the second mode.

Another advantage of this method with regard to previously described is its ability to provide estimates for the modal damping ratios. The time evolution of the modal damping ratios of the 12 identified modes during one week is presented in Figure 5.30. The second mode is the one that presents higher mean values and higher daily variability. This behaviour will be further explored in section 5.5.3.

The performance of this method in the processing of the datasets collected during one year is characterized in Table 5.3. This method presented very high success rates, seven modes were identified in all the 17 325 datasets (success rate of 100%), and only one of the modes presented a success rate lower than 99 % (mode 11). The good performance in the identification of the closely spaced modes (success ratios of 99.99 and 100%) is remarkable.

The statistics related with the natural frequencies are similar to the ones associated with the results of the FDD method (Table 5.2). Concerning the modal damping ratio estimates, apart from the second

mode, the mean values are around 0.5 %, with standard deviations roughly equal 0.1%. The mean MAC values are generally higher than 0.99. The lowest value is observed for the 11th mode, which is also the one with the lowest success rate.

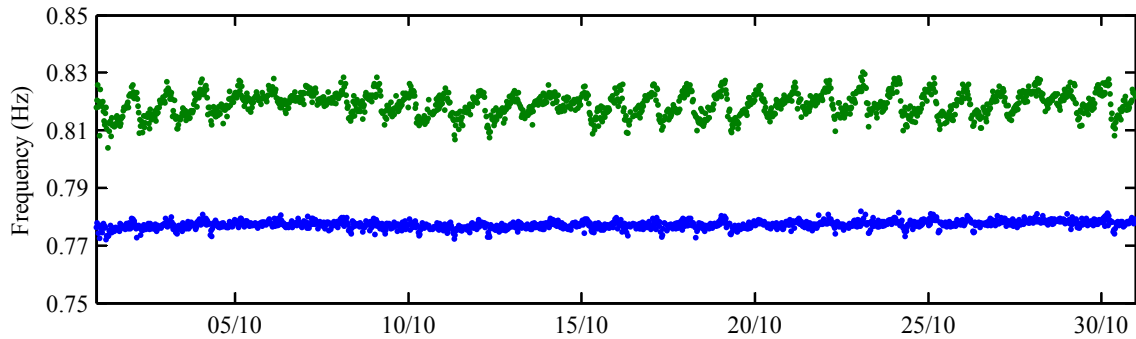


Figure 5.29 – First two natural frequencies identified with the SSI-COV method during October 2007.

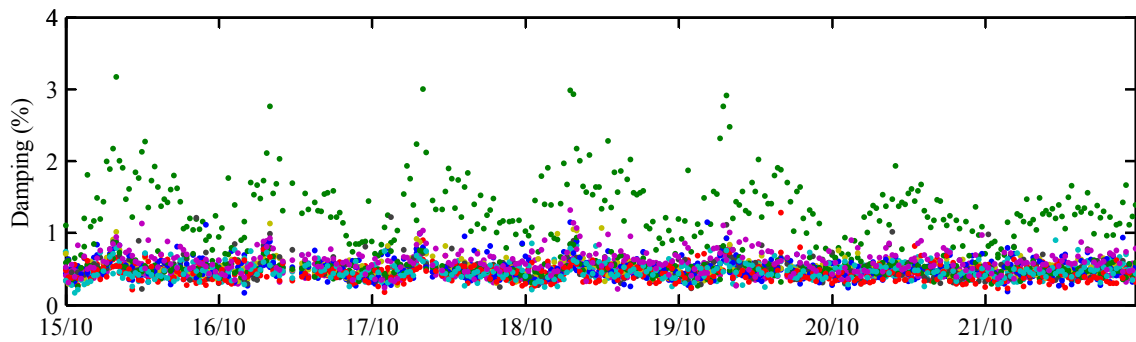


Figure 5.30 – Time evolution of modal damping ratios of the first 12 modes identified with the SSI-COV method during one week of October 2007 (second mode in green).

Table 5.3 – Results of the SSI-COV method for the period: 13/09/2007 – 12/09/2008 (total number of processed setups – 17325)

Mode	Success Rate (%)	f_{mean} (Hz)	f_{std} (Hz)	ξ_{mean} (%)	ξ_{std} (%)	MAC_{mean}	MAC_{min}
1	99.994	0.7776	0.0020	0.4520	0.1107	0.9959	0.8125
2	100	0.8195	0.0046	1.1883	0.3702	0.9989	0.9515
3	100	1.1458	0.0027	0.4718	0.1182	0.9990	0.9914
4	100	1.4151	0.0043	0.4758	0.1162	0.9996	0.9799
5	99.925	1.7507	0.0050	0.4759	0.0932	0.9904	0.8084
6	99.948	2.0113	0.0076	0.5319	0.1292	0.9995	0.8083
7	99.971	2.2249	0.0074	0.5341	0.1695	0.9994	0.8107
8	100	3.0406	0.0129	0.5427	0.1544	0.9996	0.9551
9	99.838	3.3371	0.0089	0.5164	0.1104	0.9936	0.8163
10	99.786	3.5225	0.0094	0.4261	0.1001	0.9925	0.8001
11	98.118	3.7601	0.0104	0.4734	0.1070	0.9780	0.8012
12	100	4.3788	0.0155	0.5996	0.1375	0.9993	0.9072

Automated poly Least Squares Complex Frequency Domain

The first step of the p-LSCF method is the calculation of the half spectrum matrix, whose elements are the Fast Fourier Transform of the positive lags of correlation functions, after the application of an exponential window. In the present application, the spectra were obtained from the Fast Fourier Transform of the positive lags of correlation functions with 1024 points calculated using the fast implementation of the summation formula (see section 2.3.2). An exponential window with a factor of 0.1 was applied before the conversion to the frequency domain, to minimize the leakage errors. As all the measured degrees of freedom were selected as references, the spectrum matrix is 12-by-12 (Magalhães et al. 2009g).

Then, the fitting to a theoretical spectrum was performed in the frequency range 0.5 - 5 Hz, using polynomials with orders between 1 and 18. Following the algorithm presented in section 2.3.5, the modal parameters were afterwards extracted from a state-space model derived from the estimated polynomial matrices. The stabilization diagram presented in Figure 5.31 uses the same data and stabilization criteria that were used on the one of Figure 5.24. It confirms the ability of the p-LSCF method to provide very clear stabilization diagrams.

Figure 5.32 characterizes, for the same setup, the clusters formed by all the mode estimates with positive natural frequencies and modal damping ratios extracted from all the fitted models, using the same distance limit between modes (0.02) that was adopted with the SSI-COV method. The 12 groups that contain the physical estimates clearly stand out.

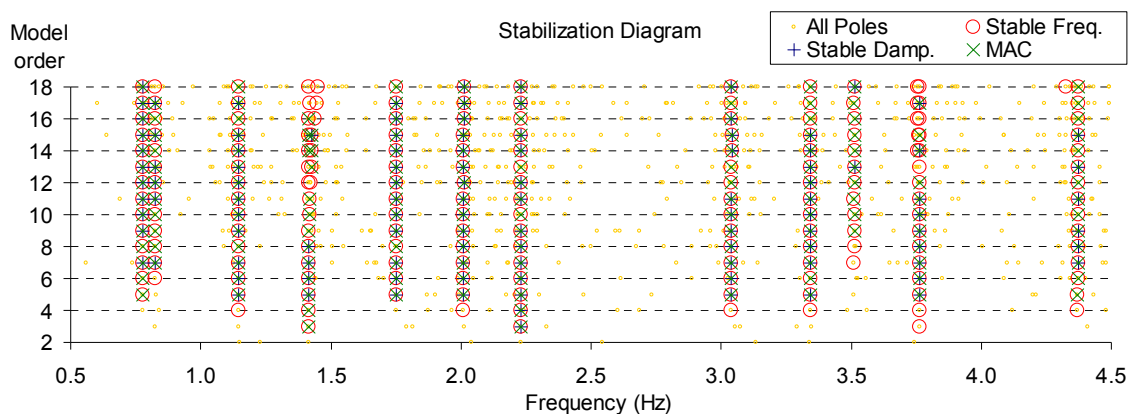


Figure 5.31 – Stabilization diagram of the data collected on 22/10/2007 23:00.

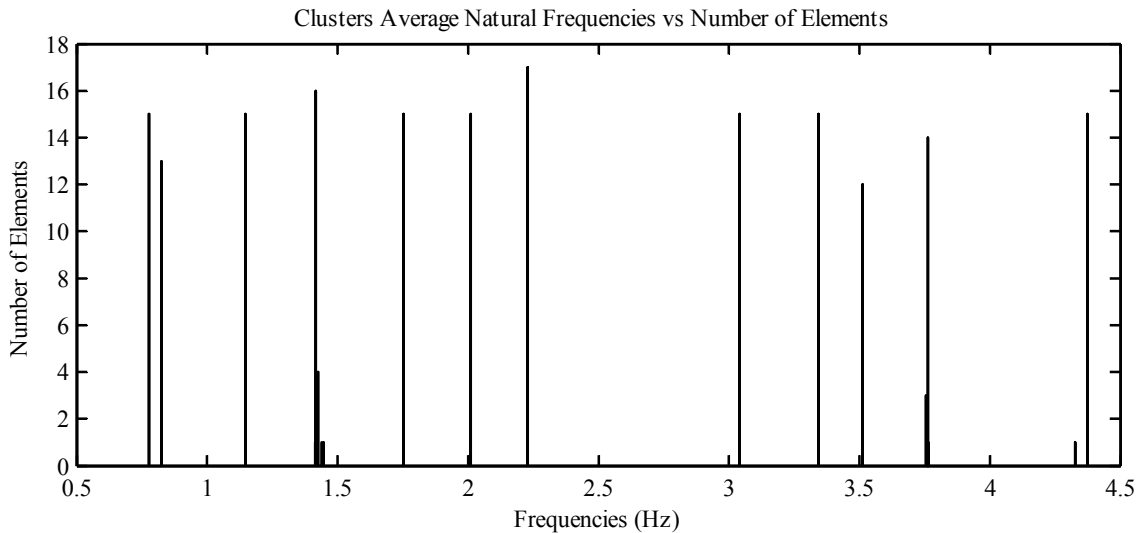


Figure 5.32 – Clusters associated with the analysis of the stabilization diagram of Figure 5.31

The modes inside the 12 groups with more elements are characterized in Figure 5.33, after and before the elimination of outliers. The comparison of these figures with their equivalents provided by the SSI-COV method shows that the scatter of the mode estimates inside the same group is much lower in the case of the p-LSCF method.

The parameters of the automated p-LSCF method used in this particular setup were firstly tested on a large amount of setups and then used for the on-line processing of the Infante D. Henrique Bridge data. The matching between each new set of mode estimates with the previous ones was performed using the same procedure and parameters that were adopted with the SSI-COV method. The reference modal parameters resulted from the application of the p-LSCF method to all the datasets collected during the 24th of November of 2007, and subsequent averaging. These are similar to the ones achieved with the application of the SSI-COV method.

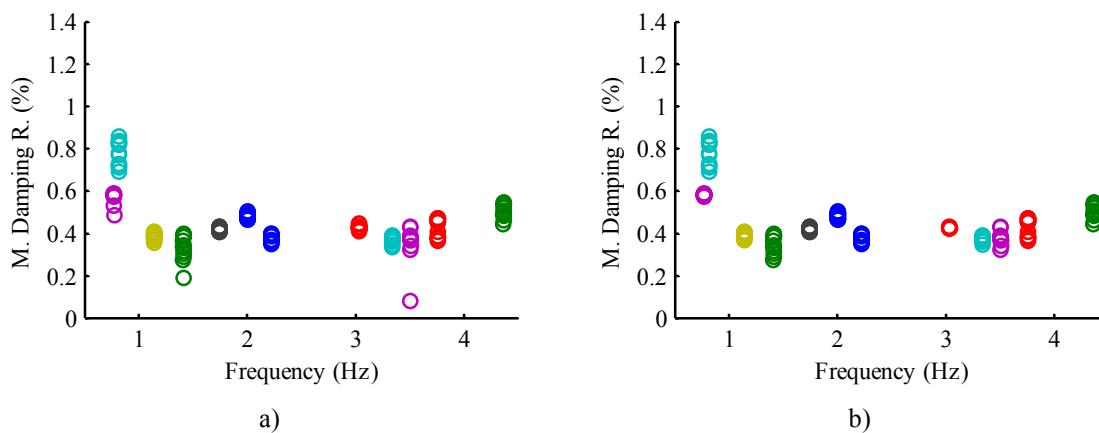


Figure 5.33 –Damping vs frequency diagrams of the mode estimates that belong to the 12 clusters with more elements, before (a) and after (b) the outliers elimination.

The continuous online application of this algorithm to the data collected in the Infante D. Henrique Bridge permitted to obtain a very reliable characterization of the time evolution of the structure modal parameters. As an illustration, Figure 5.34 presents the evolution of the modal damping ratios of all the identified modes during a normal week. The comparison of this plot with the one provided by the SSI-COV method for the same period (Figure 5.30) shows that the second one presents a slightly clearer characterization of the damping variations, especially evident for the second mode. The reasons for the observed daily variations are explained in section 5.5.3.

Table 5.4 presents the statistics of the modal parameter estimates provided by the application of the p-LSCF method to all the datasets collected during one year. The column with success rates always higher than 99% proves the robustness of this algorithm. The standard deviations displayed in Table 5.4 associated either with the natural frequencies or with modal damping ratios estimates are generally lower than the ones observed in the SSI-COV method results.

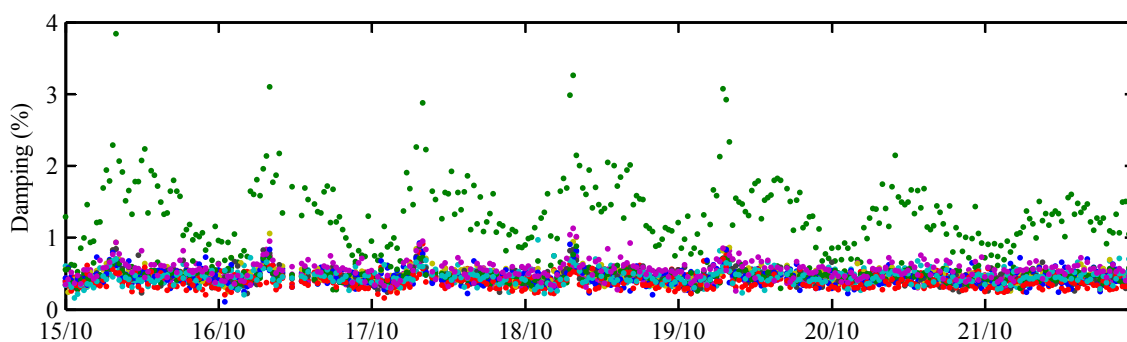


Figure 5.34 – Time evolution of modal damping ratios of the first 12 modes identified with the p-LSCF method during one week of October 2007 (second mode in green).

Table 5.4 – Results of the p-LSCF method for the period: 13/09/2007 – 12/09/2008 (total number of processed setups – 17325)

Mode	Success Rate (%)	f_{mean} (Hz)	f_{std} (Hz)	ξ_{mean} (%)	ξ_{std} (%)	MAC_{mean}	MAC_{min}
1	99.994	0.7777	0.0019	0.4379	0.0933	0.9962	0.8257
2	99.988	0.8208	0.0041	1.1841	0.3741	0.9981	0.9537
3	100	1.1459	0.0025	0.4404	0.0846	0.9998	0.9946
4	100	1.4154	0.0042	0.4482	0.0912	0.9992	0.9774
5	99.937	1.7509	0.0049	0.4411	0.0809	0.9915	0.8109
6	99.325	2.0113	0.0073	0.4751	0.0979	0.9986	0.8096
7	99.873	2.2248	0.0061	0.4424	0.1089	0.9990	0.8028
8	100	3.0408	0.0111	0.4344	0.0987	0.9993	0.9033
9	99.896	3.3371	0.0086	0.4820	0.0904	0.9945	0.8210
10	99.042	3.5214	0.0094	0.3553	0.0733	0.9908	0.8018
11	99.671	3.7603	0.0097	0.4419	0.0833	0.9925	0.8058
12	100	4.3785	0.0149	0.5352	0.1108	0.9989	0.9082

5.5.3 Analysis of the modal parameters variation

After the characterization of the performance of the algorithms for automatic modal analysis in the processing of the data collected at the Infante D. Henrique Bridge, the time evolution of the modal parameters observed during one year (from 13/09/2007 to 12/09/2008) is analysed. The above comparison of the outputs of the three tested identification methods showed that the SSI-COV and the p-LSCF methods provide more complete information than the FDD method. The results of the two parametric methods are quite similar. However, as the standard deviations of the p-LSCF method are slightly lower, its results will be adopted in the remaining analyses.

Figure 5.35 presents the evolution of the bridge first 12 natural frequencies during the period under analysis. At this scale it seems that all the natural frequencies are almost constant. However, the zoom presented in Figure 5.36 shows, as an example, the annual variation of the 4th natural frequency, which is similar to the observed for the other frequencies. This graphic also illustrates the ability of the monitoring system to well characterize very small variations of the natural frequencies, of the order of milli-Hertz.

Figure 5.37 characterizes, for the same period, the variation of the temperatures measured by 8 sensors embedded approximately in the middle of the top and bottom flanges of the deck concrete box girder at the sections marked in the scheme of Figure 5.10 (section T1 to T4). This graphic shows a minimum temperature of 5 °C in winter and maximum temperature of 31.5 °C in summer.

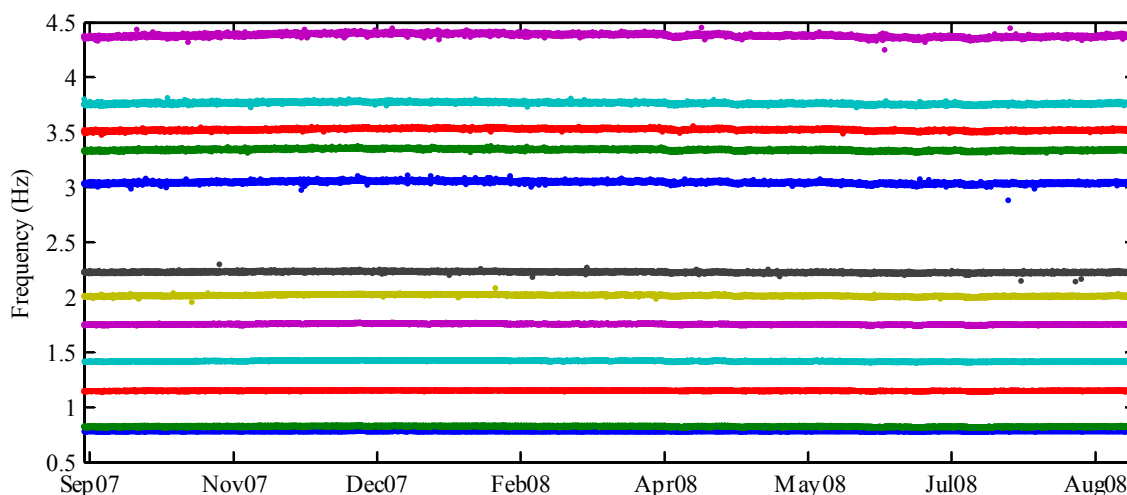


Figure 5.35 – Variation of the bridge first 12 natural frequencies identified with the p-LSCF method, from 13/09/2007 to 12/09/2008.

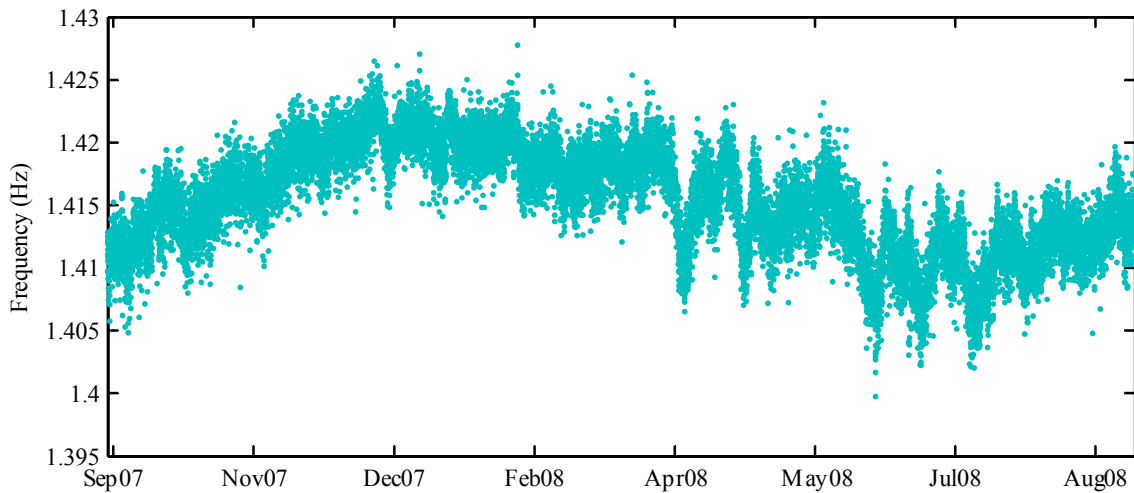


Figure 5.36 – Variation of the bridge 4th natural frequency (3rd vertical mode) from 13/09/2007 to 12/09/2008.

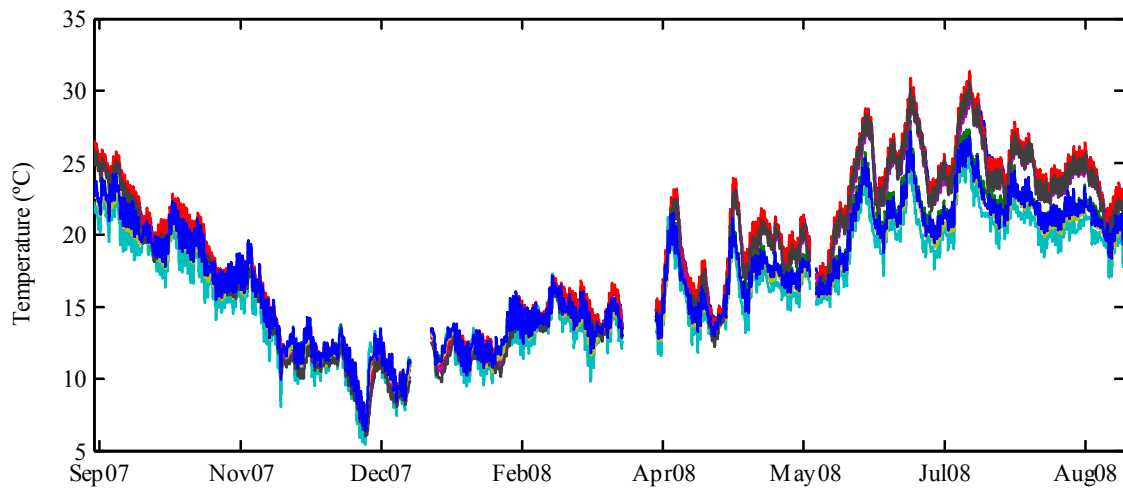


Figure 5.37 – Variation of the temperature measured by embedded temperature sensors, from 13/09/2007 to 12/09/2008.

The comparison of Figures 5.36 and 5.37 shows an evident correlation between the measured temperatures and the estimated natural frequency. This is further explored in the next section.

A second factor with relevant influence on the natural frequencies is the amplitude of the bridge vibration, which is essentially related with the traffic intensity. This dependency is characterized in Figure 5.38 for the second mode during the first week of March, using the root mean square (RMS) to quantify the vibration intensity. The second mode is the one from the twelve analysed modes that experiences higher daily fluctuations. This behaviour may well be justified by the relevant longitudinal component of this mode that mobilizes friction forces at the abutments bearings. For low vibration amplitudes the bearings behave as a fixed connection, whereas for large amplitudes the friction forces are overcome and as a consequence the natural frequency decreases (note that the scale associated with the RMS is inverted).

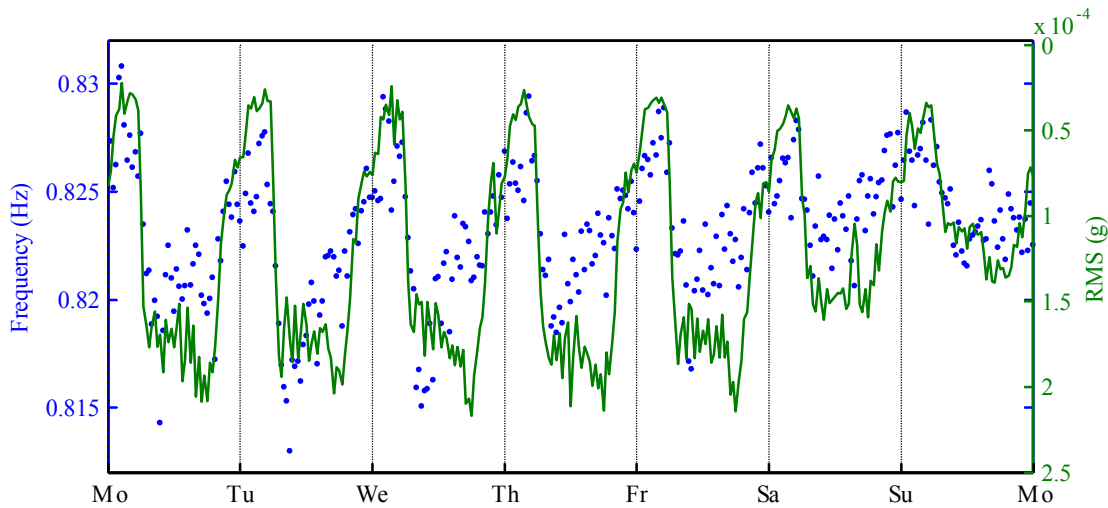


Figure 5.38 – Second natural frequency vs vertical vibration amplitude at section S3 during one week (from 03/03/2008 to 09/03/2008).

The comparison of the natural frequencies identified in the ambient vibration test with the ones provided by the monitoring system, as it is done for the second lateral mode in Figure 5.39, shows that the first set of values are consistently lower (see Table 5.4 and Figures 5.6 to 5.8). The motivation for the observed differences is certainly due to the concrete hardening manifested during the last three years (last pouring: June 2002; ambient vibration test: June 2005; dynamic monitoring: 2007/2008). This is an interesting feature of dynamic monitoring systems, as its installation on a young concrete structure allows an indirect quantification of the time evolution of the concrete elasticity modulus (as demonstrated with the laboratory tests presented in (Azenha et al. 2010)).

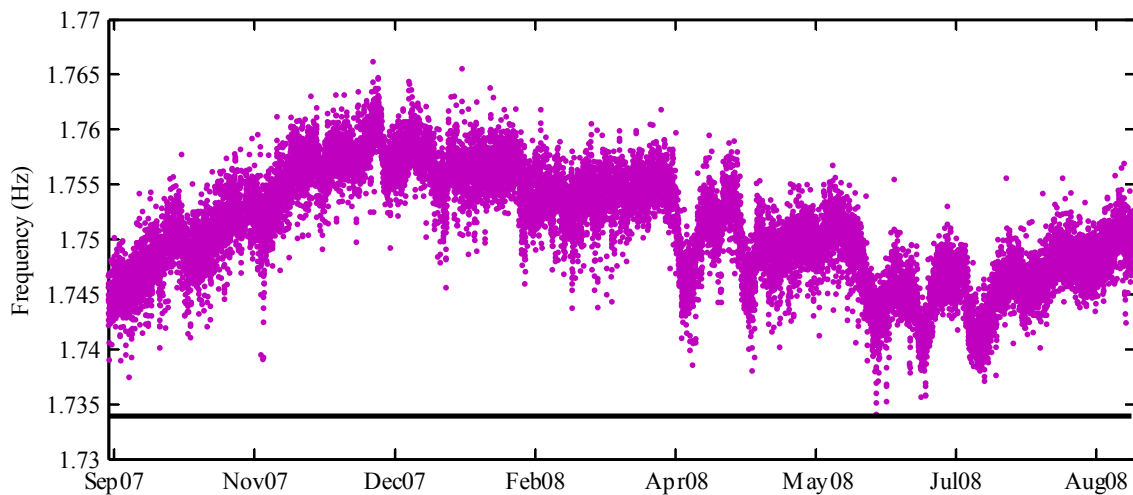


Figure 5.39 – Variation of the bridge 5th natural frequency (second lateral mode) from 13/09/2007 to 12/09/2008 and natural frequency identified with the previously developed ambient vibration test (full line at 1.734Hz).

Concerning the influence of operational factors on the bridge damping, the effect of the vibration amplitude on the modal damping ratio of the first vertical mode (2nd mode) was already illustrated by its daily variations observed in Figure 5.34. This is further proven with the plot presented in Figure

5.40, which correlates the modal damping ratios of the second mode identified during one year with the RMS values of the acceleration time series measured by one of the vertical accelerometers placed in the section where the mode shape has its largest amplitude. In spite of the observed dispersion, for the range of recorded values, the linear proportionality between the two variables is obvious.

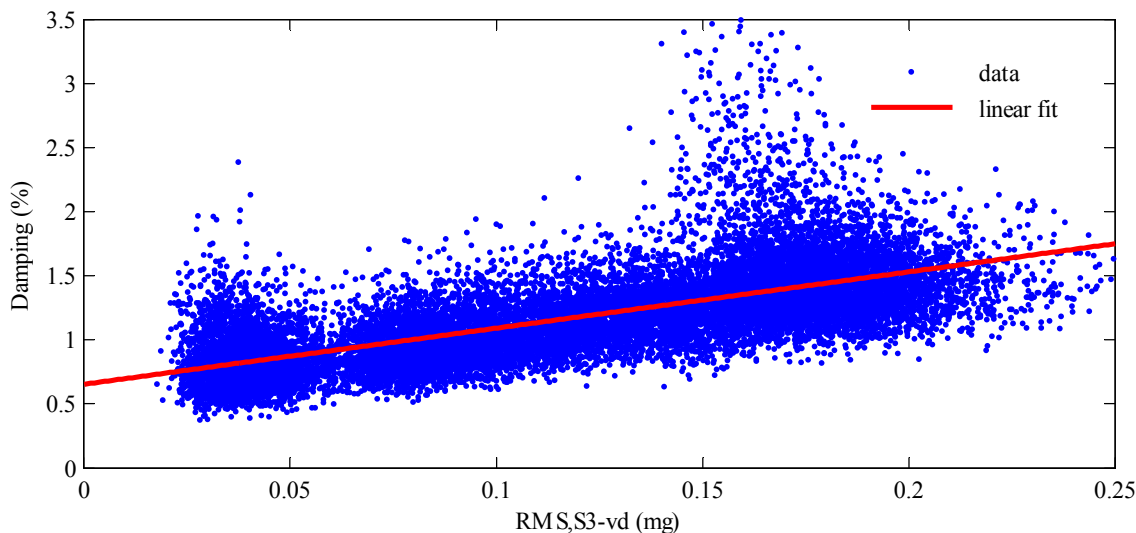


Figure 5.40 – Modal damping ratios of the first vertical mode vs RMS values of vertical acceleration time series collected at section S3.

A more close observation of Figure 5.34 also shows the existence of peaks in the damping estimates at the beginning of the first 5 days (from Monday to Friday). From the analysis of the entire database, it was possible to conclude that in the working days at the beginning of the morning an increase of the bridge damping is observed. This happens because at the bridge end on the Porto side there are traffic lights that induce traffic jams over the bridge at the morning rush hour. The increase of the damping, which consistently occurs at the same day period, is certainly motivated by the dynamic interaction between the bridge and the vehicles stopped over the bridge. It is relevant to state that this phenomenon was only identified with the application of the p-LSCF method, as it is not very clear on the estimates provided by the SSI-COV method (see Figure 5.30).

In order to better understand the effect of the traffic over the bridge on its modal parameters, an average daily evolution of the natural frequencies and modal damping ratios was evaluated. This was obtained averaging the modal parameters of all the working days of November 2007 associated with the same day period. Figure 5.41 shows the results for all the modal damping ratios of the analysed modes and for the natural frequency of the first mode. It is observed that all the modal damping ratios show a peak in the period from 7:30 to 10:00 (morning rush hour) and a less pronounced increase in the period from 6:00 to 20:00 (period with higher RMS values, see Figure 5.15), both effects being enhanced in the second mode. The effects on the natural frequencies are less prominent, but still

observable due to the high accuracy achieved in the modal identification. In the case of the natural frequency of the first mode (lateral mode), at the morning rush hour it is observed a sudden decrease of approximately 0.003 Hz, which is certainly explained by the extra mass of the cars over the bridge. The same phenomenon is also observable on modes 3 to 7. Due to the joint influence of temperature and vibration amplitude, the remaining daily variations have to be interpreted with some caution, as both vibration amplitude and temperature decrease from daylight to night.

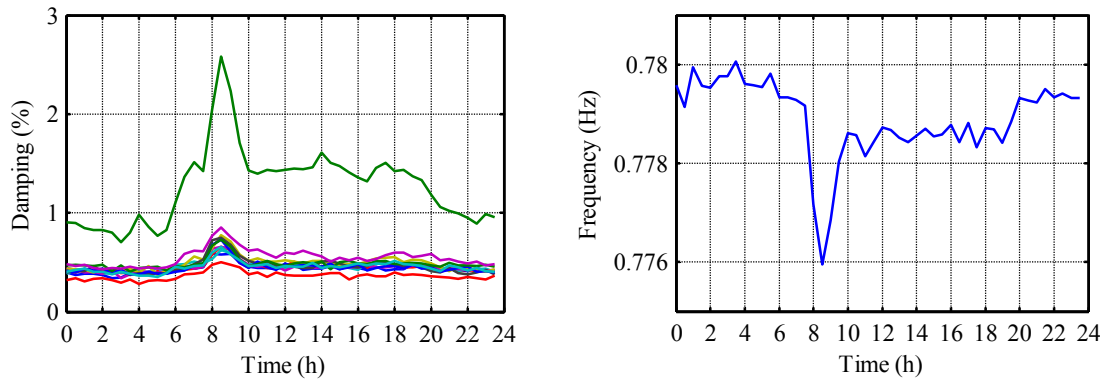


Figure 5.41 – Average day evolution of the modal damping ratios (second mode in green) and of the natural frequency of the first mode during the working days of November 2007.

5.6 Removing Environmental and Operational Effects on Natural Frequencies

The characterization of the variation of the bridge modal parameters presented in the previous section has already shown that these are essentially influenced by the temperature, by the amplitude of vibration and by the traffic over the bridge. This section aims to establish a model to remove (or at least minimize) the effects of these environmental and operational factors on the estimated natural frequencies. The different approaches that can be followed have already been described in chapter 4. There it is demonstrated that the methods that take into account the measurements of the predictors have some advantages. Therefore, in the present application, as continuous temperature measurements are available, in a first instance, a multiple linear regression model was adopted (Magalhães et al. 2009d). The data collected during the first year of the monitoring project (from 13/09/2007 to 12/09/2008) was used to establish the model and then data collected during the second year (from 13/09/2008 to 12/09/2009) was used to validate the quality of the forecasts provided by the model.

In a first step, the predictors of the regression model have to be selected. The concrete temperatures measured by the eight embedded sensors marked in Figure 5.10 are obvious candidates. Figure 5.42 characterizes their time variation during some days of September side by side with the variation of the air temperature recorded by the weather station situated in the Gaia river bank.

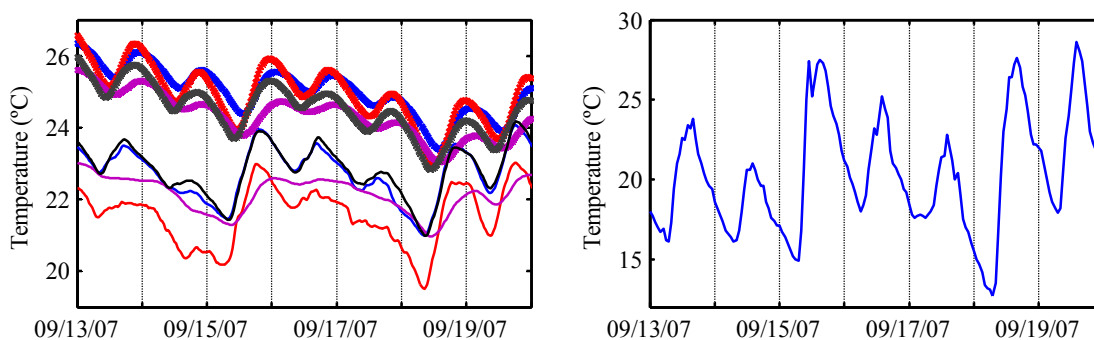


Figure 5.42 – Time evolution of the temperatures measured by the embedded sensors (T1 - blue; T2 - red; T3 - magenta; T4 - black; line-crosses - deck top; line - deck bottom) compared with the time evolution of the air temperature (plot in the right side).

Due to the high thermal inertia of the deck box girder, justified by the thickness of its walls (varying from 30 to 100 cm) and by the air mass inside the box beam, the recorded daily thermal variations are only of the order of 2 °C, despite the higher fluctuations of the outside air temperature of about 10 °C. The sensors placed at similar sections, as for instance sections T2 and T3 (Figure 5.10), should present very similar time histories, however the sensors were not positioned exactly at the same depth and

therefore some differences in terms of amplitude and time of occurrence of the daily maxima and minima are observed.

Taking into account these differences, a correlation analysis was performed with the objective of identifying the temperature time series presenting higher correlation coefficients (definition presented in chapter 4) with the time series with the evolution of the automatically identified natural frequencies. Table 5.5 presents a matrix with the correlation coefficients between all the pairs: temperature – temperature and temperature – frequency, considering one year of observations (from 13/09/2007 to 12/09/2008). The obtained results allow to group similar temperature records (the ones presenting correlation coefficients close to one) and to select the representative of each group (the one with higher correlation coefficient with the time series of the frequencies). This statistical procedure evidences two groups: one with the temperatures measured on the top flanges (T1 to T4 top) and another with the ones measured at the bottom flanges (T1 to T4 bot). The sensor placed at the bottom of section T1 (T1 bot) and the sensor positioned at top of section T4 (T4 top) were selected as representatives of each group due to their slightly higher mean correlation coefficients considering all the automatically identified natural frequencies. Still, despite the differences observed in Figure 5.42, the two selected variables present a quite high correlation factor. However, it is important to include both predictors in the model, so that the influence of the deck differential temperature is considered.

Table 5.5 – Correlation coefficients between all the pairs: temperature - temperature and temperature - frequency.

	T1 top	T1 bot	T2 top	T2 bot	T3 top	T3 bot	T4 top	T4 bot	f1	f2	f3	f4	f5	f6	f7	f8	f9	f10	f11	f12	Mean
T1 top	1.00	0.98	1.00	0.97	1.00	0.99	1.00	0.98	-0.83	-0.67	-0.78	-0.89	-0.89	-0.91	-0.69	-0.87	-0.83	-0.85	-0.83	-0.91	-0.828
T1 bot		1.00	0.99	0.99	0.98	0.99	0.99	1.00	-0.83	-0.65	-0.78	-0.90	-0.89	-0.92	-0.71	-0.88	-0.84	-0.83	-0.84	-0.90	-0.831
T2 top			1.00	0.97	1.00	0.99	1.00	0.98	-0.83	-0.65	-0.77	-0.90	-0.88	-0.91	-0.70	-0.88	-0.83	-0.84	-0.84	-0.91	-0.829
T2 bot				1.00	0.97	0.99	0.97	0.99	-0.82	-0.65	-0.77	-0.89	-0.88	-0.90	-0.69	-0.86	-0.84	-0.81	-0.83	-0.89	-0.820
T3 top					1.00	0.99	1.00	0.98	-0.84	-0.67	-0.78	-0.89	-0.89	-0.91	-0.70	-0.87	-0.84	-0.85	-0.83	-0.91	-0.831
T3 bot						1.00	0.99	0.99	-0.83	-0.67	-0.77	-0.89	-0.88	-0.90	-0.67	-0.86	-0.83	-0.85	-0.82	-0.90	-0.823
T4 top							1.00	0.98	-0.83	-0.66	-0.78	-0.91	-0.89	-0.92	-0.71	-0.88	-0.84	-0.84	-0.84	-0.91	-0.834
T4 bot								1.00	-0.83	-0.65	-0.77	-0.90	-0.88	-0.91	-0.69	-0.87	-0.83	-0.84	-0.83	-0.90	-0.825

The natural frequencies of the second and seventh mode (first vertical and first torsion modes) are the ones that present lower correlation coefficients with the measured temperatures. The correlation between the frequency of mode 6 and the temperature T4 top (pair that presents one of the higher correlation values) is illustrated in Figure 5.43. Figure 5.44 compares the time evolution of the frequency of the first mode with the temperature values measured by sensor T3 top using different vertical scales (the scale of the temperature is inverted).

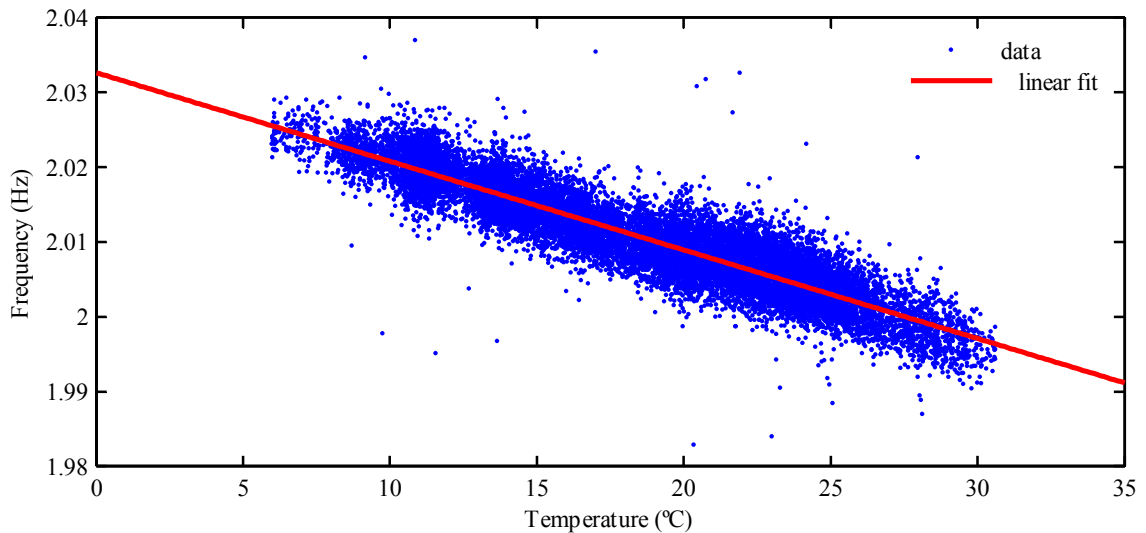


Figure 5.43 – Natural frequency of mode 6 vs temperature measured by sensor T4 top

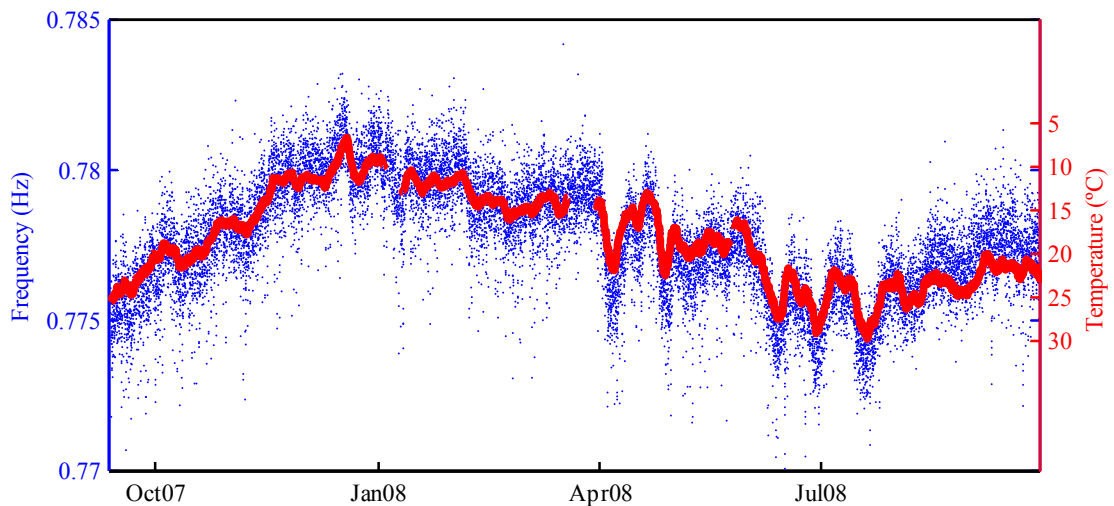


Figure 5.44 – First natural frequency (dots) vs temperature at the top of section T3.

In the previous section, the influence of the vibration amplitude on the natural frequencies has already been identified, in particular for the second mode (Figure 5.38). Table 5.6 quantifies the correlation between the RMS values of the acceleration records collected by the 12 installed sensors during a complete year and the natural frequencies identified from the same acceleration records. It is confirmed that the second mode is the one that is more influenced by the vibration amplitude. The correlation calculated between pairs of RMS values time series (not presented in the table) showed, as expected, high values (0.98 – 0.99) between RMS values associated with the same direction (lateral or vertical). Therefore, taking into account the values present in Table 5.6, a representative for each direction was chosen: RMS values of lateral acceleration at section S3 (S3 l) and RMS values of vertical acceleration at the downstream side of section S4 (S4 vd) (see Figure 5.10).

Table 5.6 – Correlation coefficients between all the acceleration RMS values and the identified natural frequencies.

	f1	f2	f3	f4	f5	f6	f7	f8	f9	f10	f11	f12
S1 l	-0.17	-0.46	-0.32	-0.09	-0.15	-0.10	-0.25	-0.10	-0.12	-0.03	-0.16	-0.10
S1 vd	-0.16	-0.46	-0.31	-0.10	-0.15	-0.11	-0.25	-0.12	-0.14	-0.04	-0.17	-0.11
S1 vu	-0.16	-0.46	-0.31	-0.10	-0.15	-0.11	-0.25	-0.11	-0.14	-0.03	-0.17	-0.11
S2 l	-0.18	-0.48	-0.33	-0.09	-0.16	-0.10	-0.26	-0.10	-0.12	-0.03	-0.15	-0.10
S2 vd	-0.18	-0.47	-0.33	-0.11	-0.16	-0.13	-0.27	-0.13	-0.15	-0.04	-0.19	-0.12
S2 vu	-0.18	-0.47	-0.33	-0.12	-0.16	-0.13	-0.28	-0.13	-0.16	-0.04	-0.19	-0.13
S3 l	-0.20	-0.49	-0.34	-0.11	-0.17	-0.12	-0.27	-0.11	-0.13	-0.04	-0.16	-0.10
S3 vd	-0.18	-0.47	-0.33	-0.12	-0.17	-0.12	-0.28	-0.13	-0.15	-0.03	-0.18	-0.12
S3 vu	-0.18	-0.47	-0.33	-0.12	-0.17	-0.13	-0.28	-0.13	-0.15	-0.03	-0.18	-0.12
S4 l	-0.19	-0.47	-0.34	-0.10	-0.16	-0.11	-0.26	-0.11	-0.13	-0.05	-0.16	-0.10
S4 vd	-0.19	-0.48	-0.34	-0.12	-0.17	-0.13	-0.28	-0.13	-0.15	-0.04	-0.18	-0.12
S4 vu	-0.19	-0.47	-0.33	-0.12	-0.17	-0.13	-0.28	-0.13	-0.15	-0.04	-0.18	-0.12

Another factor with influence on the bridge natural frequencies is the existence of traffic jams over the deck, as illustrated in Figure 5.41. This is an event that occurs during a relatively short period (1 to 2 hours) almost every working day. As there is not a direct measurement that can characterize the traffic jam, an indirect measurement has to be used. In the previous section, it was also shown that the damping is highly influenced by the existence of cars stopped over the bridge. Therefore, the estimated modal damping ratios can be used as predictors of the regression model to explain the decrease of the natural frequencies during the rush hours. Table 5.7 presents the correlation coefficient between the estimated modal damping ratios and natural frequencies, using the datasets collected during the first monitoring year. The line associated with the modal damping ratios of the second mode (d2) is the one that presents higher correlation values. As a consequence, it was selected to be a possible predictor of the regression model.

Table 5.7 – Correlation coefficients between all the modal damping ratios and the natural frequencies.

	f1	f2	f3	f4	f5	f6	f7	f8	f9	f10	f11	f12
d1	-0.20	-0.27	-0.24	-0.14	-0.18	-0.13	-0.16	-0.11	-0.09	-0.11	-0.10	-0.11
d2	-0.30	-0.48	-0.42	-0.18	-0.26	-0.18	-0.25	-0.15	-0.13	-0.18	-0.15	-0.14
d3	-0.09	-0.21	-0.16	-0.01	-0.06	0.00	-0.06	0.02	0.03	0.00	0.03	0.03
d4	-0.12	-0.20	-0.16	-0.02	-0.09	-0.05	-0.10	-0.03	-0.02	-0.05	-0.03	-0.03
d5	-0.11	-0.21	-0.16	0.00	-0.05	0.01	-0.07	0.03	0.06	0.02	0.04	0.05
d6	-0.14	-0.26	-0.21	-0.04	-0.09	-0.04	-0.11	-0.01	0.01	-0.03	0.00	0.00
d7	-0.12	-0.23	-0.19	-0.03	-0.08	-0.01	-0.08	0.00	0.04	-0.01	0.02	0.02
d8	-0.10	-0.18	-0.15	-0.03	-0.07	-0.02	-0.06	0.01	0.04	-0.01	0.03	0.03
d9	-0.07	-0.14	-0.11	0.01	-0.03	0.03	-0.05	0.05	0.08	0.06	0.06	0.07
d10	-0.16	-0.26	-0.22	-0.10	-0.13	-0.09	-0.17	-0.08	-0.06	-0.12	-0.08	-0.06
d11	-0.13	-0.23	-0.19	-0.05	-0.09	-0.04	-0.12	-0.03	0.00	-0.02	-0.02	-0.01
d12	-0.20	-0.36	-0.27	-0.09	-0.16	-0.08	-0.13	-0.06	-0.05	-0.10	-0.07	-0.07

Finally, the influence of the concrete hardening on the natural frequencies, demonstrated in the previous section (Figure 5.39), was important during the first years of the bridge, but during the monitoring period (5 year after the last pouring) this effect was less relevant. Furthermore, two years of observation are not enough to accurately characterize this slow non-linear (the increasing rate

decreases with time) process. Therefore, it was not considered in the developed regression analysis. The analysis of the time evolution of the modal parameters of a concrete structure since the end of its construction would impose the adoption of a model for the concrete hardening, as for instance the one proposed in Model Code 1990 (CEB-FIB 1993).

After this preliminary selection of the predictor variables based on correlation coefficients and also taking into account the physics of the problem, alternative regression models should be considered. In a first step, three static models with an increasing number of predictors were tested. As an increasing number of predictors may improve the quality of the fitting, but decrease the ability of the model to produce forecasts, the accuracy of the forecasts is quantified in Table 5.8 by the coefficient of determination R^2_{for} , calculated through the first equality of equation (4.7) (section 4.3.2) using the values of the natural frequencies for the period 13/09/2008 to 12/09/2009 (not considered in the construction of the models) estimated from the acceleration time series and the values forecasted by the regression models.

The obtained results show that the best model is SM 3. The addition of each new predictor improved not only the fitting but also the ability of the model to perform forecasts. The inclusion of the damping of the second mode (variable d2) had a small impact on the coefficients of determination, but the graphic presented in Figure 5.45 shows that it improved considerably the fitting of the regression model, enabling a good adjustment to the variations caused by traffic jams.

Table 5.8 – Static regression models: used predictors and coefficients of determination.

Predictors	SM1	SM2	SM3	SM1	SM2	SM3	
	R^2_{for}	R^2_{for}	R^2_{for}	R^2_{for}	R^2_{for}	R^2_{for}	
T1 bot	x	x	x	f1	0.581	0.646	0.660
T4 top	x	x	x	f2	0.489	0.748	0.762
S3 l		x	x	f3	0.482	0.618	0.641
S4 vd		x	x	f4	0.849	0.870	0.870
d2			x	f5	0.743	0.790	0.796
				f6	0.860	0.885	0.886
				f7	0.548	0.655	0.654
				f8	0.818	0.841	0.841
				f9	0.698	0.732	0.732
				f10	0.675	0.679	0.688
				f11	0.731	0.775	0.777
				f12	0.836	0.858	0.857

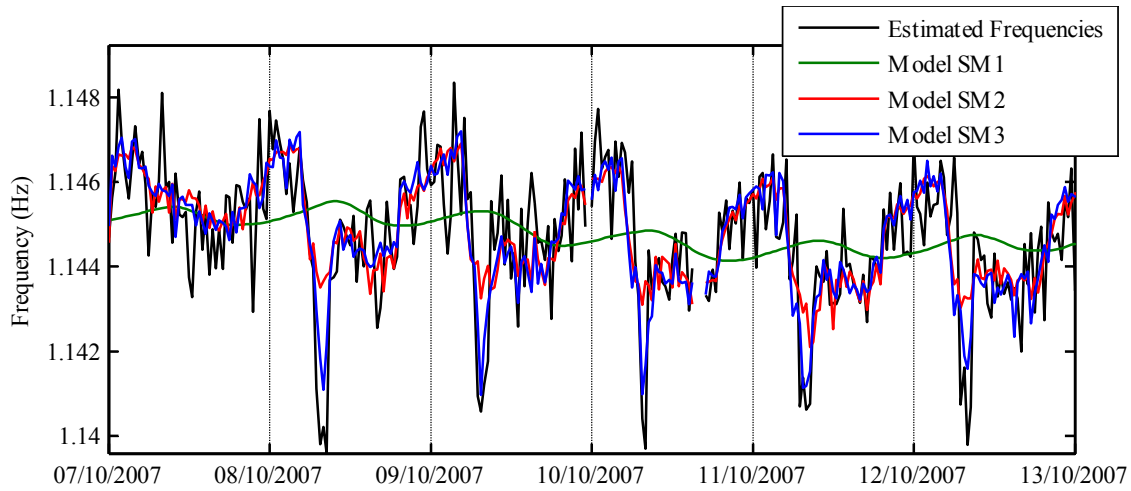


Figure 5.45 – Comparison between predicted and estimated natural frequencies of mode 3 using the static regression models SM1, SM2 and SM3.

Due to the existence of some correlation between the adopted predictors the analysis of the weigh of each predictor (β in equation (4.1), section 4.3.2) does not allow to draw conclusions about the relative importance of each predictor. Still, Figures 5.44 and 5.45 show that the temperatures are important to explain the annual variations, whereas the other variables are very relevant to model the daily fluctuation of the natural frequencies.

In order to reduce even further the differences between the predictions and the observations, and consequently increase the chances of detecting small damages, dynamic regression models were adopted. In these regression models, it is assumed that the frequencies observed at a time instant t not only depend on the temperatures observed at that time instant, but also on the temperatures observed in previous time instants. As the temperature variation recorded by the embedded sensors is quite slow (see Figure 5.42), time delays of 6, 12, 18 and 24 hours were tested in the present application. The predictors considered on the three tested dynamic models (DM1 to DM3) are characterized in Table 5.9, where T1 bot -12 means the temperature measured by sensor T1 bot 12 hours before the observation of the natural frequency that is being predicted. The adopted models are evaluated at the right side of Table 5.9, using the same index that was adopted in the case of the static models. It can be observed that DM3 is the model with the best results and that the use of past observations of temperatures slightly improves the regression models. As a result, DM3 is the regression model implemented in the on line processing of the data collected at the Infante D. Henrique Bridge.

Figure 5.46 shows the time evolution of the first natural frequency over a period of two years before and after elimination (or minimization) of the environmental and operational effects with the dynamic regression model DM3. The variation of this natural frequency is reduced to a range of about 5 milli-Hz. The gaps on the corrected frequencies are due to gaps in the temperature measurements.

Table 5.9 – Dynamic regression models: used predictors and coefficients of determination.

Predictors	DM1	DM2	DM3				
				DM1	DM2	DM3	
				R^2_{for}	R^2_{for}	R^2_{for}	
T1 bot	x	x	x	f1	0.660	0.660	0.661
T4 top	x	x	x	f2	0.800	0.783	0.799
T1 bot -6	x		x	f3	0.641	0.641	0.642
T4 top -6	x		x	f4	0.895	0.899	0.900
T1 bot -12	x	x	x	f5	0.795	0.795	0.796
T4 top -12	x	x	x	f6	0.898	0.897	0.901
T1 bot -18			x	f7	0.715	0.713	0.730
T4 top -18			x	f8	0.860	0.859	0.863
T1 bot -24		x	x	f9	0.741	0.742	0.746
T4 top -24		x	x	f10	0.714	0.720	0.724
S3 l	x	x	x	f11	0.798	0.798	0.807
S4 vd	x	x	x	f12	0.857	0.857	0.857
d2	x	x	x				

The values above 0.785 Hz observed during January of 2009 were motivated by negative temperatures which were associated with snow fall, a quite rare event in the city of Porto. It can be observed that these values were not correctly compensated by the regression model. This is comprehensible because the occurrence of negative temperatures triggers non-linear mechanisms that increase the structure stiffness (as for instance the freezing of the soil around the structure foundations) that cannot be well modelled by a linear regression model.

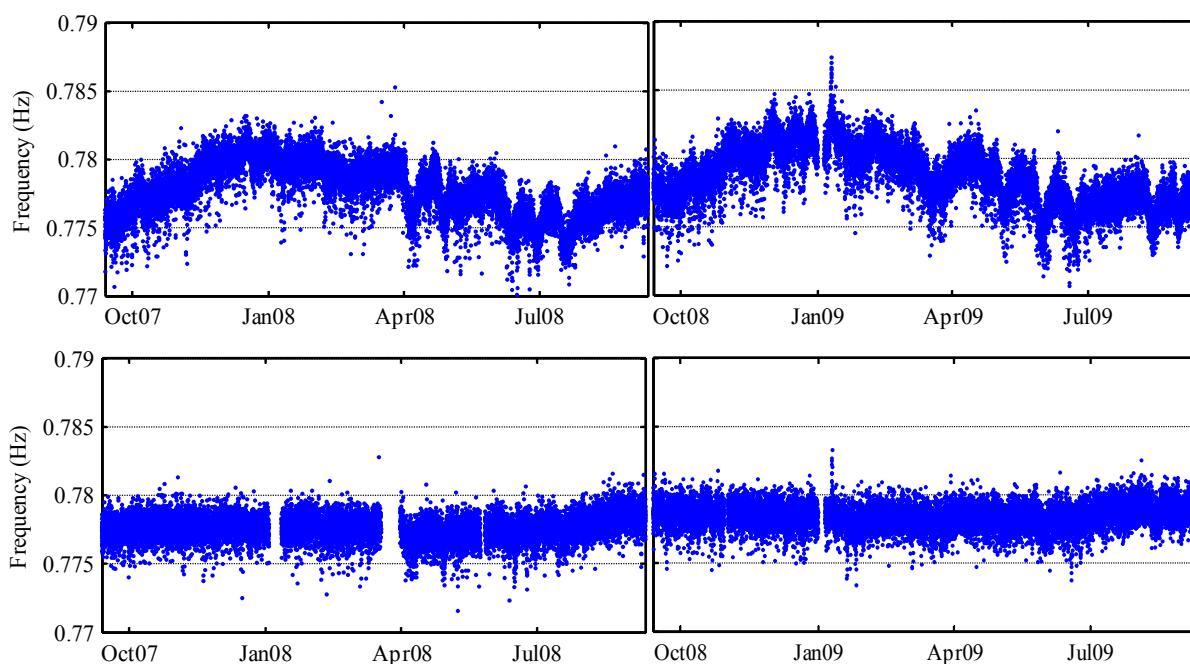


Figure 5.46 – Time evolution of the first natural frequency before and after the elimination of the environmental and operational effects (regression model DM3).

In the graphic of the corrected frequencies it is observed a slight increase of the mean natural frequency after July 2008 and July 2009, which is not consistently observed in all the natural

frequencies. A definite explanation for that slow evolution will only be possible after a larger period of observation.

The reduction of the range of variation of the natural frequencies after their correction can also be evidenced by the use of histograms. Figure 5.47 presents the histograms of the natural frequencies of the first three vertical bending modes associated with the period adopted for validation of the regression models. It is clear that after the application of regression model DM3, the frequencies are concentrated in narrower range (between 5 and 10 milli-Hz) and present histograms that resemble the ones of normal distributions.

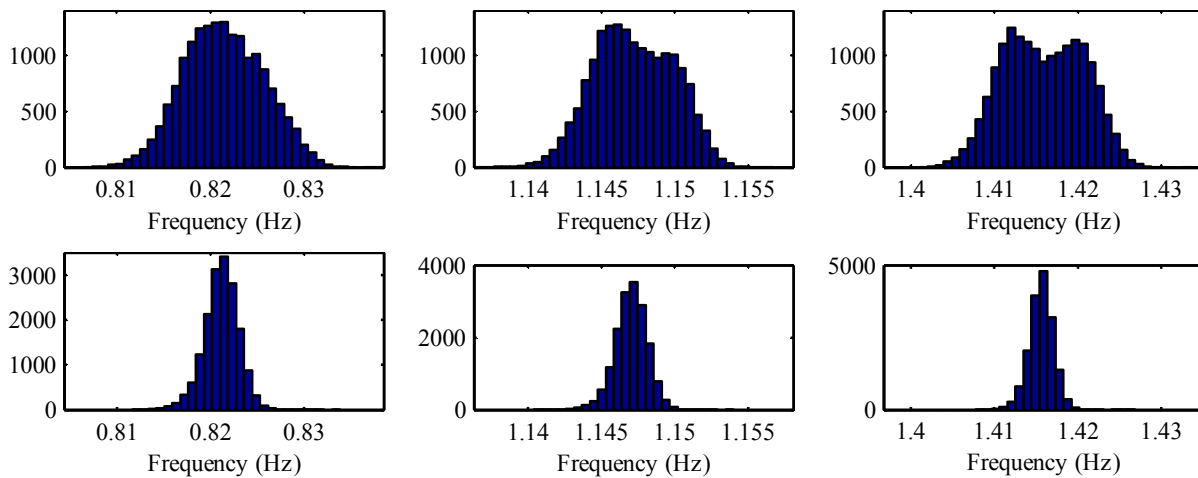


Figure 5.47 – Histograms of the natural frequencies of the first three vertical bending modes (f_2 to f_4) before and after the elimination of environmental and operational effects (regression model DM3, data from 13/09/2008 to 12/09/2009).

Important outcomes of the regression models are the confidence intervals for the forecasts of the dependent variables, in this case the natural frequencies. They permit to check if each new identified natural frequency is within the interval given by the regression model taking into account the observations of the adopted predictors. Figure 5.48 presents, for a period of about 40 days, the 95% confidence intervals calculated with equation (4.9) and the values automatically identified for the natural frequency of mode 4. As expected, the majority of the values of the frequencies (blue points) are bounded by the calculated limits (red lines). The occurrence of damages with impact on the natural frequencies would lead to a higher number (more than 5%) of frequency values outside the limits. As a consequence, this statistical tool can be adopted for damage detection.

However, this strategy for damage detection implies the verification of several variables (all the identified natural frequencies). In the next section, it is presented an alternative strategy which only involves the analysis of one parameter and that permits the identification of smaller deviations.

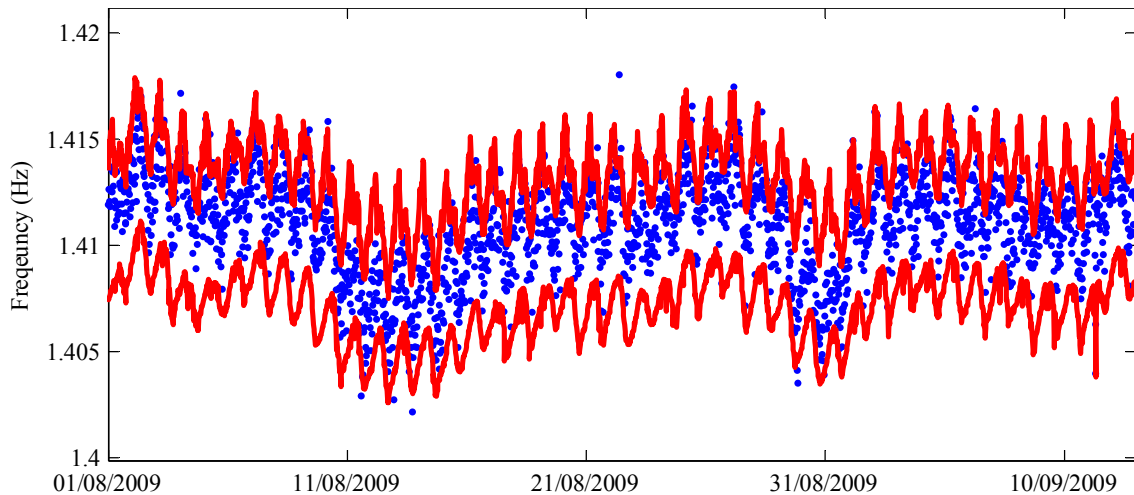


Figure 5.48 – Comparison between the automatically identified natural frequencies of mode 4 and the confidence intervals (95%) provided by model DM3.

Finally, the capability of the adopted regression model to eliminate the influence of all environmental and operational factors on the natural frequencies can be checked through the calculation of the correlation coefficients between the natural frequencies corrected by the model. The existence of a high correlation between two natural frequencies means that they are influenced by a common factor.

The results of such analysis are presented in Table 5.10, which contains the correlation coefficients between the 12 natural frequencies identified during the period from 13/09/2008 to 12/09/2009, before and after the correction provided by the regression model DM3. It can be observed that the correlation coefficients decreased significantly, in some cases from 0.8 to approximately 0. However, some correlations coefficients around 0.3 and 0.4 indicate that there is still some margin for improvement.

As a consequence, in the next section the adopted regression model is going to be complemented by a Principal Components Analysis that will reduce even further the influence of the environmental and operational factors on the identified natural frequencies.

Table 5.10 – Correlation coefficients between frequencies before and after the application of regression model DM3 (data from 13/09/2008 to 12/09/2009).

	f1	f2	f3	f4	f5	f6	f7	f8	f9	f10	f11	f12
f1	1.00	0.81	0.88	0.87	0.91	0.88	0.80	0.85	0.81	0.82	0.82	0.86
f2		1.00	0.82	0.73	0.81	0.74	0.70	0.71	0.70	0.73	0.71	0.75
f3			1.00	0.87	0.89	0.87	0.82	0.84	0.80	0.80	0.82	0.84
f4				1.00	0.91	0.94	0.83	0.92	0.86	0.85	0.88	0.91
f5					1.00	0.92	0.83	0.89	0.87	0.85	0.88	0.91
f6						1.00	0.84	0.93	0.88	0.87	0.90	0.93
f7							1.00	0.83	0.81	0.69	0.84	0.79
f8								1.00	0.87	0.85	0.89	0.91
f9									1.00	0.79	0.89	0.88
f10										1.00	0.79	0.89
f11											1.00	0.89
f12												1.00

	f1	f2	f3	f4	f5	f6	f7	f8	f9	f10	f11	f12
f1	1.00	0.32	0.35	0.28	0.42	0.23	0.30	0.15	0.18	-0.01	0.18	0.12
f2		1.00	0.21	0.20	0.35	0.14	0.22	0.08	0.19	-0.04	0.17	0.18
f3			1.00	0.32	0.34	0.29	0.32	0.21	0.10	0.11	0.15	0.08
f4				1.00	0.31	0.27	0.28	0.19	0.13	0.09	0.15	0.09
f5					1.00	0.27	0.38	0.19	0.29	-0.03	0.28	0.17
f6						1.00	0.31	0.24	0.17	0.11	0.22	0.14
f7							1.00	0.24	0.28	0.00	0.31	0.15
f8								1.00	0.14	0.08	0.20	0.12
f9									1.00	-0.06	0.35	0.22
f10										1.00	0.01	0.06
f11											1.00	0.25
f12												1.00

5.7 Damage Detection

The previous section demonstrated that with a correct post-processing of the automatically identified natural frequencies it is possible to reduce the effects of environmental and operational factors. In this section, it is evaluated if the control charts presented in section 4.3.4 are suitable to automatically detect small shifts on the natural frequencies post-processed by the adopted regression models. In particular, it is tested their ability to identify small damages simulated with a finite element model.

Damage in bridges may stem from a vast diversity of occurrences, as for instance vibrations due to an earthquake, sliding of a foundation, rupture of prestressing tendons caused by corrosion, spalling of concrete motivate by corrosion of the ordinary reinforcement or malfunction of a bearing device.

The accurate numerical modelling of damage scenarios directly motivated by the referred causes would require the development of very complex non-linear models and a large number of assumptions. As these models would provide only approximate results and also because the construction of very sophisticated numerical models is beyond the scope of this work, a simpler approach was followed. The likely consequences of extreme events or of structural ageing are modelled in a simplified manner by reductions of inertia at small segments of selected bridge components.

These damages were simulated using the tuned numerical model previously presented in section 5.3.2. Figure 5.49 shows the location and the extent of the four studied damage scenarios. All damages were simulated by a reduction in the vertical bending inertia of 10% over the length marked in the figure: D1 – 8.75m; D2 – 10.0m; D3 – 3.0m and D4 – 5.0m. These are quite small damages that do not compromise the safety of the bridge. They should be regarded as the consequences of the beginning of a deterioration process or as the result of some extreme action. It should be kept in mind that a monitoring system must be able to detect damages while they are still not very relevant, in order to permit their correction before the occurrence of a significant reduction in the safety of the infrastructure.

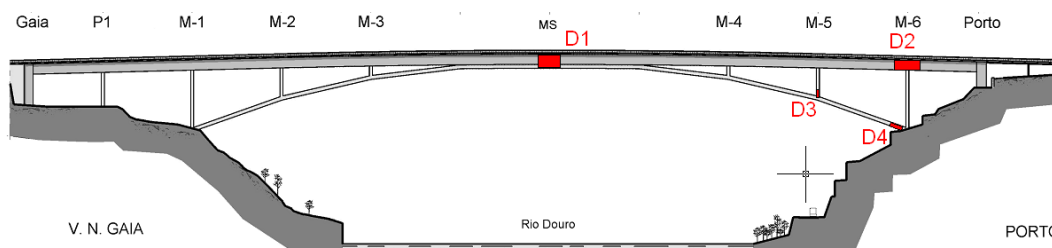


Figure 5.49 – Location and extent of the simulated damage scenarios.

Table 5.11 quantifies the effects of the considered damage scenarios on the 12 natural frequencies under analysis. As only the vertical bending inertia was changed, only the vertical bending modes suffered significant changes. Still, because the stiffness reductions are small, the variations of the natural frequencies are all lower than 0.4%.

The differences between the reference numerical frequencies and the average values identified by the monitoring system are much higher than the variations introduced by the simulated damage scenarios. Therefore, the introduction of the damage in the experimental values has to be based on the relative differences of the natural frequencies (Δ freq.). In the present application, it was assumed that each damage scenario occurred on the 13th of March of 2009, and consequently, for the test of the damage detection procedures, the natural frequencies automatically identified after this date were multiplied by the coefficient $1+(\Delta \text{ freq.})/100$, where Δ freq. assumes the values presented in Table 5.11. Taking as example the D1 scenario, for the case of mode 3, this operation is equivalent to apply a shift in the natural frequencies of approximately 1.3 milli-Hz.

Table 5.11 – Natural frequencies (in Hz) associated with damaged scenarios D1, D2, D3 and D4 compared with the numerical reference values (Ref) and with the experimental values identified with the ambient vibration test (AVT) and by the monitoring system.

Mode	Freq.	AVT (FDD)	Monitoring	Ref	D1		D2		D3		D4	
					Freq	Δ freq. (%)	Freq	Δ freq. (%)	Freq	Δ freq. (%)	Freq	Δ freq. (%)
l1	1	0.770	0.778	0.7944	0.7944	0.000	0.7944	0.000	0.7944	0.000	0.7944	0.000
v1	2	0.810	0.821	0.8103	0.8103	0.000	0.8087	-0.190	0.8094	-0.108	0.8098	-0.059
v2	3	1.135	1.146	1.1486	1.1473	-0.112	1.1483	-0.025	1.1485	-0.007	1.1484	-0.014
v3	4	1.405	1.415	1.4665	1.4647	-0.126	1.4642	-0.160	1.4646	-0.133	1.4655	-0.072
l2	5	1.734	1.751	1.7679	1.7679	0.000	1.7679	0.000	1.7679	0.000	1.7679	0.000
v4	6	1.993	2.011	2.0864	2.0863	-0.001	2.0834	-0.141	2.0858	-0.028	2.0843	-0.100
t1	7	2.212	2.225	2.1849	2.1857	0.038	2.1849	0.000	2.1849	0.000	2.1849	0.000
v5	8	3.013	3.040	3.0107	3.0066	-0.137	3.0083	-0.079	3.0094	-0.045	3.0033	-0.248
l3	9	3.309	3.337	3.3568	3.3571	0.009	3.3568	0.000	3.3568	0.000	3.3568	0.000
v a	10	3.490	3.521	3.2870	3.2870	-0.001	3.2867	-0.011	3.2788	-0.251	3.2764	-0.323
t2	11	3.734	3.760	3.6407	3.6407	0.000	3.6407	0.001	3.6407	0.000	3.6407	0.000
v6	12	4.339	4.378	4.1291	4.1290	-0.001	4.1288	-0.006	4.1290	-0.001	4.1282	-0.022

* l – lateral mode; v – vertical bending mode; t – torsion mode; v a – vertical bending mode of the arch with residual components at the deck.

As already justified in chapter 4, control charts are an interesting statistical tool to detect changes on a process characterized by several variables. For that reason, in this section, the ability of control charts to detect the changes introduced by the simulated damage scenarios is tested. It is used a Shewhart control chart based on the 12 monitored natural frequencies. The data from 13/09/2008 to 12/03/2009 was used as reference data to calculate the values of $\bar{\bar{x}}$ and S adopted in the expression of T^2 (equation (4.33)), whereas the observations between 13/03/2009 and 12/09/2009 were used to evaluate if the

simulated damages are detectable and if data associated with the non-damaged situation is not incorrectly classified.

At a first instance, a Shewhart control chart was constructed using each individual observation of the natural frequencies corrected by the regression model DM3 presented in the previous section. However, it was realized that the T^2 values presented a dispersion that would hidden modifications of the order of magnitude of the ones caused by the considered damage scenarios. It was concluded that this procedure is only adequate for the rapid identification of larger stiffness reductions, as the ones that may occur after the occurrence of an extreme event, like a strong earthquake.

Afterwards, control charts based on groups of consecutive observations were tested. Groups with 48 elements, which correspond to 1-day duration, were adopted. In the left hand side of Figure 5.50 two sets of results are presented: T^2 calculated with the observations of the 12 natural frequencies corrected by the regression model DM3, and T^2 calculated with the observations of the 12 natural frequencies shifted by the relative differences associated with damage scenario D1 in the last half of the period under analysis (from 13/03/2009 to 12/09/2009) and then also corrected by the regression model DM3. It is clear that the introduction of the damage led to higher values of T^2 . However, the considerable dispersion of the values precludes a clear distinction between the damage and non-damaged scenarios.

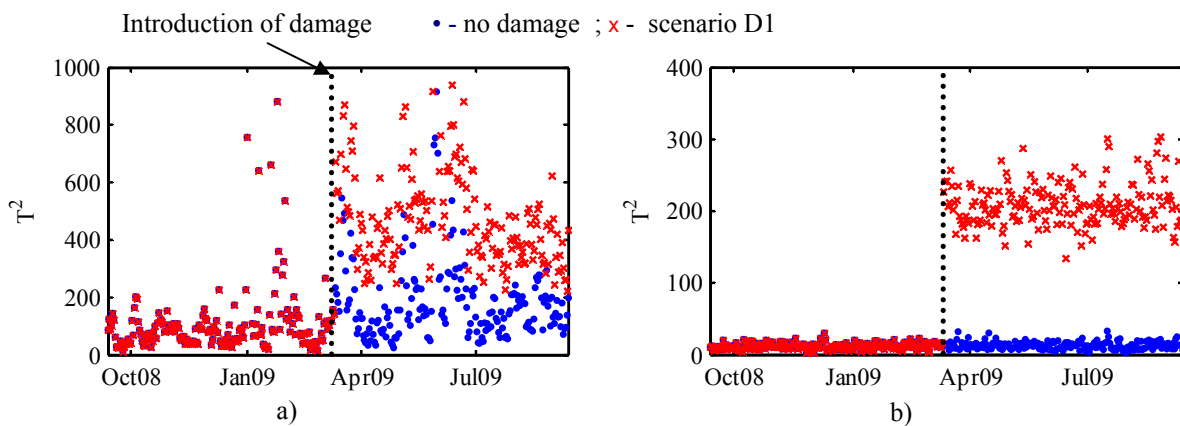


Figure 5.50 – a) Control chart constructed with the identified natural frequencies after the application of the regression model DM3 for the reference scenario and for the damage scenario D1; b) control chart constructed with artificially generated data.

In order to have a theoretical reference for the presented chart, another control chart was constructed using artificially generated data. The time evolution of the 12 natural frequencies after compensation of the environmental and operational effects was replaced by realizations of random processes with normal distributions and with the same means and standard deviations as the 12 time series with the automatically identified values corrected by the regression model. This is also represented in Figure 5.50 considering the reference and the D1 scenarios. The comparison between the two obtained charts

is relevant to show the importance of using real data instead of numerically simulated data, as it illustrates that with real data, although manipulated to artificially introduce damages, the damage identification problem becomes much more challenging.

In the presentation of the Shewhart charts in chapter 4, mathematical expressions for the upper control limit were defined (equations (4.32) and (4.34)). According to the theoretical background of this procedure, when the process is under control, or in our application when the structure is not damaged, the values of T^2 should be between zero and the upper control limit. In the control chart derived from artificially generated data the limit given by expression (4.34), equal to 21, is respected by the great majority of the points (more than 95%) when damage is not present. However, in the charts based on real data, this limit is exceeded by a large number of points even during the reference period. This happens because the real data does not respect all the assumptions adopted for the definition of the limits. In particular, it is assumed that each new observation is independent of the previous one, which is not completely true in case of the present application. Therefore, the upper control limit has to be based on the values observed for T^2 during a reference period. If a sufficiently large reference period is adopted, a confidence interval can be defined by the analysis of the histogram of the history of values obtained for T^2 .

As the results presented in Table 5.10 have shown that there is still some correlation between the natural frequency time series after the correction provided by the regression model, the regression analysis was complemented by a Principal Components Analysis (PCA) in order to improve the quality of the control charts.

Firstly, the correlation matrix of the time series with the 12 natural frequencies under analysis associated with the period from 13/09/2007 to 12/09/2008 previously corrected by the regression model DM3 was used to obtain the matrix U (equations (4.16) and (4.17)). Then, the matrix \hat{T} (equation (4.19)) was calculated from the first two columns of U (different numbers of selected principal component were tested and the selection of the first two proved to provide clear control charts). Finally, the natural frequencies previously corrected by the regression model can be transformed by equation (4.19) and the so-called residues calculated with equation (4.20). These are the new inputs for calculation of the points in the control chart.

The full procedure followed for the construction of the control chart is presented in Figure 5.51. After the tuning of the parameters of the regression model, PCA model and of the control chart using data collected before 13/03/2009, the post-processing of the data collected after 13/03/2009 can be done automatically and continuously right after the automatic identification of each new set of modal

parameters. However, as averages of 48 elements were adopted, a new point on the control chart is only marked at the end of each day.

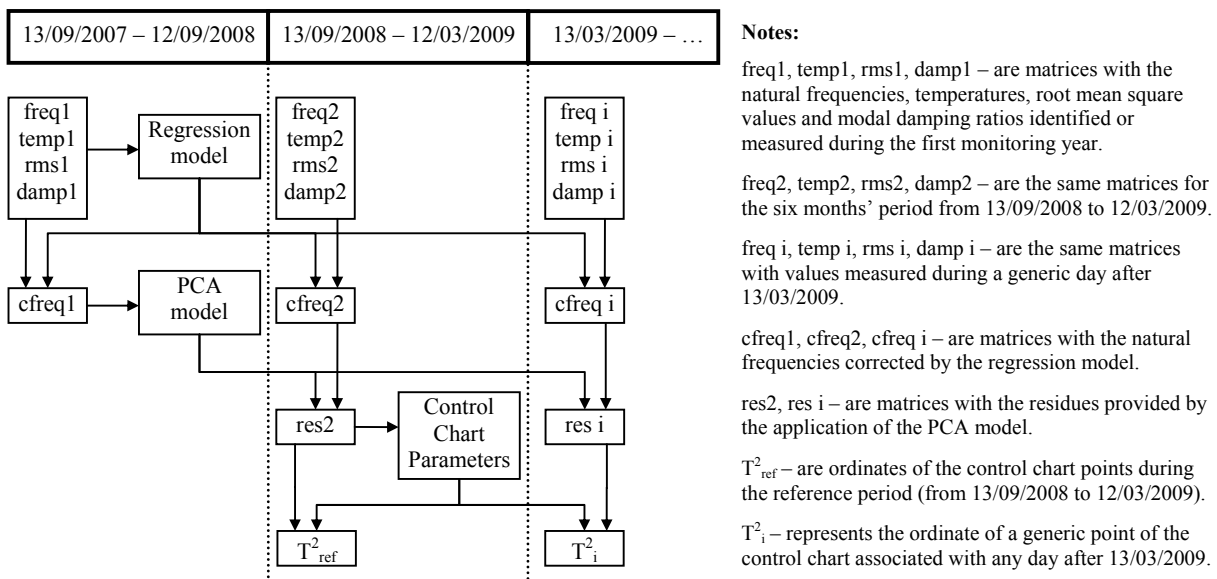


Figure 5.51 – Procedure adopted for the construction of the control chart.

Initially, this procedure was directly applied to the identified frequencies. The resulting control chart is represented in the upper left corner of Figure 5.52, where it is also marked with a red line the adopted upper control limit ($T^2 = 100$). It can be observed that the great majority of the points (more than 95%) are below the defined UCL, exceptions are just very few outliers probably due to inaccurate identification of natural frequencies. This proves that the adopted parameters do not produce false identifications of damage if the existence of damage is only considered after the occurrence of more than 2 successive points outside the control area.

After this, the ability of the presented methodology to identify the four damage scenarios characterized in Figure 5.49 was tested. The values of the automatically identified natural frequencies after 13/03/2009 were manipulated according the already described procedure to include the frequency shifts quantified in Table 5.11. Then, the same post-processing was followed (Figure 5.51). The resulting control charts are displayed in Figure 5.52.

The comparison of the two control charts associated with damage scenario D1 (Figure 5.50a and Figure 5.52b) demonstrates that the application of PCA considerable improved the quality of the charts, facilitating the identification of damage. The other control charts of Figure 5.52 also prove that the remaining 3 damages scenarios are undoubtedly detected by the proposed methodology. Still, some adjustments of the methodology can be done to try to reduce the scatter of the T^2 values after the occurrence of damage.

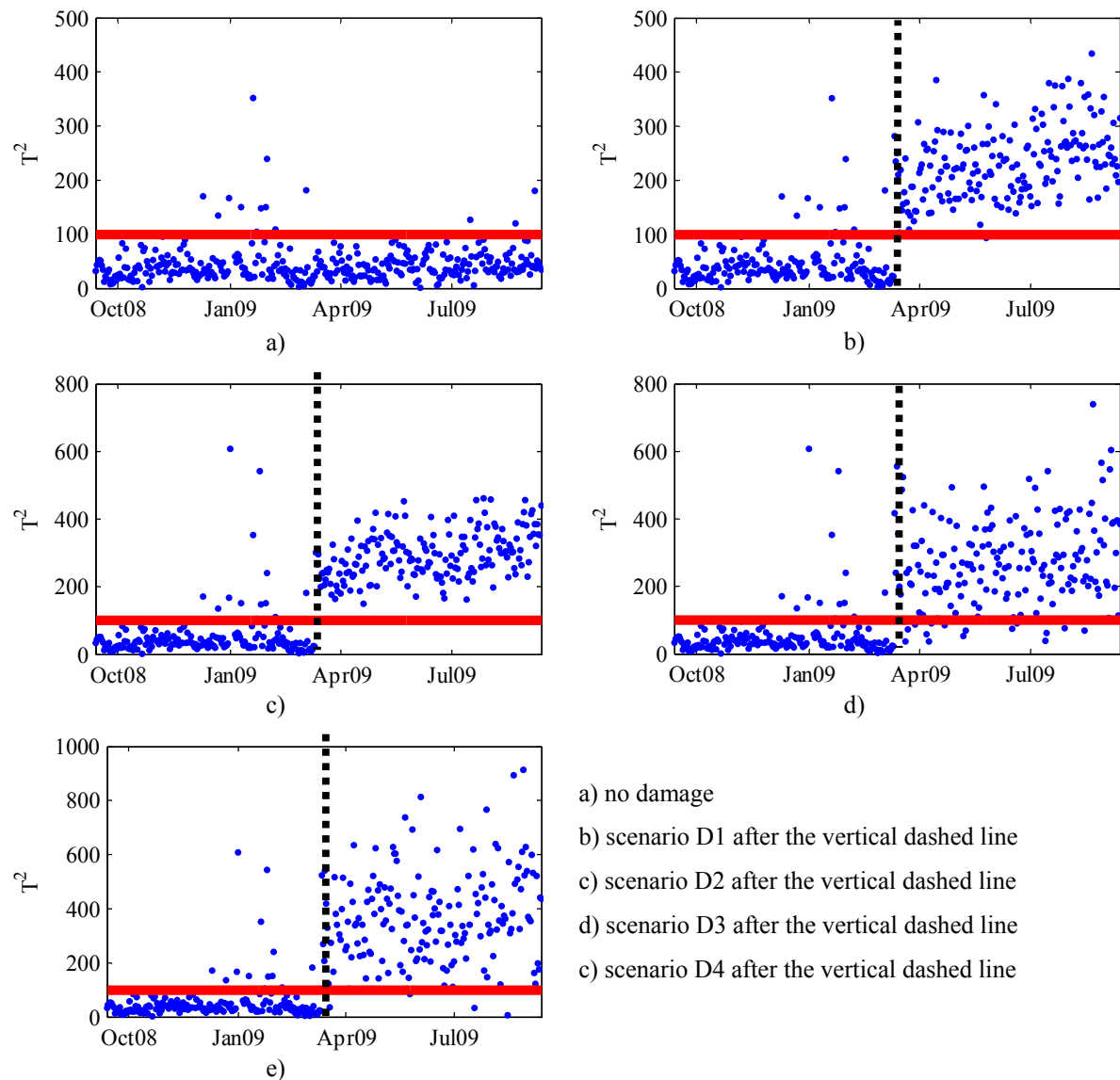


Figure 5.52 – Control Charts associated with the four considered damage scenarios with the application of PCA.

At the end of this section, it is important to refer that the capability of a monitoring system to detect an abnormal behaviour depends on the amount of data collected before the occurrence of the extraordinary event, as a larger history of data permits to determine the reference values with higher accuracy. Furthermore, the time needed to detect the damage is inversely proportional to the damage extent. Damages with an important impact on the natural frequencies can be detected in the first dataset collected after its occurrence, whereas damages with the magnitude of the ones simulated in this section are only successfully detected after some days. This is not an important limitation of this technique, as it is not crucial to rapidly detected damages with a small impact on the structural behaviour of the monitored infrastructure. The identification some days after their occurrence is adequate for the planning of maintenance or retrofiting operations.

5.8 Conclusions

This chapter started with the description of the experimental and numerical work developed before setting up a continuous dynamic monitoring system on a long span arch bridge. The preliminary ambient vibration test was essential for the design of the monitoring system, especially for the selection of the instrumented points, and for calibration of the developed numerical model. This model was fundamental to understand the strong effect of the bridge supports on its dynamic properties and then very important to simulate damage scenarios used to test the feasibility of application of vibration based damage detection techniques.

After that, some important aspects associated with the design of dynamic monitoring systems for large civil engineering structures were discussed together with the description of the solutions adopted for the hardware installed in Infante D. Henrique Bridge. It became clear that with commercially available equipment it is possible to create a monitoring system with distributed digitizers, which can be remotely configured and that permits the continuous retrieving of the collected data through the internet. Furthermore, the operation of the installed monitoring system for more than two years also demonstrated its robustness and reliability, as the number of lost setups was very reduced.

Afterwards, the application of the developed and implemented algorithms for automatic operational modal analysis was explored with the data collected by the monitoring hardware. The three algorithms, FDD, SSI-COV and p-LSCF proved to be able to perform the online automatic identification of the modal parameters of 12 vibration modes.

The automated version of the Frequency Domain Decomposition method showed high success rates even in the identification of two closely spaced modes. However, its ability to detect small frequency variations is limited by the adopted frequency resolution and, as already mention in chapter 2, it is not adequate to provide modal damping ratio estimates.

The use of the SSI-COV algorithm complemented by the new developed tool for the automatic analysis of stabilization diagrams proved also to be very efficient in the identification of the bridge first 12 natural frequencies. The results achieved during the first year of observation, which involved the analysis of more than 17000 datasets, show the high success rate of the identification algorithm (generally higher than 99%), its ability to identify closely spaced modes and the high accuracy of the estimates, enabling the detection of very small frequency shifts. It provided also meaningful modal damping ratio estimates.

The implementation of the p-LSCF method presented in chapter 2 was associated with the same procedure for automatic selection of poles that was used together with the SSI-COV method. This combination presented a very good performance: the 12 modes within the analysed frequency band were identified in more than 99% of the processed setups. The comparison of the results of this method with the ones provided by the SSI-COV method showed that its modal damping ratio estimates present a lower scatter, permitting, for instance, a better characterization of the effect of the traffic stopped over the bridge on the modal damping ratios. Consequently, the subsequent analyses were performed over the results provided by the p-LSCF method.

After this, the time series with the evolution of the natural frequencies were used to study the influence of environmental and operational variables on the modal parameters. The database collected during two years permitted to test alternative static and dynamic multiple linear regression models, which aim to explain the variations of the natural frequencies induced by other variables (as the temperatures measured at six different points of the deck). The selected dynamic model permitted to minimize the effects of environmental and operational factors on the natural frequencies and provided narrow confidence intervals for the future expected natural frequencies of the healthy structure, which permit the identification of frequency shifts due to some abnormal occurrence.

Finally, it was noticed that the correction of the natural frequencies provided by the adopted regression model could be improved with the subsequent application of the method based on a PCA presented in chapter 4. Furthermore, it was demonstrated that the construction of control charts with the outputs of the PCA permits the detection of very small frequency shifts due to numerically simulated damage scenarios.

To sum up, it was demonstrated that a dynamic monitoring system like the one installed at Infante D. Henrique Bridge permits not only to increase the understanding about the dynamic behaviour of the instrumented structure, but also to detect small variations of the modal parameters that might be indicators of the occurrence of structural degradation, of malfunction of some structural elements, as for instance a bearing device, or of damages produced by some extreme event, such as an earthquake.

This full-scale experiment was also closely related with the development of the DynaMo software presented in the previous section, as this software was first developed to meet the needs encountered in this application and then improved to become flexible to be used in the monitoring of other structures. Therefore, it driven the development of DynaMo and at the same time permitted its extensive test and the demonstration of its usefulness.

Chapter 6

DYNAMIC MONITORING OF THE BRAGA STADIUM SUSPENDED ROOF



6. DYNAMIC MONITORING OF THE BRAGA STADIUM SUSPENDED ROOF

6.1 Introduction

This chapter is dedicated to another dynamic monitoring project, this time performed over the roof of a football stadium located in Braga, a city in the North of Portugal.

The Braga Municipal Sports Stadium (figure at the chapter cover) is one of the stadia that were recently constructed in Portugal to host some of the matches of the 2004 European Football Championship. Its roof suspended by cables is unique and presented a particular challenge in terms of conception, structural design and construction.

The innovative characteristics of this roof structure, as well as the resulting flexibility, motivated extensive studies developed during the design phase by various independent entities, whose purpose was to adequately define the design wind load, to evaluate the corresponding static and dynamic behaviour, and to investigate its susceptibility to aeroelastic instabilities. These studies comprehended the development of different numerical models of the structure and a series of wind tunnel tests performed on physical models.

ViBest/FEUP was consulted in this context, at an early stage of the project, with the aim of developing a static and dynamic study of the roof structure (Caetano and Cunha 2001). The developed numerical models were used formerly in the definition of the geometric and mechanic characteristics of the cables and slabs and the calculated dynamic properties were later used in the construction of a physical model for wind tunnel tests. After the stadium construction, ViBest/FEUP was also consulted to analyse data recorded during forced and free vibration tests requested by the contractor and performed a complete ambient vibration test of the suspended roof (Magalhães et al. 2006a), in order to obtain experimental estimates of the corresponding dynamic properties and use them to validate the previously developed numerical model (Caetano et al. 2008).

The results given by the ambient vibration test were also very important for the design of the Dynamic Monitoring system that was recently installed. This monitoring system aims not only to study the influence of the wind characteristics and of the ambient temperatures on the modal properties of the structure but also to permit the detection of structural problems with consequences on the natural frequencies. In the context of the first goal, it is of special scientific relevance the evaluation of the effect of the wind velocities on the modal damping ratios and thus the quantification of aerodynamic damping components.

In the framework of the present thesis, this application is important to demonstrate that the algorithms developed for the on-line automatic identification of modal parameters are flexible to be used in diverse structures.

As this monitoring project was initiated only at the end of March 2009, the analysis presented in this chapter is not as complete as the one that was done for the Infante D. Henrique Bridge. This chapter starts with a synthesis of the main structural characteristic of the roof. Then, it comprehends the description of the experimental work performed before the installation of the monitoring equipment with relevance for the design of the monitoring system and for a better interpretation of its outputs. Afterwards, the installed hardware is characterized. And finally, the most important results obtained during nine months of monitoring are presented, giving special emphasis to the characterization of the performance of the tools for automated operational modal analysis.

6.2 Description of the Structure

The Braga Stadium was constructed on the slopes of a hill called Monte Castro, and develops as an amphitheatre over a wide rural landscape, formed only by two rows of stands, on either side of the pitch, and by a granite massif (Figure 6.1). The most noticeable element of the stadium is its roof, which is formed by pairs of full locked coil cables with diameters varying between 86 and 80mm, spaced 3.75m apart from each other, supporting two concrete slabs over the two stands of the stadium. The cables span is 202m and the slabs length is 57.3m, therefore the remaining 88.4m of the central part are free (Figure 6.2). The rain water is drained from the roof along one side only, the slope being achieved by a variation of the length of the cables. The concrete slabs have a thickness of 0.245m and are connected to the cables only in the normal direction, allowing relative tangential movements (Figure 6.3). A transversal triangular truss is suspended from the inner border of each slab acting as a stiffness beam and simultaneously accommodating the floodlights and loud speakers (Figure 6.3).

The roof cables are anchored in two large beams at the top of both stands – east and west. The east stand (Figures 6.1 and 6.2) is structurally formed by 50m high concrete walls, whose geometry was defined in order to minimize the unbalanced moments at the level of the foundation, motivated by the combination of the gravitational action of the stand and the high forces transmitted by the roof cables. In the west stand (Figure 6.2), the concrete walls are anchored in the rock and the tension forces of the roof cables are transmitted to the foundation by prestressing tendons embedded in the concrete (Furtado et al. 2005).



Figure 6.1 - Braga Municipal Sports Stadium (lateral view from the east side and top view of the roof from the west side).

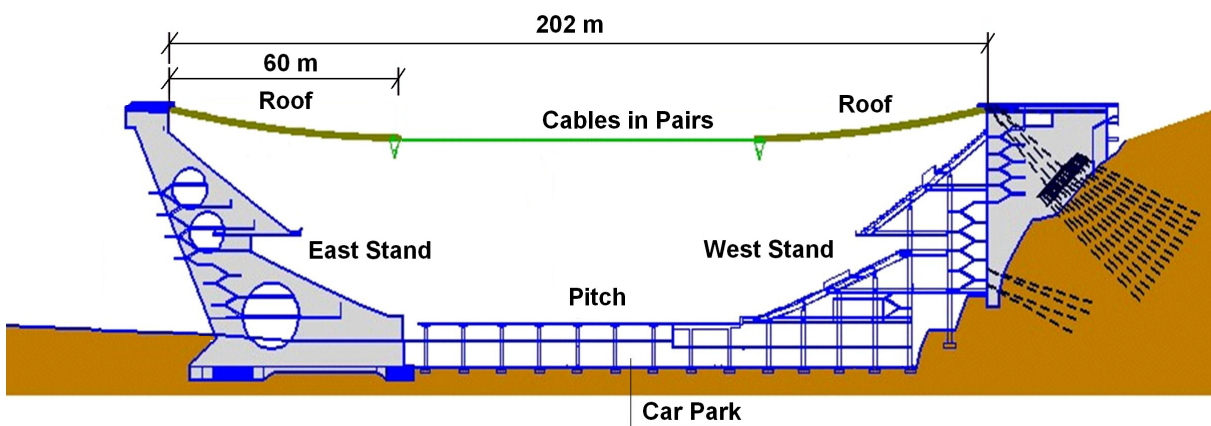


Figure 6.2 - Scheme of the Braga Stadium structure.



Figure 6.3 - Views of Braga Stadium (east stand, cables of the roof, slab of the east stand, detail of the connection between the cables and the slab, detail of the triangular truss in the inner border of the east slab and west slab).

6.3 Preliminary Experimental and Numerical Studies

6.3.1 Ambient Vibration Test

The ambient vibration test comprehended the measurement of the vertical acceleration at 42 points of the roof, using 3 strong motion recorders GSR-18 (Figure 6.4a), which are similar to the ones described in chapter 3. In the present test the adoption of wireless equipment was very convenient, as the use of cables connecting equipment placed at both sides of the suspended roof would make the test extremely complex.

The test was performed in two days. On the first day, measurements were done at the points of the west slab represented in Figure 6.4b, using 13 setups, while on the second day, measurements were carried out at the points of the west and east slabs represented in Figure 6.4c, using 15 setups (Cunha et al. 2009). For each setup, time series of 16 minutes were collected with a sampling frequency of 100Hz (minimum sampling frequency allowed by the acquisition system).

During the first day of measurements, two reference points were considered (two recorders were permanently placed at points 1 and 7 during all setups). After a preliminary analysis of the data, it was concluded that, for the frequency range of interest (0-1Hz), all the modes could be detected by the reference sensor placed at point 7. Thus, in order to reduce the duration of the test, it was decided to use just this reference for the remaining setups. The test developed on the second day provided a set of new responses at the east slab and more response measurements at the west side slab that allowed the improvement of the spatial resolution used in the characterization of the mode shapes.

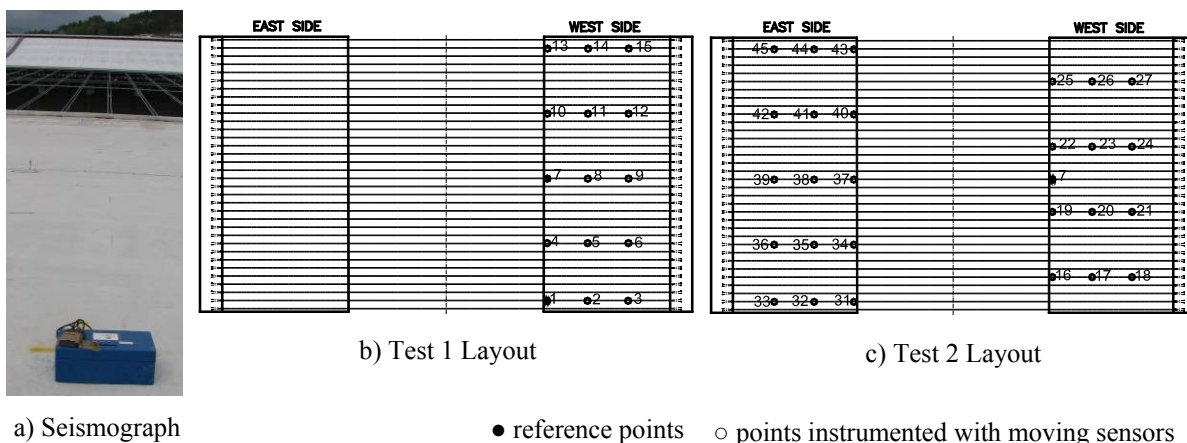


Figure 6.4 - Placement of one of the used seismographs (a) and measurement points of the ambient vibration test: b) 1st day; c) 2nd day.

The data collected during the ambient vibration test was processed by several output-only algorithms (FDD, SSI-COV and SSI-DATA), which provided almost coincident results for the natural frequencies and mode shapes and similar estimates of the modal damping ratios (Magalhães et al. 2008c). Here, only the natural frequencies and mode shapes provided by the FDD method are presented. This method was applied using the Artemis software (http://www.svibs.com/documentation/case_braga_stadium.htm), basing the identification on spectrum matrices with a resolution of 0.00488Hz, which allowed the achievement of spectra with clear peaks and sufficient accuracy in the identification of the natural frequencies (the frequency resolution is approximately 1.8% of the lowest natural frequency).

Figure 6.5 presents the configurations of the first 15 identified mode shapes, showing the good quality of the results, as quite smooth shapes were obtained, and the existence of pairs of closely spaced modes, mainly justified by the slope of the roof to drain the rain water, which breaks the symmetry of the structure with respect to the middle axis parallel to the cables. The lower spatial resolution of the measurements performed in the east slab explains the inferior quality of the estimates for mode shapes f_{11} to f_{15} in this slab. Mode shapes f_{12} and f_{13} seem to be only observable in the west and east slabs, respectively. The not clear configurations of the 15th and subsequent modes shows that the spatial resolution of the used measurement mesh is only suitable to well characterize the first 14 modes.

6.3.2 Numerical modelling

In order to better interpret the dynamic behaviour of the constructed roof and increase the confidence on the collected experimental data, the tri-dimensional numerical model developed at ViBest/FEUP to support the design was upgraded to take into account some structural modifications dictated by the construction process (Caetano et al. 2008).

The modal parameters (natural frequencies and mode shapes) were calculated using the tangent stiffness matrix of the global structure after application of permanent loads, which was evaluated taking into account the geometric nonlinear characteristics of this cable structure and simulating the progressive application of loads during the construction phase.

The first six mode shapes and the corresponding natural frequencies are presented in Figure 6.6. The comparison of the numerical results with their experimental counterparts, further explored in (Caetano et al. 2008), evidences the achievement of an excellent correlation, both in terms of natural frequencies and mode shapes (Figures 6.5 and 6.6).

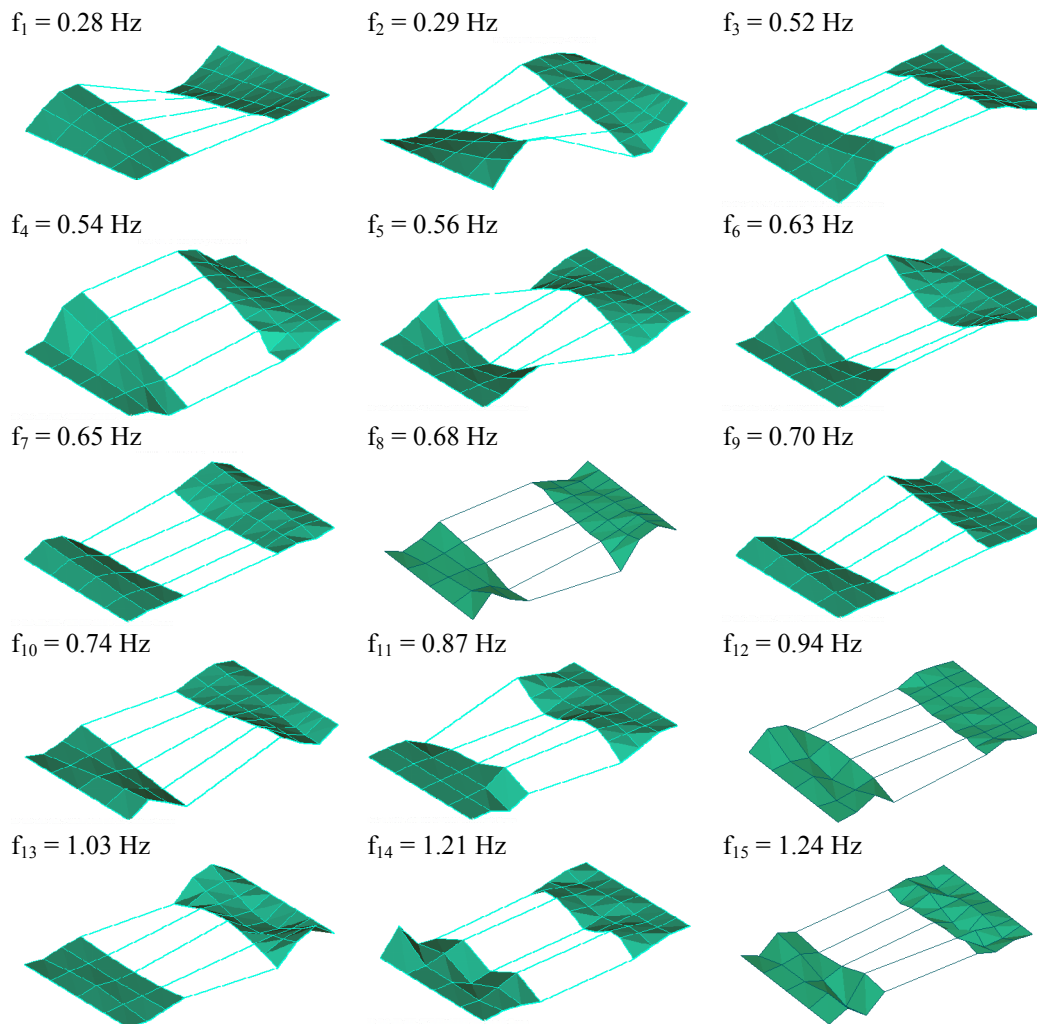


Figure 6.5 – Natural frequencies and mode shapes estimated by the FDD method.

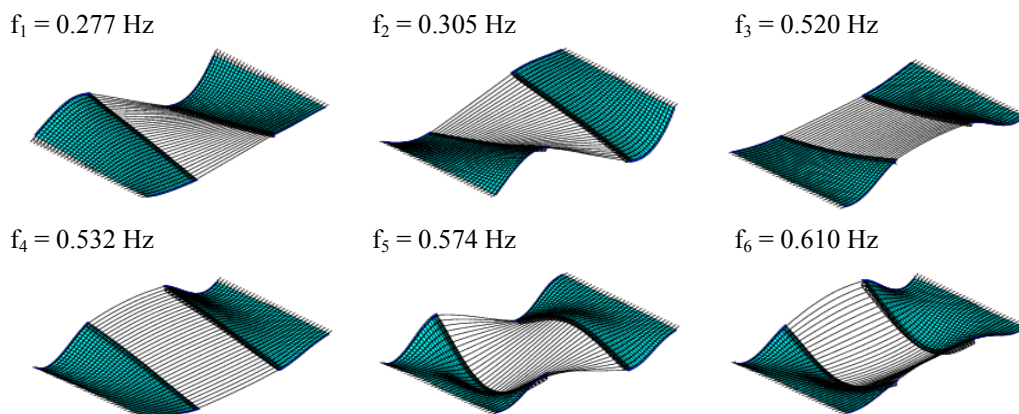


Figure 6.6 - Calculated frequencies and mode shapes of the first six modes.

6.4 Monitoring System Description

The outstanding characteristics of the structure and the need of a tight control of the corresponding behaviour and geometry during the construction justified the installation of a monitoring system with several components: static, dynamic and wind characterization.

The static monitoring system comprehends a series of load cells installed in the anchorages of the roof cables, sensors embedded in the concrete structure (strain gauges, clinometers and thermometers) and instrumentation of the rock massifs and foundations, with load cells installed in the anchors to the earth and in-place inclinometers. This system was essential during the construction, especially at the stage of installation of the roof precast panels.

The dynamic monitoring system installed during the construction is composed by six accelerometers, installed in the inner edges of the concrete slabs, three sensors in each slab. Its main goal is the characterization of the levels of vibration of the roof. This is complemented by instrumentation for the characterization of the wind action by means of two anemometers and cells to measure the wind pressure on the underside and top of the roof slabs.

In March 2009, a new independent and complementary Dynamic Monitoring system was installed by ViBest/FEUP on the west slab of the stadium roof. This comprehends very sensitive accelerometers that permit the use of the recorded acceleration time series for the continuous identification of the roof modal parameters (natural frequencies, modal damping ratios and mode shapes), which can be subsequently used to experimentally characterize the effects of the wind on the roof dynamic behaviour and to evaluate the roof structural condition, using the procedure characterized and applied in the context of the monitoring of the Infante D. Henrique Bridge (chapter 5).

This more recent system is essentially composed by six force balance accelerometers (FBA ES-U2), a digitizer (Q330) and a robust field processor (Slate)(Magalhães et al. 2009c). These components are the same as the ones installed at the monitoring application described in the previous chapter and so, their technical characteristics have already been presented.

The six accelerometers were installed on the top of the roof according to the scheme presented in Figure 6.7, placed inside boxes for protection against rain and other environmental aggressions (Figure 6.8) and mounted to measure the acceleration in the vertical direction. These are connected by cables to the digitizer that was stored, together with the field processor (Figure 6.8), inside a technical room with power supply and an ADSL connection for remote access and data retrieving. With the intention

of minimizing the total length of cables, two junction boxes were adopted to gather in one cable the signals and power supply of groups of 3 accelerometers. The internal clock of the digitizer is continuously set by GPS.

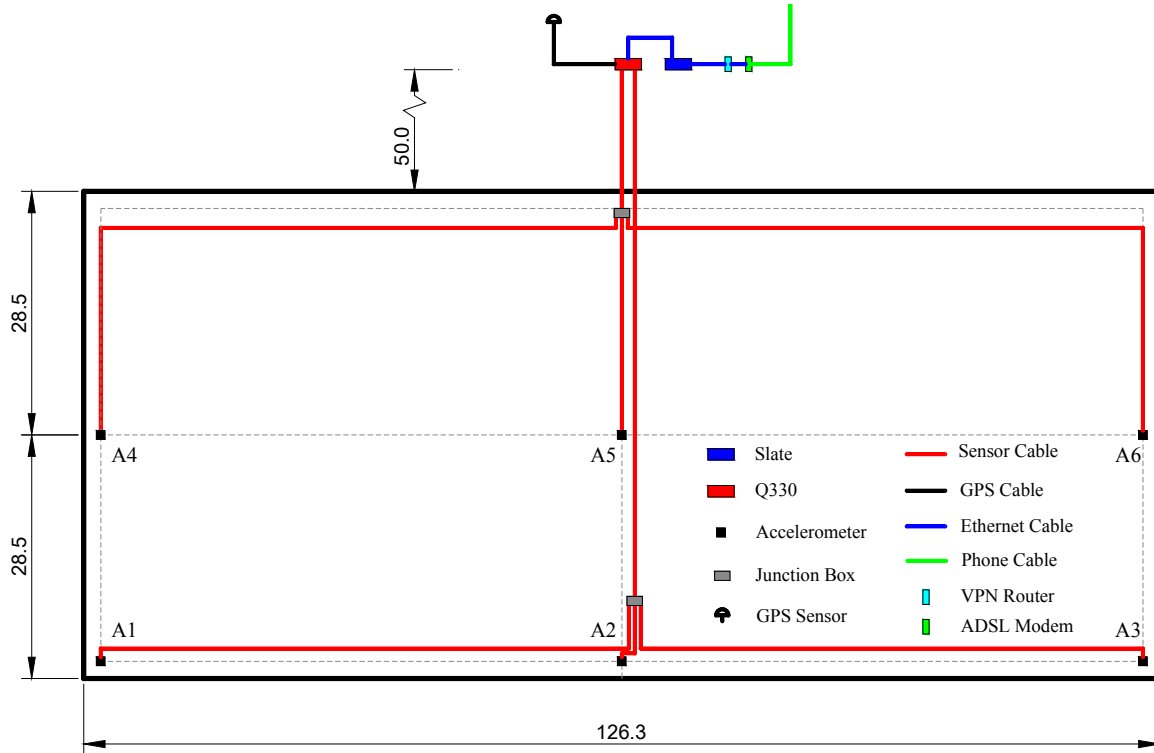


Figure 6.7 - Plan of the Monitoring System of the Braga Stadium roof (view of the top face of the west slab).

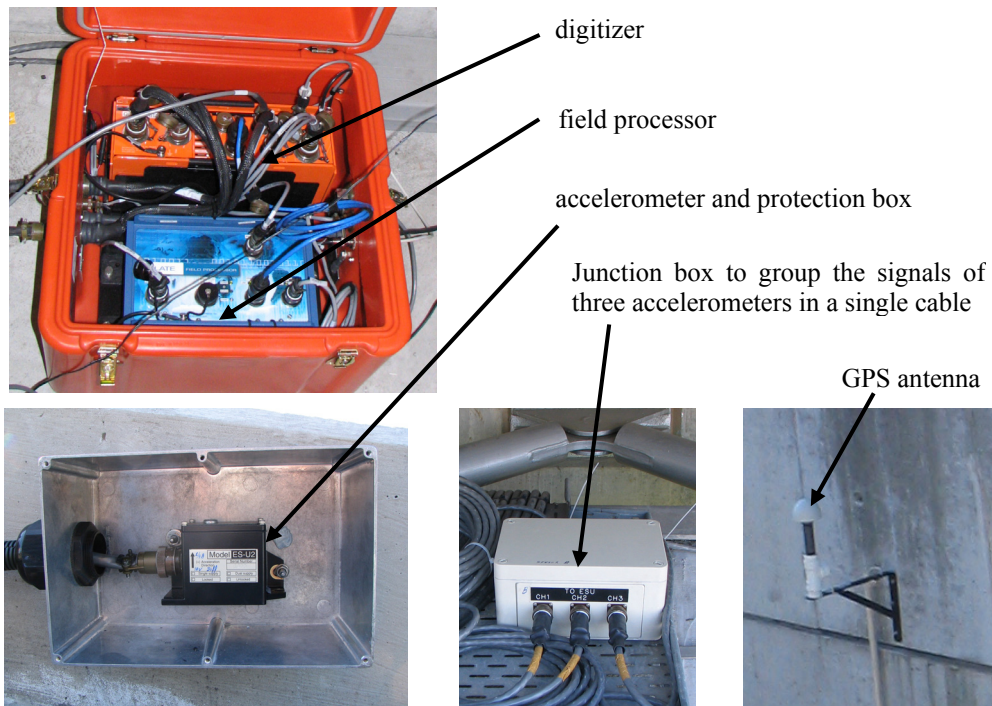


Figure 6.8 - Dynamic Monitoring system components and installation details.

6.5 Monitoring Results

The Dynamic Monitoring system installed in the west slab of the roof of the Braga Stadium is in operation since 25/03/2009. This section presents the analysis of the setups collected until the end of 2009. During this period, a technical problem occurred leading to an interruption in the data recording from 15/05/2009 to 11/06/2009. Besides this disturbance, all the remaining setups of this 9 months period were recorded and processed.

As the period of observation is shorter than one year, the establishment of correlations between the modal parameters and the environmental variables recorded by the monitoring hardware installed during construction is reserved to a future work. Thus, this section only presents the results provided by the recently installed monitoring system.

6.5.1 Characterization of the measured signals

The digitizers were configured to continuously measure the signals recorded by the six accelerometers with a sampling rate of 20Hz. The field processor was programmed to store the collected signals in text files with a time length of one hour. Taking into account the natural frequencies of the roof presented in section 6.3, the selected sampling frequency is a very conservative value that was chosen with the goal of creating a database that may be used later for other purposes than modal analysis. The length of one hour is a compromise between the aim of obtaining reliable estimates of the modal damping ratios and the objective of characterizing the daily variations of the modal parameters.

The continuously created data files have been processed by the DynaMo software, presented in chapter 4 and extensively used in chapter 5. After the storage of the original text files in an organized backup, the one hour length acceleration time series are pre-processed. This includes the elimination of linear trends, the application of a band pass filter with lower and upper cutting frequencies of 0.1 and 2Hz and a re-sampling with a frequency of 5Hz. The elimination of the signals frequency content below 0.1Hz was important to remove fluctuations in the signals average values that should be close to zero to well characterize the dynamic component of the accelerations.

Figure 6.9 presents two examples of acceleration time series after the application of the previously described pre-processing. The first plot shows the existence of very low levels of vibration during the night, generally lower than $50\mu\text{g}$, which are interrupted by impulse responses with amplitudes between $200\mu\text{g}$ and $400\mu\text{g}$. The cause for these low amplitude impulsive loads has not been confirmed yet.

Figure 6.10 characterizes the vibration intensity during one week using the maxima and RMS (root mean square) values of the collected acceleration time series. This shows the daily variation of the vibration amplitude and the existence of higher levels of vibration during the weekend (28, 29th March), certainly due to events taking place in the stadium.

The evolution of the maxima of the pre-processed acceleration time series during all the observation period is depicted in Figure 6.11. This shows that, if only the contribution of frequencies between 0.1 and 2Hz is considered, accelerations are generally lower than 5mg and have never risen above 25mg.

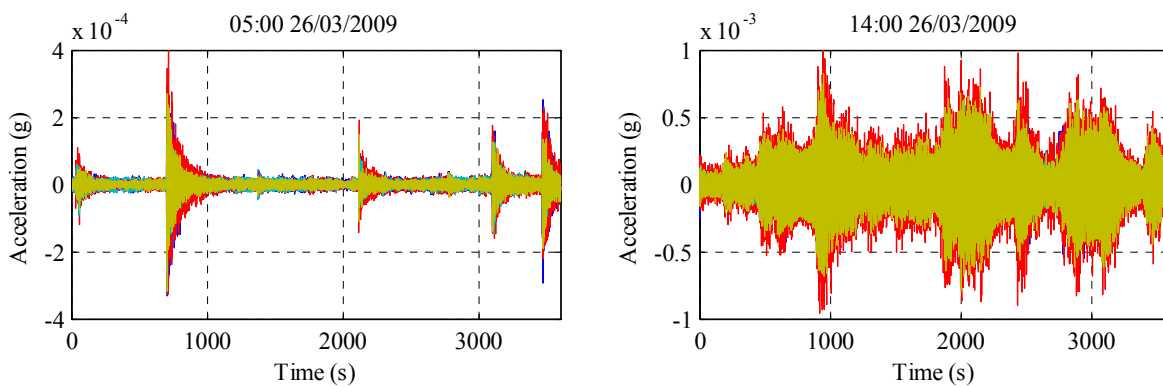


Figure 6.9 - Examples of acceleration time series after pre-processing: a) 05:00 26/03/2009; b) 14:00 26/03/2009.

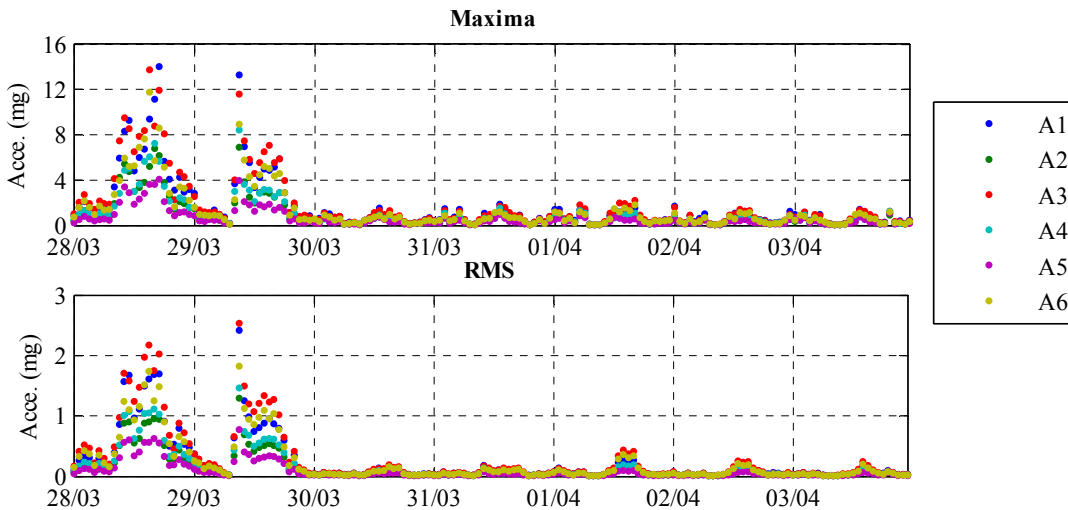


Figure 6.10 - Characterization of the time evolution of the levels of vibration during one week (from 28/03/2009 to 3/04/2009).

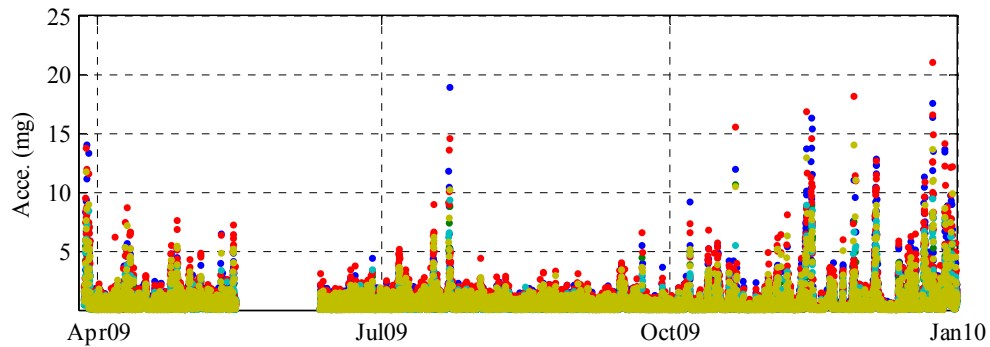


Figure 6.11 - Characterization of the time evolution of the maxima of the acceleration time series from 25/03/2009 to 31/12/2009.

The colour map presented in Figure 6.12 illustrates the frequency content of data continuously collected during one week. This comprehends 168 spectra of the first singular value of spectrum matrices derived from one hour long time series with a frequency resolution of 0.0012Hz. The hotter colours mean more energy and therefore the vertical alignments in red/yellow characterize the time evolution of the excited natural frequencies. The comparison of the mean natural frequencies of these vertical alignments with the natural frequencies provided by the ambient vibration test (Figure 6.5) shows an excellent agreement. The natural frequency around 0.94Hz is less evident in the colour map because it is associated with a mode with relevant movements only on the east slab (f_{12} , Figure 6.5).

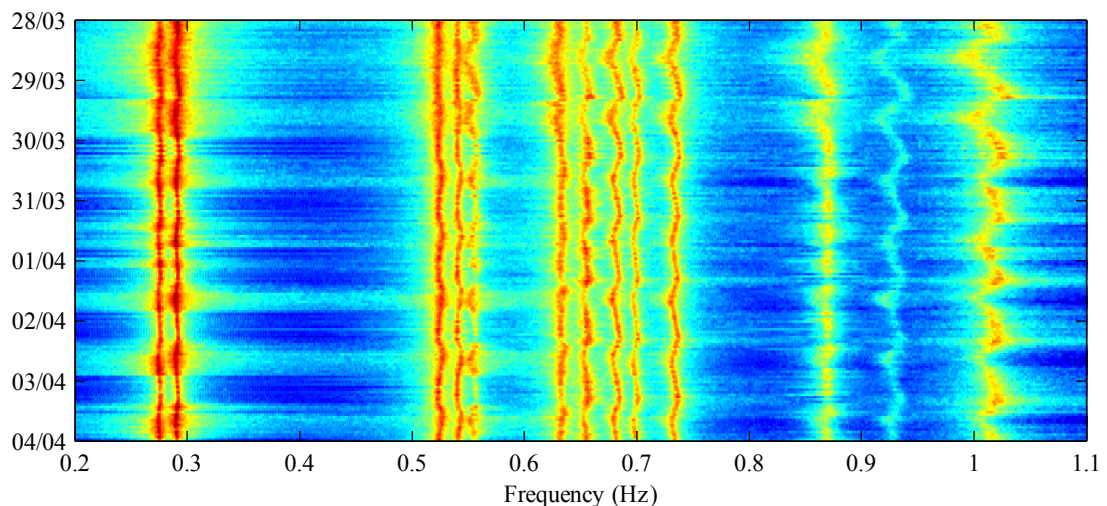


Figure 6.12 - Colour map with the variation of the signals frequency content over time (from 28/03/2009 to 03/04/2009).

6.5.2 Automatic modal parameters identification

As one of the goals of this application was to further test the algorithm developed to perform the automatic identification of modal parameters using parametric methods, the acceleration time series collected at the roof of the Braga Stadium have been processed by the automatic versions of the SSI-

COV and p-LSCF methods. The colour map presented in Figure 6.12 shows that the frequency range 0.2 to 1.1Hz already contains a considerable number of resonant frequencies. So, the application of both methods is restricted to this frequency band.

Automated SSI-COV

The SSI-COV method starts with the calculation of a matrix with the correlations of the recorded time series. After some preliminary tests, it was concluded that good results could be obtained using the complete correlation matrix, instead of selecting a subset of references, and adopting for the length of correlation functions 200 points (200/5 = 40 seconds → 40 x 0.28 = 11.2 periods of the lowest frequency). The application of the SSI-COV algorithm to correlation matrices calculated with the previously defined parameters gives stabilization diagrams similar to the ones shown in Figure 6.13. These are associated with the time series presented in Figure 6.9 and demonstrate that the acceleration time series collected during the night led to clearer stabilization diagrams. Anyway, in both diagrams there are 12 vertical alignments of stable poles that stand out. These 12 alignments are consistent with the resonant frequencies that are enhanced in Figure 6.12. The mode with natural frequency around 0.94Hz (f_{12}), essentially associated with the east slab, is not evidenced by the majority of the analysed stabilization diagrams.

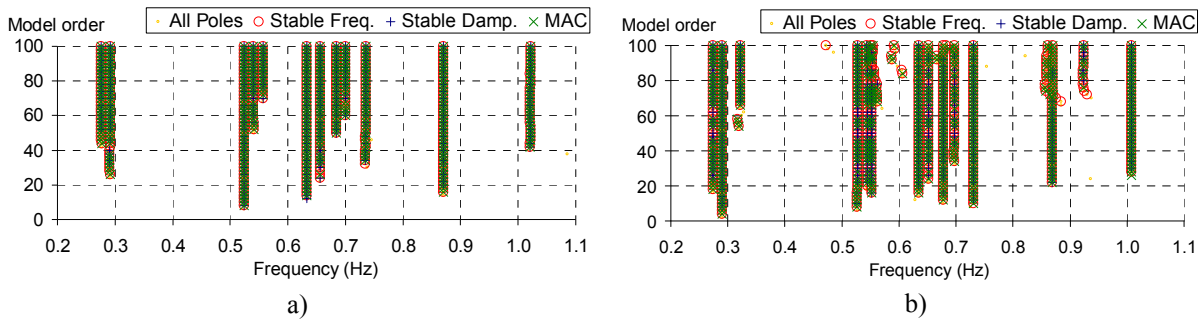


Figure 6.13 – Stabilization diagrams produced by the application of the SSI-COV method to setups: a) 05:00 26/03/2009, b) 14:00 26/03/2009

The poles of the stabilization diagrams that represent the same physical modes are easily grouped by the hierarchical clustering algorithm presented in section 2.4.4, as it is proven in Figure 6.14. This algorithm was configured to group all the poles of the stabilization diagram, stable and not stable, to use as maximum distance between modes of the same cluster 0.02 (see eq. (2.94)) and to select the 14 groups with more elements. Figure 6.15 characterizes the mode estimates of the stabilization diagram presented in Figure 6.13a selected by the clusters algorithm and then processed by a routine that eliminates the extreme values of the modal damping ratios.

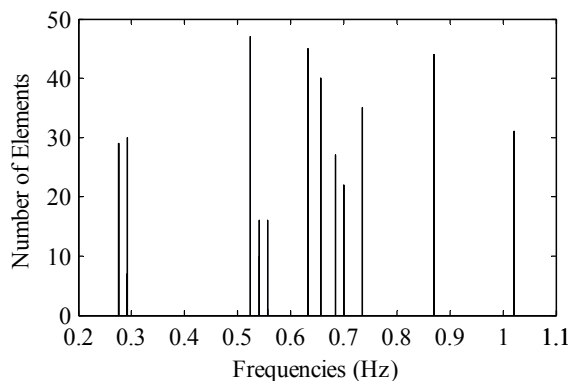


Figure 6.14 – Number of elements of the clusters formed with all the poles of the stabilization diagram presented in Figure 6.13a

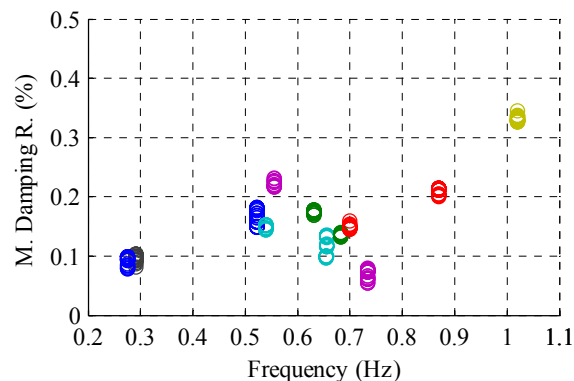


Figure 6.15 – Damping vs frequency of the mode estimates that belong to the 12 clusters with more elements after the outliers elimination.

For the matching of the estimates from consecutive setups, it was adopted the same procedure that is followed in the monitoring of Infante D. Henrique Bridge. In each setup, the mean modal parameters of 14 selected clusters are compared with reference modal parameters. These reference values are the mean of the modal parameters given by the application of the SSI-COV method to all the setups collected during the 26 of March of 2009. As the frequency f_{12} only appears in very few setups, its mode was not included in the reference set. Only the estimates that differ less than 10 % from the reference values of the natural frequencies and that present a MAC higher than 0.8 with regard to the reference modes are selected.

The performance of the automated SSI-COV in the processing of all the setups collected from 06/03/2009 to 31/12/2009 is characterized in Table 6.1.

Table 6.1 – Results of the SSI-COV method for the period: 25/03/2009 – 31/12/2009 (total number of processed setups – 6104)

Mode	Success Rate (%)	f_{mean} (Hz)	f_{std} (Hz)	ξ_{mean} (%)	ξ_{std} (%)	MAC_{mean}	MAC_{min}
1	99.23	0.2751	0.0007	0.2363	0.1465	0.992	0.802
2	99.90	0.2906	0.0010	0.2125	0.1454	0.999	0.829
3	99.93	0.5256	0.0015	0.2160	0.0957	0.996	0.831
4	99.51	0.5421	0.0014	0.1830	0.0946	0.980	0.804
5	90.83	0.5542	0.0054	0.4092	0.2178	0.969	0.800
6	99.69	0.6326	0.0019	0.2843	0.1123	0.991	0.809
7	97.64	0.6545	0.0015	0.2173	0.0757	0.980	0.802
8	99.98	0.6812	0.0040	0.1640	0.0724	0.995	0.827
9	98.94	0.6979	0.0020	0.1548	0.0794	0.989	0.807
10	99.97	0.7326	0.0026	0.1447	0.0645	0.997	0.801
11	96.33	0.8667	0.0039	0.3637	0.1596	0.991	0.800
13	99.93	1.0160	0.0061	0.4387	0.1152	0.997	0.827

The second column of the table shows that, also in this application, it was possible to achieve very high success rates (always above 90%) in the automatic identification of modal parameters. The lowest success rate is associated with mode 5, which is not significantly excited during all the setups, as it is evidenced by the colour map presented in Figure 6.12.

Automated p-LSCF

The first step of the p-LSCF method is the calculation of half-spectrum matrices from the acquired acceleration time series. In the present application, each element of these matrices is calculated from the FFT of the positive lags of correlation functions with a length of 512 points, after the application of an exponential window with a factor of 0.1. All the measured degrees of freedom were selected as references, so the spectrum matrices are 6-by-6.

Then, the experimental spectra are fitted by theoretical spectra in the frequency range 0-2.5Hz, adopting polynomials with orders between 1 and 30. Following the algorithm presented in section 2.3.5, stabilization diagrams like the ones presented in Figure 6.16 are obtained. These diagrams, which are associated with the same time series that were adopted for the construction of the stabilization diagram presented in Figure 6.13, permit the immediate identification of 12 alignments of stable poles.

Figure 6.17 characterizes, for the setup at 05:00 26/03/2009, the clusters formed by all the mode estimates with positive natural frequencies and modal damping ratios extracted from all the fitted models, using the same distance limit between modes (0.02) that was adopted with the SSI-COV method. The 12 groups that contain the physical estimates clearly stand out. The mode estimates inside these 12 groups are characterized in Figure 6.18, after the elimination of the extreme values of modal damping ratios. The results are similar to those provided by the SSI-COV method (Figure 6.15).

Finally, the matching between each new set of mode estimates and the previous ones is performed using the same procedure and parameters that are adopted with the SSI-COV method. The overall performance of the automated p-LSCF in the processing of all the setups collected from 25/03/2009 to 31/12/2009 is characterized in Table 6.2.

The comparison between Tables 6.1 and 6.2 shows that the p-LSCF presented slightly better success rates. The mean natural frequencies provided by the two methods are almost coincident and the similarity of the mean modal damping ratio estimates is remarkable. Like in the bridge application, the scatter of the damping estimates provided by the p-LSCF method is slightly lower.

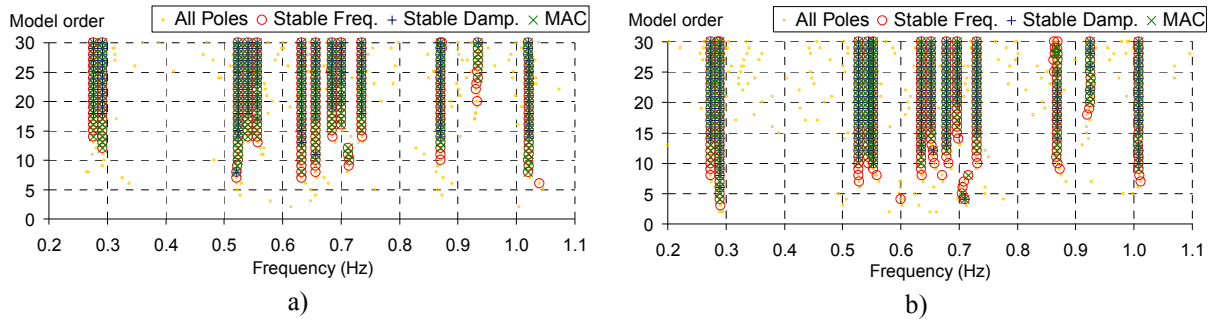


Figure 6.16 – Stabilization diagrams produced by the application of the p-LSCF method to the setups: a) 05:00 26/03/2009, b) 14:00 26/03/2009

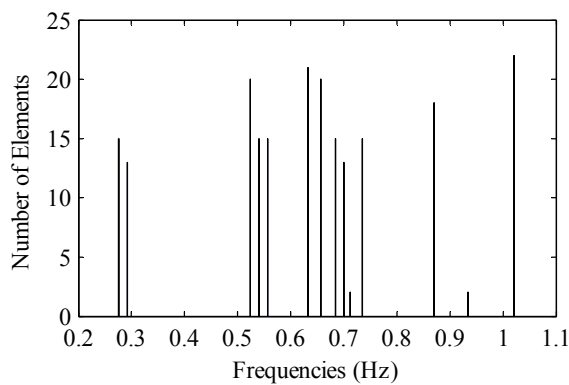


Figure 6.17 – Number of elements of the clusters formed with all the poles of the stabilization diagram presented in Figure 6.16a

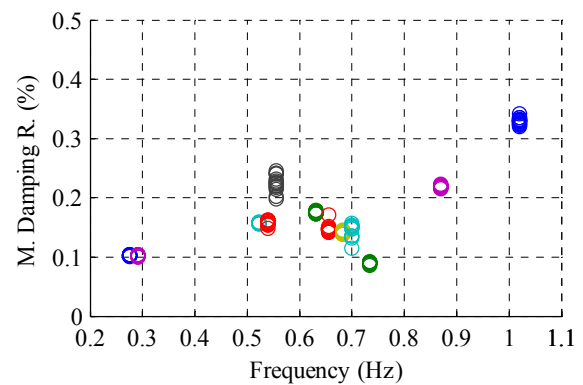


Figure 6.18 – Damping vs frequency of the mode estimates that belong to the 12 clusters with more elements after the outliers elimination.

Table 6.2 – Results of the p-LSCF method for the period: 25/03/2009 – 31/12/2009 (total number of processed setups – 6104)

Mode	Success Rate (%)	f_{mean} (Hz)	f_{std} (Hz)	ξ_{mean} (%)	ξ_{std} (%)	MAC_{mean}	MAC_{min}
1	99.79	0.2751	0.0007	0.2294	0.1261	0.992	0.807
2	99.98	0.2906	0.0010	0.2020	0.1191	0.999	0.851
3	99.97	0.5256	0.0015	0.2148	0.0899	0.996	0.842
4	99.64	0.5421	0.0013	0.1790	0.0710	0.980	0.801
5	91.78	0.5539	0.0040	0.3881	0.1462	0.967	0.800
6	99.93	0.6325	0.0020	0.2812	0.1027	0.990	0.810
7	98.49	0.6545	0.0015	0.2102	0.0640	0.981	0.801
8	100	0.6814	0.0053	0.1592	0.0675	0.994	0.805
9	99.31	0.6978	0.0023	0.1407	0.0549	0.989	0.802
10	99.97	0.7325	0.0028	0.1436	0.0596	0.997	0.800
11	96.97	0.8666	0.0040	0.3169	0.1271	0.974	0.800
13	100	1.0158	0.0061	0.4351	0.1033	0.997	0.895

6.5.3 *Analysis of the modal parameters variation*

This sub-section is dedicated to the analysis of the variation of modal parameters automatically identified by the p-LSCF method during the period from 25/03/2009 to 31/12/2009. As demonstrated in the previous paragraphs, the results provided by the SSI-COV method are similar.

Figure 6.19 characterizes the time evolution of 12 natural frequencies of the roof during the whole period under analysis, with an interruption from 15/05/2009 to 11/06/2009. It proves once more the ability of the implemented algorithms to successfully track the evolution of a considerable number of natural frequencies. The zoom around the values of the first natural frequency shows that after October 2009 (autumn and winter period), its average increases and that the scatter around the average decreases. This behaviour is justified by the decrease of the average temperature of the roof structural elements and by the decrease of the daily variations of the temperature from summer to winter.

The graphic presented in Figure 6.20, just concentrated in one week, illustrates even better the influence of temperature on natural frequencies. Particularly clear in the zoom that shows the daily variations of the natural frequencies of the 3rd, 4th and 5th modes. First of all, the accuracy of the identification algorithm to characterize variations of the order of milli-Hz has to be pointed out. Then, it is interesting to observe that the temperature variation has different consequences on different types of modes: the natural frequency of mode 5 varies in opposite sense with regard to the frequency variations observed in modes 3 and 4.

A temperature increase has two consequences on the structure of the roof: it leads to a decrease of the elasticity modulus of the concrete of the slabs and it produces an increase of the cables length, and so, an increase in the sag of the cables. The modes that present mode shapes with low curvatures of the concrete slabs and symmetry with respect to a horizontal axis perpendicular to the cables and crossing the cables at their mid-span, modes 3, 4 and 6 (see Figure 6.5), present an increase of their natural frequencies when the temperature increases (higher values of the natural frequencies during daylight time). On the contrary, the other modes are more affected by the influence of temperature on the stiffness of the concrete slabs and therefore their natural frequencies present higher values during the night or beginning of the morning, when the structure presents lower temperatures.

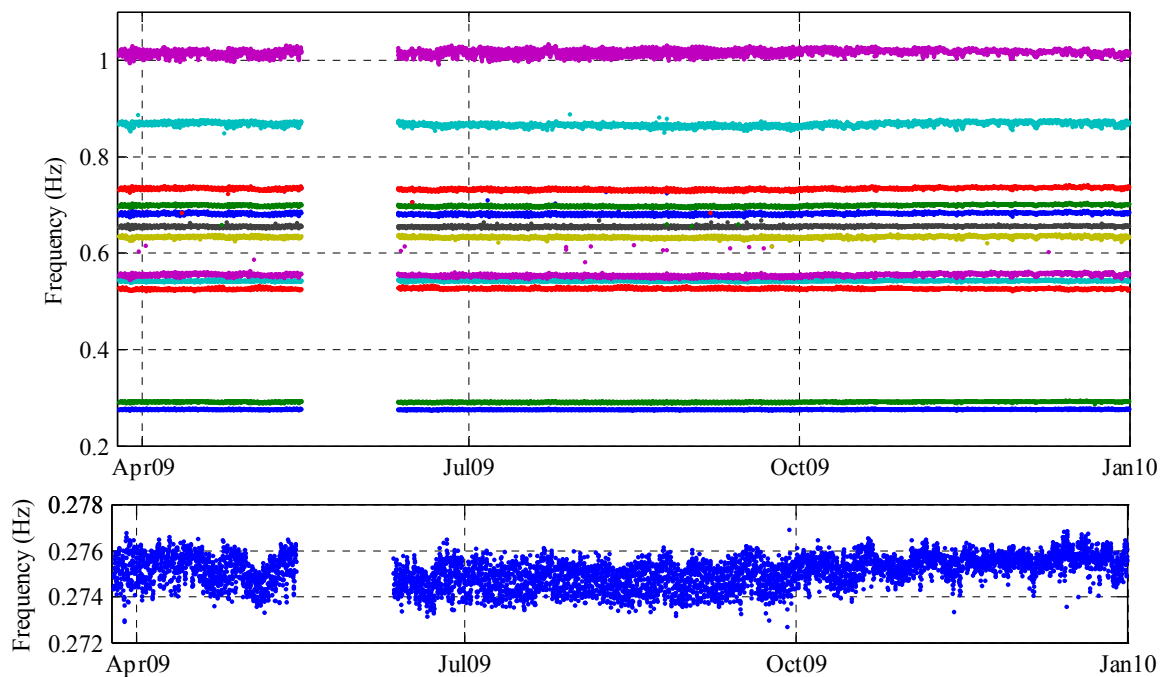


Figure 6.19 – Time evolution of natural frequencies from 25/03/2009 to 31/12/2009, all frequencies and zoom around the first frequency.

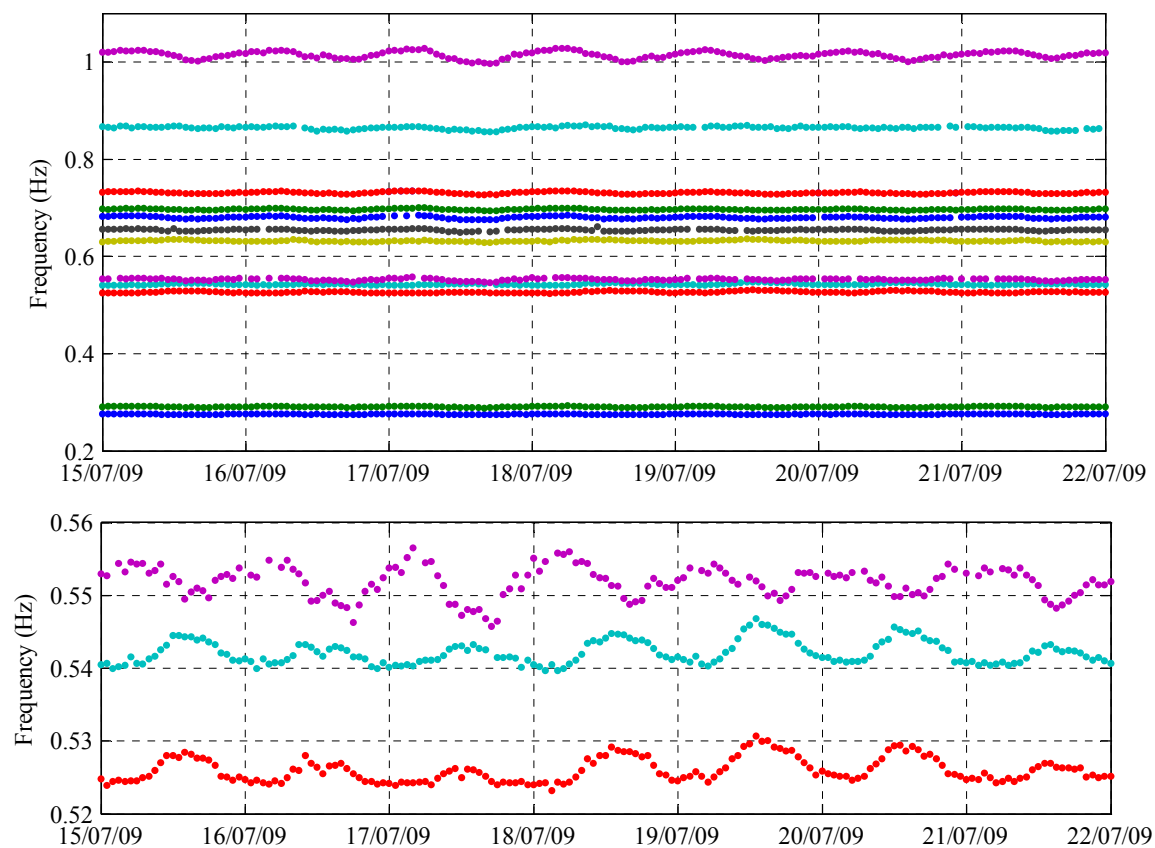


Figure 6.20 – Time evolution of natural frequencies during the week from 15/07/2009 to 22/07/2009, all frequencies and zoom around the 3rd, 4th and 5th frequencies.

The time evolution of modal damping ratios is much less clear than the presented for natural frequencies. This is mainly due to the higher uncertainty associated with the estimates of these parameters and to the fact that they are significantly influenced by a large variety of factors, like the wind characteristics or the vibration amplitude. Figure 6.21 groups the modal damping ratio estimates obtained during the period under analysis for the first six modes in histograms, which permit the identification of the dominant values, the characterization of their variability and the definition of confidence intervals.

The results obtained with the monitoring system for the damping confirm the extremely low values provided by the ambient vibration and free vibration tests, already presented in section 3.5.7. The results produced by the dynamic monitoring system are much more reliable than those provided by the ambient vibration test, because longer time series have been used (1 hour instead of 16 minutes) and because a much larger variety of loading scenarios (different wind conditions and vibration amplitudes) have been covered. The mean values presented in Tables 6.1 and 6.2 are in good agreement with the values estimated by the free vibration tests (Figure 3.56, section 3.5.7).

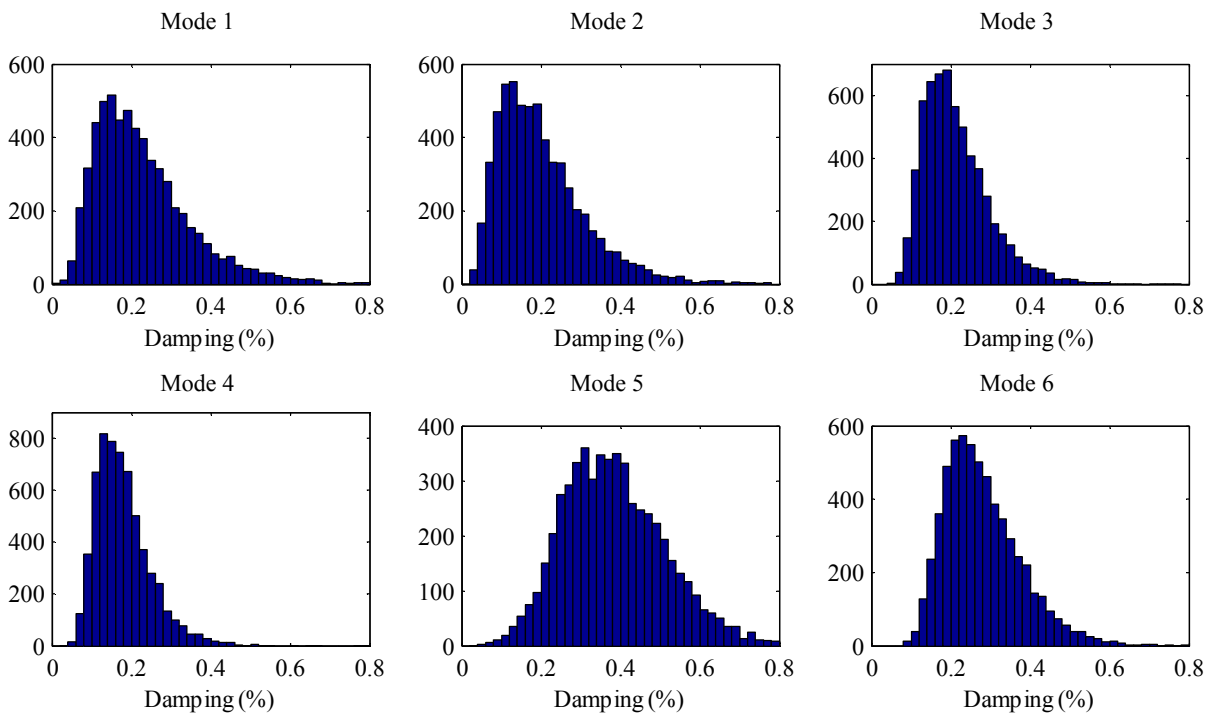


Figure 6.21 – Histograms of the modal damping ratios of modes 1 to 6.

6.6 Conclusions

This chapter starts with the description of the experimental work developed before the design of a dynamic monitoring system for a cable suspended roof of a stadium. Then, the installed equipment is characterized and finally, the main results associated with the first nine months of observation are presented.

The preparation phase included an ambient vibration test of the roof that provided modal parameters estimates of high quality with an excellent correlation with the values obtained with a previously developed numerical model. Then, this information was of paramount importance for the design of a Dynamic Monitoring system, whose main purpose is the continuous identification of the most relevant modal parameters.

The first nine months of operation of the installed monitoring system have already permitted to prove that the developed and implemented routines for automatic identification of modal parameters make possible a very detailed characterization of the time evolution of the natural frequencies of 12 modes in the frequency range 0-1.1Hz, and also the quantification of the corresponding modal damping ratios. This exercise was very important to demonstrate that the DynaMo software presented in chapter 4 is flexible enough to be used on diverse civil engineering structures.

The analysis of the data produced by the continuous dynamic monitoring system of the Braga Stadium is far from being finished. In the near future, the observed variations of the natural frequencies are going to be correlated with the temperatures measured by the static monitoring system installed during the construction of the stadium, and a model to reduce the effects of environmental and operational factors on natural frequencies, like the ones presented in chapter 4 and applied in chapter 5, is going to be established. This will then permit to test the ability of the monitoring system to detect small structural changes that might be due to damages.

Furthermore, the continuously estimated modal damping ratios are going to be correlated with the data collected by the anemometers and pressure cells installed in the roof, with the final goal of experimentally quantify aerodynamic damping components. This is an important research topic since these damping components, which can be negative and thus reduce the structural damping, play an important role in the dynamic response of flexible structures to the wind action.

Chapter 7

CONCLUSIONS AND FUTURE RESEARCH



7. CONCLUSIONS AND FUTURE RESEARCH

7.1 Conclusions

This work was focused on the use of operational modal analysis in the testing and monitoring of bridges and special structures. It included the development, implementation and application of tools that permit an efficient processing of data collected during ambient vibration tests of large structures and the on-line continuous and automatic transformation of time series recorded by long-term dynamic monitoring systems into useful information for the owners or operators of important civil infrastructures.

The thesis comprehends an overview of the algorithms for operational modal analysis, followed by a detailed description of three state-of-the-art identification techniques: Frequency Domain Decomposition, Covariance driven Stochastic Subspace Identification and poly-Least Squares Complex Frequency Domain. These were firstly assessed with numerical simulations and then applied to very complete databases collected at the Millau Viaduct and at the Humber Bridge, taking advantage of algorithms that permit the global processing of several setups. Additionally, the accuracy of modal damping ratio estimates provided by ambient vibration tests was evaluated using data from ambient and free vibration tests developed in five relevant structures: Vasco da Gama Cable-Stayed Bridge, Millau Viaduct, Pedro e Inês Footbridge, Grand Ravine Bridge and the suspended roof of the Braga Stadium.

Concerning the use of operational modal analysis in the context of continuous dynamic monitoring, the description of a new technique to automate the identification of modal parameters and an overview of the tools available to reduce the effects of environmental and operational factors on natural frequencies, with the goal of obtaining an index for damage detection, is followed by the presentation of two monitoring projects: one at the Infante D. Henrique Bridge and another at the roof of the Braga Stadium. Both applications were based on a new monitoring software package (DynaMo) where all the previously characterized tools were integrated.

The developed research permitted to achieve the following main conclusions, which synthesize the partial conclusions previously presented at the end of each chapter.

- Data collected during the ambient vibration tests of Millau Viaduct and Humber Bridge permitted to explore four different strategies to process multiple setups using two of the most powerful system identification methods: SSI-COV and p-LSCF.

The application of the p-LSCF method to the data collected at the Millau Viaduct demonstrated that the traditional approach, based on an independent analysis for each setup, made possible the identification of all the relevant modes and the characterization of the scatter of the corresponding natural frequencies and modal damping ratios during the test. However, its application is very time consuming and some mode shape components could not be determined. On the other hand, one of the tested approaches based on the global processing of all the setups, the PoGER approach (section 2.5.3), applied also together with the p-LSCF method proved to be able to provide similar estimates for the natural frequencies and more complete mode shapes with much less effort, as only one very clear stabilization diagram had to be interpreted.

The large amount of data collected during the ambient vibration test of the Humber Bridge permitted to test the PoGER approach together with the SSI-COV and p-LSCF methods. The majority of the results were similar (the largest discrepancies were observed on the modal damping ratios), but the time domain method was able to successfully identify a higher number of modes. However, the analysis with the new proposed combined procedure, based on a first global processing followed by an automatic independent processing of each setup (see section 2.5.5), was the one that provided the most complete results, as the mean estimates of the global analysis were complemented by the characterization of the scatter of the natural frequencies and modal damping ratios during the testing period.

- Although modern output-only modal identification techniques, in conjunction with the use of appropriate state-of-the-art vibration measurement equipment, can provide very accurate estimates of natural frequencies and mode shapes, even when closely spaced modes are present, it was observed that the corresponding damping estimates show a significant scatter and that the differences between the damping values provided by different identification methods are always higher than those observed for the remaining modal parameters. Therefore, the accuracy of the damping estimates provided by operational modal analysis was investigated with numerical simulations (section 2.3) and by the comparison of the results provided by Ambient Vibration Tests (AVT) and Free Vibration Tests (FVT) performed in five relevant civil engineering structures (section 3.5).

The numerical simulations demonstrated that an incorrect selection of the user-defined parameters of each identification algorithm or the use of time series with an insufficient length can lead to highly biased estimates of damping. Taking into account the results of the simulations, suggestions on how to make an adequate choice of the inputs of the three analyzed methods (EFDD, SSI-COV and p-LSCF) are provided. The tested parametric identification

methods (SSI-COV and p-LSCF) performed much better than the EFFD method, as they provided estimates for modal damping ratios with lower bias and random errors and are less sensitive to the length of the time series and to the adopted user-defined parameters. However, it became clear that even in ideal conditions (simulated data, right choice of parameters and time series with more than 1 hour), the relative standard deviations of the estimates provided by the former methods present values around 10%. The improvement proposed for the EFFD method (section 2.3.3) permitted to significantly reduce the bias error of the estimates achieved with this non-parametric method, especially when only short time series are available, but even so, the results were not as good as the ones provided by the SSI-COV and p-LSCF methods.

The results associated with the five structures, where both ambient and free vibration tests were performed, confirmed the high scatter of the modal damping estimates provided by operational modal analysis (relative standard deviation of the order of 50%), justified not only by the uncertainties of the identification algorithms, but also by the influence on damping of wind intensity (aerodynamic damping) and vibration amplitude, as it is impossible to guarantee stationary conditions during the entire testing period. Nevertheless, in all the cases, the majority of modal damping ratio estimates obtained from the free decays are within the interval defined by the average values \pm the standard deviation of the estimates of the ambient vibration tests. This conclusion is very important to increase the confidence in the results provided by ambient vibration tests, which are much more practical and less expensive.

- The continuous dynamic monitoring system installed in the Infante D. Henrique Bridge permitted to extensively test the algorithm developed to perform the automatic identification of modal parameters based on both the SSI-COV and the p-LSCF methods. With regard to the also tested automated FDD method, the two parametric methods presented the advantage of providing estimates of modal damping ratios and of not limiting the accuracy in the identification of the natural frequencies by a pre-set frequency resolution. Furthermore, the on-line continuous application of the SSI-COV and p-LSCF methods, during more than two years, showed high success rates (generally higher than 99%) and demonstrated their ability to identify closely spaced modes and to permit the detection of very small frequency shifts. Both provided also meaningful modal damping ratios estimates. The comparison of the outputs of the two parametric methods showed that the modal damping ratio estimates obtained with the p-LSCF method present a lower scatter, permitting, for instance, a better characterization of the effect of vehicles stopped on the bridge on these modal parameters.

- The post-processing of the modal parameters automatically identified at the Infante D. Henrique Bridge during more than two years permitted to test the capability of alternative static and dynamic multiple linear regression models to minimize the effects of environmental and operational factors on natural frequencies. A dynamic model that includes as predictors temperatures measured by sensors embedded in the structure, the vibration amplitude and the modal damping ratio estimates of the first vertical mode (to indirectly characterize the influence of traffic jams on natural frequencies) led to narrow confidence intervals for the expected natural frequencies of the healthy structure, allowing the detection of frequency shifts of some milli-Hz that might be due to some abnormal occurrence. Additionally, it was noticed that the results provided by the adopted regression model could be improved with the subsequent application a model based on a Principal Components Analysis of the time series with the natural frequencies previously corrected by the regression model. Furthermore, it was proven that the construction of control charts with the outputs of the PCA permits the detection of very small frequency shifts (around 0.15%) due to numerically simulated damage scenarios. Thus, it was demonstrated that the adopted processing strategy permits the detection of realistic damages at an early phase of appearance.
- The software for continuous dynamic monitoring (DynaMo) developed during the present work was successfully tested in the application on the Infante D. Henrique Bridge. It proved to be robust and efficient on the managing of the acquired data files, on the data processing, which includes automatic identification of modal parameters, elimination of environmental and operational effects on natural frequencies and construction of a control chart that permits the automatic detection of abnormal changes, and on the construction of a database with the history of the relevant outputs of data processing.
- The first nine months of operation of the monitoring system installed on the suspended roof of the Braga Stadium permitted to prove that the automated SSI-COV and p-LSCF methods were able to provide a very detailed characterization of the time evolution of the natural frequencies of 12 modes in the frequency range 0-1.1Hz and also the quantification of the corresponding modal damping ratios. This was an important exercise to demonstrate that the DynaMo software is flexible to be used in a large variety of civil engineering structures.

7.2 Future Research

The work presented in this thesis included the development of important tools to extract useful information from data collected during dynamic tests or by continuous dynamic monitoring systems. However, several new developments and more full-scale applications are still needed to make dynamic testing and monitoring even more advantageous. Therefore, some research topics in line with the developed work are presented in the following paragraphs.

- The techniques to simultaneously process data collected during several setups of an ambient vibration test need to be further explored through numerical simulations and other full-scale applications, to better understand how they perform under non-stationary conditions of the input and also of the modal parameters of the tested structures, which may vary significantly due to, for instance, temperature variations during the test.
- Further work is needed to reduce the uncertainty of the estimates of modal damping ratios provided by ambient vibration tests or to, at least, accurately characterize the uncertainty associated with the obtained values in order to make a well-founded decision about the necessity to perform additional free vibration tests.
- The algorithms for the automatic identification of modal parameters have to be tested in further examples and if necessary improved to become more efficient not only in the context of monitoring projects, but also to assist in the processing of data collected during ambient vibration tests.
- The models to eliminate the effects of temperature on natural frequencies presented in this work are statistical models which do not explicitly take into account the physics of the problem. Numerical simulations of the influence of temperature on modal parameters using thermo-mechanical models, validated with small laboratory experiments and observations on full-scale applications, might contribute to a better understanding of the involved mechanisms and subsequently to the creation of better models to correct the estimated resonant frequencies.
- The database created by the monitoring project established in the Infante D. Henrique Bridge is certainly useful to perform benchmark studies to evaluate alternative algorithms, developed by different research groups, for automatic identification of modal parameters, for elimination of environmental and operational effects on natural frequencies and for damage detection. These are fundamental for an objective selection of the best processing techniques.

- The presented monitoring software (DynaMo) still needs some improvements to become more efficient, more user-friendly and more flexible to be adopted in any monitoring application. Furthermore, it is worthwhile to develop software to perform the management of data collected in several structures and of the corresponding results, which would be certainly very useful for operators of a network of instrumented structures.
- The analysis of the data collected in the Braga Stadium roof is far from being finished. In a next step, the observed variations of natural frequencies are going to be correlated with the also monitored environmental data, and a model to reduce the effect of the environmental and operational effects on natural frequencies is going to be established. Then, this will permit to test the ability of the monitoring system for damage detection. Furthermore, the continuously estimated modal damping ratios are going to be correlated with the recorded wind data, with the final goal of experimentally quantifying aerodynamic damping components. This is an important research topic since damping plays an important role on the dynamic response of flexible structures to the wind action.

REFERENCES



8. REFERENCES

- Abdel-Ghaffar, A. M.; Scanlan, R. H. (1985) Ambient Vibration Studies of the Golden Gate Bridge: I. Suspended Structure and II. Pier-Tower Structure. *ASCE Journal of Engineering Mechanics*, 111(4), 463-499.
- Abe, M.; Fujino, Y. (2009) Bridge Monitoring in Japan. *Encyclopedia of Structural Health Monitoring*, C. Boller, F. Chang, and Y. Fujino, eds., Vol. 5, John Wiley & Sons.
- Adão da Fonseca, A.; Bastos, R.; Cunha, Á.; Caetano, E. (2002) Monitoring of Temporary Cables in "Infante D. Henrique Bridge". In *Proceedings of Structural Health Monitoring*, Paris, France.
- Adão da Fonseca, A.; Millanes Mato, F. (2005) Infante Henrique Bridge over the River Douro, Porto, Portugal. *Structural Engineering International*, 15(2), 85-87.
- Aktan, A. E.; Catbas, F. N.; Grimmelman, K. A.; Pervizpour, M. (2003) *Development of a Model Health Monitoring Guide for Major Bridges*. Drexel Intelligent Infrastructure and Transportation Safety Institute.
- Alampalli, H. (1998) Influence of in-service Environmental on Modal Parameters In *Proceedings of IMAC 16, International Modal Analysis Conference*, Santa Barbara, CA, USA.
- Allemang, R. J.; Brown, D. L. (1982) A Correlation Coefficient for Modal Vector Analysis. In *Proceedings of IMAC 1, International Modal Analysis Conference*, Orlando, Florida, USA.
- Andersen, P. (1997) *Identification of Civil Engineering Structures using Vector ARMA Models*. PhD Thesis, Aalborg University, Denmark.
- Azenha, M.; Magalhães, F.; Faria, R.; Cunha, Á. (2010) Measurement of concrete E-modulus evolution since casting: A novel method based on ambient vibration. *Cement and Concrete Research*, doi:10.1016/j.cemconres.2010.02.014.
- Bendat, J.; Piersol, A. (1980) *Engineering Applications of Correlation and Spectral Analysis*. John Wiley & Sons, USA.
- Bisby, L. A. (2004) *An Introduction to Structural Health Monitoring*. ISIS Canada (www.isiscanada.com).
- Boller, C.; Chang, F.-K.; Fujino, Y. (2009) *Encyclopedia of Structural Health Monitoring*. John Wiley & Sons

Brincker, R.; Andersen, P.; Jacobsen, N.-J. (2007) Automated Frequency Domain Decomposition for Operational Modal Analysis. In *Proceedings of IMAC 25, International Modal Analysis Conference*, Orlando, Florida, USA.

Brincker, R.; Krenk, S.; Kirkegaard, P.; Rytter, A. (1992) Identification of Dynamical Properties from Correlation Function Estimates. *Bygningsstatistiske Meddelelser*, 63, 1-38.

Brincker, R.; Ventura, C.; Andersen, P. (2001) Damping Estimation by Frequency Domain Decomposition. In *Proceedings of IMAC 19, International Modal Analysis Conference*, Kissimmee, Florida, USA.

Brincker, R.; Zhang, L.; Andersen, P. (2000) Modal Identification from Ambient Responses Using Frequency Domain Decomposition. In *Proceedings of IMAC 18, International Modal Analysis Conference*, San Antonio, USA.

Brownjohn, J.; Dumanoglu, A.; Severn, R.; Blakeborough, A. (1989) Ambient Vibration Survey of the Bosphorus Suspension Bridge. *Earthquake Engineering and Structural Dynamics*, 18(2), 263-283.

Brownjohn, J. M.; Dumanoglu, A. A.; Severn, R. T.; Taylor, C. A. (1986) *Ambient Vibration Survey of the Humber Suspension Bridge*. University of Bristol.

Brownjohn, J. M. W. (2007) Structural Health Monitoring of Civil Infrastructures. *Philosophical Transactions of The Royal Society A*, 365(1851), 589-622.

Brownjohn, J. M. W.; Carden, P. (2008) Real-time operation modal analysis of Tamar Bridge In *Proceedings of IMAC 26, International Modal Analysis Conference*, Orlando, Florida, USA.

Brownjohn, J. M. W.; Durnanoglu, A. A.; Severn, R. T. (1992) Ambient vibration survey of the Fatih Sultan Mehmet (Second Bosphorus) Suspension Bridge. *Earthquake Engineering and Structural Dynamics*, 21(10), 907-924.

Brownjohn, J. M. W.; Magalhães, F.; Caetano, E.; Cunha, Á. (2010) Ambient vibration re-testing and operational modal analysis of the Humber Bridge. *Engineering Structures*, doi:10.1016/j.engstruct.2010.02.034.

Brownjohn, J. M. W.; Worden, K. (2008) *Novel Data Mining and Performance Diagnosis Systems for Structural Health Monitoring of Suspension Bridges*. EPSRC Research Project (<http://gow.epsrc.ac.uk/ViewGrant.aspx?GrantRef=EP/F035403/1>).

Caetano, E. (2000) *Dynamics of Cable-stayed Bridges: Experimental Assessment of Cable-Structure Interaction*. PhD Thesis, Faculty of Engineering of the University of Porto, Portugal.

-
- Caetano, E.; Cunha, Á. (2001) *Numerical modelling of the Structural Behaviour of the New Braga Stadium Roof*. Report ViBest/FEUP
- Caetano, E.; Cunha, Á.; Magalhães, F. (2004) *Modal Identification of Millau Viaduct, Contribution of FEUP*. Report ViBest/FEUP.
- Caetano, E.; Cunha, Á.; Magalhães, F. (2008) Numerical and experimental studies of Braga sports stadium suspended roof. *Structure and Infrastructure Engineering*, doi:10.1080/15732470802087906.
- Caetano, E.; Cunha, Á.; Magalhães, F.; Moutinho, C. (2010a) Studies for controlling human-induced vibration of the Pedro e Inês footbridge, Portugal. Part 1: Assessment of dynamic behaviour *Engineering Structures*, 32(4), 1069-1081.
- Caetano, E.; Cunha, Á.; Moutinho, C.; Magalhães, F. (2010b) Studies for controlling human-induced vibration at the Pedro e Inês Footbridge, Portugal. Part 2: Implementation of tuned mass dampers. *Engineering Structures*, 32(4), 1082-1091.
- Caetano, E.; Magalhães, F.; Cunha, Á.; Flamand, O.; Grillaud, G. (2007) Comparison of stochastic identification methods applied to the natural response of Millau Viaduct. In *Proceedings of EVACES, Experimental Vibration Analysis for Civil Engineering Structures*, Porto, Portugal.
- Cantieni, R. (2005) Experimental Methods used in System Identification of Civil Engineering Structures. In *Proceedings of IOMAC, International Operational Modal Analysis Conference*, Copenhagen, Denmark.
- Carden, E. P.; Brownjohn, J. M. W. (2008) Fuzzy Clustering of Stability Diagrams for Vibration-Based Structural Health Monitoring. *Computer-Aided Civil and Infrastructure Engineering*, 23(5), 360-372.
- Carter, D. S. (1937) Observed Vibrations of Bridges. *Bulletin of the Seismological Society of America*, 27(4), 267-303.
- Cauberghe, B. (2004) *Applied Frequency-Domain System Identification in the Field of Experimental and Operational Modal Analysis*. PhD Thesis, Vrije Universiteit Brussel, Belgium.
- CEB-FIB (1993) *Model Code 1990*. Thomas Telford.
- CEN (2004) *Eurocode 2: Design of concrete structures - Part 1-1: General rules and rules for buildings*. Brussels.
- Clough, R. W.; Penzien, J. (1993) *Dynamics of Structures*. McGraw-Hill.

Cooley, J. W.; Tukey, J. W. (1965) An Algorithm for the Machine Calculation of Complex Fourier Series. *Mathematics of Computation*, 19(90), 297-301.

Corrêa, M. R.; Costa, A. C. (1992) *Dinamic tests of the bridge over the Arade River*. Cable-stayed Bridges of Guadiana and Arade, book (in portuguese) edited by J. A. Fernandes e L. O. Santos, LNEC.

Crawford, R.; Ward, H. S. (1964) Determination of the Natural Period of Buildings. *Bulletin of the Seismological Society of America*, 54(6), 1743-1756.

Croiset, J.-E.; Ryckaert, J.; Viel, G.; Spielmann, A. (2006) A new bridge for Reunion Island in the Indian Ocean intended to sit lightly on the island's fragile environment. *Bridge Design & Engineering*, 44.

Cunha, Á.; Caetano, E. (2006) Experimental Modal Analysis of Civil Engineering Structures. *Sound and Vibration*, 6(40), 12-20.

Cunha, A.; Caetano, E.; Delgado, R. (2001) Dynamic Tests on a Large Cable-Stayed Bridge. An Efficient Approach. *Journal of Bridge Engineering, ASCE*, 6(1), 54-62.

Cunha, Á.; Caetano, E.; Magalhães, F. (2007) Output-only Dynamic Testing of Bridges and Special Structures. *Structural Concrete (Fib)*, 8(2), 67-85.

Cunha, Á.; Calçada, R. (2000) Ambient vibration test of a steel trussed arch bridge. In *Proceedings of IMAC 18, International Modal Analysis Conference*, San Antonio, USA,.

Cunha, Á.; Magalhães, F.; Caetano, E. (2006) Output-only Modal Identification of Luiz I Bridge before and after Rehabilitation. In *Proceedings of ISMA, International Conference on Noise and Vibration Engineering*, Leuven, Belgium.

Cunha, Á.; Magalhães, F.; Caetano, E. (2009) Suspended Roof of Braga Sports Stadium, Portugal. *Encyclopedia of Structural Health Monitoring*, C. Boller, F. Chang, and Y. Fujino, eds., John Wiley & Sons, 2253-2264.

De Boe, P.; Golinval, J.-C. (2003) Principal Component Analysis of a Piezosensor Array for Damage Localization. *Structural Health Monitoring*, 2(2), 137-144.

De Troyer, T.; Guillaume, P.; Pintelon, R.; Vanlanduit, S. (2009) Fast Calculation of Confidence Intervals on Parameter Estimates of Least-Squares Frequency-Domain Estimators. *Mechanical Systems and Signal Processing*, 23(2), 261-273.

-
- Deraemaeker, A.; Reynders, E.; De Roeck, G.; Kullaa, J. (2008) Vibration-based structural health monitoring using output-only measurements under changing environment. *Mechanical Systems and Signal Processing*, 22(1), 34-56.
- Devriendt, C.; Guillaume, P. (2007) The use of Transmissibility Measurements in Output-Only Modal Analysis. *Mechanical Systems and Signal Processing*, 21(7), 2689-2696.
- Diord, S.; Magalhães, F.; Cunha, Á. (2009) *DynaMo Viewer User's Guide*. Report ViBest/FEUP.
- Doebling, S. W.; Farrar, C. R.; Prime, M. B.; Shevitz, D. W. (1996) *Damage Identification and Health Monitoring of Structural and Mechanical Systems from Changes in their Vibration Characteristics: a Literature Review*. LA-13070-MS, Los Alamos National Laboratory, Los Alamos.
- Dohler, M.; Reynders, E.; Magalhães, F.; Mevel, L.; De Roeck, G.; Cunha, A. (2010) Pre- and Post-identification Merging for Multi-Setup OMA with Covariance-Driven SSI. In *Proceedings of IMAC 28, International Modal Analysis Conference*, Jacksonville, Florida, USA.
- Ewins, D. J. (2000) *Modal Testing: theory and practice*. Research Studies Press, U.K.
- Farrar, C. R.; Doebling, S. W.; Cornwell, P. J.; Straser, E. G. (1997) Variability of Modal Parameters Measured on the Alamosa Canyon Bridge In *Proceedings of IMAC 15, International Modal Analysis Conference*, Orlando, Florida, USA.
- Federal Highway Administration (2008) *2008 status of the nation's highways, bridges and transit: Conditions and performance - report to congress*. Technical Report, U. S. Department of Transportation.
- Felber, A. J. (1993) *Development of a Hybrid Bridge Evaluation System*. PhD Thesis, University of British Columbia, Vancouver, Canada.
- Felber, A. J.; Cantieni, R. (1996) Advances in Ambient Vibration Testing: Ganter Bridge, Switzerland. *Structural Engineering International*, 3, 187-190.
- FIB (2003) *Monitoring and Safety Evaluation of Existing Concrete Structures* FIB Bulletin 22.
- Flamand, O. (2009) *Essais de caractérisation dynamique du Viaduc de La Grande Ravine*. CSTB Report EN-CAPE 09.073 C - V0 Nantes, France.
- Flamand, O.; Grillaud, G. (2005) *Identification modale du Viaduc de Millau*. CSTB, Report EN-CAPE 05.007 C – V0 Nantes, France.
- Flamand, O.; Grillaud, G. (2006) Dynamic testing of the Millau Viaduct. In *Proceedings of Third International Conference on Bridge Maintenance, Safety and Management*, Porto, Portugal.
-

Fraser, M.; He, X.; Elgamal, A.; Conte, J. P. (2007) Structural Monitoring of the I-5/voigt Drive Bridge, San Diego County, California In *Proceedings of EVACES, Experimental Vibration Analysis for Civil Engineering Structures*, Porto, Portugal.

Furtado, R.; Quinaz, C.; Bastos, R. (2005) New Braga Municipal Stadium, Braga. *Structural Engineering International*, 15(2), 72-76.

Gentile, C.; Bernardini, G. (2008) Output-only modal identification of a reinforced concrete bridge from radar-based measurements. *NDT&E International*, 41(7), 544-553.

Goethals, I.; Vanluyten, B.; De Moor, B. (2004) Reliable spurious mode rejection using self learning algorithms. In *Proceedings of ISMA, International Conference on Noise and Vibration Engineering*, Leuven, Belgium.

Guillaume, P.; Hermans, L.; Van der Auweraer, H. (1999) Maximum Likelihood Identification of Modal Parameters from Operational Data. In *Proceedings of IMAC 17, International Modal Analysis Conference*, Kissimmee, Florida, USA.

Guillaume, P.; Verboven, P.; Vanlanduit, S.; Van der Auweraer, H.; Peeters, B. (2003) A Poly-Reference Implementation of the Least-Squares Complex Frequency-Domain Estimator. In *Proceedings of IMAC 21, International Modal Analysis Conference*, Kissimmee, Florida, USA.

Hair, J.; Anderson, R.; Tatham, R.; Black, W. (1998) *Multivariate Data Analysis*. Prentice Hall.

Heylen, W.; Lammens, S.; Sas, P. (2007) *Modal Analysis Theory and Testing*. KULeuven, Belgium.

Hu, W.-H.; Moutinho, C.; Magalhães, F.; Caetano, E.; Cunha, Á. (2009) Analysis and Extraction of Temperature Effects on Natural Frequencies of a Footbridge based on Continuous Dynamic Monitoring. In *Proceedings of IOMAC, International Operational Modal Analysis Conference*, Portonovo (Ancona), Italy.

IABSE (2009) *Recent Major Bridges*. IABSE Workshop, Shanghai.

Jacobsen, N.-J.; Andersen, P.; Brincker, R. (2008) Applications of Frequency Domain Curve-fitting in the EFDD Technique. In *Proceedings of IMAC 26, International Modal Analysis Conference*, Orlando, Florida, USA.

James, G. H.; Carne, T. G.; Lauffer, J. P.; Nard, A. R. (1992) Modal Testing Using Natural Excitation. In *Proceedings of IMAC 10, International Modal Analysis Conference*, San Diego, USA.

Johnson, R. A.; Wichern, D. W. (1992) *Applied Multivariate Statistical Analysis*. Prentice Hall.

Juang, J.-N. (1994) *Applied System Identification*. Prentice Hall Englewood Cliffs, New Jersey, USA.

-
- Juang, J.-N.; Pappa, R. S. (1985) An Eigensystem Realization Algorithm for Modal Parameter Identification and Model Reduction. *Journal of Guidance, Control, and Dynamics*, 8(5), 620-627.
- Ko, J. M.; Ni, Y. Q. (2005) Technology developments in structural health monitoring of large-scale bridges. *Engineering Structures*, 27(12), 1715-1725.
- Koh, H.-M.; Lee, H.-S.; Kim, S.; Choo, J. F. (2009) Monitoring of Bridges in Korea. Encyclopedia of Structural Health Monitoring, C. Boller, F. Chang, and Y. Fujino, eds., Vol. 5, Chapter 124, John Wiley & Sons
- Kullaa, J. (2003) Damage Detection of the Z24 Bridge using Control Charts. *Mechanical Systems and Signal Processing*, 17(1), 163-170.
- Kullaa, J. (2004) Structural Health Monitoring of a Crane in Variable Configurations. In *Proceedings of ISMA, International Conference on Noise and Vibration Engineering*, Leuven, Belgium.
- Kung, S. Y. (1978) A new Identification and Model Reduction Algorithm via Singular Value Decomposition. In *Proceedings of 12th Asilomar Conference on Circuits, Systems and Computers*, USA.
- Liu, C.; DeWolf, J. T. (2007) Effect of Temperature on Modal Variability of a Curved Concrete Bridge under Ambient Loads. *Journal of Structural Engineering*, 133(12), 1742-1751.
- Ljung, L. (1999) *System Identification: Theory for the user*. Prentice Hall, New Jersey.
- Londono, N. A. (2006) *Use of Vibration Data for Structural Health Monitoring of Bridges*. PhD Thesis, Carleton University, Ottawa.
- Macdonald, J. H. G.; Daniell, W. E. (2005) Variation of Modal Parameters of a Cable-stayed Bridge Identified from Ambient Vibration Measurements and FE Modelling. *Engineering Structures*, 27(13), 1916-1930.
- MacLamore, V. R.; Hart, G. C.; Stubbs, I. R. (1971) Ambient Vibration of two Suspension Bridges. *Journal of the Structural Division, ASCE*, 97(ST10), 2567-2582.
- Magalhães, F.; Brownjohn, J. M.; Caetano, E.; Cunha, Á. (2009a) Challenges in Identification of the Humber Bridge Modal Parameters based on an Ambient Vibration Test. In *Proceedings of IOMAC, International Operational Modal Analysis Conference*, Ancona, Italy.
- Magalhães, F.; Caetano, E.; Cunha, Á. (2006a) Operational Modal Analysis of the Braga Sports Stadium Suspended Roof. In *Proceedings of IMAC 24, International Conference of Modal Analysis*, St. Louis, Missouri, USA.
-

Magalhães, F.; Caetano, E.; Cunha, Á. (2007a) Challenges in the Application of Stochastic Modal Identification Methods to a Cable-Stayed Bridge. *Journal of Bridge Engineering* 12(6), 746-754.

Magalhães, F.; Caetano, E.; Cunha, Á. (2007b) Dynamic Testing of the New Coimbra Footbridge before Implementation of Control Devices. In *Proceedings of IMAC 25, International Modal Analysis Conference*, Orlando, Florida, USA.

Magalhães, F.; Caetano, E.; Cunha, Á. (2008a) *Ambient Vibration Test of the Humber Bridge - FEUP Preliminary Report*. Report ViBest/FEUP.

Magalhães, F.; Caetano, E.; Cunha, Á. (2008b) Dynamic Tests and Continuous Monitoring of a Moveable Cable-Stayed Bridge. In *Proceedings of Footbridge 2008*, Porto, Portugal.

Magalhães, F.; Caetano, E.; Cunha, Á. (2008c) Operational modal analysis and finite element model correlation of the Braga Stadium suspended roof. *Engineering Structures*, 30(6), 1688-1698.

Magalhães, F.; Caetano, E.; Cunha, Á. (2009b) *Dynamic Tests of the "Viaduc de La Grande Ravine"*. Report ViBest/FEUP.

Magalhães, F.; Cunha, Á.; Caetano, E. (2008d) Dynamic Monitoring of a Long Span Arch Bridge. *Engineering Structures*, 30(11), 3034-3044.

Magalhães, F.; Cunha, Á.; Caetano, E. (2009c) Installation of a Continuous Dynamic Monitoring system at Braga Stadium Suspended Roof: initial results from automated modal analysis. In *Proceedings of EVACES, Experimental Vibration Analysis for Civil Engineering Structures*, Wroclaw, Poland.

Magalhães, F.; Cunha, Á.; Caetano, E. (2009d) One-year Dynamic Monitoring of a Bridge: modal parameters tracking under the influence of environmental effects. In *Proceedings of SHMII-4, International Conference on Structural Health Monitoring of Intelligent Infrastructure*, Zurich, Switzerland.

Magalhães, F.; Cunha, Á.; Caetano, E. (2009e) Online automatic identification of the modal parameters of a long span arch bridge. *Mechanical Systems and Signal Processing*, 23(2), 316-329.

Magalhães, F.; Cunha, Á.; Caetano, E.; Adão da Fonseca, A.; Bastos, R. (2006b) Evaluation of the dynamic properties of the Infante Dom Henrique Bridge. In *Proceedings of IABMAS*, Porto, Portugal.

Magalhães, F.; Cunha, Á.; Caetano, E.; Brincker, R. (2009f) Damping Estimation using Free Decays and Ambient Vibration Tests. *Mechanical Systems and Signal Processing*, doi:10.1016/j.ymssp.2009.02.011.

-
- Magalhães, F.; Reynders, E.; Cunha, Á.; De Roeck, G. (2009g) Online automatic identification of modal parameters of a bridge using the p-LSCF method. In *Proceedings of IOMAC, International Operational Modal Analysis Conference*, Ancona, Italy.
- Maia, N.; Silva, J. (1997) *Theoretical and Experimental Modal Analysis*. Research Studies Press Ltd.
- Marecos, J. (1954) *Observation and Test of a the Bridge of the Sousa River*. LNEC report (in portuguese).
- Marecos, J.; Castanheta, M. (1970) *Observation of the Bridge over the Tagus river. Stresses and Displacements in the Main Structure*. LNEC report (in Portuguese).
- Marecos, J.; Pereira, J.; Castanheta, M. (1967) *Load test of the Tagus Bridge: Suspension Bridge*. LNEC Report (in portuguese).
- Mathworks (2009) *Statistics Toolbox 7 - User's Guide*.
- MatLab (2000a) *Signal Processing Toolbox For Use with MATLAB, User's Guide, Version 5*. The MathWorks.
- MatLab (2000b) *Using MATLAB Version 6*. The MathWorks.
- Mevel, L.; Basseville, M.; Benveniste, A.; Goursat, M. (2002) Merging Sensor Data from Multiple Measurement Set-ups for Non-stationary Subspace-based Modal Analysis. *Journal of Sound and Vibration*, 249(4), 719-741.
- Montgomery, D. (2005) *Introduction to Statistical Quality Control*. John Wiley & Sons.
- Ni, Y. O.; Hua, X. G.; Fan, K. Q.; Ko, J. M. (2005) Correlating Modal Properties with Temperature using Long-term Monitoring Data and Support Vector Machine Technique. *Engineering Structures*, 27, 1762-1773.
- Oppenheim, A. V.; Schaffer, R. W. (1975) *Digital Signal Processing* Prentice-Hall.
- Pakzad, S. N.; Fences, G. L. (2009) Statistical Analysis of Vibration Modes of a Suspension Bridge Using Spatially Dense Wireless Sensor Network. *Journal of Structural Engineering*, 135(7), 863-872.
- Pappa, R.; James III, G.; Zimmerman, D. (1998) Autonomous Modal Identification of the Space Shuttle Tail Rudder. *Journal of Spacecraft and Rockets*, 35(2), 163-169.
- Parloo, E. (2003) *Application of Frequency-Domain System Identification Techniques in the Field of Operational Modal Analysis*. PhD Thesis, Vrije Universiteit Brussel, Belgium.

Peeters, B. (2000) *System Identification and Damage Detection in Civil Engineering*. PhD Thesis, Katholieke Universiteit Leuven, Belgium.

Peeters, B.; Couvreur, G.; Razinkov, O.; Kundig, C.; Van der Auweraer, H.; De Roeck, G. (2003) Continuous Monitoring of the Oresund Bridge: System and Data Analysis. In *Proceedings of IMAC 21, International Modal Analysis Conference*, Kissimmee, Florida, USA.

Peeters, B.; De Roeck, G. (2000) Reference Based Stochastic Subspace Identification in Civil Engineering. *Inverse Problems in Engineering*, 8(1), 47-74.

Peeters, B.; De Roeck, G. (2001) One-year monitoring of the Z24-Bridge: environmental effects versus damage events. *Earthquake Engineering and Structural Dynamics*, 30(2), 149-171.

Peeters, B.; De Roeck, G.; Caetano, E.; Cunha, A. (2002) Dynamic Study of the Vasco da Gama Bridge. In *Proceedings of ISMA, International Conference on Noise and Vibration Engineering*, Leuven, Belgium.

Peeters, B.; Van Der Auweraer, H. (2005) PolyMax: a Revolution in Operational Modal Analysis. In *Proceedings of IOMAC, International Operational Modal Analysis Conference*, Copenhagen, Denmark.

Peeters, B.; Van Der Auweraer, H.; Guillaume, P.; Leuridan, J. (2004) The PolyMAX Frequency-Domain Method: a New Standard for Modal Parameters Estimation? *Shock and Vibration*(11), 395-409.

Pereira, J. (1962) *Dynamic Measurements in Bouça Dam*. LNEC report (in portuguese).

Prevosto, M. (1982) *Algorithmes D'Identification des Caractéristiques Vibratoires de Structures Mécaniques Complexes*. PhD Thesis, Université de Rennes I, France.

Reynders, E. (2009) *System Identification and Modal Analysis in Structural Mechanics*. PhD Thesis, KULeuven.

Reynders, E.; Magalhães, F.; De Roeck, G.; Cunha, Á. (2009) Merging Strategies for Multi-Setup Operational Modal Analysis: Application to the Luiz I steel Arch Bridge. In *Proceedings of IMAC 27, International Modal Analysis Conference*, Orlando, Florida, USA.

Reynders, E.; Pintelon, R.; De Roeck, G. (2008a) Uncertainty Bounds on Modal Parameters obtained from Stochastic Subspace Identification. *Mechanical Systems and Signal Processing*, 22(4), 948-969.

Reynders, E.; Schevenels, M.; De Roeck, G. (2008b) *MACEC: A Matlab toolbox for experimental and operational analysis* Department of Civil Engineering, K. U. Leuven.

-
- Rodrigues, J. (2004) *Stochastic modal identification. Methods and applications in civil engineering structures*. PhD Thesis (in Portuguese), University of Porto (FEUP/LNEC).
- Rodrigues, J.; Brincker, R.; Andersen, P. (2004) Improvement of Frequency Domain Output-Only Modal Identification from the Application of the Random Decrement Technique. In *Proceedings of IMAC 22, International Modal Analysis Conference*, Dearborn, USA.
- Rodrigues, J.; Ledesma, M. (2009) Modal Identification of Railway Bridges from Ambient and Free Vibration Records. In *Proceedings of IOMAC, International Operational Modal Analysis Conference*, Portonovo (Ancona), Italy.
- Rohrman, R. G.; Baessler, M.; Said, S.; Schmid, W.; Ruecker, W. F. (2000) Structural Causes of Temperature Affected Modal Data of Civil Structures Obtained by Long Time Monitoring. In *Proceedings of IMAC 18, International Modal Analysis Conference*, San Antonio, TX, USA.
- Scionti, M.; Lanslots, J.; Goethals, I.; Vecchio, A.; Van der Auweraer, H.; Peeters, B.; De Moor, B. (2003) Tool to Improve detection of Structural changes from In-Flight Flutter Data. In *Proceedings of Eighth International Conference on recent advances in Structural Dynamics*, Southampton, UK.
- Shih, C. Y.; Tsuei, Y. G.; Allemang, R. J.; Brown, D. L. (1988) Complex Mode Indicator Function and its application to spatial domain parameter estimation. *Mechanical Systems and Signal Processing*, 2(4), 367-377.
- Siringoringo, D. M.; Fujino, Y. (2008) System Identification of a Suspension Bridge from Ambient Vibration Response. *Engineering Structures*, 30(2), 462-477.
- Sohn, H.; Farrar, R.; Hemez, M.; Czarnecki, J.; Shunk, D.; Stinemates, W.; Nadler, R. (2002) *A review of Structural Health Monitoring Literature: 1996-2001*. Los Alamos National Laboratory, Los Alamos.
- Sohn, H.; Worden, K.; Farrar, C. R. (2003) Statistical damage classification under changing environmental and operational conditions. *Journal of Intelligent Material Systems and Structures*, 13(9), 561-574.
- Steenackers, G.; Guillaume, P. (2005) Structural Health Monitoring of the Z-24 Bridge in the Presence of Environmental Changes using Modal Analysis. In *Proceedings of IMAC 23, International Modal Analysis Conference*, Orlando, Florida, USA.
- SVS (1999-2004). ARTeMIS Extractor Pro, Release 3.41. Structural Vibration Solutions, Aalborg, Denmark.

Trifunac, M. (1972) Comparison between Ambient and Forced Vibration Experiments. *Earthquake Engineering and Structural Dynamics*, 1, 133-150.

Van Overschee, P.; De Moor, B. (1996) *Subspace Identification for Linear Systems*. Kluwer Academic Publishers, Leuven, Belgium.

Vanlanduit, S.; Parloo, E.; Cauberghe, B.; Guillaume, P.; Verboven, P. (2005) A Robust Singular Value Decomposition for Damage Detection under Changing Operational Conditions and Structural Uncertainties. *Journal of Sound and Vibration*, 284(3-5), 1033-1050.

Vapnik, V. N. (1999) An overview of Statistical Learning Theory. *IEEE Transaction on Neural Networks*, 10(5), 988-999.

Verboven, P.; Guillaume, P.; Cauberghe, B.; Parloo, E.; Vanlanduit, S. (2003) Stabilization Charts and Uncertainty Bounds for Frequency-Domain Linear Least Squares Estimators. In *Proceedings of IMAC 21, International Modal Analysis Conference*, Kissimmee, Florida, USA.

Verboven, P.; Parloo, E.; Guillaume, P.; Van Overmeire, M. (2001) Autonomous Modal Parameter Estimation based on a Statistical Frequency Domain Maximum Likelihood Approach. In *Proceedings of IMAC 19, International Modal Analysis Conference*, Kissimmee, Florida, USA.

Verboven, P.; Parloo, E.; Guillaume, P.; Van Overmeire, M. (2002) Autonomous Structural Health Monitoring - Part I: Modal Parameter Estimation and Tracking. *Mechanical Systems and Signal Processing*, 16(4), 637-657.

Virlogeux, M.; Servant, C.; Cremer, J.-M.; Martin, J.-P.; Buonomo, M. (2005) Millau Viaduct, France. *Structural Engineering International*, 15(1), 4-7.

Welch, P. D. (1967) The use of Fast Fourier Transform for the Estimation of Power Spectra: a Method based on Time Averaging over short Modified Periodograms. *IEEE Transaction on Audio and Electro-Acoustics*, AU-15(2).

Wenzel, H.; Pichler, D. (2005) *Ambient Vibration Monitoring*. John Wiley & Sons.

Whelan, M. J.; Gangone, M. V.; Janoyan, K. D.; Jha, R. (2009) Real-time wireless vibration monitoring for operational modal analysis of an integral abutment highway bridge. *Engineering Structures*, 31(10), 2224-2235.

Wong, K.-Y. (2004) Instrumentation and Health Monitoring of Cable-supported Bridges. *Structural Control and Health Monitoring*, 11(2), 91-124.

Xu, Y. L.; Ko, J. M.; Zhang, W. S. (1997) Vibration studies of Tsing Ma suspension bridge. *ASCE Journal of Bridge Engineering*, 2(4), 149-156.

Yan, A.-M.; De Boe, P.; Golinval, J.-C. (2004) Structural Damage Diagnosis by Kalman Model Based on Stochastic Subspace Identification. *Structural Health Monitoring*, 3(2), 103-110.

Yan, A.-M.; Kerschen, G.; De Boe, P.; Golinval, J.-C. (2005a) Structural Damage Diagnosis under varying Environmental Conditions - Part I: A Linear Analysis. *Mechanical Systems and Signal Processing*, 19(4), 847-864.

Yan, A.-M.; Kerschen, G.; De Boe, P.; Golinval, J.-C. (2005b) Structural damage diagnosis under varying environmental conditions - part II: local PCA for non-linear cases. *Mechanical Systems and Signal Processing*, 19(4), 865-880.